

**Development of pharmacological modulators  
for the orphan G protein-coupled receptor GPR17  
and their application for the investigation of  
molecular signal transduction pathways**

**Dissertation**

zur

Erlangung des Doktorgrades (Dr. rer. nat.)

der

Mathematisch-Naturwissenschaftlichen Fakultät

der

Rheinischen Friedrich-Wilhelms-Universität Bonn

vorgelegt von

Andreas Spinrath

aus

Mönchengladbach

Bonn, Januar 2011



Angefertigt mit Genehmigung der Mathematisch-Naturwissenschaftlichen Fakultät  
der Rheinischen Friedrich-Wilhelms Universität Bonn.

1. Referent: Prof. Dr. Evi Kostenis  
2. Referent: Prof. Dr. Christa E. Müller  
Tag der Promotion: 17.Juni 2011  
Erscheinungsjahr: 2011



Die vorliegende Arbeit wurde in der Zeit von September 2006 bis Januar 2011 am Institut für Pharmazeutische Biologie der Rheinischen Friedrich-Wilhelms Universität Bonn unter der Leitung von Frau Prof. Dr. Evi Kostenis durchgeführt.

Mein besonderer Dank gilt Frau Prof. Dr. Evi Kostenis, die mich ermutigt und es mir ermöglicht hat, diese Arbeit anzufertigen. Ich danke ihr für ihre freundliche Betreuung und Unterstützung und ihre stete Diskussionsbereitschaft.

Frau Prof. Dr. Christa E. Müller danke ich für die freundliche Übernahme des Koreferats sowie Herr Prof. Dr. Klaus Mohr und Herr Prof. Dr. Ivar von Kügelgen für die Mitwirkung in meiner Promotionskommission.

Ich danke der Deutschen Forschungsgemeinschaft für die finanzielle Unterstützung in Form eines Promotionsstipendiums im Rahmen des Graduiertenkollegs 677 „Struktur und molekulare Interaktion als Basis der Arzneimittelwirkung.“



Meiner Frau Marieke, meiner Tochter Annemarie  
und  
meinen Eltern





## DIRECTORY

<b>CHAPTER I: INTRODUCTION .....</b>	<b>1</b>
1.1 G protein-coupled receptors and their signal transduction pathways.....	1
1.2 Orphan G protein-coupled receptors and their deorphanisation .....	4
1.3 G protein-coupled receptor 17 (GPR17) .....	5
1.4 Scope of the present study .....	8
<b>CHAPTER II: RESULTS .....</b>	<b>9</b>
2.1 Generation of recombinant cell systems stably expressing GPR17.....	9
2.2 Examination of positive pharmacological GPR17 modulators.....	10
2.2.1 Compound analysis using the calcium assay .....	10
2.2.2 GPR17 agonist RA-II-150 does not activate related P2Y receptors .....	19
2.2.3 Compound analysis using inositol phosphate accumulation assays .....	20
2.2.4 Compound analysis using the dynamic mass redistribution assay.....	22
2.3 Uracil nucleotides proposed as GPR17 agonists.....	29
2.3.1 Compound analysis using calcium assays .....	29
2.3.2 Compound analysis using DMR technology based assays.....	31
2.4 CysLT <sub>1</sub> receptor antagonists proposed as GPR17 antagonists.....	32
2.4.1 Compound analysis using calcium assays .....	32
2.4.2 Compound analysis using inositol phosphate accumulation assays .....	34
2.5 Investigations of signal transduction pathways coupled to GPR17 and discovery of a novel calcium release mechanism in 1321N1 cells .....	36
2.5.1 PTX pretreatment reveals participation of the G <sub>i</sub> pathway in the calcium mobilisation mechanism.....	36
2.5.2 Confirmation of GPR17 G <sub>i</sub> coupling by determination of cAMP decrease .	37
2.5.3 A phosphatidylinositol-specific phospholipase C is involved in the calcium release mechanism in 1321N1-GPR17 cells.....	40
2.5.4 GPR17 activation does not lead to an accumulation of inositol phosphates in 1321N1-GPR17 cells .....	43
2.5.5 Intracellular calcium stores are the major sources of GPR17-mediated..... calcium flux .....	44
2.5.6 IP <sub>3</sub> receptors on intracellular calcium stores gate the efflux of calcium .....	45
2.5.7 The role of calmodulin in the calcium release mechanism .....	48

2.5.8 Protein kinases and their influence on the calcium release mechanism ...	50
2.6 Characterisation of potential endogenous ligands of GPR17 .....	52
2.6.1 Selected endogenous compounds and biosynthesis pathway	
intermediates as potential GPR17 ligands .....	52
2.6.2 Selected amino acids and folic acid as potential ligands of GPR17.....	52
2.6.3 Selected intermediates of the citric acid cycle as potential GPR17	
ligands .....	54
2.6.4 Selected purines and pyrimidine bases and a nucleoside as	
potential GPR17 ligands .....	54
2.6.5 Neurotransmitters and their metabolites as modulators of GPR17 .....	56
2.7 Products from natural sources as GPR17 modulators .....	57
2.7.1 Compounds from marine and endophytic fungi and marine sponges .....	57
2.7.2 Compounds from bacterial sources .....	62
2.7.3 Compounds from terrestrial plants.....	63
2.8 Characterisation of synthetic anthraquinone compounds as negative	
modulators of GPR17.....	70
2.8.1 Substitution of the anthraquinone scaffold with a phenyl group.....	71
2.8.2 Substitution of the anthraquinone with a side chain containing a benzyl	
or phenethyl scaffold or an ethylthiophenyl side chain.....	79
2.8.3 Substitution of the anthraquinone containing an aliphatic scaffold.....	81
2.8.4 Substitution of the anthraquinone with a side chain containing	
a naphthalene or anthracene scaffold.....	82
2.8.5 Substitution of the anthraquinone with a side chain consisting of	
two substituted or unsubstituted phenyl rings bridged by different atoms.	84
2.8.6 Substitution of the anthraquinone containing a side chain consisting	
of a phenyl ring and a triacetyl or pyrimidinyl ring .....	87
2.8.7 Substitution of the anthraquinone containing a side chain consisting of a	
phenyl ring substituted with at least a sulphonate or carboxylate group ...	90
<b>CHAPTER III: Discussion .....</b>	<b>95</b>
3.1 Identified GPR17 ligands – useful <i>in vitro</i> tools .....	95
3.2 First indications of functionally selective GPR17 ligands.....	97
3.3 Novel calcium mobilisation mechanism proposed for GPR17 .....	98
3.4 Screening of natural products does not deorphanise GPR17, but identifies	
novel antagonist lead structures.....	100

---

3.5 Anthraquinone derivatives as potent <i>in vitro</i> GPR17 antagonists .....	102
3.6 Putative <i>in vivo</i> role of GPR17 .....	103
<b>CHAPTER IV: SUMMARY .....</b>	<b>105</b>
<b>CHAPTER V: EXPERIMENTAL SECTION.....</b>	<b>106</b>
5.1 Devices and materials.....	106
5.1.1 Devices .....	106
5.1.2 Consumables .....	108
5.1.3 Kits .....	111
5.1.4 Radioligands .....	111
5.1.5 Software .....	112
5.2 Cell culture.....	113
5.2.1 Cell lines.....	113
5.2.2 Materials and supplements for cell culture .....	114
5.2.4 Media for mammalian cells.....	116
5.2.4 Cell culture techniques .....	117
5.3 Molecular biology .....	122
5.3.1 Solutions for molecular biology .....	122
5.3.2 Bacteria .....	123
5.3.3 Media for bacterial cultures .....	124
5.3.4 Enzymes .....	124
5.3.5 Vectors and molecular weight markers .....	125
5.3.6 Protocols for molecular biological techniques .....	125
5.4 Functional assays .....	134
5.4.1 Solutions for functional assays.....	134
5.4.2 Microplates for functional assays .....	138
5.4.3 Protocols for functional GPCR analysis.....	139
<b>CHAPTER VI: TABLE OF ABBREVIATIONS .....</b>	<b>150</b>
<b>CHAPTER VII: REFERENCES .....</b>	<b>156</b>
<b>ACKNOWLEDGEMENTS .....</b>	<b>169</b>
<b>REGISTER OF PUBLICATIONS .....</b>	<b>171</b>



---

## CHAPTER I: INTRODUCTION

---

### 1.1 G protein-coupled receptors and their signal transduction pathways

G protein-coupled receptors (GPCR) can be classified into five major families. The largest family is the Rhodopsin-like receptor family, while the other smaller families are the Secretin family, the Adhesion family, the Glutamate family and the Frizzled/Taste family.<sup>[1]</sup>

The members of the Rhodopsin-like receptor family, in particular, are one of the most important therapeutical drug targets on the pharmaceutical market, because they are involved in a broad spectrum of diseases like stroke, asthma, schizophrenia, cancer, neurological pain, migraine, allergies, gastric ulcers, diabetes, obesity and hypertension.<sup>[2-4]</sup>

GPCRs are proteins located in the cytoplasmic membrane. They consist of seven  $\alpha$ -helical transmembrane domains that are connected by intracellular and extracellular loops; the N-terminus is extracellular and the C-terminus intracellular. These receptors are classically activated upon ligand binding and transduce signals from the extracellular compartment to the interior via biochemical processes involving GTP-binding proteins, so-called G proteins. Activated GPCRs act as guanine nucleotide exchange factors (GEFs) for the  $G_{\alpha}$  subunit of a heterotrimeric G protein, catalyzing the release of GDP and the binding of GTP for G protein activation. The activated G protein subunits  $G_{\alpha}$  and  $G_{\beta\gamma}$  can then associate with downstream effectors to modulate various aspects of cellular physiology. The downstream effector activated or inhibited by the G protein divides the group of G proteins into the following classes:  $G_q$ ,  $G_s$ ,  $G_{i/o}$  and  $G_{12/13}$  (Figure 1).<sup>[5]</sup> Each class activates specific signal transduction pathways within the cell.

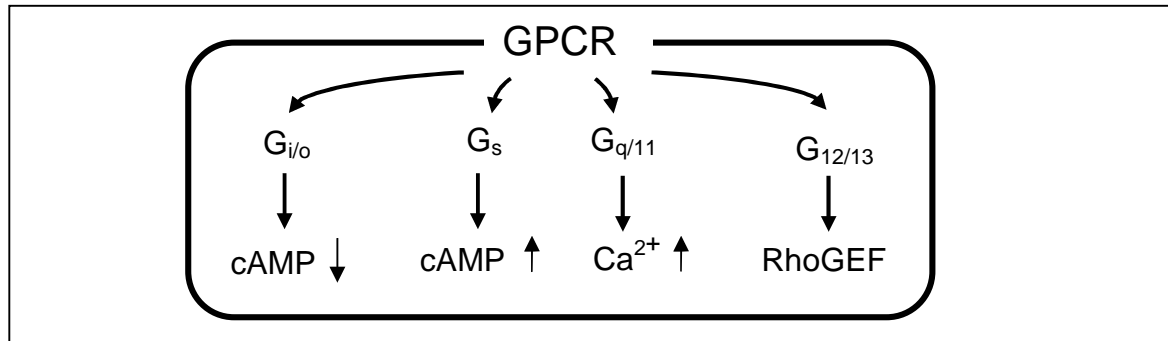


**Figure 1.** Different signal transduction pathways are linked to G protein-coupled receptors (GPCR). Upon stimulation, GPCRs activate one or more different classes of G proteins ( $G_{i/o}$ ,  $G_s$ ,  $G_{q/11}$ ,  $G_{12/13}$ ) which promote the activation of certain signal transduction pathways, resulting either in an accumulation, in a concentration decrease of intracellular second messengers (cAMP,  $Ca^{2+}$ ) or in an activation of other downstream molecules (RhoGEF).

### G protein-dependent signal transduction pathways

Upon activation, the heterotrimeric  $G_q$  protein dissociates into its  $G_{\alpha q}$  and  $G_{\beta\gamma}$  subunits. The  $G_{\alpha q}$  subunit recruits phospholipase C, which catalyses the degradation of phosphatidylinositol 4,5-bisphosphate ( $PIP_2$ ) to inositol 1,4,5-triphosphate ( $IP_3$ ) and diacylglycerol (DAG).  $IP_3$  subsequently binds to  $IP_3$  sensitive receptors on intracellular calcium stores, leading to a release of calcium from these stores. In the presence of calcium and DAG protein kinase C (PKC) is activated, which modulates different target proteins by phosphorylation and hence further signal transduction pathways.<sup>[6]</sup> Among these, the mitogen-activated protein kinase (MAPK) pathway is activated by PKC. The MAPK pathway activates among others the transcription factor cAMP-response element binding protein (CREB).<sup>[7]</sup>

The  $G_{\alpha s}$  subunit activates the enzyme adenylyl cyclase, which catalyses the formation of cyclic adenosine monophosphate (cAMP) from adenosine monophosphate. cAMP regulates cardiac hypertrophy, insulin secretion, cytoskeletal dynamics, the cell cycle, proliferation, transcriptional activation and neurite outgrowth.<sup>[8-14]</sup> These processes are modulated by the ability of cAMP to regulate different proteins like protein kinase A (PKA) and exchange proteins activated by cAMP (EPAC), which probably act as transcription regulators.<sup>[15]</sup> PKA regulates important proteins involved in signalling processes such as GPCRs,  $IP_3$  receptors and transcription factors like CREB by phosphorylation.<sup>[15-21]</sup>

The heterotrimeric G protein, consisting of a  $G_{\alpha i/o}$  and a  $G_{\beta\gamma}$  subunit, modulates diverse pathways. As the adversary of the  $G_{\alpha s}$  protein, the  $G_{\alpha i/o}$  subunit inhibits the adenylyl cyclase. Furthermore, the  $G_{\beta\gamma}$  subunit activates PLC isoforms and both subunits activate the MAPK pathway.<sup>[22-25]</sup>

Finally, the activation of the  $G_{12/13}$  pathway plays a key role in stress fibre formation, nuclear signalling and cell transformation.<sup>[26, 27]</sup> These processes are initiated upon  $G_{\alpha 12/13}$  subunit-dependent activation of a family of Rho guanine nucleotide exchange factors (RhoGEFs). The  $G_{\alpha 12/13}$  family of G proteins therefore acts directly upstream of RhoA by binding and activating a distinct family of RhoGEFs.<sup>[28, 29]</sup>

### **Ligand and G protein-independent functions and signal transduction pathways**

It has been reported that GPCRs have functions that are not dependent on their ability to activate G proteins. These functions are based on their ability to interact with each other or with other membrane bound proteins. The function of GPCRs and/or their surface expression can be modified by the formation of GPCR heteromers like GPR17 and type 1 cysteinyl-leukotriene receptor (CysLT<sub>1</sub>), the subtype 1 melatonin receptor (MT<sub>1</sub>) and GPR50 or the subtype D Mas-related gene (MrgD) and MrgE.<sup>[30-32]</sup> Furthermore, the formation of heterodimers can be essential for the export of a receptor to the cell surface and G protein coupling.<sup>[33]</sup> In addition, a GPCR cannot only be modulated by its own ligand but also by a ligand that binds to its heterodimer partner. This modulation has been shown for the heterodimers of taste receptors: T1R<sub>3</sub> forms a heterodimer with either T1R<sub>1</sub> or T1R<sub>2</sub>. Both cyclamate and lactisole regulate the pharmacology of the respective heterodimer by binding to T1R<sub>3</sub>.<sup>[34]</sup>

For a long time,  $\beta$ -arrestin and G protein-coupled receptor kinases (GRK) have been known to play a central and coordinated role in the 'desensitisation' of G protein activation by GPCRs, but it now becomes clear that GPCRs can also signal through these two protein families.

It has been shown that  $\beta$ -arrestin activates ERK1/2 as well as p38 MAPK pathways upon receptor stimulation.<sup>[35, 36]</sup> Furthermore, GPCRs respond to  $\beta$ -arrestin mediated by RhoA.<sup>[37]</sup> The protein kinase B pathway is modulated by

protein phosphatase 2A (PP2A), which is activated by  $\beta$ -arrestin.<sup>[38]</sup> In addition, GPCRs activate c-Src in a  $\beta$ -arrestin-dependent fashion. c-Src is a member of the nonreceptor tyrosin kinase family, which also results in the activation of the ERK cascade.<sup>[39]</sup>

GRKs have been identified as modulators of  $\beta$ -arrestin signalling on the one hand and on the other hand as direct interactors with protein kinase B and MEK1, a MAPK kinase.<sup>[40, 41]</sup> Protein kinase B and MEK1 are inhibited by the interaction with GRK.<sup>[42, 43]</sup>

There are several GPCRs which are constitutively active independently of any ligand. Examples of GPCRs that function by their constitutive activity, are the human orphan herpesvirus-8-encoded receptor ORF74, which is responsible for its oncogenic potential to cause Kaposi's sarcoma-like lesions, the Epstein-Barr virus (EBV) induced receptor 2 (EBI2), the  $G_s$  coupled receptor GPR3, which prevents premature ovarian ageing and maintains meiotic arrest in oocytes, as well as GPR3, GPR6 and GPR12, which promote neurite outgrowth.<sup>[14, 44-47]</sup>

## 1.2 Orphan G protein-coupled receptors and their deorphanisation

At present, there are still approximately 100 orphan receptors. Orphan receptors are GPCRs whose endogenous ligand is not identified.<sup>[3]</sup> Owing to their relevance as potential drug targets, it is not surprising that the deorphanisation of GPCRs is a major goal in the development of new therapeutic approaches.

The chief strategy in the deorphanisation of GPCRs is the so-called reverse pharmacology.<sup>[3]</sup> This strategy is composed of two steps. First, the orphan receptor has to be recombinantly overexpressed in an appropriate cell system. Eukaryotic cells are therefore transfected with the corresponding receptor cDNA in an appropriate expression vector. Second, potential receptor ligands can be tested with regard to their binding abilities or their ability to change intracellular second messenger levels as a result of receptor activation. Membranes of the receptor expressing cells or whole cells are used for this purpose.<sup>[48]</sup>



### 1.3 G protein-coupled receptor 17 (GPR17)

Bläsius *et. al.* were the first to report on a novel orphan G protein-coupled receptor primarily expressed in the brain.<sup>[49]</sup> The coding sequence of this receptor localized on human chromosomal band 2q21 has been identified on a cDNA clone called R12.<sup>[49, 50]</sup> The cDNA clone consists of three exons and two introns. Two receptor versions, a long and a short version, are possible because there are two starting codons in exon 2 as well as in exon 3. These two versions are generated by alternative splicing of the receptor mRNA.

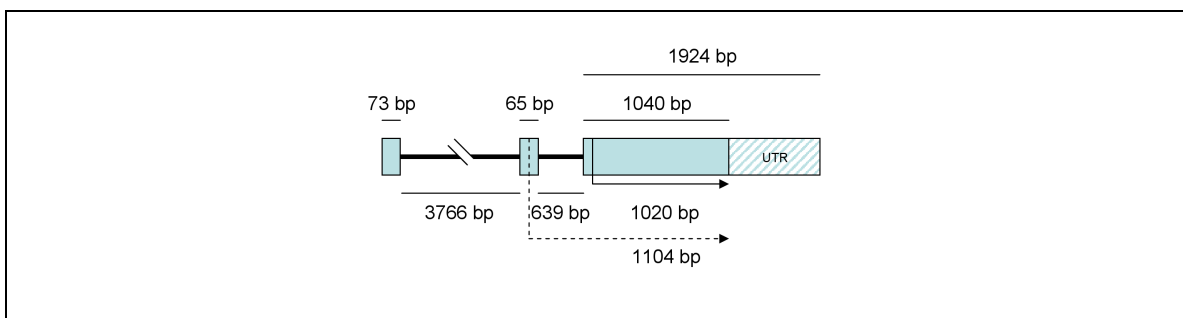


**Figure 2.** Structure of cDNA clone R12 coding for the human GPR17 as described by Bläsius *et. al.*<sup>[49]</sup> R12 consists of three exons (grey), two introns and a 3'-untranslated region (UTR). There are in-frame starting codons on exons 2 and 3, so that two GPR17 proteins are possible, a long (1104 bp) and a short version (1020 bp).

As already mentioned GPR17 is mainly expressed in the brain.<sup>[49, 51]</sup> However, it is also expressed in heart, kidney and in peripheral blood monocytes.<sup>[30, 51, 52]</sup> CD11c<sup>+</sup> dendritic cells and bone marrow-derived macrophages developed from monocytes also express GPR17.<sup>[53]</sup>

The GPR17 expression pattern has been further investigated within different regions and distinct cell types of the brain. GPR17 is expressed highly in hypothalamus, cerebellum, amygdala, cerebellar hemisphere, frontal cortex, hippocampus and putamen.<sup>[54]</sup> Reports concerning the expression of GPR17 in different cell types within the brain are contrary. The following cell types have been identified to express GPR17: pyramidal neurons, hippocampal neuroprogenitor cells, microglia/macrophages, adult oligodendrocyte precursor cells, ependymal cells lining the central cord, nerve growth factor (NGF) induced rat

pheochromocytoma cells (PC12), and CD11c<sup>+</sup> dendritic cells.<sup>[51, 53, 55-57]</sup> By contrast, it has been reported that GPR17 expression is restricted to oligodendrocytes and that it is not expressed in neurons or astrocytes.<sup>[58, 59]</sup> However, there are several indications that GPR17 expression is induced under certain conditions, such as after ischemic events, which might explain the contrary reports.

Ciana *et. al.* proposed that GPR17 belongs to the group of P2Y receptors and cysteinyl-leukotriene receptors (CysLT) (Figure 3).<sup>[51]</sup> They therefore aligned the protein sequence of nucleotide receptors P2Y<sub>1</sub>, P2Y<sub>2</sub>, P2Y<sub>4</sub>, P2Y<sub>6</sub>, P2Y<sub>11</sub>, P2Y<sub>12</sub>, P2Y<sub>13</sub> and P2Y<sub>14</sub> with the CysLT receptors type 1 and 2 (CysLT1, CysLT2). Based on the results of the alignment, they created a phylogenetic tree. This phylogenetic tree shows two distinct clusters of receptors: P2Y<sub>1</sub>-like and P2Y<sub>12</sub>-like receptors. The first cluster consists of P2Y<sub>1</sub>, P2Y<sub>2</sub>, P2Y<sub>4</sub>, P2Y<sub>6</sub> and P2Y<sub>11</sub> while the second contains P2Y<sub>12</sub>, P2Y<sub>13</sub> and P2Y<sub>14</sub> as well as the CysLT receptors type 1 and 2 and GPR17 (Figure 3).

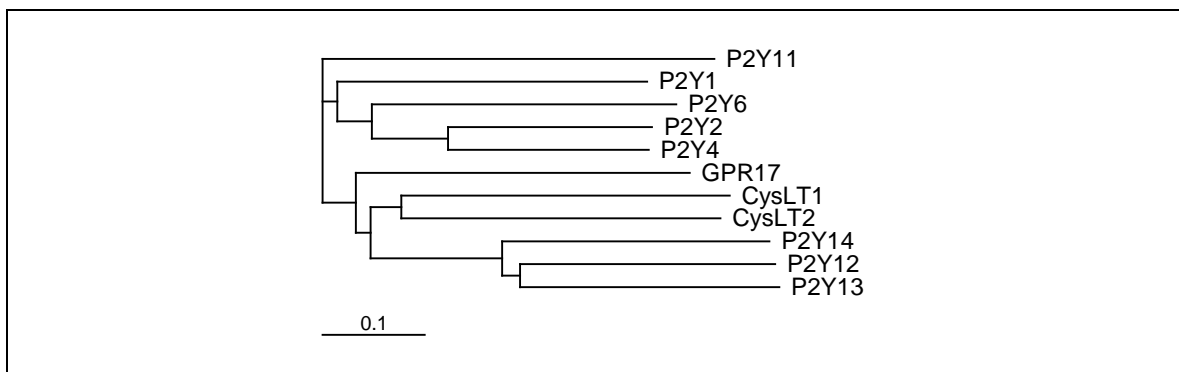


**Figure 3.** Phylogenetic tree showing the relationship between GPR17, P2Y- and cysteinyl-leukotriene receptors. The figure has been modified according to Ciana *et. al.*<sup>[51]</sup>

Until 2006, GPR17 belonged to the group of orphan GPCRs, but then Ciana *et. al.* claimed that GPR17 is a dual uracil nucleotides and cysteinyl-leukotriene receptor. The uracil nucleotide UDP and its derivatives UDP-glucose and UDP-galactose as well as the CysLTs leukotrienes C<sub>4</sub> (LTC<sub>4</sub>) and D<sub>4</sub> (LTD<sub>4</sub>) have been characterised as agonists for GPR17. Moreover, the characterisation of GPR17 reveals that it has the ability to couple to the G<sub>i</sub> and G<sub>q</sub> pathways.<sup>[51]</sup> The CysLT receptor antagonists montelukast and pranlukast as well as cangrelor, a P2Y<sub>12</sub>/P2Y<sub>13</sub>

receptor antagonist and MRS2179, a P2Y<sub>1</sub> receptor antagonist, have been reported as potent GPR17 antagonists.<sup>[51]</sup> It has been shown that ATP<sub>γ</sub>S acts as an antagonist for the longer splice variant of GPR17 and that it couples to K<sup>+</sup> channels.<sup>[60]</sup>

Yet there are also contrary results indicating the ability of the published agonists and antagonists to activate or inhibit GPR17. Maekawa *et. al.* reported that both the human and the mouse GPR17 do not respond to LTC<sub>4</sub> and LTD<sub>4</sub>, and that the mouse receptor cannot be activated by UDP-glucose.<sup>[30]</sup> Partially in line with these observations, Benned-Jensen and Rosenkilde described that LTC<sub>4</sub> and LTD<sub>4</sub> neither activate nor bind to GPR17. Furthermore they could not confirm binding of montelukast to GPR17.<sup>[54]</sup> Instead, Maekawa *et. al.* proposed ligand-independent functions of GPR17. They claimed that GPR17 negatively regulates the function and/or surface expression of the type 1 cysteinyl-leukotriene receptor (CysLT<sub>1</sub>) in a ligand-independent manner.<sup>[30, 61]</sup>

First reports suggest that GPR17 plays a key role in the development of brain injury after ischemic events. After ischemia, GPR17 expression is up-regulated in the affected areas and GPR17 knock-down as well as pharmacological GPR17 inhibition protect the brain from injury.<sup>[51]</sup> On the other hand, GPR17 promotes pre-oligodendrocyte differentiation to mature myelinating cells, the infiltration of the lesioned area with microglia cells expressing GPR17 and remodelling processes of the injured area.<sup>[56]</sup> A comparable GPR17 function has been observed after spinal cord injury. Here, GPR17 seems to be responsible for the degradation of neurons and oligodendrocytes in the lesioned area in the early phases after injury, whereas microglia and ependymal cells expressing GPR17 in a later state initiate local remodelling and repair processes, respectively.<sup>[57]</sup> There is further evidence that GPR17 plays a role in remodelling and repair mechanisms: GPR17 is expressed in nerve growth factor (NGF) treated PC12 cells, and GPR17 stimulation with proposed GPR17 agonists leads to pro-survival effects as well as to neurite outgrowth of these cells.<sup>[62]</sup> Contrary to these findings, Chen *et. al.* report that GPR17 inhibits oligodendrocyte maturation and thus myelinogenesis, which implies that GPR17 does not act as a modulator of brain repair after injury.<sup>[58]</sup>

In addition to functions in the brain or spinal cord after ischemia or in myelination processes, GPR17 acts as a negative regulator of the CysLT<sub>1</sub> receptor, a mediator of inflammatory processes.<sup>[30]</sup> It has been reported that coexpression of GPR17

and CysLT<sub>1</sub> blocks signalling of the CysLT<sub>1</sub> receptor. Furthermore, there are indications that GPR17 negatively regulates the *in vivo* CysLT<sub>1</sub> receptor surface expression.<sup>[30, 61]</sup> The modulating effect on the CysLT<sub>1</sub> receptor and its impact on inflammation have been shown. In two inflammation models, a model for the detection of vascular permeability in mast cell-mediated passive cutaneous anaphylaxis (PCA) and a pulmonary inflammation model, GPR17 knock-down leads to an increased inflammatory response as well as in the second model to an enhanced CysLT<sub>1</sub> receptor expression level.<sup>[30, 61]</sup>

### 1.4 Scope of the present study

GPR17 acts as a mediator in pathological processes like ischemia and inflammation and is therefore a predestined therapeutic target. Since contrary functions are described for GPR17 in these diseases, the development of pharmacological tools for the activation and inhibition of GPR17 is of outstanding relevance.

A suitable recombinant cell system based on the strategy of reverse pharmacology has to be generated for the identification and characterisation of novel GPR17 activators.

A small GPR17 ligand, previously identified in studies by our group, and its derivatives synthesised in collaboration with the group of Professor C. E. Müller, University of Bonn, have to be characterised in different functional assays.

Signal transduction pathways which couple to GPR17 and their crosstalk have to be characterised in different, appropriate second messenger assays (cAMP, IP<sub>3</sub>, calcium) as well as with the novel label-free dynamic mass redistribution technology (DMR).

Compounds from different natural sources which mimic the published GPR17 ligands or our own ligands are tested to identify novel agonistic and inhibitory lead structures.

Finally, a series of P2Y<sub>2</sub> and P2Y<sub>12</sub> receptor antagonists and their derivatives containing an anthraquinone scaffold are tested for their ability to inhibit GPR17.

---

## CHAPTER II: RESULTS

---

### 2.1 Generation of recombinant cell systems stably expressing GPR17

It was necessary to generate an appropriate test system in order to identify novel GPR17 ligands and characterise signal transduction pathways which couple to GPR17. Since it was postulated by Ciana *et. al.* that GPR17 is activated by uracil nucleotides such as UDP, UDP-glucose and UDP-galactose, 1321N1 astrocytoma cells were chosen as an appropriate test system, because it was known that this cell line does not express endogenous nucleotide receptors.<sup>[63, 64]</sup> The stable transfection of this cell line with GPR17 was performed using a retrovirus. Both the cell line and the retroviral expression system were kindly provided by Professor C. E. Müller, Pharmaceutical Institute, Pharmaceutical Chemistry I, University of Bonn.

In order to investigate potential differences in receptor signalling as a function of the cellular background, GPR17 was expressed and analysed in a further cell system. This cell system, a recombinant Chinese hamster ovary (CHO) cell line stably expressing GPR17, was generated previously by our group. The CHO cell line was transfected with the Flp-In™ T-Rex™ expression system. Here, expression of GPR17 was induced after adding doxycycline.

## 2.2 Examination of positive pharmacological GPR17 modulators

### 2.2.1 Compound analysis using the calcium assay

Based on the classification of GPR17 into the group of P2Y receptors, a selection of nucleotides and synthetic nucleotide mimetics was tested for their ability to activate GPR17 (AG Kostenis, unpublished data). These investigations identified a small compound, which is available from ChemDiv Inc., San Diego, CA 92121, USA (ID 3341-1774) and activates GPR17. The ligand, also referred to as RA-II-150, has an indole scaffold and mimics the phosphate groups of a nucleotide such as UDP with its two carboxylic groups. Furthermore, the aromatic substructure of the indole is dichloro-substituted at positions 4 and 6 (Figure 4).

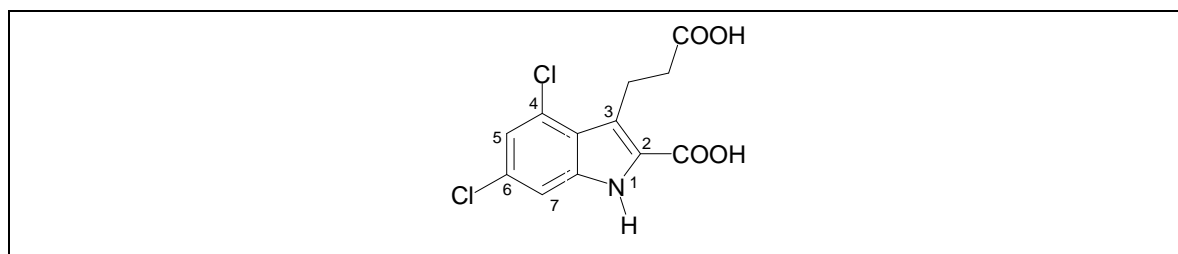


**Figure 4.** A small nucleotide mimetic, found in previous studies in our group, was identified as a GPR17 agonist. In the working group of Professor C. E. Müller, University of Bonn, it was synthesised by Rhallid Akkari. The different possible substitution positions of the indole scaffold are numbered consecutively.

RA-II-150, and later all of its derivatives, were characterised in a cell population based calcium assay. These derivatives had been synthesised in collaboration with the working group of Professor C. E. Müller, Pharmaceutical Institute, Pharmaceutical Chemistry I, University of Bonn.

Upon addition, RA-II-150 showed a GPR17-dependent increase of intracellular calcium in 1321N1 cells as well as CHO cells stably expressing GPR17, but not in the corresponding native cells (Figure 5 and Figure 6).

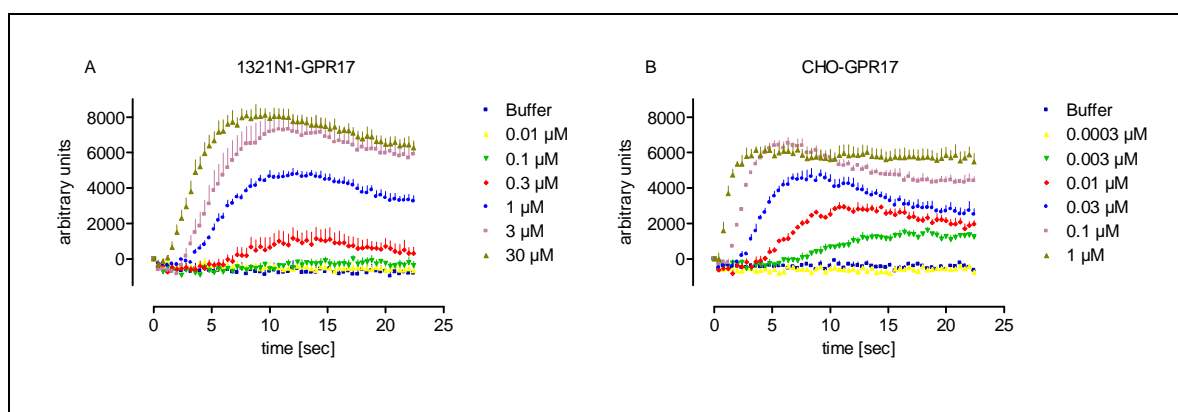


**Figure 5.** Real-time calcium efflux measurements in 1321N1 (A) and CHO (B) cells expressing GPR17 recombinantly after addition of RA-II-150 in the specified concentration. In both cell systems, concentration-dependent calcium mobilisation occurred. Representative data are shown for both cell systems ( $n = 1$  of 29).

The  $pEC_{50}$  of RA-II-150 is 6.09 ( $\pm 0.06$ ) in the 1321N1 cell system and 8.20 ( $\pm 0.08$ ) in the CHO cell system. Interestingly, the potencies of RA-II-150 and its active derivatives are higher in the CHO cells than in the astrocytoma cells. This relation may be due to differences in the receptor expression level in both cell lines or to the presence of so-called “spare receptors.” This term means that a full agonist can cause a maximum response while occupying only a fraction of the total receptor population. Thus, not all of the receptors in the cell are required to achieve a maximum response. Yet although the receptors may not all be needed for a maximum response, they all contribute to the measured responses, so that the potency of full agonists is enhanced by the presence of the spare receptors.<sup>[65]</sup> In this particular case the recombinant CHO cell system appears to be a pharmacological system that includes spare receptors. Unfortunately, both explanations for the differences in the  $pEC_{50}$  values between the different cell lines cannot be verified with the assay used. Further investigations have therefore to be undertaken.

In both cell systems the following compounds are active in addition to RA-II-150: RA-III-40, RA-III-55, KL16-1, KL28 and KL126. In the recombinant CHO cell system RA-III-20, RA-III-56, KL16-2, KL21, KL91, KL94 and KL118 are also active (Figure 6). KL94 seems to be a partial GPR17 agonist (Figure 6).

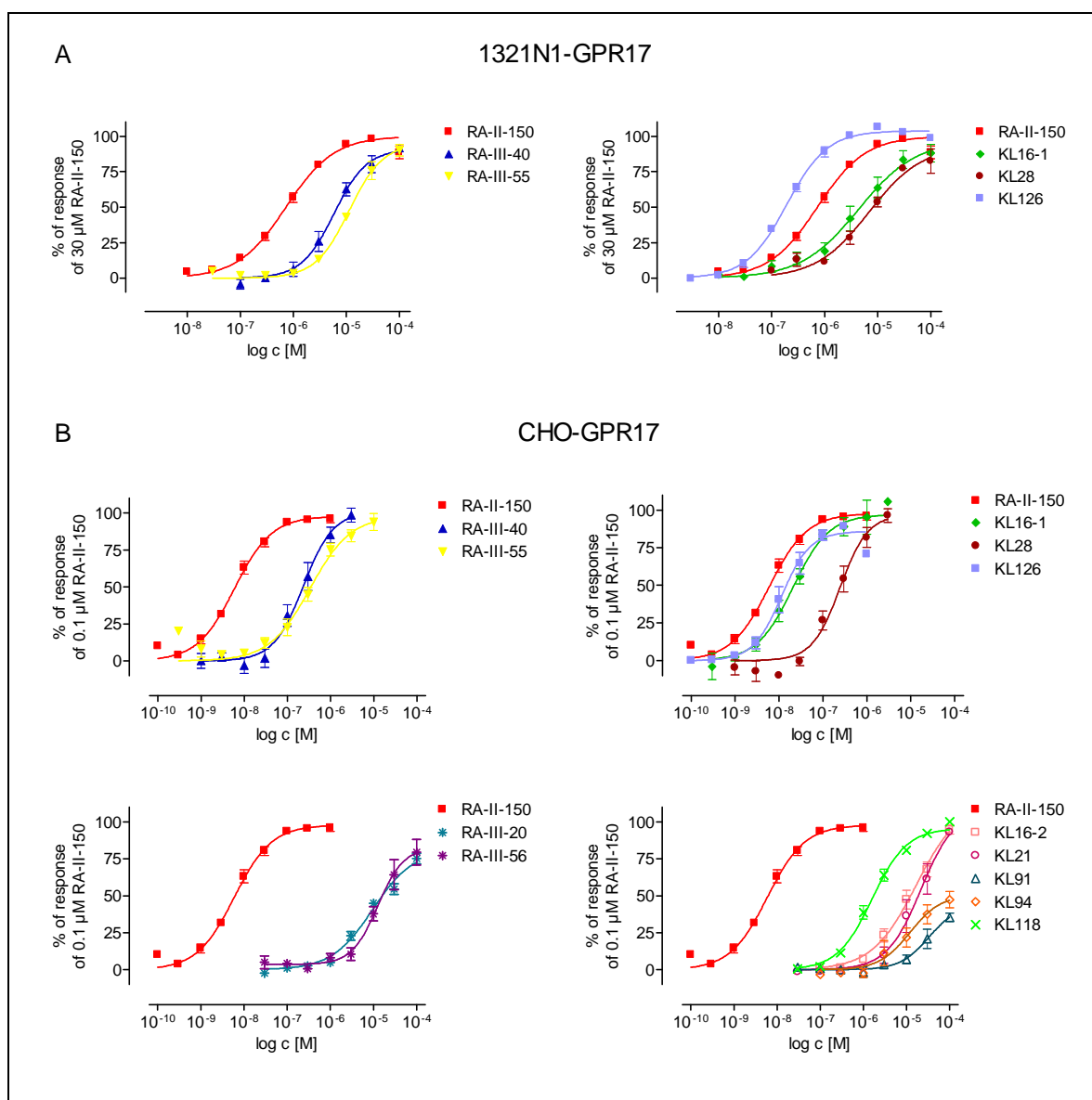


**Figure 6.** Dose response curves of compounds being active in the 1321N1 (A) and CHO cell systems (B) expressing GPR17 recombinantly ( $n = 3-29$ ). For reference purposes the DRC of the lead compound RA-II-150 is shown in all plots (closed red squares). The  $pEC_{50}$  values of all compounds are summarised in Table 1.

After RA-II-150 was identified as a potent GPR17 activator in both cell systems, 21 derivatives of the lead compound RA-II-150 had been synthesised and analysed in both cell systems (Table 1). All test compounds share an indole scaffold which carries a carboxylic group at position 2. As already described for RA-II-150, the potencies of all other test compounds are increased in CHO cells compared with astrocytoma cells.

There are several indications of a structure activity relationship. The deletion of the



3-(2-carboxyethyl) group terminates stimulatory properties of the compound (KL99). Yet whether both the 3-(2-carboxyethyl) group and the 2-carboxylic group or only 3-(2-carboxyethyl) are needed for compound activity cannot be verified, because until now it had not been possible to remove the 2-carboxylic group. The importance of the 3-(2-carboxyethyl) group is evident from its exchange with a 3-(3-carboxypropyl) (KL72) or a 3-(2-carboxyethyl-1-en-1-yl) group (KL118): While KL118 is inactive in the 1321N1-GPR17 cell system and weakly active in the CHO-GPR17 cell system, KL72 is completely inactive in both systems. In addition, the deletion of the 3-(2-carboxyethyl) group cannot be compensated by the introduction of a 1-carboxymethyl group at position 1 (KL110). This compound is inactive in both cell lines (Table 1).

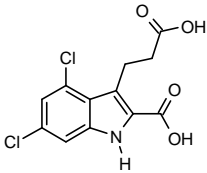
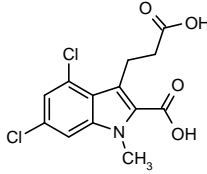
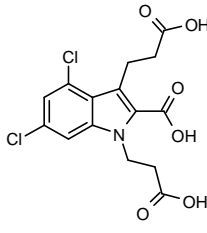
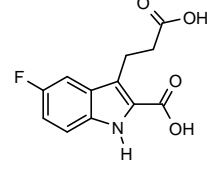
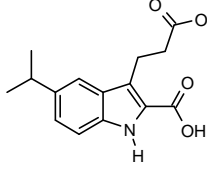
Substitutions at position 1 are tolerated if they are charged. Depending on the cell line, a lipophilic methyl group at this position leads to a loss of function or a considerable decrease in ligand potency (RA-III-20), while the insertion of a further 2-carboxyethyl group results in a significant decrease in compound activity (RA-III-40) without this activity actually disappearing.

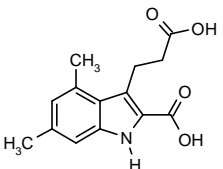
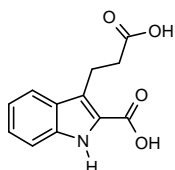
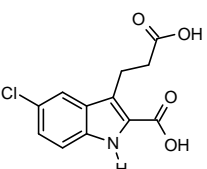
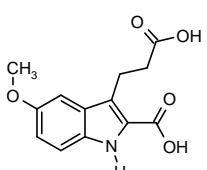
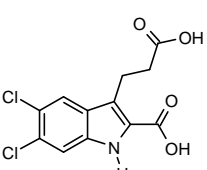
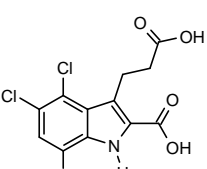
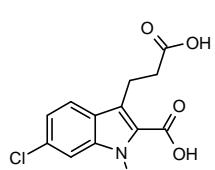
Many different substitution patterns on the aromatic ring substructure of the indole scaffold were realised to investigate their influence on compound activity. This activity disappears almost completely, if the ring is unsubstituted (RA-III-56) and decreases dramatically, if the 4,6-dichloro substitution pattern is exchanged for a 4,6-dimethyl (RA-III-55) or 4,6-difluoro pattern (KL28). However, these two compounds are still active in both cell systems. With a 4,6-dibromo substitution pattern (KL126), activity is enhanced in the 1321N1-GPR17 cell system but slightly decreased in the CHO-GPR17 system compared to the activity of RA-II-150 in the corresponding cell system (Table 1). It seems to be important that substitutions at these positions are bulky and less electronegative.

Furthermore, the crucial relevance of the chlorination at position 6 compared to that at position 4 was shown by testing derivatives which are only chlorinated at one of these positions. While the activity of 6-chlorinated compound (KL16-1) is only slightly decreased, the potency of the 4-chlorinated compound (KL16-2) decreases dramatically (Table 1).

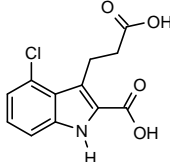
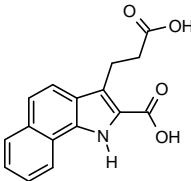
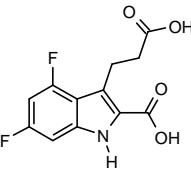
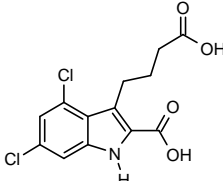
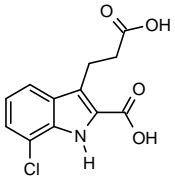
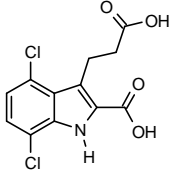
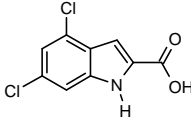
Obviously, a substitution at position 5 terminates any compound activity. Even if a 5-substituted compound shares structural elements with very potent compounds, the activity is lost (Table 1).

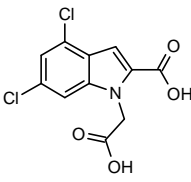
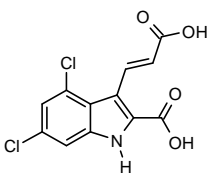
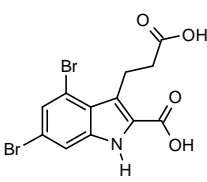
**Table 1.** Potencies and efficacies of RA-II-150 and its derivatives in the 1321N1-GPR17 and CHO-GPR17 cell systems. The pEC<sub>50</sub> values of six and thirteen compounds, respectively, are determined. Data in recombinant 1321N1 and CHO cells are normalised to the response of 30 µM and 0.3 µM RA-II-150 (column 3), respectively. For all other compounds the activity is below the determination limit or the compounds are inactive (n = 3-29). Unspecific effects of active compounds are tested on native 1321N1 or CHO-K1 cells. Here, data are normalised to the response of 100 µM carbachol or 100 µM ATP (column 4) (n = 3-4). Inactive compounds were not tested on native 1321N1 or CHO-K1 cells (n. a.). \* The pEC<sub>50</sub> of KL91 is calculated after extrapolation, because the maximum response was not reached up to a concentration of 100 µM.

Chemical structure and internal designation of the test compounds	pEC <sub>50</sub> (± SEM) 1321N1-GPR17/ CHO-GPR17	% of response of 30 µM compound (± SEM) 1321N1-GPR17/ CHO-GPR17 cells	% response of 30 µM compound (± SEM) Native 1321N1 cells/CHO-K1 cells
 RA-II-150	6.09 (0.06)/ 8.20 (0.08)	100 (0.00)/ 100 (0.00) (0.3 µM compound)	-0.49 (1.88)/ 0.17 (1.27) (0.1 µM compound)
 RA-III-20	n. d./ 5.05 (0.12)	16.1 (4.45)/ 54.6 (3.60)	-3.50 (1.63)/ 0.92 (3.96)
 RA-III-40	5.28 (0.08)/ 6.73 (0.12)	80.4 (6.05)/ 85.2 (5.19) (1 µM compound)	1.16 (0.60)/ 0.59 (0.93) (1 µM compound)
 RA-III-52	n. d./ n. d.	8.70 (5.93)/ 11.0 (6.51)	n. a./ 2.39 (4.22)
 RA-III-54	n. d./ n. d.	6.33 (2.25)/ 7.13 (5.96)	n. a./ 0.82 (1.62)

Chemical structure and internal designation of the test compounds	pEC <sub>50</sub> (± SEM) 1321N1-GPR17/ CHO-GPR17	% of response of 30 μM compound (± SEM) 1321N1-GPR17/ CHO-GPR17 cells	% response of 30 μM compound (± SEM) Native 1321N1 cells/CHO-K1 cells
 RA-III-55	4.86 (0.10)/ 6.47 (0.05)	75.8 (6.36)/ 68.2 (1.86) (1 μM compound)	0.79 (0.54)/ 1.19 (1.19) (1 μM compound)
 RA-III-56	n. d./ 4.78 (0.10)	7.56 (1.74)/ 64.3 (10.2)	n. a./ 6.50 (5.37)
 RA-III-57	n. d./ n. d.	11.1 (1.77)/ 11.6 (1.46)	-2.95 (1.10)/ 4.02 (1.13)
 RA-III-64	n. d./ n. d.	5.27 (3.44)/ 7.34 (3.93)	n. a./ 1.36 (3.43)
 RA-III-65A	n. d./ n. d.	11.2 (8.20)/ 6.47 (2.02)	0.70 (2.30)/ 4.43 (1.69)
 RA-III-65B	n. d./ n. d.	15.9 (11.6)/ 1.08 (1.08)	0.81 (2.26)/ 2.79 (2.25)
 KL16-1	5.43 (0.14)/ 7.69 (0.10)	83.5 (6.20)/ 94.3 (6.66) (1 μM compound)	3.76 (2.67)/ 1.23 (1.90) (0.3 μM compound)

## CHAPTER II: RESULTS

Chemical structure and internal designation of the test compounds	pEC <sub>50</sub> (± SEM) 1321N1-GPR17/ CHO-GPR17	% of response of 30 μM compound (± SEM) 1321N1-GPR17/ CHO-GPR17 cells	% response of 30 μM compound (± SEM) Native 1321N1 cells/CHO-K1 cells
 KL16-2	n. d./ 4.96 (0.16)	52.2 (16.3)/ 67.8 (4.93)	-2.36 (0.80)/ 4.44 (0.83)
 KL21	n. d./ 4.82 (0.18)	0.33 (2.23)/ 61.3 (10.2)	n. a./ 0.65 (2.34)
 KL28	5.13 (0.13)/ 6.79 (0.10)	77.2 (2.23)/ 96.5 (4.58) (3 μM compound)	1.93 (1.38)/ 0.99 (2.08) (3 μM compound)
 KL72	n. d./ n. d.	0.60 (0.60)/ 27.3 (9.23)	n. a./ 1.47 (2.57)
 KL91	n. d./ 4.72 (0.18)*	-4.87 (3.01)/ 20.9 (6.54)	n. a./ 3.73 (0.94)
 KL94	n. d./ 4.97 (0.11)	1.23 (1.04)/ 37.5 (6.46)	n. a./ 1.28 (1.13)
 KL99	n. d./ n. d.	1.17 (0.59)/ 3.65 (1.62)	n. a./ 3.16 (0.92)

Chemical structure and internal designation of the test compounds	pEC <sub>50</sub> (± SEM) 1321N1-GPR17/ CHO-GPR17	% of response of 30 μM compound (± SEM) 1321N1-GPR17/ CHO-GPR17 cells	% response of 30 μM compound (± SEM) Native 1321N1 cells/CHO-K1 cells
 KL110	n. d./	0.09 (0.29)/	n. a./
	n. d.	2.39 (0.73)	n. a.
 KL118	n. d./	21.8 (3.63)/	-2.17 (1.48)/
	5.82 (0.10)	92.3 (1.14)	0.19 (2.20)
 KL126	6.71 (0.01)/	106 (1.24)	0.11 (0.67)/
	7.87 (0.16)	(10 μM compound)/ 89.3 (1.47) (0.3 μM compound)	0.18 (0.08) (0.3 μM compound)

The substitution pattern of KL94 is a combination of the substitution pattern of KL16-2 on the one hand and KL91 on the other hand. KL16-2 and KL91 are monochlorinated at positions 4 and 7 respectively, while KL94 is 4,7-dichlorinated. KL16-2 and KL91 are similarly potent to KL94 (Table 1). When additionally chlorinated at position 5 compared with KL94, RA-III-65B does not show any activity (Figure 6). Interestingly, the chlorination at position 7 seems to lead to a partial agonism of test compounds. All other active test compounds are full agonists.

All compounds with the ability to activate GPR17 in the 1321N1 and/or CHO cell systems do not cause an unspecific increase of the intracellular calcium concentration in native 1321N1 or CHO-K1 cells (Table 1).

To sum up, the 3-(2-carboxyethyl), the hydrogen at position 5 and the bulky, less electronegative substitution at position 4 are essential structural elements of GPR17 agonists with an indole scaffold (Figure 7).

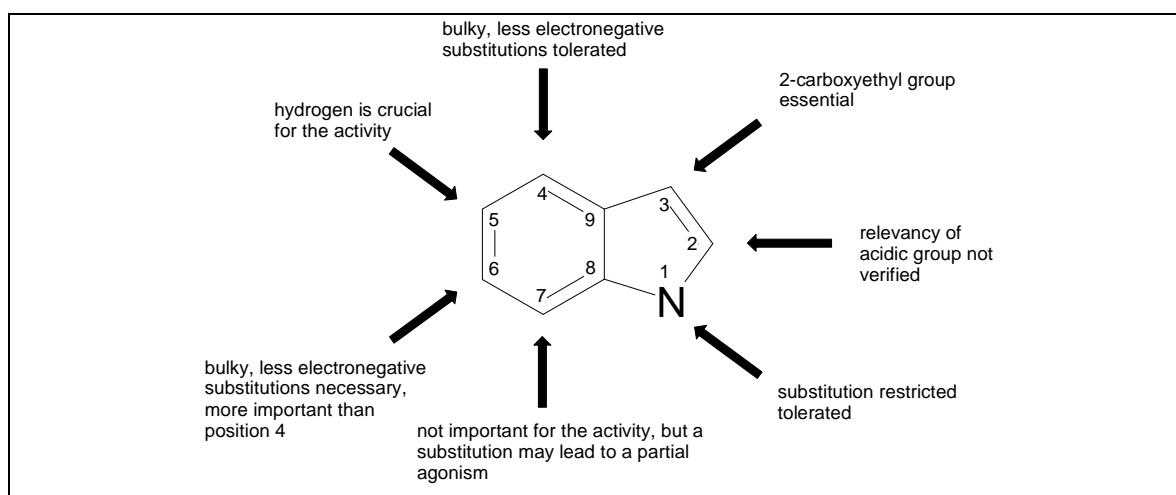


**Figure 7.** Structure activity relationship of GPR17 agonists with an indole scaffold. Whereas acidic groups at positions 2 and 3 as well as bulky, less electronegative substitutions at position 4 and a hydrogen at position 5 are important for activity, substitutions at position 7 are well tolerated and may lead to partial agonism.

A Pearson correlation of their  $pEC_{50}$  values was performed to permit a comparison of the compound potencies in both cell lines. This correlation is based on the assumption that both X and Y values, in this case the  $pEC_{50}$  values in both cell lines, are sampled from populations that follow an at least approximately Gaussian distribution. The P value of 0.04 was computed as a two-tailed value, and a confidence interval of 95% was chosen. The r value is 0.83 and the coefficient of determination  $r^2$  for this correlation is 0.69 (Figure 8), which means there is a good correlation between the compound potencies in both cell lines.

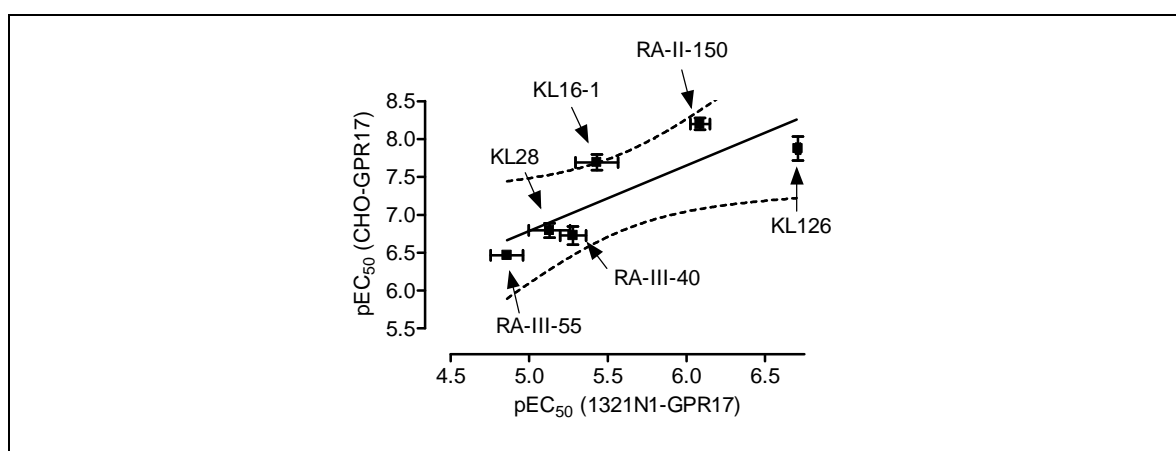


**Figure 8.** Correlation between the  $pEC_{50}$  values of the compounds which are active in the 1321N1-GPR17 and CHO-GPR17 cell systems. The dotted lines indicate the 95% confidence interval. The P value of the correlation is 0.04.

### 2.2.2 GPR17 agonist RA-II-150 does not activate related P2Y receptors

Since there are many reasons for the appearance of side-effects of a drug, such as the modulation of molecules besides the desired target, the selectivity of RA-II-150 to GPR17 needs to be determined. Therefore it was analysed whether RA-II-150 activates the related human nucleotide receptors P2Y<sub>2</sub> and P2Y<sub>4</sub>. Both nucleotide receptors are recombinantly expressed in 1321N1 astrocytoma test systems. Since these receptors couple to the calcium signal transduction pathway, the receptor activation was determined by measuring calcium concentration increase after adding the compound.<sup>[66]</sup> This analysis showed the selectivity of RA-II-150 for GPR17, because it did not activate the tested nucleotide receptors up to a concentration of 30  $\mu$ M (Figure 9). This information is very important for further *in vitro* or *in vivo* studies of diseases, because with a specific compound the effect observed in this kind of model can be attributed to the modulation of GPR17 by the compound.

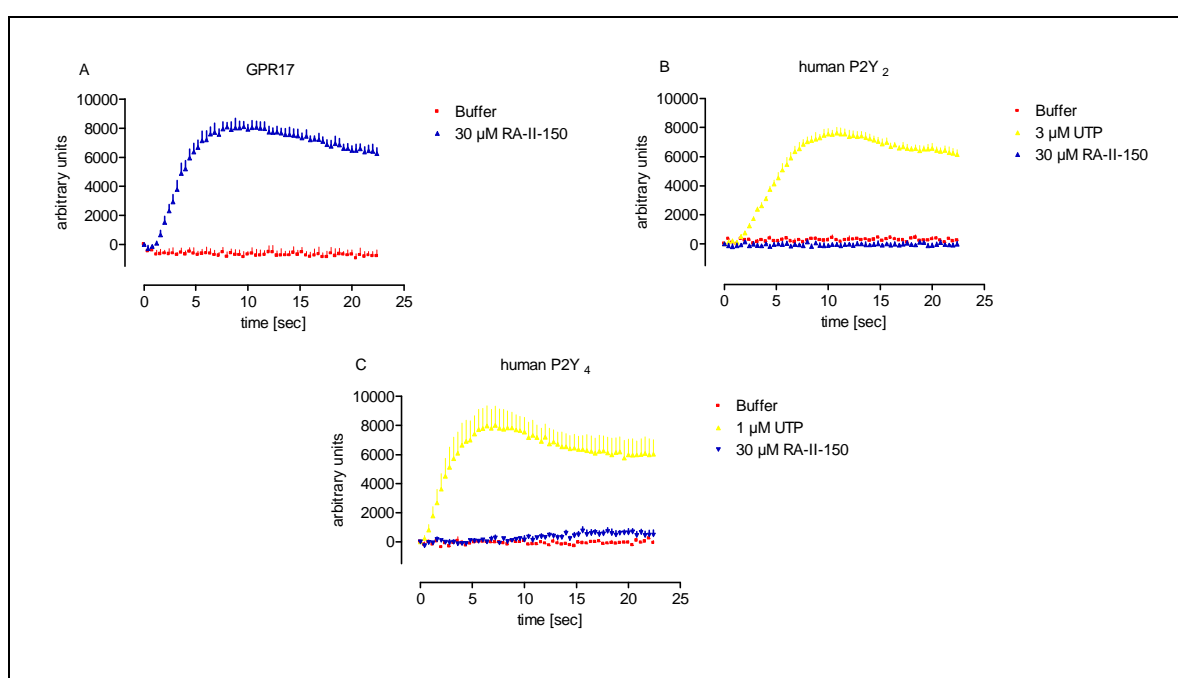


**Figure 9.** Determination of the selectivity of RA-II-150 for GPR17. Representative real-time measurements of changes in the intracellular calcium concentration after adding 30  $\mu$ M RA-II-150 to recombinant 1321N1 astrocytoma cells stably expressing GPR17 (A), human P2Y<sub>2</sub> (B) and human P2Y<sub>4</sub> (C) are shown. The response of the human P2Y<sub>2</sub> and P2Y<sub>4</sub> receptor to 30  $\mu$ M RA-II-150 is compared to the corresponding response to 3  $\mu$ M or 1  $\mu$ M UTP. Neither the human P2Y<sub>2</sub> nor the human P2Y<sub>4</sub> can be activated by RA-II-150.

### 2.2.3 Compound analysis using inositol phosphate accumulation assays

Next, selected compounds were analysed in inositol phosphate accumulation assays using the more sensitive recombinant CHO-GPR17 cell system. Constitutive GPR17 activity in this cell system can be excluded, because the basal inositol phosphate levels in recombinant and native CHO cells are identical (Figure 10A).

After addition, all selected compounds lead to a concentration-dependent accumulation of inositol phosphates (Figure 10B). The potencies decrease within the series: RA-II-150 [ $pEC_{50}$  6.27], KL16-1 [ $pEC_{50}$  5.28], RA-III-40 [ $pEC_{50}$  5.04], KL28 [ $pEC_{50}$  4.72] and RA-III-55 [ $pEC_{50}$  4.65] (Table 2).

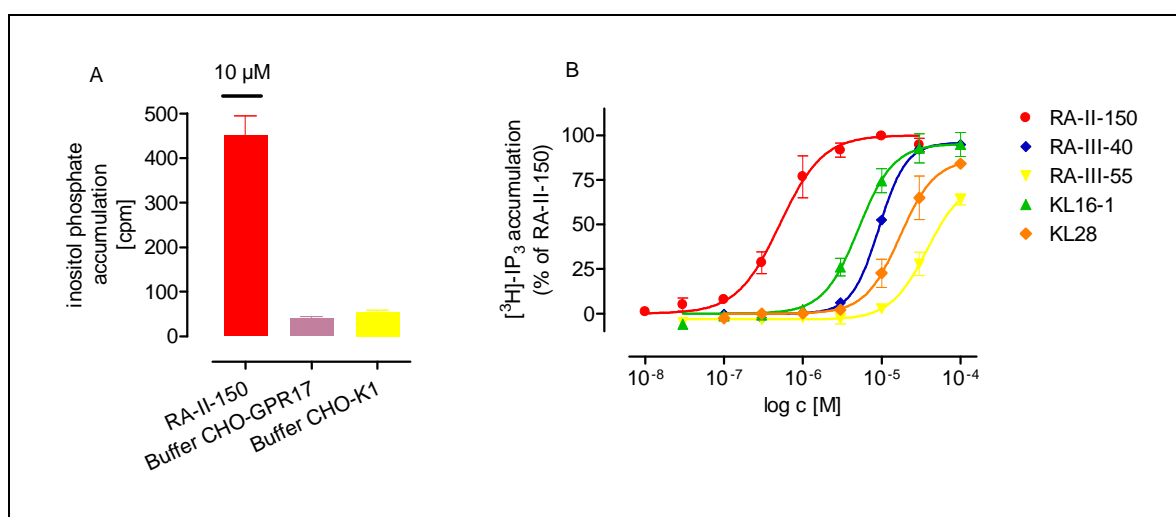


**Figure 10.** Inositol phosphate accumulation assays with CHO-GPR17 cells. While the basal inositol phosphate level in native and CHO-GPR17 cells does not differ significantly, it increases when agonist is added in CHO-GPR17 cells (A) ( $n = 2-5$ ). The dose response curves of selected GPR17 agonists in the CHO-GPR17 cell system are shown in (B) ( $n = 3-5$ ). Data are normalised to the response of 10  $\mu$ M RA-II-150.



**Table 2.** pEC<sub>50</sub> values and efficacies of selected agonists of GPR17 in the CHO cell system. The efficacies are referred to the response of 10 μM RA-II-150 (column 3) (n = 3-5).

Test compound	CHO-GPR17 cells	
	pEC <sub>50</sub> (± SEM)	% of response of 100 μM (± SEM)
RA-II-150	6.27 (0.13)	100 (0.00) (10 μM compound)
RA-III-40	5.04 (0.02)	94.8 (1.08)
RA-III-55	4.65 (0.11)	84.8 (4.92)
KL16-1	5.28 (0.06)	94.8 (6.78)
KL28	4.72 (0.16)	84.1 (1.79)

In the inositol phosphate accumulation assay the dose response curves for all compounds are obviously shifted to the right compared to those in the calcium assay. All agonists in this assay with the exception of RA-III-55 appear to be full GPR17 agonists. The DRC of RA-III-55 does not reach the upper plateau up to a concentration of 100 μM. Unfortunately, it is not possible to increase the RA-III-55 concentration, because of cytotoxic solvent concentration reaching at agonist concentrations more than 100 μM, so that it remains unclear whether RA-III-55 is a partial or a full GPR17 agonist here.

A Pearson correlation was performed to permit a comparison of the compound potencies in the inositol phosphate accumulation assay and the cell population based calcium assay. The P value of 0.02 was computed as a two-tailed value and a confidence interval of 95% was chosen. The r value is 0.93 and the coefficient of determination  $r^2$  for this correlation is 0.86 (Figure 11), meaning that the potencies in both assays correlate with each other.

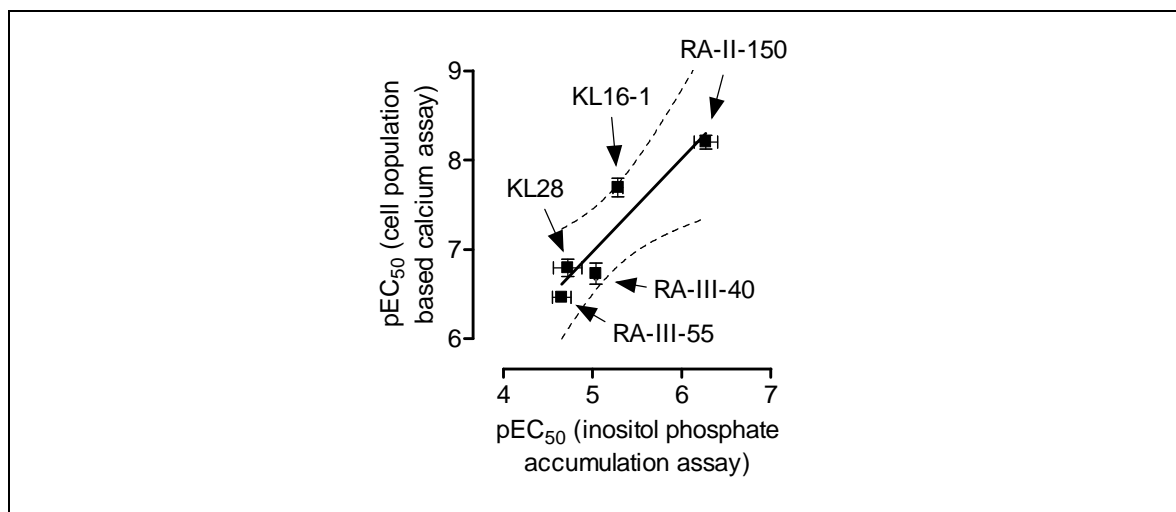


**Figure 11.** Comparison of the calcium assay and the inositol phosphate accumulation assay. The P value of the linear regression analysis is 0.02. The dotted lines indicate the 95% confidence interval.

#### 2.2.4 Compound analysis using the dynamic mass redistribution assay

The lead compound RA-II-150 as well as RA-III-40, RA-III-55, KL16-1 and KL28 were analysed in dynamic mass redistribution assays (DMR) in both recombinant cell lines (only RA-II-150 and KL16-1 in 1321N1-GPR17 cells). Representative agonist DMR signatures in 1321N1-GPR17 (Figure 12A and B) are shown. For the recombinant 1321N1 cell system pEC<sub>50</sub> values of 6.44 ( $\pm$  0.13) and 5.66 ( $\pm$  0.15) were calculated for RA-II-150 and KL16-1. The following pEC<sub>50</sub> values were calculated for selected GPR17 agonists in CHO-GPR17 cells: 7.49 ( $\pm$  0.08) (RA-II-150), 5.75 ( $\pm$  0.14) (RA-III-55), 5.56 ( $\pm$  0.16) (RA-III-40), 6.57 ( $\pm$  0.10) (KL16-1), 5.03 ( $\pm$  0.42) (KL28) (Figure 12C and I; Table 3). Compared to the DRCs of RA-II-150 and KL16-1 in the 1321N1-GPR17 cell system, the corresponding DRCs in the CHO-GPR17 cell system are shifted to the left (Figure 12C and I). The same behaviour was observed in the cell population based calcium assay (Figure 6 and Table 1). Interestingly, the DRCs in the recombinant CHO cell system, as determined in the DMR assay, are shifted to the right compared to those in the calcium assay, while the opposite can be observed in case of the 1321N1-GPR17 cell system. Here, the agonists are more potent in the DMR assay than in the calcium assay (Table 1 and Table 3).

The DMR signatures of all agonists within a cell system are very similar. However, the shape of the signature differs slightly between the two cell lines. A rapidly increasing positive wavelength shift can be observed in both cell lines. The signal decreases again after the maximum is reached. The total wavelength shift is higher in the CHO cell line than in the astrocytoma cell line. Both the increase and the decrease in the positive wavelength shift are faster in the astrocytoma cell line than in the CHO cell line (Figure 12). In 1321N1-GPR17 cells the rapid signal decrease is replaced by a further slight signal increase (“shoulder”) at high concentrations, which is subsequently replaced by a permanent signal decrease (Figure 12A and B). This “shoulder” cannot be observed at concentrations below 1  $\mu\text{M}$ . At 0.3  $\mu\text{M}$  the signal remains on the same level after the rapid decrease. At concentrations below 0.3  $\mu\text{M}$  the signal decreases again to the basal level, leading to the formation of a single peak (Figure 12A and B).

In CHO-GPR17 cells at high concentrations the signal increases again after the maximum has been reached. It then remains approximately at the same level. At concentrations of less than 1  $\mu\text{M}$  no further significant increase of the signal occurs; instead there is a slow decrease, which is replaced by a signal that remains constant (Figure 12C-G).

The DMRs of GPR17 are different in the two cell lines, reflecting the cell line-specific signalling of GPR17. In both cell lines the DMRs are partially comparable to those published for a  $G_i$  coupled receptor.<sup>[67]</sup> A  $G_i$  component explains the initial, fast, positive DMR upon activation of the receptor. The  $G_i$  pathway activation was verified by performing cAMP assays (2.5.2).

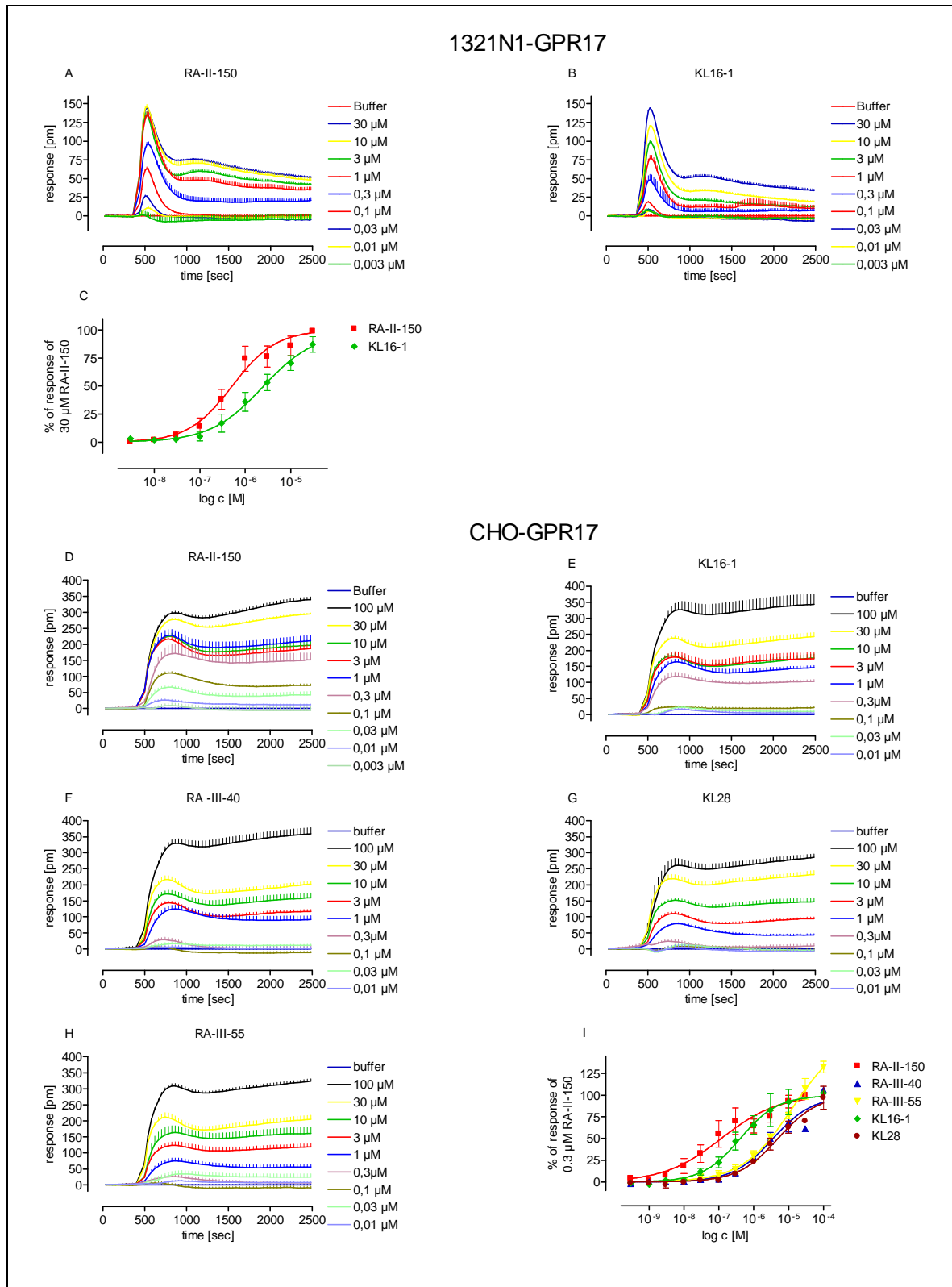


**Figure 12.** Positive DMR and the resulting DRCs (A-C) in 1321N1-GPR17 and CHO-GPR17 cells (D-I) as a result of receptor activation by the specified agonist. The figure shows the averaged (+ error bar in one direction), baseline corrected signatures of a representative experiment (n = 3-6).

**Table 3.** Collection of potencies and efficacies of selected compounds analysed in the DMR assay ( $n = 3-6$ ). The data are normalised to the response of  $30 \mu\text{M}$  (column 3) or  $10 \mu\text{M}$  RA-II-150 (column 5).

Test compound	1321N1-GPR17		CHO-GPR17 cells	
	$pEC_{50}$ ( $\pm$ SEM)	% of response of $100 \mu\text{M}$ ( $\pm$ SEM)	$pEC_{50}$ ( $\pm$ SEM)	% of response of $100 \mu\text{M}$ ( $\pm$ SEM)
RA-II-150	6.44 (0.13)	100	7.49 (0.08)	100
RA-III-40	n. a.	n. a.	5.75 (0.14)	63.6 (9.55)
RA-III-55	n. a.	n. a.	5.56 (0.16)	76.6 (3.66)
KL16-1	5.66 (0.15)	85.3 (7.15)	6.57 (0.10)	72.3 (9.50)
KL28	n. a.	n. a.	5.03 (0.42)	63.1 (7.06)

A negative control with untransfected, native 1321N1 or CHO-K1 cells showed that these cells did not respond to the GPR17 agonists up to a concentration of  $30 \mu\text{M}$  or  $10 \mu\text{M}$  respectively (Figure 13A and B). Representative DMR signatures of the corresponding agonists are shown in Figure 13A and B.  $100 \mu\text{M}$  carbachol and ATP were used as endogenous controls.

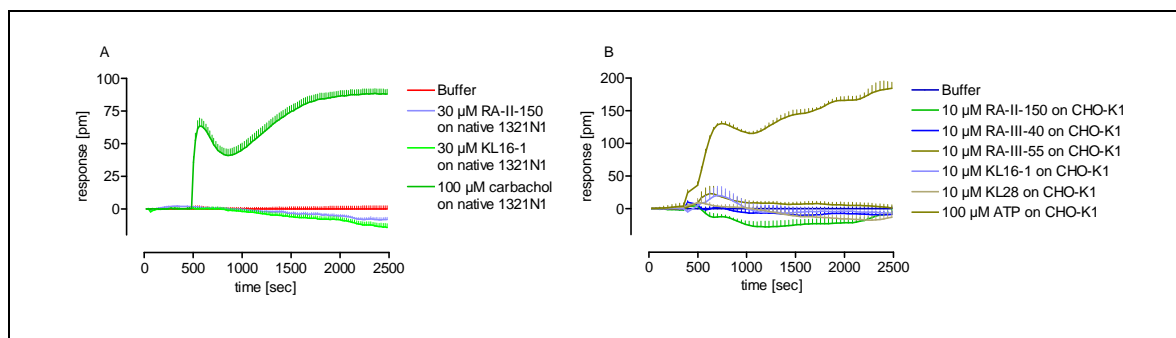


**Figure 13.** Representative DMR signatures of GPR17 agonists are shown on native 1321N1 (A) and CHO-K1 cells (B). Native cells do not respond to GPR17 agonists but to the corresponding control agonists carbachol and ATP respectively ( $n = 1$  of 2-6).

Next, it was investigated whether the initial fast rising part of the signature is due to the activation of the  $G_i$  pathway. Cells were therefore pretreated with PTX. The positive DMRs in recombinant 1321N1 cells decrease considerably and full activation cannot be achieved in PTX pretreated cells (Figure 14A-D). The

“shoulder” observed in 1321N1-GPR17 cells at high concentrations disappears completely. Interestingly, the DMR does not disappear completely, suggesting another, as yet undefined, signalling pathway that is engaged by GPR17. This is possibly an instance of a  $G_{12/13}$  signal transduction pathway or  $\beta$ -arrestin recruitment. Nevertheless, the substantial contribution of the  $G_i$  pathway to the DMR of all test compounds was demonstrated in 1321N1-GPR17 cells.

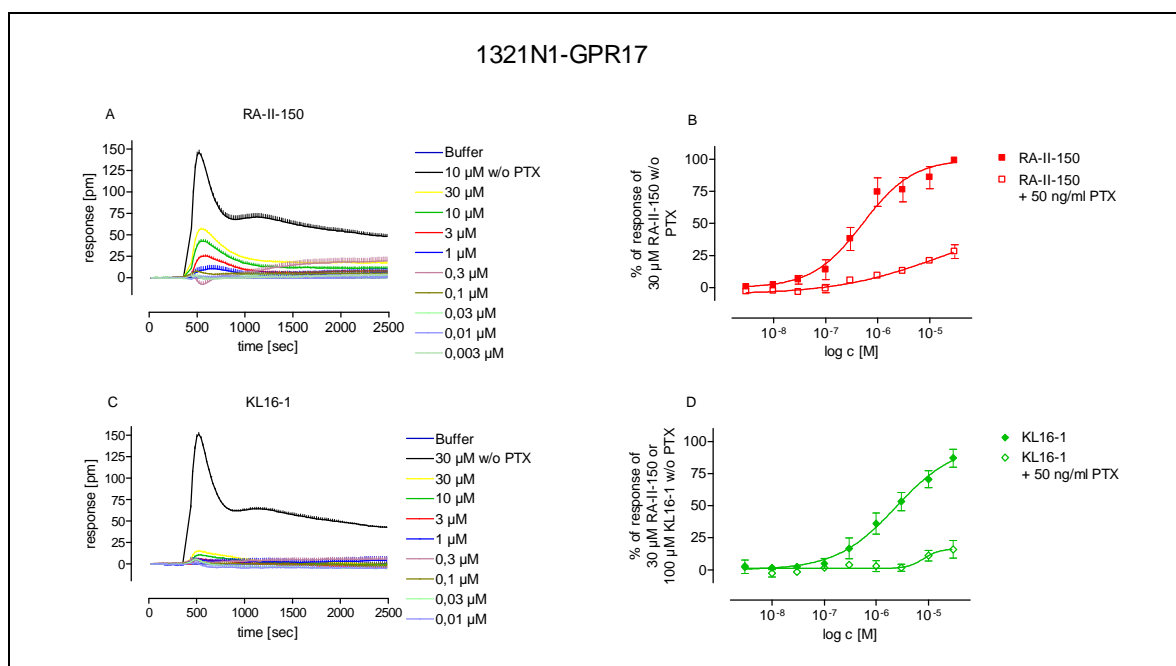


**Figure 14.** Effects of PTX pretreatment on the DMR of RA-II-150 and KL16-1 in 1321N1-GPR17 cells. Signatures of a representative experiment with PTX pretreated recombinant 1321N1-GPR17 cells and two selected GPR17 agonists are presented in (A) and (C). A signature of the corresponding agonist with untreated cells is also shown. PTX treatment has a strong impact on the DMR of RA-II-150 and KL16-1 in 1321N1-GPR17 (A and C). Even if full activation is not achieved, GPR17 still responds to its agonist. The corresponding DRCs are given in (B) and (D).

A similar behaviour was observed in CHO-GPR17 cells (Figure 15). In this cell line the signal elevation at the same concentration decreases drastically in pretreated cells. At high concentrations, on the other hand, the signal rises again (Figure 15). The DMR shapes of these signals are comparable to those described in the literature for the  $G_q$  signal transduction pathway.<sup>[67]</sup> The DRCs of all tested GPR17 agonists are shifted to the right under the influence of PTX compared to standard assay conditions.

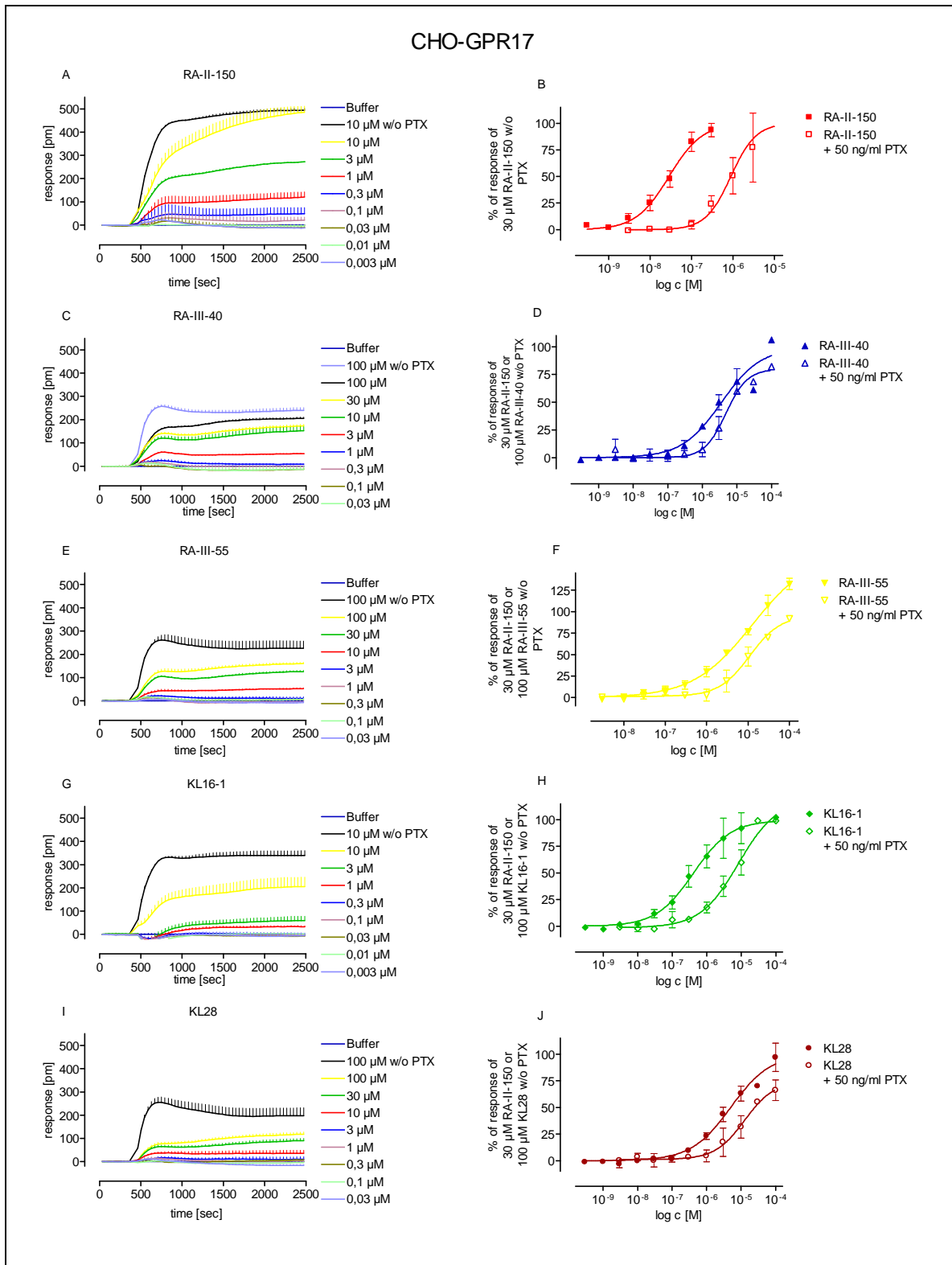


**Figure 15.** Effects of PTX pretreatment on the DMR of selected GPR17 agonists in CHO-GPR17 cells. Signatures of a representative experiment with PTX pretreated recombinant CHO-GPR17 cells and selected GPR17 agonists are presented in (A), (C), (E), (G) and (I). A signature of the corresponding agonist with untreated cells is also shown in each case. PTX treatment has a strong impact on the DMR of all test compounds in CHO-GPR17 cells (A and C). Even if all compound DRCs are shifted to the right, full activation appears to be possible (B, D, F, H and J).

The agonist potencies in the inositol phosphate accumulation assay correlate with those in the DMR assay for both untreated and PTX treated cells (Figure 16A and B). Both correlations fit ( $r^2$  0.90 and 0.86). But it was expected that the data from the inositol phosphate accumulation assays fit more to the DMR data with PTX treated cells than to the DMR data with the untreated cells, because under the influence of PTX the  $G_i$  signalling is blocked and it was expected to analyse the  $G_q$  pathway in isolation with the DMR assay under these conditions. In this case the DMR should be equivalent to the data from the inositol phosphate accumulation assay. This observation indicates that the remaining DMR signal in CHO cells after PTX treatment consists of the  $G_q$ -dependent signal transduction pathway and another yet unidentified pathway.

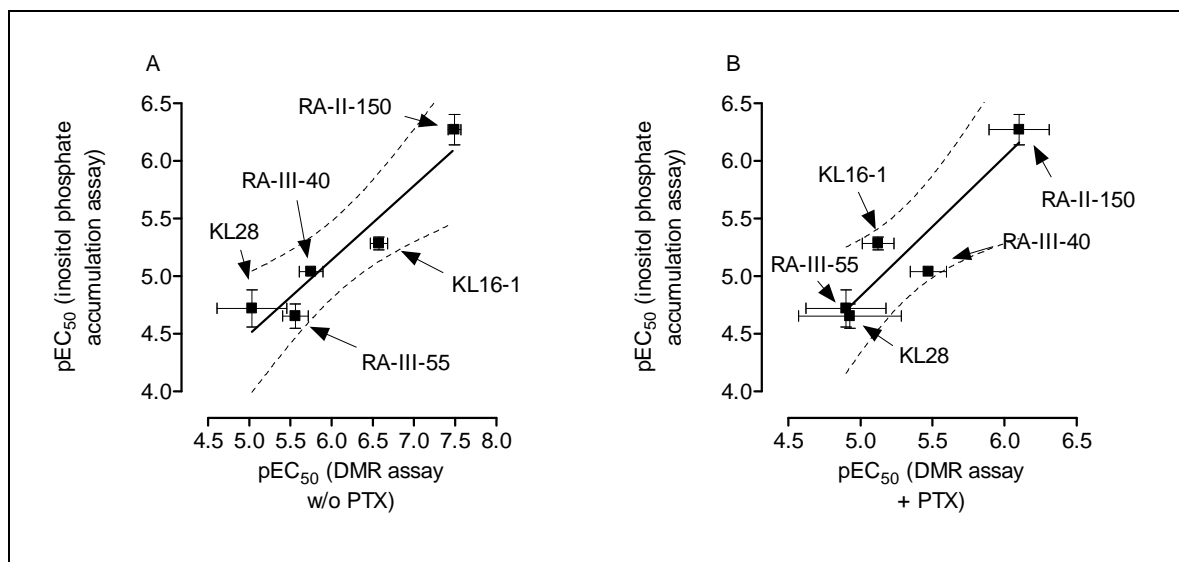


**Figure 16.** Comparison of the pEC<sub>50</sub> values of selected GPR17 agonists with CHO-GPR17 cells in the inositol phosphate accumulation assay and the DMR assay under standard conditions (A) and under PTX conditions (B). The P values of the linear regression analysis are 0.01 and 0.02. The dotted lines indicate the 95% confidence interval.



## 2.3 Uracil nucleotides proposed as GPR17 agonists

### 2.3.1 Compound analysis using calcium assays

In 2006, Ciana *et. al.* claimed that GPR17 can be activated by UDP, UDP-glucose and UDP-galactose (Figure 17).<sup>[51]</sup> According to this report GPR17 activation leads to an adenylyl cyclase inhibition, an increased intracellular calcium concentration and GTP<sub>γ</sub>S binding. The EC<sub>50</sub> values of these compounds are 1.14 μM UDP, 12 μM UDP-glucose and 1.1 μM UDP-galactose.<sup>[51]</sup>

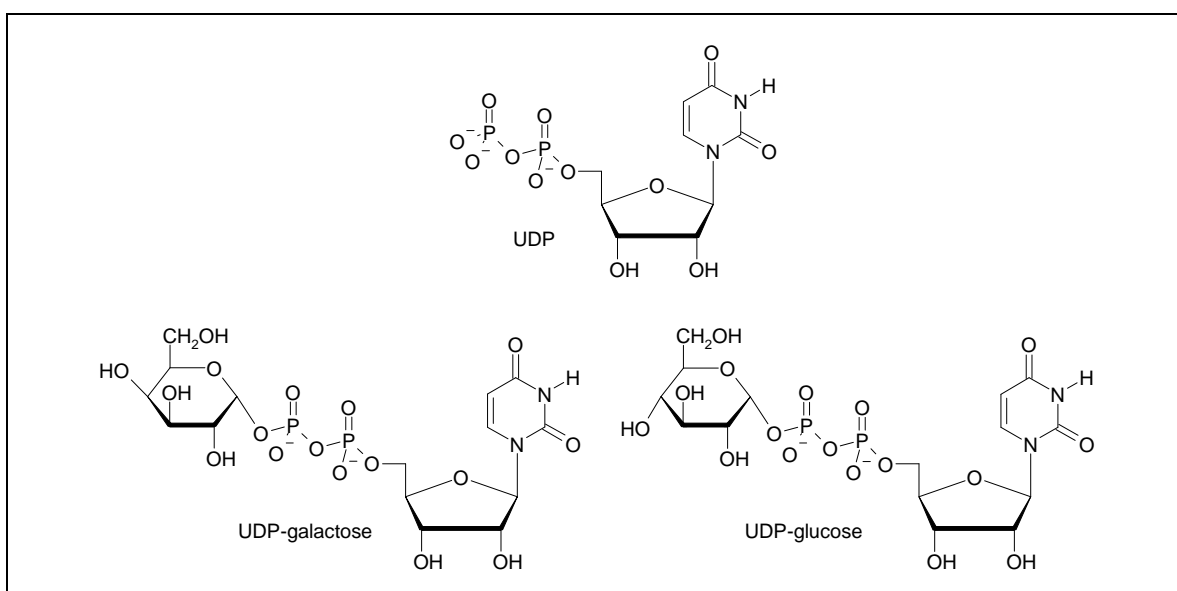


**Figure 17.** Uracil nucleotides proposed as GPR17 agonists.<sup>[51]</sup>

At the beginning, the ability of uracil nucleotides UDP, UDP-glucose and UDP-galactose to increase the intracellular calcium concentration was investigated in recombinant 1321N1 cells stably expressing GPR17.

Compared to RA-II-150, neither UDP and UDP-glucose nor UDP-galactose causes a calcium response up to 100 μM in 1321N1-GPR17 cells (Figure 18A and B).

When UDP-glucose and UDP-galactose are added, no calcium mobilisation is

detectable in recombinant CHO-GPR17 cells (Figure 18C and D). After adding, 30  $\mu$ M UDP, the intracellular calcium concentration is increased (Figure 18C and D). An even stronger response to the addition of UDP occurs in native CHO-K1 cells, indicating that this response is due to the activation of endogenously expressed P2Y receptors in CHO cells and not to the activation of GPR17 (Figure 18E and F).

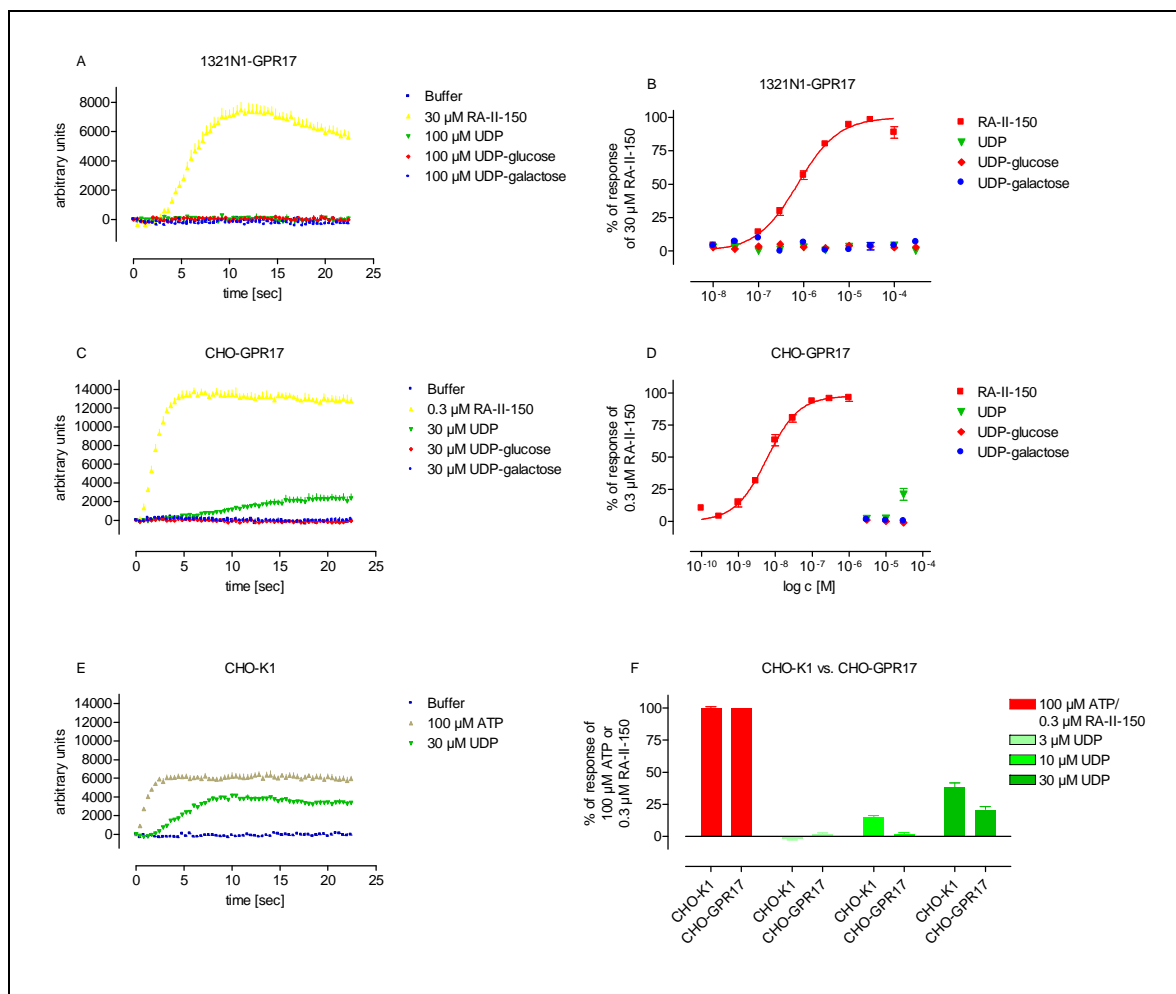


**Figure 18.** Representative calcium traces of uracil nucleotides in 1321N1-GPR17 (A), CHO-GPR17 (C) and native CHO-K1 (E) cells. The corresponding normalised DRCs or data are shown in (B), (D) and (F). The addition of uracil nucleotides does not cause an increase in the intracellular calcium concentration in 1321N1-GPR17 cells (A and B). Whereas the addition of UDP to CHO-GPR17 cells leads to calcium mobilisation, CHO-GPR17 cells do not respond to UDP-glucose or UDP-galactose (C and D). However, CHO-K1 cells also respond to UDP in a concentration-dependent manner (F), meaning that the response of CHO-GPR17 to UDP is not due to the activation of GPR17.

The response of 1321N1-GPR17 cells to 300  $\mu$ M UDP-galactose was analysed in a single-cell calcium assay. UDP-galactose fails to increase the intracellular calcium concentration also in this assay (Figure 19). By contrast, GPR17 is activated by RA-II-150.

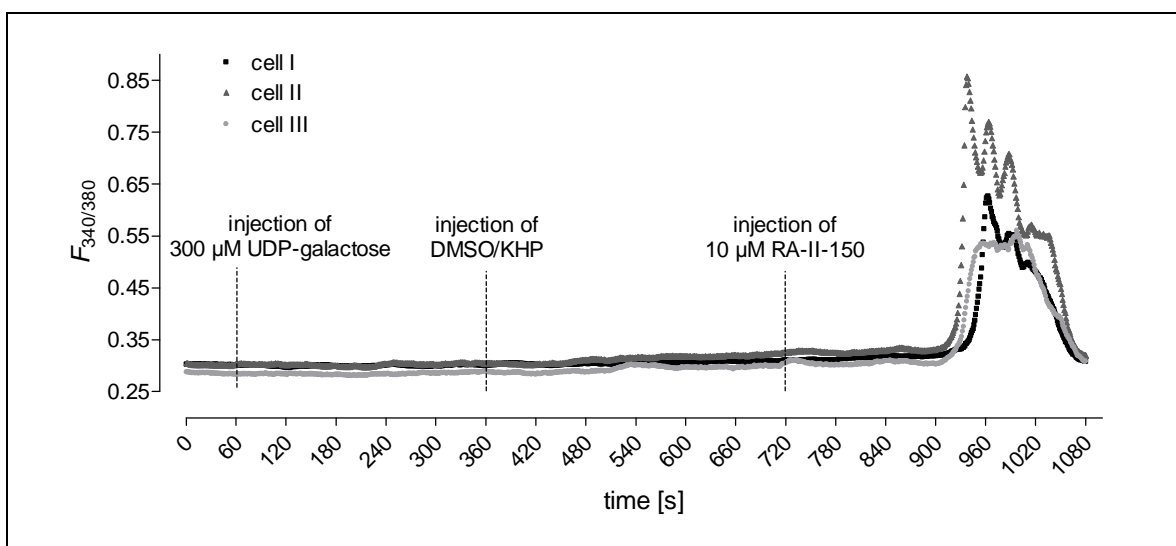


**Figure 19.** Representative real-time calcium measurement data in a single-cell calcium assay in 1321N1-GPR17 cells. Each signature represents the response of a single cell. No calcium response is detectable following UDP-galactose superfusion. After UDP-galactose elution, 10  $\mu$ M RA-II-150 is superfused to the cells and calcium mobilisation occurs.

### 2.3.2 Compound analysis using DMR technology based assays

Since uracil nucleotides did not increase the intracellular calcium concentration, it was investigated whether the addition of these compounds causes DMR in 1321N1-GPR17 and CHO-GPR17 cells. UDP-glucose and UDP-galactose fail to cause DMR in either 1321N1-GPR17 or CHO-GPR17 cells (Figure 20A and B). The injection of UDP in this assay leads to stronger DMR signals in native CHO-K1 cells in comparison to CHO-GPR17 cells, indicating that the response to the addition of UDP is due to the activation of endogenously expressed receptors, namely P2Y receptors, and not to the activation of GPR17 in this cell line (Figure 20B)

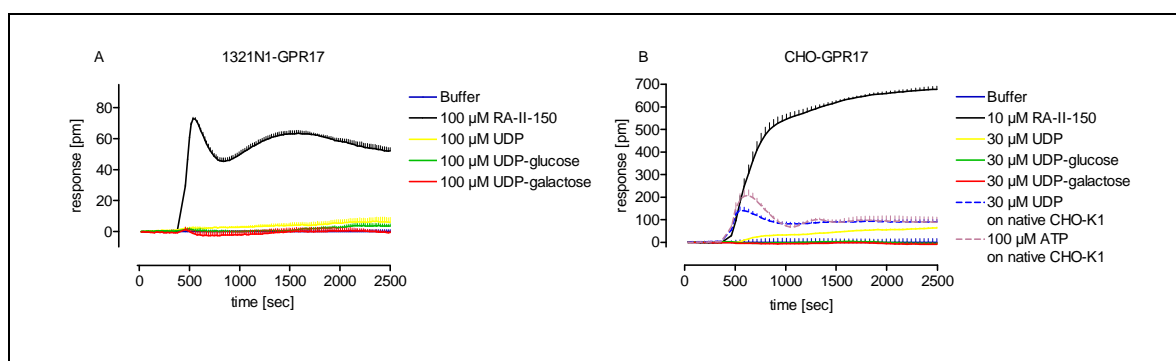


**Figure 20.** Uracil nucleotides do not lead to GPR17-dependent DMR in recombinant 1321N1-GPR17 (A) and CHO-GPR17 (B) cells ( $n = 2-3$ ). DMR occurring upon UDP addition in CHO-GPR17 cells is also observable - and even stronger - in native CHO-K1 cells ( $n = 2-3$ ), which is may be due to endogenously expressed P2Y receptors and not to the activation of GPR17.

## 2.4 CysLT<sub>1</sub> receptor antagonists proposed as GPR17 antagonists

### 2.4.1 Compound analysis using calcium assays

Among others, Ciana *et. al.* identified and characterised montelukast and pranlukast (Figure 21), two CysLT<sub>1</sub> specific antagonists, as potent GPR17 antagonists.<sup>[51, 68]</sup> The IC<sub>50</sub> values for the characterised antagonists determined in GTP<sub>γ</sub>S binding experiments are in the nanomolar and subnanomolar range.

In the following, pranlukast, montelukast and zafirlukast, another CysLT<sub>1</sub> receptor antagonist, were tested in calcium assays for their ability to inhibit GPR17. All tested CysLT<sub>1</sub> receptor antagonists inhibit GPR17 (Figure 22), but an analysis of the corresponding antagonist DRCs revealed that both pranlukast and montelukast are considerably less potent than published (Figure 22D). Their potency is decreased by a factor of 240 and 255 respectively (Table 4).

No unspecific increase of intracellular calcium is detectable after adding 30 μM of one of the CysLT<sub>1</sub> receptor antagonists (Table 4).

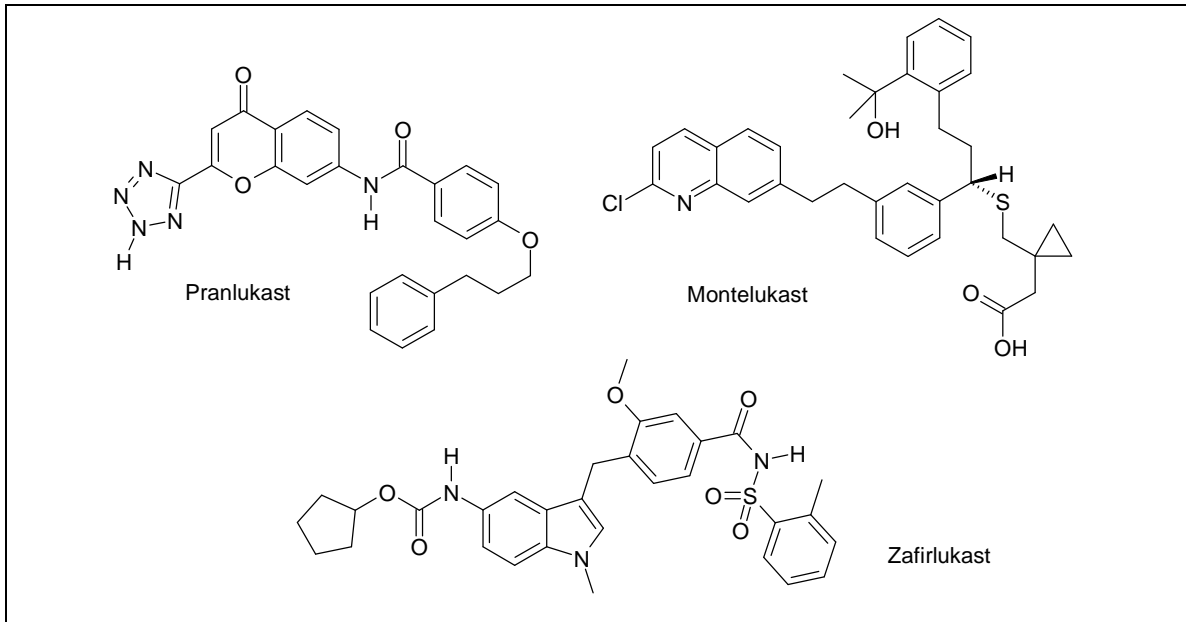


**Figure 21.** Pranlukast and montelukast, two potent CysLT<sub>1</sub> receptor antagonists, were proposed as antagonists of GPR17.<sup>[51, 68]</sup> Zafirlukast, another potent CysLT<sub>1</sub> receptor antagonist, was also tested in this thesis.

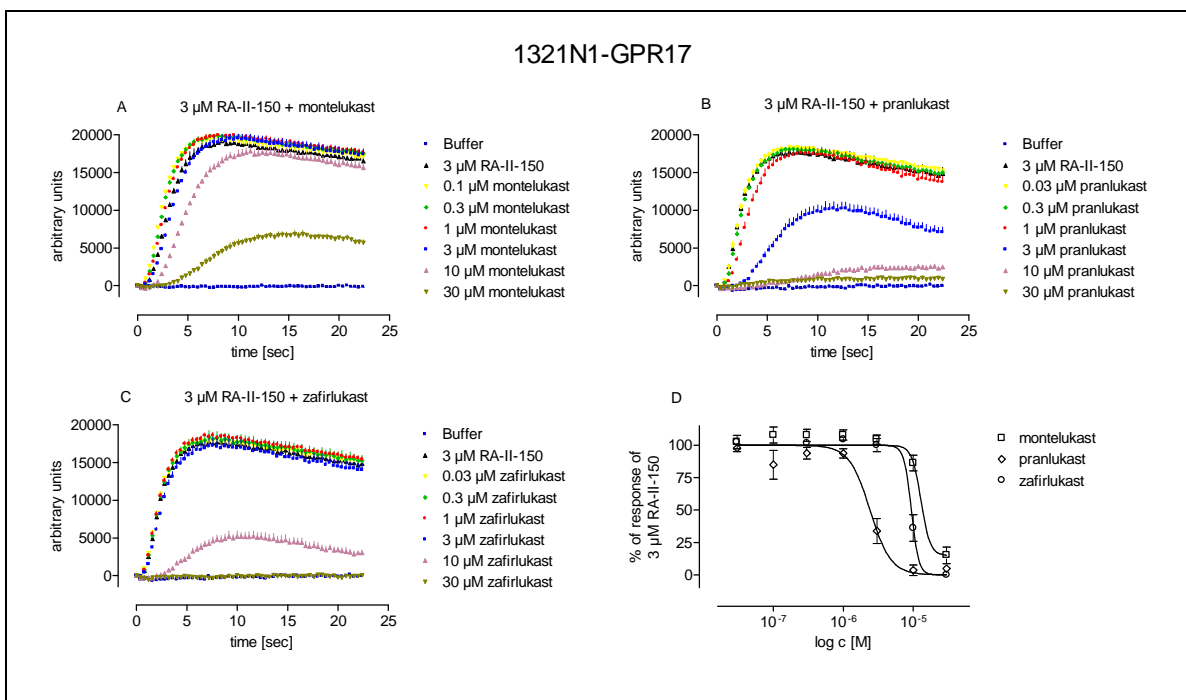


**Figure 22.** Analysis of antagonistic effects of montelukast and zafirlukast in calcium assays. The representative calcium real-time responses of 1321N1-GPR17 cells after adding 3  $\mu\text{M}$  RA-II-150 in the absence of a corresponding CysLT<sub>1</sub> receptor antagonist or in the presence of a defined concentration of montelukast (A), pranlukast (B) or zafirlukast (C) are presented here. Dose response curves were calculated from this data (D).

**Table 4.** Collection of  $pIC_{50}$  values and inhibition data of CysLT<sub>1</sub> receptor antagonists tested in the recombinant 1321N1-GPR17 cell system (n = 3-5). Test compounds were applied in a concentration of 30  $\mu$ M. The data are normalised to the response of 3  $\mu$ M (column 3) or 30  $\mu$ M RA-II-150 (column 4).

Chemical structure of the test compounds	1321N1-GPR17		
	$pIC_{50}$ ( $\pm$ SEM)	% of inhibition by test compound ( $\pm$ SEM)	% of response of test compound ( $\pm$ SEM)
Montelukast	4.85 (0.05)	84.9 (6.43)	0.92 (0.30)
Pranlukast	5.57 (0.02)	95.2 (1.53)	1.23 (1.62)
Zafirlukast	5.06 (0.06)	97.3 (2.85)	0.27 (0.28)

#### 2.4.2 Compound analysis using inositol phosphate accumulation assays

The CysLT<sub>1</sub> receptor antagonists montelukast, pranlukast and zafirlukast were also tested in inositol phosphate accumulation assays for their ability to inhibit GPR17 activation in the recombinant CHO-GPR17 cell system. No unspecific inositol phosphate accumulation occurs in the presence of 30  $\mu$ M test compound (Figure 23A). Montelukast does not significantly inhibit GPR17 in this assay (Figure 23B), but pranlukast and zafirlukast do (Figure 23B). The corresponding DRCs for pranlukast and zafirlukast are shown in Figure 23C.

Pranlukast and zafirlukast inhibit the RA-II-150-dependent activation of GPR17 in both this assay and the cell population based calcium assay (Table 4). The DRCs in the inositol phosphate accumulation assay are shifted slightly to the left compared to those in the calcium assay. Pranlukast is more potent than zafirlukast in both assays. Montelukast inhibits GPR17 in the calcium assay but not in the IP<sub>3</sub> accumulation assay (Table 5).

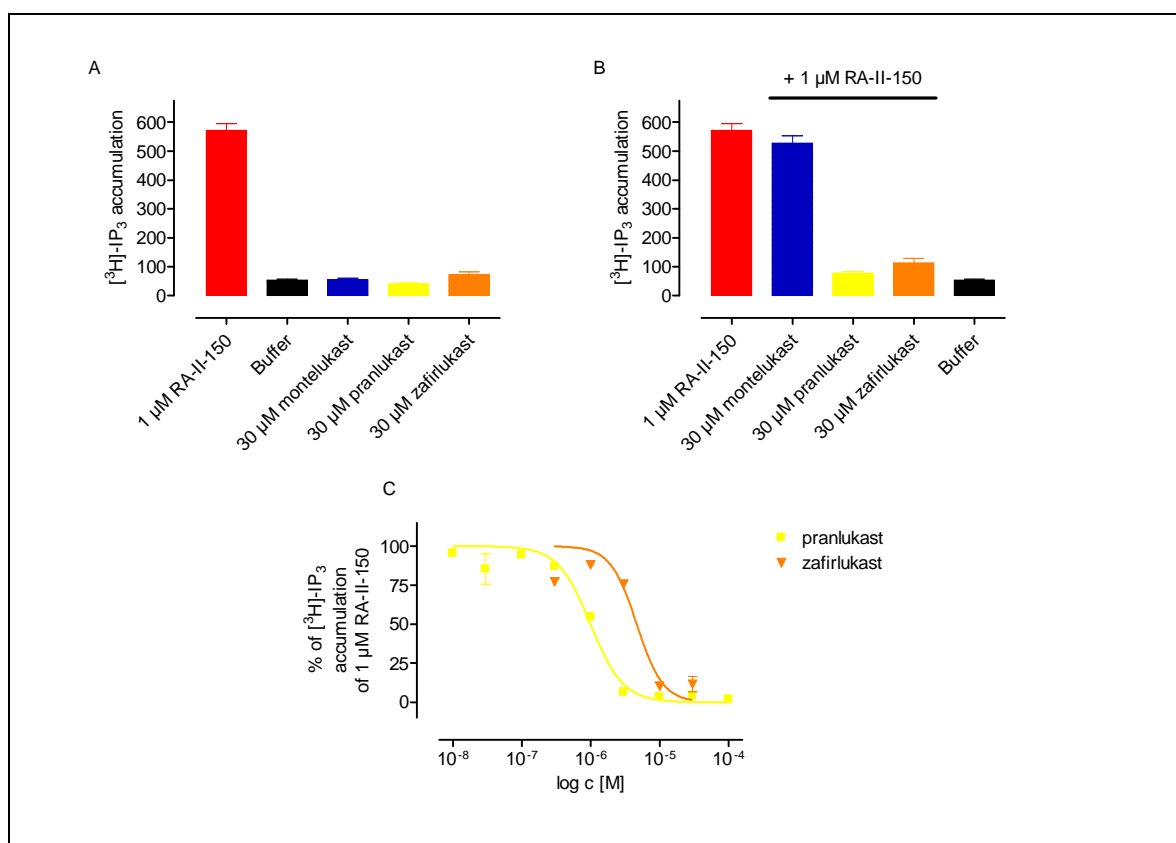


**Figure 23.** The addition of the CysLT<sub>1</sub> receptor antagonists pranlukast, montelukast and zafirlukast does not cause an unspecific inositol phosphate accumulation in CHO-GPR17 cells (A) (n = 3-4). Whereas montelukast does not inhibit GPR17 activation up to a concentration of 30 μM, GPR17 is blocked by pranlukast and zafirlukast (B) (n = 3-4). DRCs of pranlukast (n = 3) and zafirlukast (n = 1) were determined by analysing an inositol phosphate accumulation of 1 μM RA-II-150 in the presence of a defined antagonist concentration (C).

**Table 5.** pIC<sub>50</sub> values and inhibition values of montelukast, pranlukast and zafirlukast at a concentration of 30 μM (n = 1-3). The inhibition values are normalised to the response of 1 μM RA-II-150.

CHO-GPR17 cells		
Test compound	pIC <sub>50</sub> (± SEM)	% of inhibition of test compound (± SEM)
Montelukast	n. d.	14.0 (6.49)
Pranlukast	6.04 (0.08)	95.8 (1.51)
Zafirlukast	5.32 (0.00)	88.3 (5.05)

## **2.5 Investigations of signal transduction pathways coupled to GPR17 and discovery of a novel calcium release mechanism in 1321N1 cells**

Cell population based calcium assays (Figure 5) with 1321N1-GPR17 and CHO-GPR17 cells as well as fluorescence microscopy based single cell calcium assays (Figure 19) with recombinant 1321N1-GPR17 cells suggested a GPR17 coupling to the calcium signalling cascade. This classical calcium cascade consists of phospholipase C, which is activated by a  $G_{\alpha q}$  subunit or a  $G_{\beta\gamma}$  subunit liberated from PTX-sensitive  $G_i$  family proteins, and  $IP_3$  receptors on intracellular calcium stores, which are activated by  $IP_3$ , a product of the PLC-catalysed reaction. The intracellular calcium stores are emptied after the  $IP_3$  receptors have been activated.

### **2.5.1 PTX pretreatment reveals participation of the $G_i$ pathway in the calcium mobilisation mechanism**

It is well known that the  $G_{\beta\gamma}$  subunit liberated from PTX-sensitive  $G_i$  family proteins also activates PLC- $\beta$  isoforms (except PLC- $\beta_4$ ) as well as PLC- $\epsilon$ .<sup>[24, 25, 69, 70]</sup> For this reason the involvement of the  $G_i$  pathway in the calcium mobilisation mechanism was analysed. The participation of the  $G_i$  pathway was confirmed by PTX pretreatment, since in pretreated 1321N1-GPR17 cells the calcium response disappeared (Figure 24A and B), while the calcium response of endogenously expressed muscarinic  $M_3$  receptors was not affected, indicating the functionality of the cells under these conditions (Figure 24C).

By contrast, the calcium mobilisation is also affected in CHO-GPR17 cells, but GPR17 is still completely activated at higher agonist concentrations (Figure 24D and E). The  $pEC_{50}$  of RA-II-150 is decreased from 8.20 in untreated cells to 7.16 ( $\pm 0.14$ ) in PTX-pretreated cells.



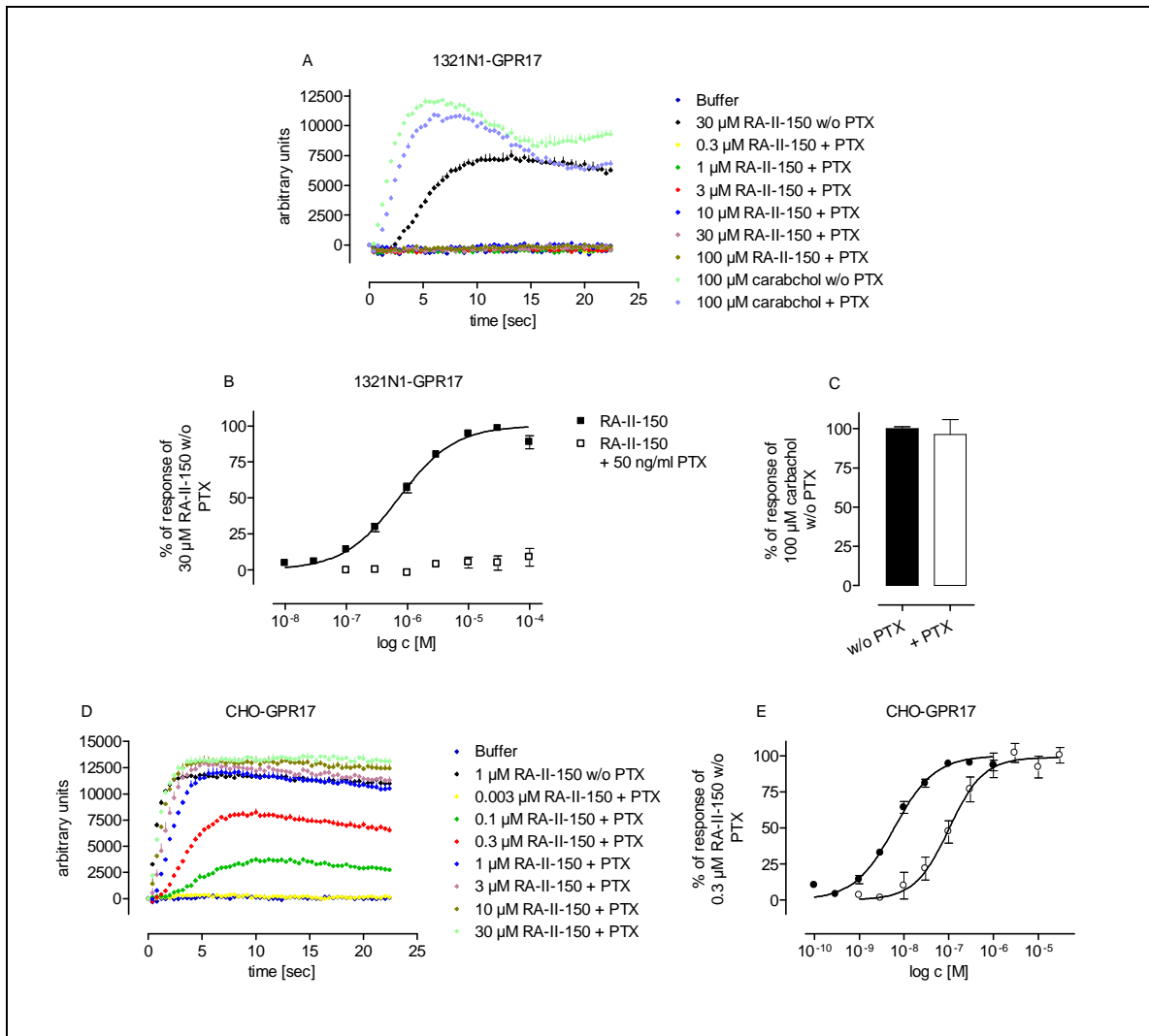


**Figure 24.** Influence of PTX on the calcium release in 1321N1-GPR17 and CHO-GPR17 cells. (A) Representative real-time measurements of the changes in intracellular calcium in PTX-pretreated 1321N1-GPR17 upon agonist addition. Under these conditions the calcium mobilisation of GPR17 is completely blocked so that no DRC can be determined for RA-II-150 (B). By contrast, the calcium signalling of endogenously expressed muscarinic  $M_3$  receptor is not affected by PTX pretreatment (C). Representative real-time measurements of the changes in intracellular calcium levels in PTX-treated CHO-GPR17 upon RA-II-150 addition (D) and corresponding DRC showing that GPR17 is still fully activated, but its DRC has been shifted to the right (E).

## 2.5.2 Confirmation of GPR17 $G_i$ coupling by determination of cAMP decrease

The results of the calcium assays with PTX-treated 1321N1-GPR17 and CHO-GPR17 cells indicated the dependence on, or contribution to, respectively

the  $G_i$  pathway in the calcium response of GPR17. The  $G_i$  coupling of GPR17 was analysed using the HTRF<sup>®</sup> cAMP assay. Constitutive  $G_i$  activity of GPR17 can be ruled out because the  $pEC_{50}$  value of forskolin is determined to be 6.14 in recombinant 1321N1-GPR17 cells and 5.75 in native cells (Figure 25). In the event of constitutive  $G_i$  activity, the potency should have been decreased.

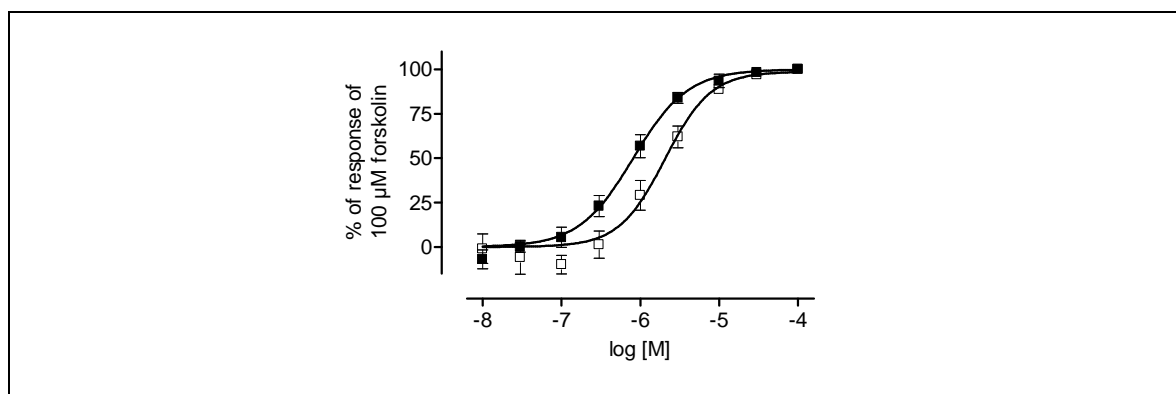


**Figure 25.** GPCR-independent adenylyl cyclase activation by forskolin in native 1321N1 cells (open squares) and recombinant 1321N1-GPR17 cells (closed squares) ( $n = 3-4$ ). The DRC for forskolin in the recombinant cell system is shifted slightly to the left. The data were normalised to the cAMP accumulation of 100  $\mu$ M forskolin.

The  $G_i$  coupling of GPR17 was then analysed in detail using RA-II-150 as a representative agonist. A concentration of 1  $\mu$ M forskolin, which causes approximately 55% of the maximum forskolin response (Figure 25), was added to the cells in parallel with different RA-II-150 concentrations for this analysis. These investigations indicated an agonist concentration-dependent inhibition of the forskolin-dependent adenylyl cyclase activation. The  $G_i$  signal transduction cascade is activated at low agonist concentrations (Figure 26), while at RA-II-150 concentrations higher than 0.1  $\mu$ M a stimulatory  $G_s$  signal cascade outweighs the inhibitory response (Figure 26). This behaviour results in a bell-shaped dose response curve (Figure 26). In native astrocytoma cells this behaviour cannot be observed, meaning that the effect of RA-II-150 in the recombinant cell system is due to the activation of GPR17.

Since PTX pretreatment blocked the observed inhibition of the adenylyl cyclase, it can be confirmed that this inhibitory effect is due to the activation of the  $G_i$  signal transduction cascade by GPR17 (Figure 27).<sup>[71]</sup> Furthermore, under these

conditions the activation of the stimulatory  $G_s$  pathway disappeared, indicating that the activation of this pathway is dependent on a previous activation of the  $G_i$  pathway (Figure 27).

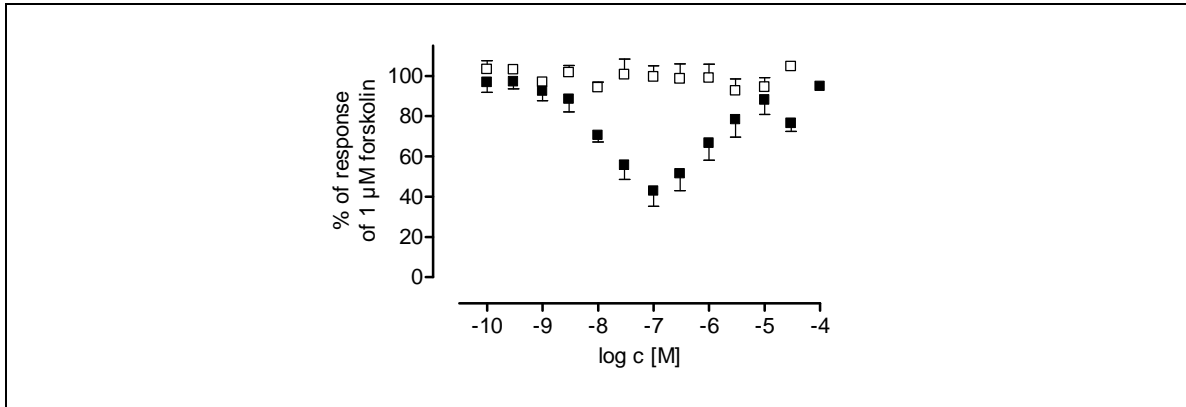


**Figure 26.** Dose response curves of 1321N1-GPR17 and native 1321N1 cells as deduced from cAMP assays. Challenge of 1321N1-GPR17 cells with RA-II-150 (closed squares) ( $n = 6$ ) leads to a bell-shaped DRC, while treatment of native 1321N1 cells with the lead agonist (open squares) does not show any effect ( $n = 3$ ).

The activation of the  $G_i$  and  $G_s$  pathways by selected GPR17 agonists in the CHO-GPR17 cells was already shown by Stephanie Hennen (unpublished data) and Marieke Böckman genannt Dallmeyer.<sup>[72]</sup>

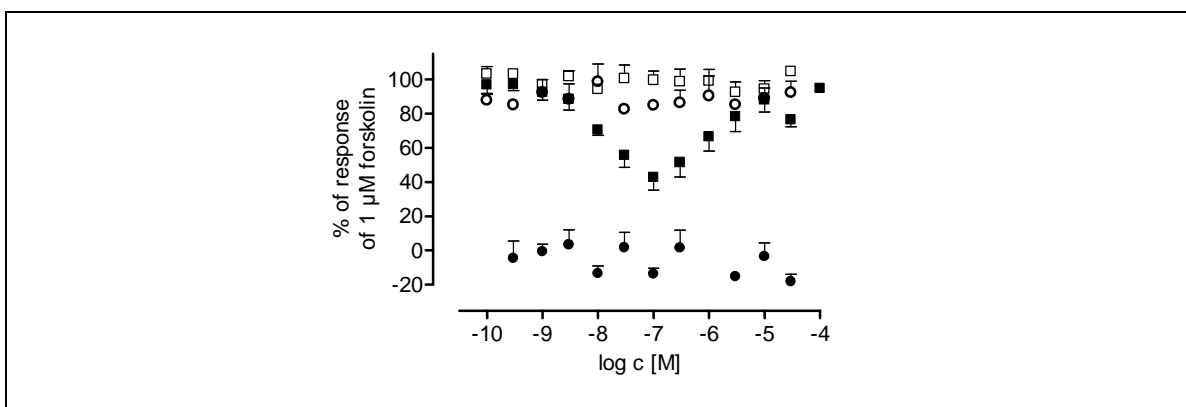


**Figure 27.** Dose response curves of 1321N1-GPR17 and native 1321N1 cells as deduced from cAMP assays. Challenge of 1321N1-GPR17 cells with RA-II-150 (closed squares) ( $n = 6$ ) leads to a bell-shaped DRC, while treatment of native 1321N1 cells with the lead agonist (open squares) does not show any effect ( $n = 3$ ). After PTX pretreatment the  $G_i$  response of GPR17 disappears (open circles) ( $n = 4$ ). Furthermore, no  $G_s$  coupling can be detected (closed circles) ( $n = 6$ ).

### **2.5.3 A phosphatidylinositol-specific phospholipase C is involved in the calcium release mechanism in 1321N1-GPR17 cells**

The data from the calcium assay indicated the contribution of phospholipase C by the  $G_{\beta\gamma}$  subunit liberated from PTX-sensitive proteins of the  $G_i$  family in 1321N1 cells as well as the participation of the  $G_q$  pathway in CHO-GPR17. For this reason the influence of the PLC inhibitor U-73122 and its inactive derivative U-73343 on the calcium mobilisation mechanism was investigated (Figure 28).

The addition of an effective concentration of the PLC inhibitor U-73122 (2.5  $\mu$ M for the 1321N1-GPR17 cell system and 5  $\mu$ M in the CHO-GPR17 cell system) does not lead to an increase in the intracellular calcium concentration (Figure 28A and D), meaning that the inhibitory effects are not due to unspecific calcium mobilisation but to PLC inhibition. In the presence of the PLC inhibitor the maximal calcium response of RA-II-150 decreases significantly in the recombinant 1321N1 astrocytoma cell system (Figure 28B and C) as well as in the CHO-GPR17 cell system (Figure 28E and F). The  $pEC_{50}$  values of RA-II-150 in the corresponding cell system are 6.16 ( $\pm$  0.16) and 7.24 ( $\pm$  0.13), respectively (under standard conditions: 6.09 ( $\pm$  0.06) and 8.20 ( $\pm$  0.08)). By contrast, the inactive U-73122 homolog does not influence the calcium mobilisation in either cell system (Figure 28B, C and E, F). This means that phospholipase C is involved in the calcium mobilisation mechanism in both cell systems.

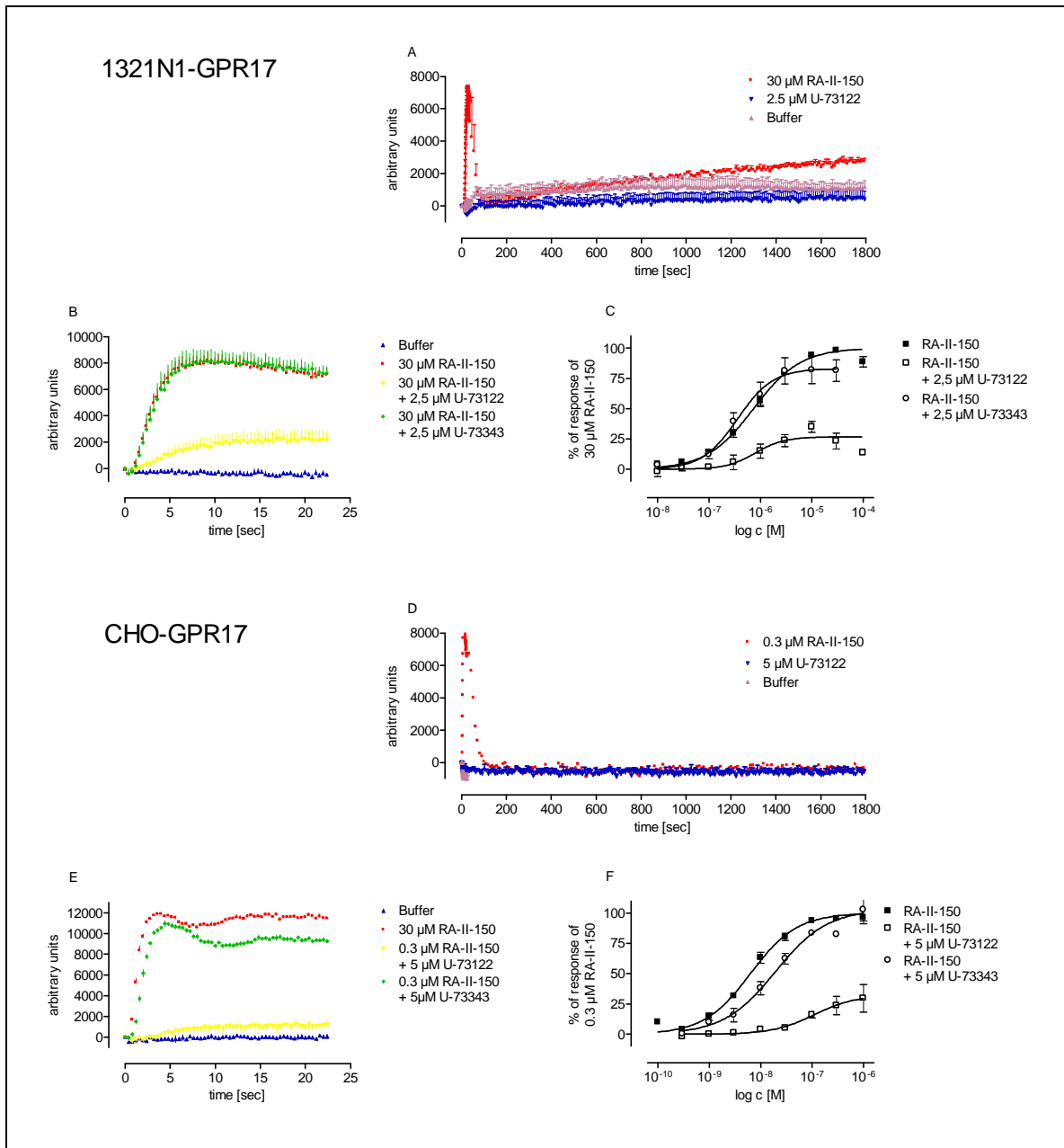


**Figure 28.** Investigations concerning the influence of the PLC-inhibitor U-73122 on the calcium release in 1321N1-GPR17 cells and CHO-GPR17 cells. The intracellular calcium concentration increases neither in 1321N1-GPR17 nor in CHO-GPR17 upon PLC inhibitor addition (A and D). The calcium mobilisation in 1321N1-GPR17 (B, C) and CHO-GPR17 (E, F) cells is decreased in the presence of the PLC inhibitor U-73122, but not in the presence of the inactive derivative U-73343 ( $n = 3-10$ ). Representative real-time calcium signatures are shown in (B) and (E), whereas in (C) and (F) the DRC of RA-II-150 under standard assay conditions is compared to that of RA-II-150 in the presence of 2.5  $\mu\text{M}$  U-73122 or U-73343 (1321N1-GPR17 cells) or 5  $\mu\text{M}$  U-73122 or U-73343 (CHO-GPR17 cells).

Next, it was investigated whether a phosphatidylinositol-specific phospholipase C (PI-PLC) is involved in the calcium release mechanism. The PI-PLC was therefore

selectively blocked by edelfosine.<sup>[73, 74]</sup> Within 30 minutes after adding edelfosine, the intracellular calcium concentration is not elevated (Figure 29A). A significant decrease in intracellular calcium mobilisation can be observed in the presence of 2.5  $\mu\text{M}$  edelfosine, while the calcium signal disappears in the presence of 5  $\mu\text{M}$  (Figure 29B and Figure 29C). The agonist potency in the presence of the inhibitor (2.5  $\mu\text{M}$ ) is slightly increased compared to its potency under standard conditions (Figure 29D). Calcium signalling is completely blocked in the presence of 5  $\mu\text{M}$  edelfosine (Figure 29D). These results indicate the contribution of a PI-PLC.

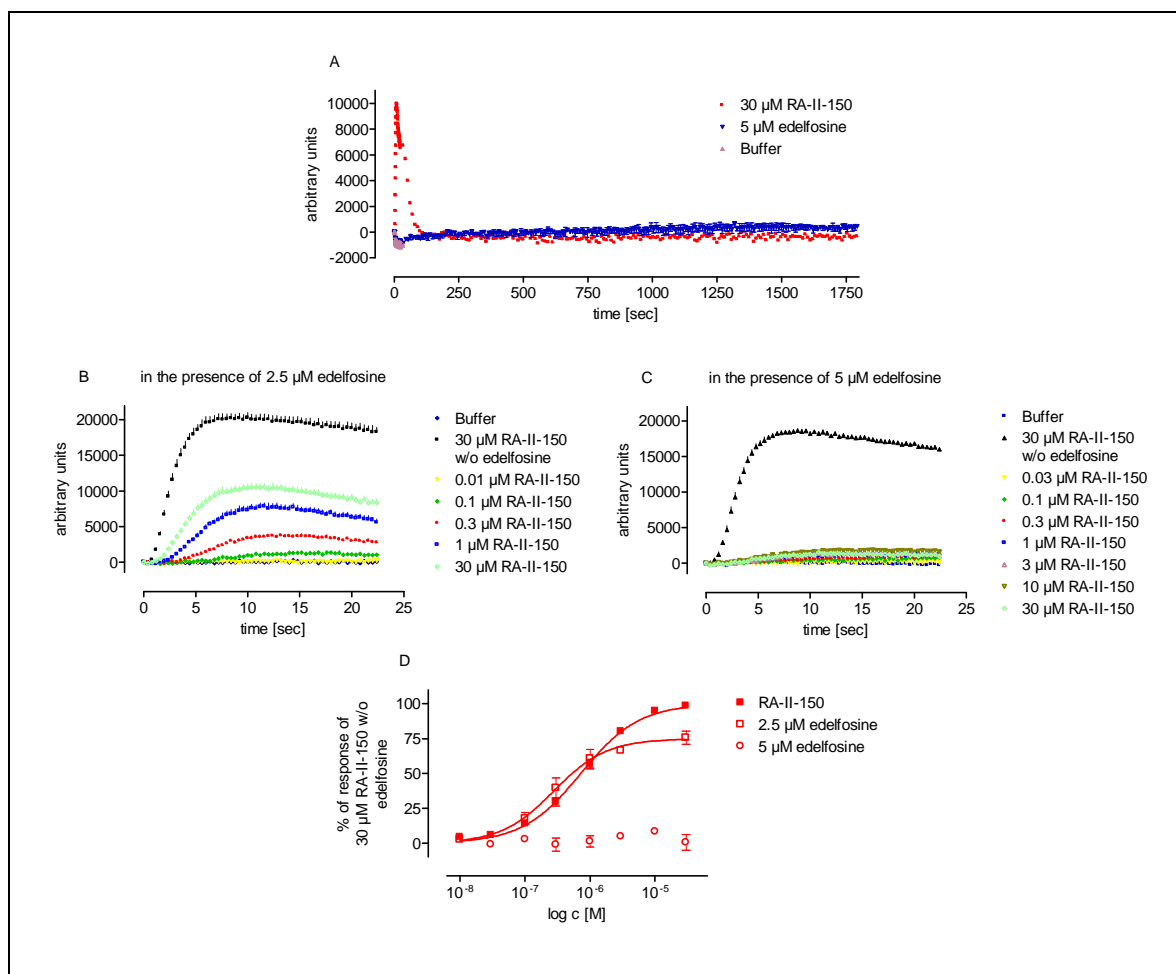


**Figure 29.** Influence of the PI-PLC-specific inhibitor on the calcium release in 1321N1-GPR17 cells upon agonist addition. No significant calcium mobilisation in 1321N1-GPR17 cells can be detected within 30 minutes after adding 5  $\mu\text{M}$  of the phosphatidylinositol-specific phospholipase C inhibitor edelfosine (A). The maximum calcium response of GPR17 upon RA-II-150 addition decreases with the concentration of edelfosine (B and C) ( $n = 2-9$ ). DRCs in the presence of different inhibitor concentrations are shown in (D) ( $n = 2-29$ ). In the presence of 2.5  $\mu\text{M}$  edelfosine the potency of RA-II-150 is slightly increased compared to that under standard conditions ( $n = 3-29$ ).

### 2.5.4 GPR17 activation does not lead to an accumulation of inositol phosphates in 1321N1-GPR17 cells

Since the data from the calcium assay suggested the involvement of a PI-PLC in the calcium release mechanism in 1321N1 cells, and the activation of the PLC in CHO-GPR17 was verified by inositol phosphate accumulation assays (Figure 10 and Figure 30A), it was very surprising that no inositol phosphate accumulation was detected in 1321N1-GPR17 cells upon agonist addition (Figure 30B). Carbachol was used as an endogenous control for assay conditions. These data indicate a novel calcium release mechanism in 1321N1-GPR17 cells, which depends on PI-PLC activation without leading to an inositol phosphate accumulation.

The involvement of the PLC in CHO-GPR17 was investigated further by its inhibition. The inositol phosphate accumulation decreases upon agonist addition in CHO-GPR17 depending on the inhibitor concentration (Figure 30A). In CHO-GPR17 neither 5  $\mu\text{M}$  nor 10  $\mu\text{M}$  U-73122 leads to an inositol phosphate accumulation (Figure 30C).

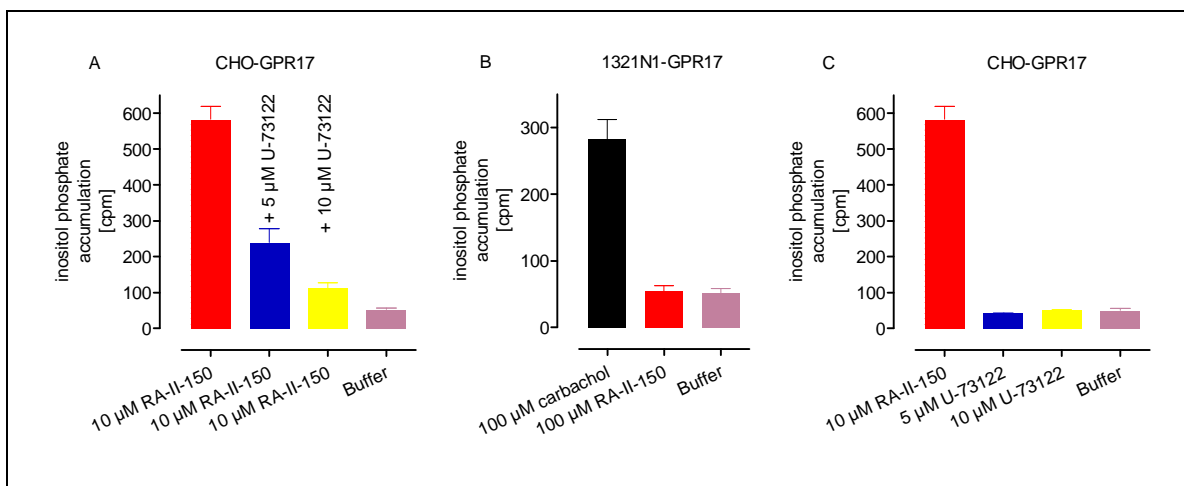


**Figure 30.** Inositol phosphate accumulation analysis in CHO-GPR17 and 1321N1-GPR17 cells. The inositol phosphate accumulation decreases upon inhibitor addition dependent on its concentration (A). Cells are stimulated with 10  $\mu\text{M}$  RA-II-150. In 1321N1-GPR17 the intracellular inositol phosphate concentration is not elevated upon agonist addition (up to 100  $\mu\text{M}$  RA-II-150) (B). Carbachol is used as an endogenous control. No unspecific inositol phosphate accumulation is detectable after adding 5  $\mu\text{M}$  or 10  $\mu\text{M}$  U-73122 in CHO-GPR17 cells (C).

### **2.5.5 Intracellular calcium stores are the major sources of GPR17-mediated calcium flux**

Next, the calcium source from which the detected calcium is released was identified. There are basically two possibilities. Either calcium can be released from intracellular calcium stores, for example the endoplasmic reticulum, as a result of receptor activation, or it is pumped into the cell from the extracellular environment. These two possibilities were investigated using the sarco/endoplasmic reticulum  $\text{Ca}^{2+}$  transport ATPases (SERCA) inhibitor thapsigargin as well as assay conditions without extracellular calcium.<sup>[75]</sup>

Thapsigargin depletes intracellular calcium stores within 30 minutes after addition (Figure 31A). Thus, thapsigargin selectively inhibits SERCA channels, which pump cytoplasmic calcium back into intracellular calcium stores. This inhibition leads to an elevation of the cytoplasmic calcium level.<sup>[76]</sup>

The calcium responses of GPR17 towards RA-II-150 disappear after pretreatment with thapsigargin (Figure 31B und D), indicating that intracellular calcium stores are the major calcium source.

Nevertheless, it was investigated whether the calcium response of GPR17 consists at least partially of calcium from the extracellular environment. For this purpose the standard Krebs HEPES buffer (KHB) was replaced with a calcium-free KHB. Whereas the GPR17-dependent maximum calcium response significantly decreases under these conditions (Figure 31C and E), the  $\text{pEC}_{50}$  value of RA-II-150 ( $\text{pEC}_{50}$  6.00 ( $\pm$  0.09)) is not affected (standard conditions:  $\text{pEC}_{50}$  6.09 ( $\pm$  0.06)).

These results indicate the minor relevancy of extracellular calcium for the calcium response of GPR17 in 1321N1 cells.



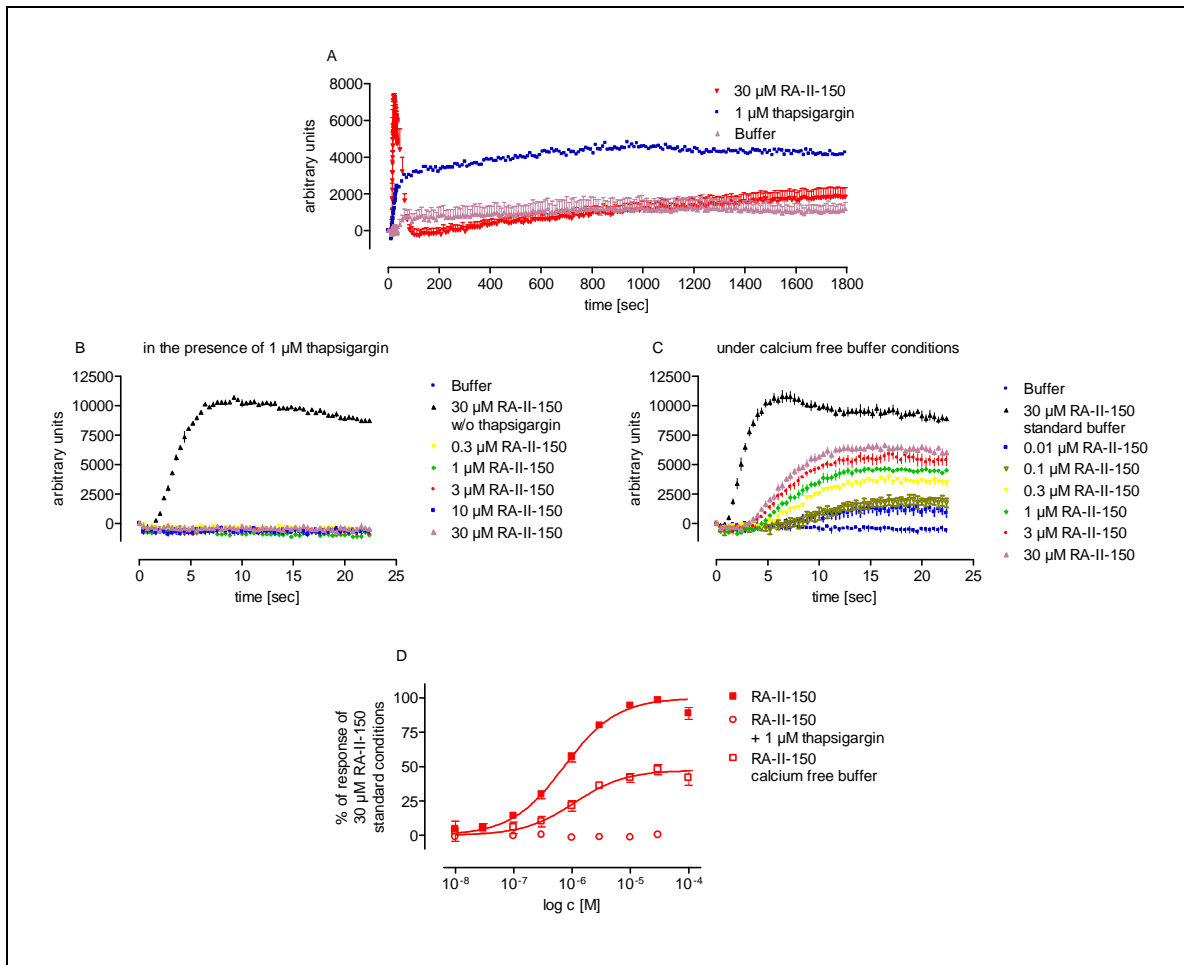


**Figure 31.** Investigations of the calcium source of the calcium response. Treatment with 1  $\mu$ M thapsigargin, an inhibitor of the sarco/endoplasmic reticulum  $\text{Ca}^{2+}$  ATPase, leads to the depletion of the intracellular calcium stores (A). After preincubation with 1  $\mu$ M thapsigargin, no calcium response is detectable upon GPR17 activation (B). Under calcium-free buffer conditions the calcium response of GPR17 (C) is significantly decreased but does not disappear (P value < 0.0001) (n = 3-7). These results are rendered in the DRCs of RA-II-150 under corresponding conditions (D).

### 2.5.6 $\text{IP}_3$ receptors on intracellular calcium stores gate the efflux of calcium

After intracellular calcium stores had been identified as the main calcium source, it was investigated whether ryanodine receptors (RYRs) or  $\text{IP}_3$ -dependent receptors ( $\text{IP}_3\text{R}$ ) are responsible for the release of calcium to the cytoplasm.

The role of ryanodine receptors was investigated first. RYRs are cation channels in the membrane of intracellular calcium stores like the endoplasmic reticulum that

upon stimulation pump calcium to the cytoplasm. RYRs are inhibited by an effective concentration of dantrolene (20  $\mu\text{M}$ ).<sup>[77, 78]</sup> The effect of 20  $\mu\text{M}$  dantrolene on the maximum calcium response of GPR17 towards their agonists RA-II-150 was determined. Within a time period of 30 minutes there is no elevation of the intracellular calcium level in 1321N1-GPR17 cells (Figure 32A). Furthermore, dantrolene does not attenuate the maximal calcium response of GPR17 (Figure 32B). By contrast, the  $\text{pEC}_{50}$  value of RA-II-150 is significantly increased in the presence of dantrolene ( $\text{pEC}_{50}$  6.85 ( $\pm$  0.03)) compared to its  $\text{pEC}_{50}$  under standard conditions ( $\text{pEC}_{50}$  6.09 ( $\pm$  0.06)) (Figure 32E).

$\text{IP}_3$  receptors are intracellular ligand-gated  $\text{Ca}^{2+}$  release channels localised primarily in the endoplasmic reticulum membrane.<sup>[79]</sup> This type of channel can be blocked by 2-aminoethoxydiphenyl borate (2-APB).<sup>[80]</sup> 2-APB does not elevate the intracellular calcium level in 1321N1-GPR17 cells upon addition (Figure 32C). In the presence of 2-APB the elevation of calcium concentration is decreased significantly compared to the calcium response under standard conditions (Figure 32D). The  $\text{pEC}_{50}$  of RA-II-150 in the presence of 2-APB is significantly increased from 6.09 ( $\pm$  0.06) to 6.56 ( $\pm$  0.04) (Figure 32E).

Since dantrolene does not attenuate the agonist-induced calcium rise but 2-APB attenuates it by more than 20%, the contribution of  $\text{IP}_3$  receptors can be confirmed. The significantly increased potency of RA-II-150 in the presence of both inhibitors is probably due to a shift in the calcium equilibrium from the cytoplasm towards the intracellular calcium stores.

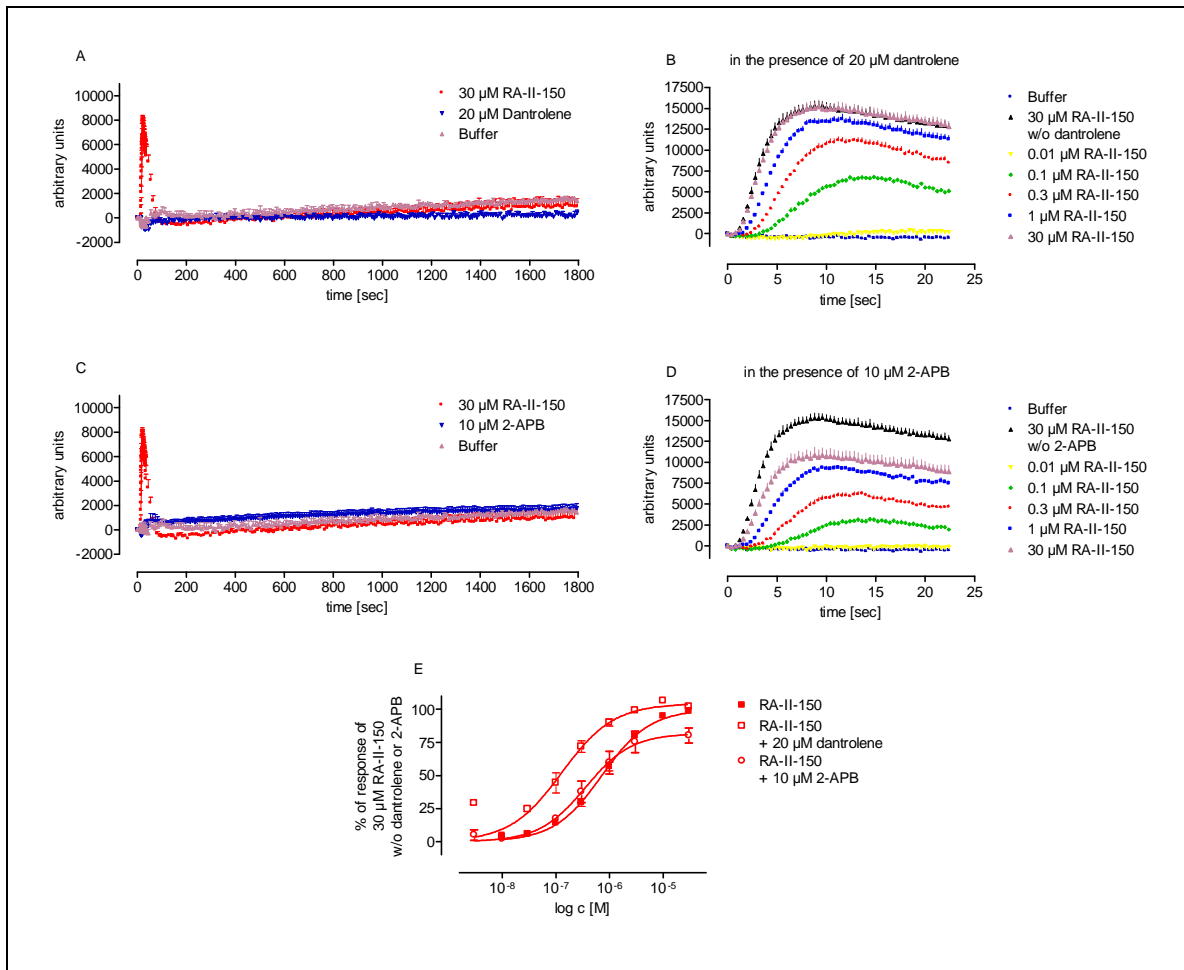


**Figure 32.** Analysis of the calcium source in 1321N1-GPR17 cells. Dantrolene, a ryanodine receptor inhibitor, does not elicit unspecific calcium mobilisation in 1321N1-GPR17 cells within 30 minutes after injection (A). Representative calcium signatures of RA-II-150 in the presence of 20  $\mu\text{M}$  dantrolene show that the maximum response of RA-II-150 is not affected (B). Upon addition of 2-APB, an  $\text{IP}_3$  receptor antagonist, the intracellular calcium concentration is also not affected (C). Representative calcium signals show that in the presence of 2-APB the maximum response is significantly decreased (D;  $P < 0.01$ ;  $n = 3-4$ ). The potency of the GPR17 agonist RA-II-150 is increased in the presence of 2-APB (D;  $n = 3-29$ ). The potency of RA-II-150 in the presence of dantrolene as well as of 2-APB is significantly increased ( $p\text{EC}_{50}[\text{dantrolene}] 6.85 \pm 0.03$ ;  $p\text{EC}_{50}[\text{2-APB}] 6.56 (\pm 0.04)$ ;  $p\text{EC}_{50}[\text{standard}] 6.09 (\pm 0.06)$ ) ( $n = 3-29$ ) (E).

### 2.5.7 The role of calmodulin in the calcium release mechanism

Next, the involvement of calmodulin in the release mechanism was investigated. Calmodulin is a ubiquitous and highly conserved calcium binding protein. It confers to calcium-dependent regulation of many proteins, including ion channels like ryanodine as well as IP<sub>3</sub> receptors in the endoplasmic reticulum membrane.<sup>[81-83]</sup>

N-(6-aminohexyl)-5-chloro-1-naphthalenesulphonamide hydrochloride (W-7) and fluphenazine are two calmodulin inhibitors which have been used to verify the participation of calmodulin in the calcium release mechanism.<sup>[84, 85]</sup>

First, the possibility that the addition of 30 μM W-7 or fluphenazine causes an unspecific calcium mobilisation in 1321N1-GPR17 is ruled out (Figure 33A).

In the presence of W-7 and fluphenazine the maximum elevation of calcium concentration elevation upon GPR17 activation is significantly decreased, whereby the effect of fluphenazine is stronger than that of W-7 (Figure 33B and C). The potency of RA-II-150 increases in the presence of W-7 and fluphenazine from a pEC<sub>50</sub> value of 6.09 (± 0.06) to 6.61 (± 0.09) and 6.46 (± 0.09), respectively (Figure 33D).

Since calmodulin inhibits the IP<sub>3</sub> receptor-mediated calcium release from intracellular stores by direct interaction with these channels, it was expected that the calcium release would be enhanced in the presence of a calmodulin inhibitor.<sup>[86, 87]</sup> Surprisingly, the opposite is observed. However, these results can be explained by the unspecific effects of the antagonists that are used. It was reported that both inhibitors block IP<sub>3</sub> receptors directly in a calmodulin-independent manner.<sup>[88-90]</sup> These data are consistent with the 2-APB data that identifies IP<sub>3</sub> receptors as the responsible calcium release channels.

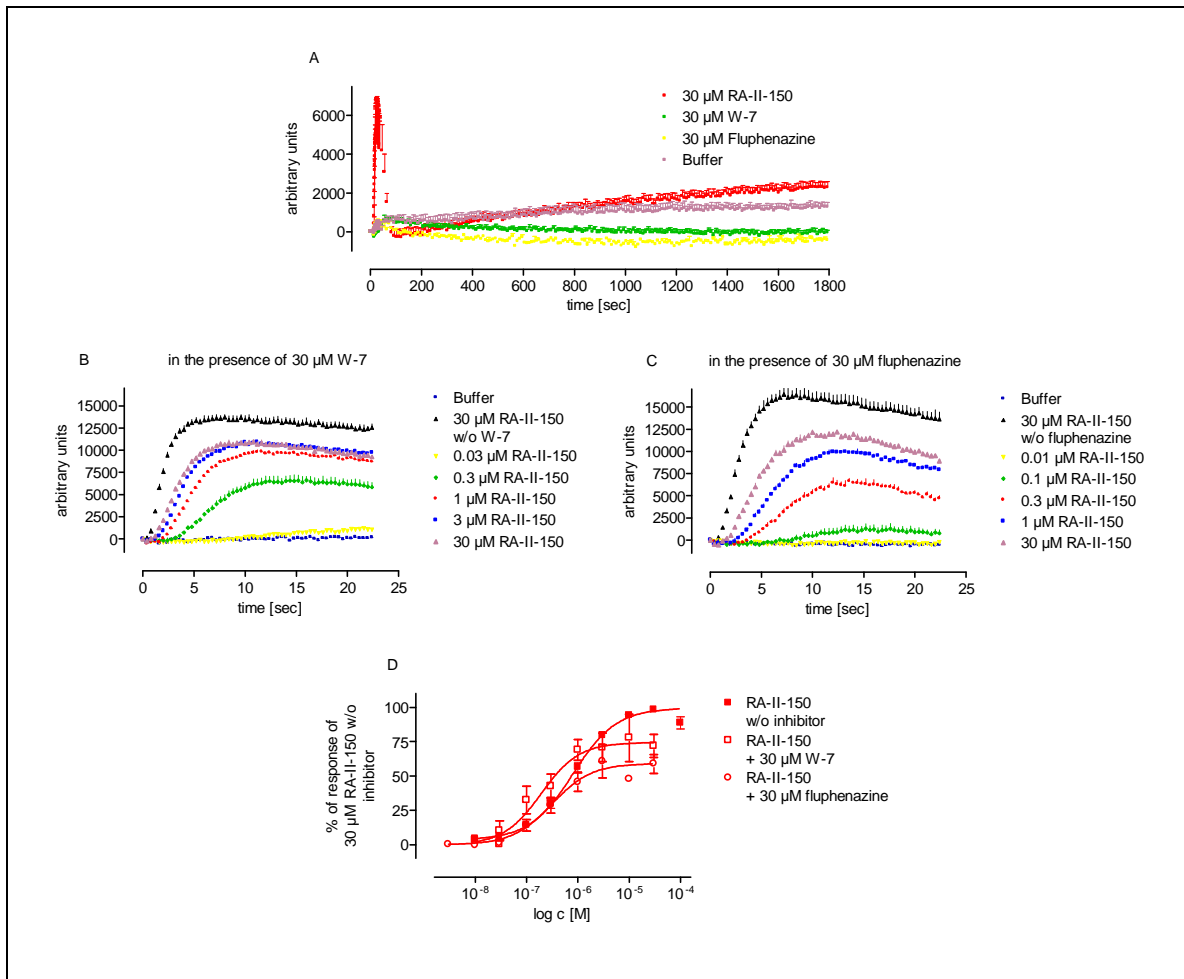


**Figure 33.** Investigations of the role of calmodulin in the calcium release mechanism in 1321N1-GPR17 cells. The effect of two calmodulin inhibitors on the calcium mobilisation mechanism of the calcium signalling of GPR17 after adding RA-II-150 was tested. Within 30 minutes of adding 30  $\mu\text{M}$  W-7 or fluphenazine, respectively, no unspecific calcium mobilisation but rather a decrease in cytoplasmic calcium is detected (A). Representative real-time measurements of intracellular calcium changes upon agonist addition in the presence of 30  $\mu\text{M}$  W-7 (B) or fluphenazine (C) reveal that the maximum calcium response is decreased in contrast to the response under standard conditions. The effect of 30  $\mu\text{M}$  fluphenazine (D;  $n = 5-6$ ) on the maximum calcium response is stronger than that of 30  $\mu\text{M}$  W-7 (D;  $n = 6-7$ ). The potency of RA-II-150 is significantly increased in the presence of both compounds ( $P$  values  $< 0.01$  and  $< 0.05$ ;  $n = 5-29$ ).

### 2.5.8 Protein kinases and their influence on the calcium release mechanism

Finally, the putative influence of protein kinases A (PKA) and protein kinase C (PKC) on the calcium signalling of GPR17 was investigated. Protein kinases modulate a variety of processes within the cell by phosphorylation of the proteins involved. PKA and PKC phosphorylate IP<sub>3</sub> receptors and G protein-coupled receptors and modulate their functions in this way.<sup>[17-20]</sup>

For this reason it was investigated, whether the inhibition of PKA or PKC influences the calcium response of GPR17 upon receptor activation in 1321N1-GPR17 cells.

PKA was inhibited by 1  $\mu$ M H 89 and PKC by 1  $\mu$ M bisindolylmaleimide GF 109203X.<sup>[91, 92]</sup> Neither H 89 nor GF 109203X causes an unspecific calcium elevation in 1321N1-GPR17 within a period of 30 minutes after addition (Figure 34A).

Interestingly, the maximum response is not affected in the presence of the PKA inhibitor and the pEC<sub>50</sub> value ( $6.77 \pm 0.11$ ) is significantly increased (Figure 34B and D), while in the presence of the PKC inhibitor the maximum response of GPR17 upon agonist addition is significantly increased by approximately 50%, and the pEC<sub>50</sub> is unchanged (Figure 34C and D).

The effect of the corresponding protein kinase inhibitor suggests that both kinases modulate the calcium response. Protein kinase C seems to be responsible for the inactivation or desensitisation of certain constituents of the calcium mobilisation mechanism, while the involvement of PKA remains enigmatic. In both cases it remains unclear which pathway constituent is modulated by the phosphorylation of these protein kinases. Further investigations concerning this are necessary.

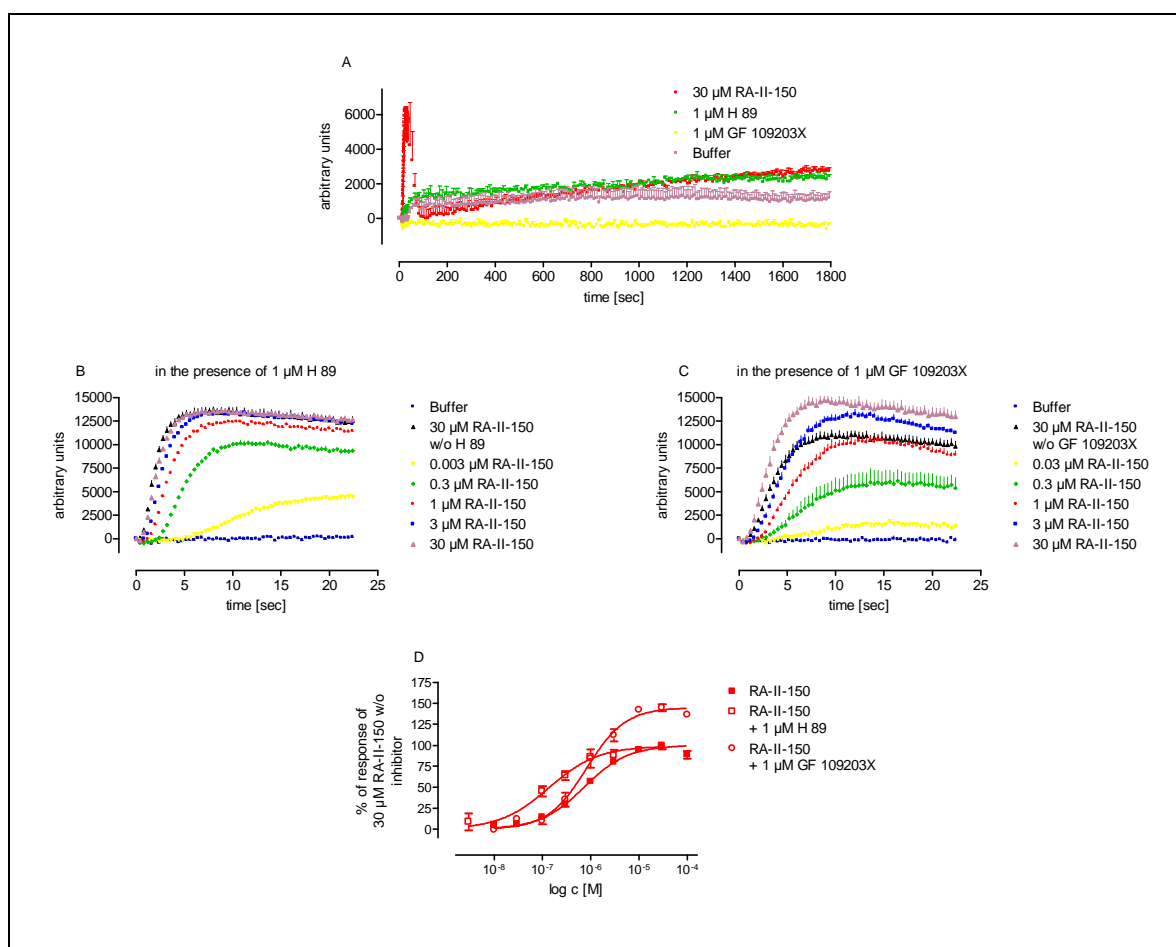


**Figure 34.** Investigations of the modulatory role of protein kinases A and C on the calcium release mechanism in 1321N1-GPR17 cells. Neither 1  $\mu\text{M}$  of the PKA inhibitor H 89 nor 1  $\mu\text{M}$  of the PKC inhibitor GF 109203X cause unspecific calcium mobilisation in 1321N1-GPR17 cells (A). Real-time measurements of the changes in the intracellular calcium concentration upon agonist addition reveal that the maximum calcium response of GPR17 towards RA-II-150 is not significantly affected in the presence of H 89 (B) but is affected in the presence of GF 109203X (C;  $P$  value < 0.001). The  $\text{pEC}_{50}$  value of RA-II-150 is significantly increased in the presence of H 89 (D;  $P$  value < 0.01), while it is not affected in the presence of GF 109203X ( $n = 4-29$ ).

## **2.6 Characterisation of potential endogenous ligands of GPR17**

### **2.6.1 Selected endogenous compounds and biosynthesis pathway intermediates as potential GPR17 ligands**

To gain an insight into the role of an orphan receptor, it is important on the one hand to know when and where it is expressed and on the other to know its endogenous ligand.

For this reason several types of natural products were tested in the cell population based calcium assay.<sup>[66]</sup> It was investigated whether these compounds activate or inhibit GPR17.

### **2.6.2 Selected amino acids and folic acid as potential ligands of GPR17**

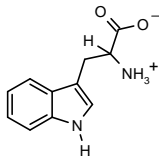
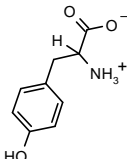
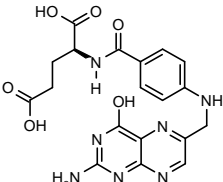
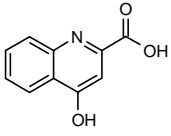
Tryptophane, tyrosine, folic acid and kynurenic acid were tested first. Tryptophane shares the indole scaffold as well as the carboxylic group at a similar position to RA-II-150. Tyrosine shows the carboxylic group at the same distance from a ring structure as the lead compound. Folic acid contains two carboxylic groups and an amino group with the same constitution as in the lead compound RA-II-150.

Tryptophane is metabolised in the kynurenine pathway. Several metabolites of this pathway are proposed to be involved in the pathogenesis of Alzheimer's disease.<sup>[93]</sup> One of these metabolites is kynurenic acid, which is an endogenous antagonist of the N-methyl-*D*-aspartate receptor.<sup>[94]</sup> The antagonistic effect of kynurenic acid leads to a reduction in neuronal damage in primary neuronal cultures exposed to excitotoxins, a reduction in the infarct volume after middle cerebral artery occlusion in rats and the protection of hippocampal pyramidal neurones after transient carotid occlusion in gerbils.<sup>[95-97]</sup>



However, neither the amino acids tryptophane and tyrosine nor folic acid and kynurenic acid activate or inhibit GPR17 (Table 6).

**Table 6.** Summary of the stimulatory and inhibitory effects of test compounds (n = 3-5). Test compounds were applied in a concentration of 30  $\mu$ M. The data are normalised to the response of 30  $\mu$ M (column 2) or 3  $\mu$ M RA-II-150 (column 3). Kynurenic acid was originally provided by Professor Reuter, Institute for Pharmaceutical Biology, University of Jena and a gift of Professor E. Leistner, Institute of Pharmaceutical Biology, University of Bonn.

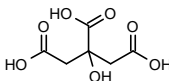
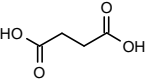
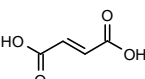
1321N1-GPR17 cells		
Test compound	% of response of test compound ( $\pm$ SEM)	% of inhibition by test compound ( $\pm$ SEM)
 Tryptophane	-0.44 (1.14)	0.43 (1.19)
 Tyrosine	0.36 (0.43)	1.90 (1.76)
 Folic acid	0.43 (1.43)	6.51 (1.69)
 Kynurenic acid	0.19 (0.78)	1.13 (5.91)

### 2.6.3 Selected intermediates of the citric acid cycle as potential GPR17 ligands

Next, three free acids of citric acid metabolites were tested. All the compounds share two carboxylic components with the lead structure RA-II-150.

Neither citric acid and succinic acid nor fumaric acid activate or inhibit GPR17 in calcium assays up to a concentration of 30  $\mu$ M (Table 7).

**Table 7.** Summary of the stimulatory and inhibitory effects of natural occurring organic acids (n = 3-9). Test compounds were applied in a concentration of 30  $\mu$ M. The data are normalised to the response of 30  $\mu$ M (column 2) or 3  $\mu$ M RA-II-150 (column 3).

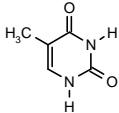
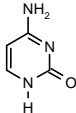
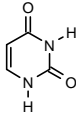
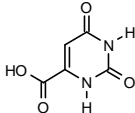
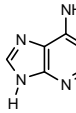
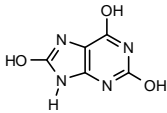
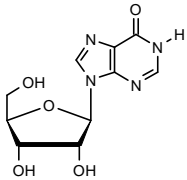
Test compound	1321N1-GPR17 cells	
	% of response of test compound ( $\pm$ SEM)	% of inhibition of test compound ( $\pm$ SEM)
 Citric acid	0.03 (0.27)	1.43 (2.14)
 Succinic acid	0.15 (0.65)	6.78 (1.80)
 Fumaric acid	1.63 (1.48)	4.74 (2.72)

### 2.6.4 Selected purines and pyrimidine bases and a nucleoside as potential GPR17 ligands

Purine and pyrimidine bases are structural elements of nucleic acids. Several of these bases were tested together with orotic acid, an intermediate of the pyrimidine nucleotide synthetic pathway, uric acid and inosine. The latter is commonly found in transfer RNAs.<sup>[98, 99]</sup>

None of the tested compounds showed an ability to activate GPR17 or inhibit the RA-II-150-dependent activation of GPR17 (Table 8).

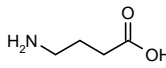
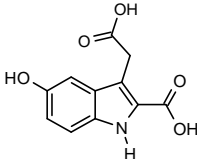
**Table 8.** Summary of the stimulatory and inhibitory effects of test compounds (n = 3-6). Test compounds were applied in a concentration of 30  $\mu$ M. The data are normalised to the response of 30  $\mu$ M (column 2) or 3  $\mu$ M RA-II-150 (column 3).

Test compound	1321N1-GPR17 cells	
	% of response of test compound ( $\pm$ SEM)	% of inhibition by test compound ( $\pm$ SEM)
 Thymine	2.30 (1.63)	0.78 (2.56)
 Cytosine	3.48 (0.92)	0.70 (2.87)
 Uracil	0.43 (0.98)	7.63 (2.22)
 Orotic acid	2.25 (0.76)	0.05 (4.07)
 Adenine	2.20 (0.66)	2.60 (3.86)
 Uric acid	7.63 (2.22)	5.74 (3.07)
 Inosine	3.33 (2.39)	0.46 (3.31)

### 2.6.5 Neurotransmitters and their metabolites as modulators of GPR17

GPR17 expression occurs in tissue which undergoes ischemic damages.<sup>[51]</sup> One of these tissues is the brain. For this reason  $\gamma$ -aminobutyric acid (GABA), the most important inhibitory neurotransmitter in the mammalian central nervous system, and 5-hydroxyindoleacetic acid (5-HIAA), the main metabolite of serotonin, were tested. 5-HIAA is interesting, because its chemical structure shows some similarities to that of RA-II-150. It is composed of an indole scaffold and two carboxylic groups (Table 9). However, neither 5-HIAA nor GABA activate or inhibit GPR17 (Table 9).

**Table 9.** Summary of the agonistic and inhibitory effects of  $\gamma$ -aminobutyric acid (GABA) and 5-hydroxyindoleacetic acid (n = 3-4). Test compounds were applied in a concentration of 30  $\mu$ M. The data are normalised to the response of 30  $\mu$ M (column 2) or 3  $\mu$ M RA-II-150 (column 3).

Test compounds	1321N1-GPR17 cells	
	% of response of test	% of inhibition by test
	compound ( $\pm$ SEM)	compound ( $\pm$ SEM)
 $\gamma$ -aminobutyric acid	0.69 (0.53)	4.56 (2.15)
 5-hydroxyindoleacetic acid	0.74 (2.24)	6.68 (8.95)

In summary, it was not possible to identify the endogenous ligand of GPR17. Only a small number of endogenous compounds were tested here, however, which share structural similarities with the identified agonists and proposed agonists of GPR17. There are probably other essential, but unknown, functional groups in addition to those already identified, in a defined arrangement that are essential features of the endogenous ligand. Until now, GPR17 remains an orphan G protein-coupled receptor.

## 2.7 Products from natural sources as GPR17 modulators

### 2.7.1 Compounds from marine and endophytic fungi and marine sponges

The relevance of compounds from natural, especially marine, sources is summarised in many review articles.<sup>[100-103]</sup> In 2006 more than 650 new compounds from marine sources with biological activities were isolated.<sup>[101]</sup> Mayer *et. al.* report in their review on the preclinical pharmacology of 183 chemically characterised marine compounds.<sup>[103]</sup> The molecular target was identified for 58 of these compounds.<sup>[103]</sup> Most of the compounds are antitumor, antiviral, antibacterial, and antifungal reagents, though compounds were also identified which bind to structures localised on the cell surface. The nicotinic acetylcholine receptor and the ionotropic glutamate receptor are just two examples.<sup>[103]</sup>

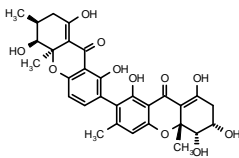
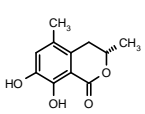
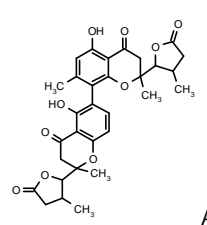
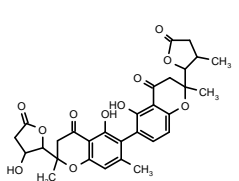
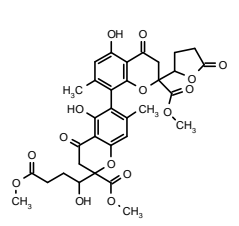
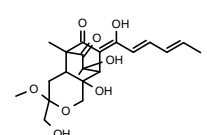
In collaboration with the working group of Professor G. M. König, Institute of Pharmaceutical Biology, University of Bonn, a library of different classes of natural products from different sources was made available and tested in the cell population based calcium assay.<sup>[66]</sup> It was investigated whether these compounds activate or inhibit GPR17.

Dr. Alexander Pontius isolated mellein, a new aromatic polyketide, ascochrom as well as AK 6, AK 7 and 707-4.4-R-2, three heterodimeric chromanones, from different algicolous or endophytic fungi.<sup>[104-106]</sup> Dr. Kerstin Neumann isolated KN935 from the marine derived fungus *Trichoderma saturnisporium* as part of her PhD thesis.

The analysis of these compounds showed that all compounds are inactive (Table 10).

## CHAPTER II: RESULTS

**Table 10.** Agonistic and inhibitory effects of different compounds isolated by Dr. Alexander Pontius. None of the tested compounds showed any agonistic or antagonistic effect (n = 3-4). Test compounds were applied in a concentration of 30  $\mu$ M. The data are normalised to the response of 30  $\mu$ M (column 2) or 3  $\mu$ M RA-II-150 (column 3).

Internal designation of the test compound	1321N1-GPR17 cells	
	% of response of test compound	% of inhibition by test compound
	( $\pm$ SEM)	( $\pm$ SEM)
 Ascochrom	0.09 (0.94)	0.46 (2.44)
 Mellein	0.95 (1.78)	0.67 (5.06)
 AK6	0.19 (0.41)	10.1 (3.73)
 AK7	-0.22 (0.65)	-7.36 (4.03)
 707-4.4-R-2	0.09 (0.81)	2.29 (7.42)
 KN935	0.18 (1.92)	6.23 (5.56)

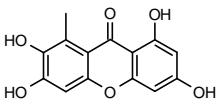
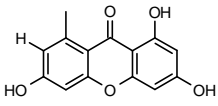
Next, Anomalin A and 3,6,8-trihydroxy-1-methylxanthone were tested. Both were isolated by Ahmed Abdel Lateff and containing a xanthone scaffold.<sup>[107]</sup> The xanthone scaffold of both compounds carries a methyl substitution at position one and hydroxyl substitutions at positions three, six and eight. Anomalin A is differentiated from 3,6,8-trihydroxy-1-methylxanthone by a further hydroxyl substitution at position two (Table 11).

Both compounds were tested for their ability to activate GPR17. Neither anomalin A nor 3,6,8-trihydroxy-1-methylxanthone increased the amount of intracellular calcium (Table 11).

Interestingly, both compounds inhibit GPR17. Anomalin A exhibits a  $pIC_{50}$  of 5.20 and is more potent than 3,6,8-trihydroxy-1-methylxanthone ( $pIC_{50}$  of 4.68 (extrapolated)) (Table 11 and Figure 35).

It was not possible to test these compounds on other related receptors for selectivity purposes because access to them is limited.

**Table 11.** Agonistic and inhibitory effects of Anomalin A and 3,6,8-trihydroxy-1-methylxanthone. Both compounds showed antagonistic effects but no agonistic effects (n = 4-7). Test compounds were applied in a concentration of 30  $\mu$ M (or 10  $\mu$ M). The data are normalised to the response of 30  $\mu$ M (column 3) or 3  $\mu$ M RA-II-150 (column 4).

Internal designation of the test compounds	1321N1-GPR17 cells		
	$pIC_{50}$ ( $\pm$ SEM)	% of response of test compound ( $\pm$ SEM)	% of inhibition by test compound ( $\pm$ SEM)
 Anomalin A	5.20 (0.11)	9.96 (2.11)	86.7 (4.49)
 3,6,8-trihydroxy-1-methylxanthone	4.68 (0.02)	0.11 (0.66) (10 $\mu$ M compound)	62.0 (2.01)

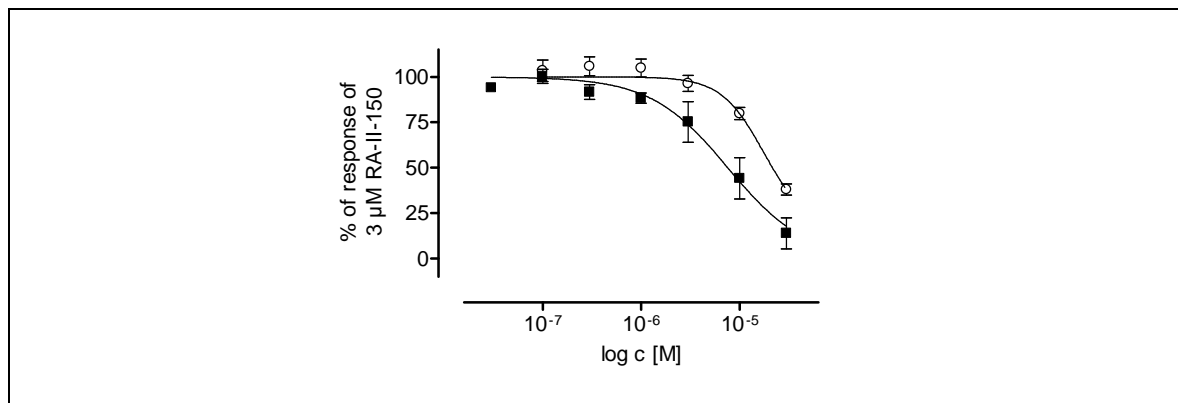


**Figure 35.** Dose response curves of anomalin A (closed squares) and 3,6,8-trihydroxy-1-methylxanthone (open circles). The  $pIC_{50}$  values in 1321N1-GPR17 cells are  $5.20 \mu\text{M}$  ( $\pm 0.11$ ) for anomalin A and  $4.68$  ( $\pm 0.02$ ) ( $n = 4-7$ ) for 3,6,8-trihydroxy-1-methylxanthone.

Finally, a serial of compounds derived from sponges of the species *Dysidea* were tested.<sup>[108, 109]</sup> These compounds are polybrominated and share a diphenyl ether scaffold (Figure 36).

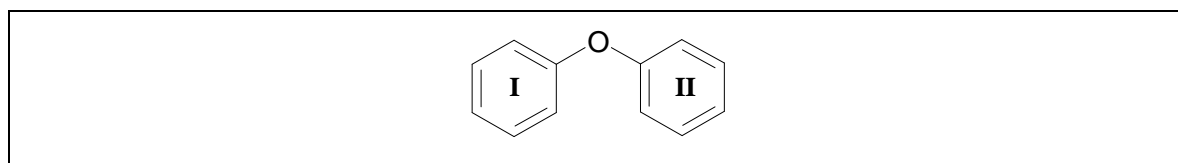


**Figure 36.** Diphenyl ether scaffold of test compounds extracted from sponges of the species *Dysidea*. The aromatic rings are numbered.

Four compounds, numbered *Dysidea* sp. 1 to sp. 4, were tested. All the compounds consist of a dibrominated ring II, with an identical substitution pattern, and a dibrominated (*Dysidea* sp. 3) or tribrominated ring I (*Dysidea* sp. 1, sp. 2 and sp. 3) (Table 12). Furthermore, both ring systems are substituted with a single hydroxyl or methyl ether group (Table 12).

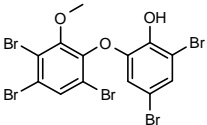
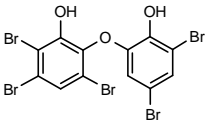
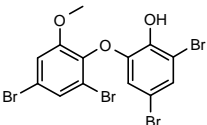
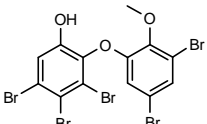
After adding  $30 \mu\text{M}$  test compound, no increase in intracellular calcium concentration is detected but all compounds inhibit GPR17 activation. The compound potencies decrease as followed: *Dysidea* sp. 2 ( $pEC_{50}$  5.37) > *Dysidea* sp. 1 ( $pEC_{50}$  5.14) > *Dysidea* sp. 4 ( $pEC_{50}$  5.04) > *Dysidea* sp. 3 ( $pEC_{50}$  5.03) (Table 12 and Figure 37). *Dysidea* sp. 2, the only compound with a single hydroxyl



group at each ring system, is the most potent compound in this series.

It was not possible to test these compounds on other related receptors for selectivity purposes because access to them is limited.

**Table 12.** Agonistic and inhibitory effects of different Dysidea species (n = 3-5). Test compounds were applied in a concentration of 30  $\mu$ M. The data are normalised to the response of 30  $\mu$ M (column 3) or 3  $\mu$ M RA-II-150 (column 4).

Internal designation of the test compounds	1321N1-GPR17 cells		
	pIC <sub>50</sub> ( $\pm$ SEM)	% of response of test compound ( $\pm$ SEM)	% of inhibition by test compound ( $\pm$ SEM)
 Dysidea sp. 1	5.14 (0.01)	0.70 (1.10)	90.0 (4.33)
 Dysidea sp. 2	5.37 (0.02)	1.63 (3.24)	99.8 (2.99)
 Dysidea sp. 3	5.03 (0.06)	-1.92 (1.16)	86.1 (5.79)
 Dysidea sp. 4	5.04 (0.04)	-1.29 (1.07)	102 (0.91)

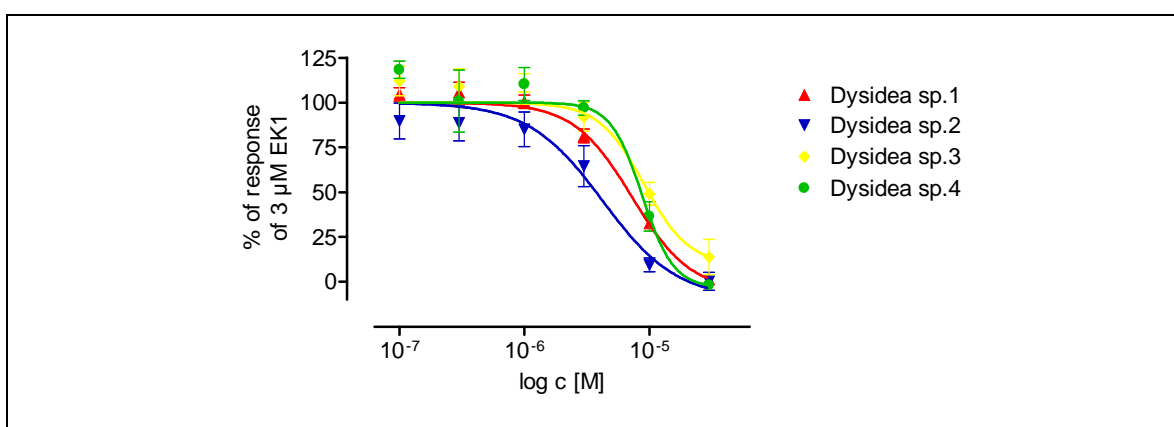


**Figure 37.** Dose response curves of Dysidea sp. 1 (red triangle), sp. 2 (blue triangle), sp. 3 (yellow rhombus) and sp. 4 (green circle). All the compounds show antagonistic activities, though Dysidea sp. 2 is the most potent antagonist.

A comparison of the structure of anomalin A and its derivative identified the hydroxylic group at position 2 as very important for compound potency. The elimination of this group leads to a considerable decrease in potency. No further information is available about important structural elements. Interestingly, the diphenyl ether scaffold of the Dysidea species is completely integrated in the xanthone scaffold of anomalin A and its derivative. However, the scaffold of anomalin A and its derivative is planar, while the aromatic Dysidea rings rotate around the bridging atom. A planar structure and free rotation of both rings around the linking bridge are not possible, because of the ring substitution pattern. Furthermore, the formation of ether at one of the two hydroxylic groups leads to decreased compound potency, indicating the relevance of the free hydroxylic groups.

### 2.7.2 Compounds from bacterial sources

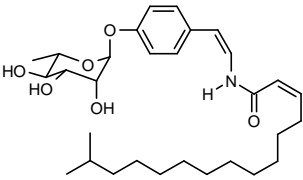
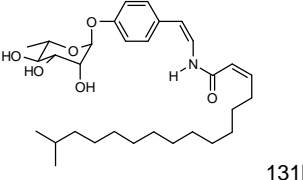
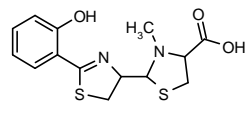
Bacteria are another very important source of new compounds. For this reason a few compounds from this source were tested.

Both 131A and 131B, which were isolated by Dr. Birgit Ohlendorf from the proteobacteria *Mycococcus* sp., have a tyrosine derived core structure glycosylated with rhamnose and acylated with unusual fatty acids such as (Z)-15-methyl-2-hexadecenoic or (Z)-2-hexadecenoic acid.

Pyochelin, a sideophore which was isolated by Dr. Harald Gross, was also tested.<sup>[110]</sup>

All the compounds fail to activate or inhibit GPR17 up to a concentration of 30  $\mu$ M (Table 13).

**Table 13.** Summary of the agonistic and inhibitory effects of 131A, 131B and pyochelin (n = 3-6). Test compounds were applied in a concentration of 30  $\mu$ M. The data are normalised to the response of 30  $\mu$ M (column 2) or 3  $\mu$ M RA-II-150 (column 3).

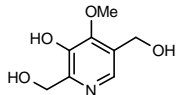
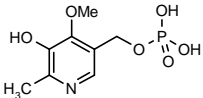
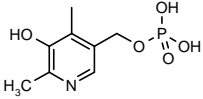
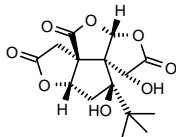
Internal designation of the test compounds	1321N1-GPR17 cells	
	% of response of test compound ( $\pm$ SEM)	% of inhibition by test compound ( $\pm$ SEM)
 131A	0.83 (1.19)	10.4 (2.32)
 131B	2.17 (5.43)	0.78 (6.13)
 Pyochelin	0.24 (2.04)	1.24 (1.71)

### 2.7.3 Compounds from terrestrial plants

Higher plants in particular have a long history of use in the treatment of human diseases, which is why this part focuses on compounds derived from this source. There are many plant-derived drugs on the market or in clinical trials.<sup>[111]</sup> All the compounds described in this part were kindly provided by Professor E. Leistner, Institute of Pharmaceutical Biology, University of Bonn, unless otherwise mentioned.

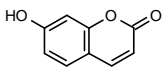
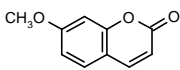
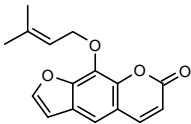
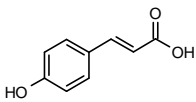
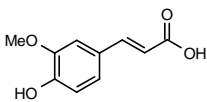
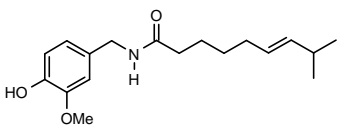
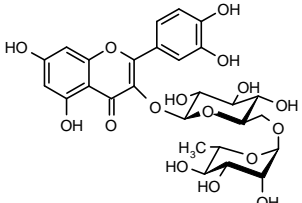
4'-O-Methylpyridoxine, better known as ginkgotoxin, was tested together with its 5' phosphorylated derivative (4'-O-deoxypyridoxine-5'-phosphate). 4'-O-deoxypyridoxine-5'-phosphate is commercially available while bilobalide was provided by the Dr. Willmar Schwabe GmbH and Co. KG, Karlsruhe. All the compounds in this series fail to activate or inhibit GPR17 (Table 14).

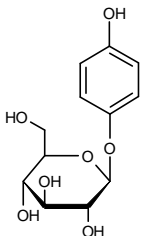
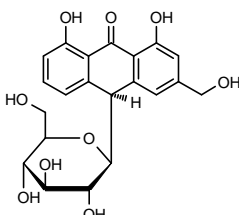
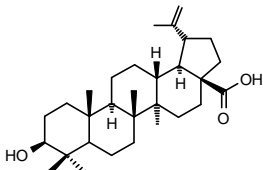
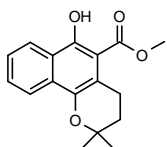
**Table 14.** Agonistic and inhibitory effects of Ginkgotoxin, its derivatives and bilalolide. The natural products of this series do not activate or inhibit GPR17 (n = 3-6). Test compounds were applied in a concentration of 30  $\mu$ M. The data are normalised to the response of 30  $\mu$ M (column 2) or 3  $\mu$ M RA-II-150 (column 3).

Test compounds	1321N1-GPR17 cells	
	% of response of test compound ( $\pm$ SEM)	% of inhibition by test compound ( $\pm$ SEM)
 4'-O-Methylpyridoxine (Ginkgotoxin)	1.79 (0.58)	3.99 (4.29)
 4'-O-Methylpyridoxine-5'-phosphate (Ginkgotoxin phosphate)	3.14 (0.74)	1.50 (4.06)
 4'-Deoxyxypyridoxine-5'-phosphate	2.76 (0.63)	4.94 (3.58)
 Bilalolide	0.30 (1.01)	3.16 (4.38)

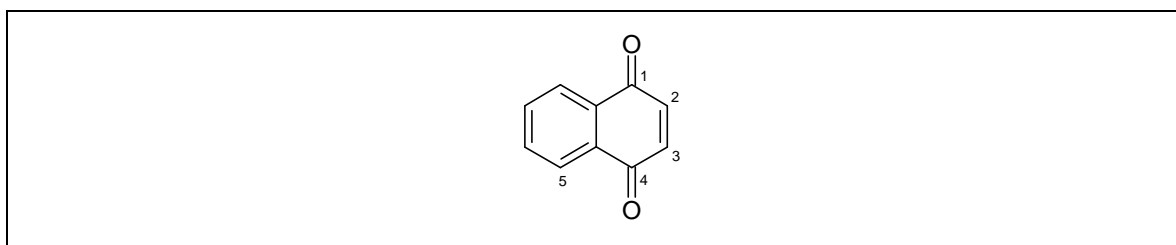
Umbelliferone, herniarin and imperatorin share a coumarin scaffold. p-Coumaric acid is a derivative of cinnamic acid which can be synthesised from phenylalanine and ferullic acid. The alkaloid capsaicin, rutin, a citrus flavonoid glycoside, arbutin, aloin, betulinic acid, which has a pentacyclic triterpene carboxylic acid scaffold, and mollugin were also tested. However, none of compounds shows any activity.

**Table 15.** Agonistic and inhibitory effects of different natural occurring compounds. All the compounds fail to activate or inhibit GPR17 RA-II-150 ( $n = 3-5$ ). Test compounds were applied in a concentration of 30  $\mu\text{M}$ . The data are normalised to the response of 30  $\mu\text{M}$  (column 2) or 3  $\mu\text{M}$  RA-II-150 (column 3). All the compounds are commercially available.

Chemical structure and designation of the test compounds	1321N1-GPR17 cells	
	% of response of test compound	% of inhibition by test compound
	( $\pm$ SEM)	( $\pm$ SEM)
 Umbelliferone	-1.84 (0.50)	5.65 (2.78)
 Herniarin	-0.43 (0.53)	11.0 (1.45)
 Imperatorin	-0.53 (0.83)	2.11 (3.51)
 p-Coumaric acid	0.93 (1.08)	8.85 (1.35)
 Ferulic acid	-0.93 (0.39)	-1.39 (1.46)
 Capsaicin	1.16 (0.73)	0.70 (4.58)
 Rutin	0.02 (2.16)	4.62 (9.04)

Chemical structure and designation of the test compounds	1321N1-GPR17 cells	
	% of response of test	% of inhibition by test
	compound ( $\pm$ SEM)	compound ( $\pm$ SEM)
 <p>Arbutin</p>	2.71 (1.27)	3.70 (6.99)
 <p>Aloin</p>	0.32 (0.75)	2.11 (4.04)
 <p>Betulinic acid</p>	-0.12 (0.60)	0.27 (2.20)
 <p>Mollugin</p>	0.97 (1.59)	0.57 (5.49)

A series of compounds with a naphthoquinone scaffold were tested next (Figure 38).

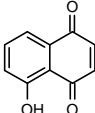
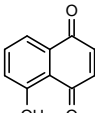
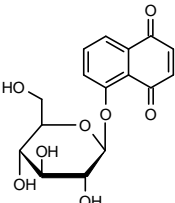
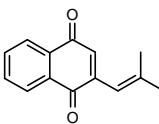
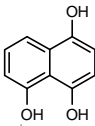
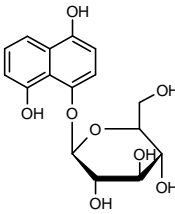


**Figure 38.** Naphthoquinone scaffold of juglone and its derivatives. The positions of the substitutions are numbered.

Juglone, its  $\beta$ -D-glucoside and hydrojuglone and its  $\beta$ -D-glucopyranoside neither

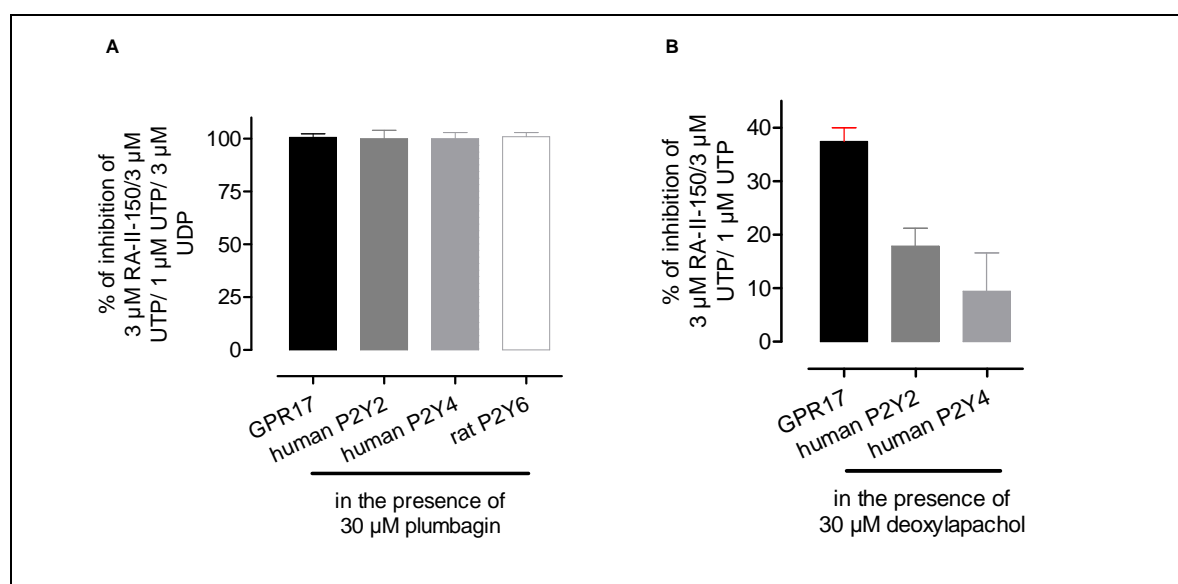
activate nor inhibit GPR17. Plumbagin and deoxylapachol, two derivatives of juglone, do not activate GPR17 but inhibit GPR17 activation in a concentration-dependent manner. The receptor activation is inhibited by 99.8% and 37.4% respectively in the presence of 30  $\mu\text{M}$  plumbagin and deoxylapachol (Table 16).

**Table 16.** Agonistic and inhibitory effects of compounds containing a naphthoquinone scaffold. The compounds were tested for their ability to activate or inhibit GPR17 in a calcium assay ( $n = 3-7$ ). Test compounds were applied in a concentration of 30  $\mu\text{M}$ . The data are normalised to the response of 30  $\mu\text{M}$  (column 2) or 3  $\mu\text{M}$  RA-II-150 (column 3).

Test compounds	1321N1-GPR17 cells	
	% of response of test compound ( $\pm$ SEM)	% of inhibition by test compound ( $\pm$ SEM)
 Juglone	1.74 (1.05)	6.34 (5.95)
 Plumbagin	0.21 (1.07)	99.8 (0.97)
 Juglone- $\beta$ -D-glucoside	2.07 (1.08)	3.30 (2.75)
 Deoxylapachol	1.48 (0.53)	37.4 (2.58)
 Hydrojuglone	-2.13 (1.07)	6.98 (2.64)
 4,8-Dihydroxy-1-naphthalenyl- $\beta$ -D-glucopyranoside	0.43 (0.85)	10.7 (3.14)

The selectivity of plumbagin and deoxylapachol was investigated by testing their inhibitory effects on related receptors like human P2Y<sub>2</sub> and P2Y<sub>4</sub> as well as rat P2Y<sub>6</sub>. Apparently, plumbagin also blocks the calcium response of human P2Y<sub>2</sub>, human P2Y<sub>4</sub> and rat P2Y<sub>6</sub> towards their corresponding standard agonists (Figure 39A). Even human P2Y<sub>2</sub> and P2Y<sub>4</sub> are blocked by deoxylapachol, the inhibitory effect of which is more selective for GPR17 than for the other two receptors (Figure 39B).

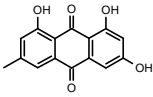
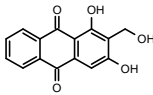
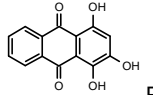
Finally, a serial of natural products which share an anthraquinone scaffold were tested.<sup>[112, 113]</sup> Whereas emodin and lucidin neither activate nor inhibit GPR17, purpurin inhibited GPR17 activation without leading to any increase in intracellular calcium concentration on its own (Table 17).



**Figure 39.** Investigations of compound selectivity. Since plumbagin blocks related receptors, such as human P2Y<sub>2</sub>, P2Y<sub>4</sub> and rat P2Y<sub>6</sub>, its inhibitory effect is not selective for GPR17 (A). By contrast, deoxylapachol is more selective for GPR17 than plumbagin (B). Therefore, the receptor calcium response upon addition of 3 μM UTP, 1 μM UTP or 3 μM UDP in the presence of 30 μM test compound was related to the corresponding response in the absence of test compound.



**Table 17.** Summary of the agonistic and inhibitory effects of different natural products ( $n = 3-5$ ). Test compounds were applied in a concentration of  $30 \mu\text{M}$ . The data are normalised to the response of  $30 \mu\text{M}$  (column 2) or  $3 \mu\text{M}$  RA-II-150 (column 3). All the test compounds are commercially available.

Test compounds	1321N1-GPR17 cells	
	% of response of test compound	% of inhibition by test compound
	( $\pm$ SEM)	( $\pm$ SEM)
 Emodin	0.97 (1.16)	2.53 (10.1)
 Lucidin	1.48 (0.67)	0.26 (3.73)
 Purpurin	4.06 (0.73)	71.1 (2.33)

Purpurin was tested for its ability to inhibit other related receptors of GPR17. The inhibitory effect of purpurin is selective for GPR17 compared to the activity on human  $\text{P2Y}_2$  and  $\text{P2Y}_4$  (Figure 40).

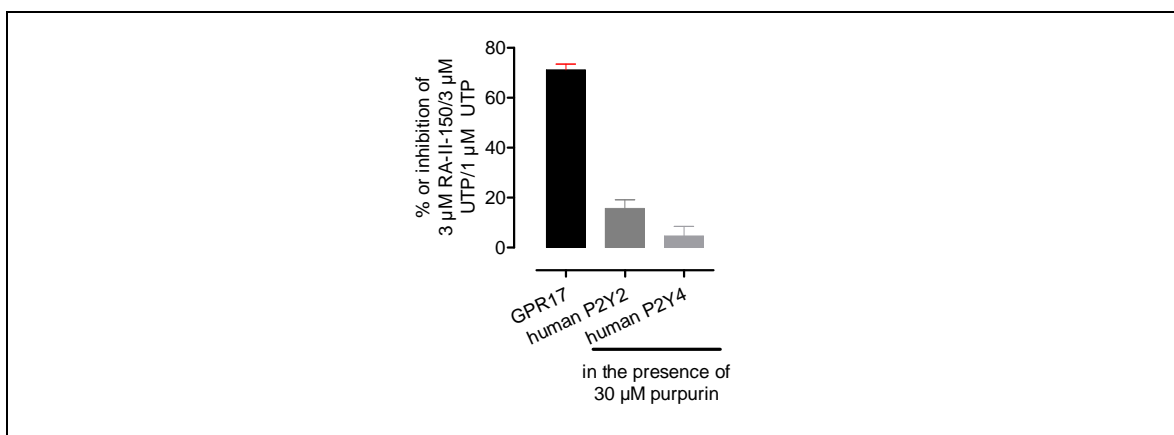


**Figure 40.** Determination of compound selectivity. The inhibitory effect of purpurin on human  $\text{P2Y}_2$  and  $\text{P2Y}_4$  receptor is less than on GPR17 in a calcium assay ( $n = 3-4$ ).

Plumbagin and deoxylapachol, both GPR17 inhibitors, share a 1,4-naphthoquinone scaffold whereas juglone with the same scaffold and hydrojuglone with a very similar scaffold are inactive. It seems that further

methylation or 2-methylpropenylation at a certain position is essential for activity. In addition, the hydroxylation of the 1,4-naphthoquinone scaffold terminates compound activity. The scaffold of these two compounds is a substructure of the purpurin scaffold, another inhibitor of GPR17. However, a comparison of purpurin, which is multiply hydroxylated, with related structures does not allow any definite statement about essential substitution patterns.

## 2.8 Characterisation of synthetic anthraquinone compounds as negative modulators of GPR17

As already described earlier, GPR17 is closely related to the P2Y receptor family. Compounds with an anthraquinone scaffold (Figure 41), such as reactive blue 2, had been characterised as antagonists for P2Y<sub>12</sub>.<sup>[114]</sup> A few further investigations concerning the antagonistic behaviour of these compounds were carried out on the P2Y<sub>1</sub>-like receptor, the P2Y<sub>2</sub> receptor, the P2Y<sub>12</sub> receptor, the P2X receptors and ectonucleoside triphosphate diphosphohydrolases.<sup>[115-120]</sup> These compounds were synthesised by Dr. Stefanie Weyler and Dr. Younis Baqi of the group of Professor C. E. Müller, Pharmaceutical Institute, Pharmaceutical Chemistry I, University of Bonn.<sup>[119, 121, 122]</sup> They share a 1,4-diamino-2-sulfoanthraquinone scaffold which is substituted with different aliphatic or aromatic side chains over the amino group at position 4 (Figure 41).

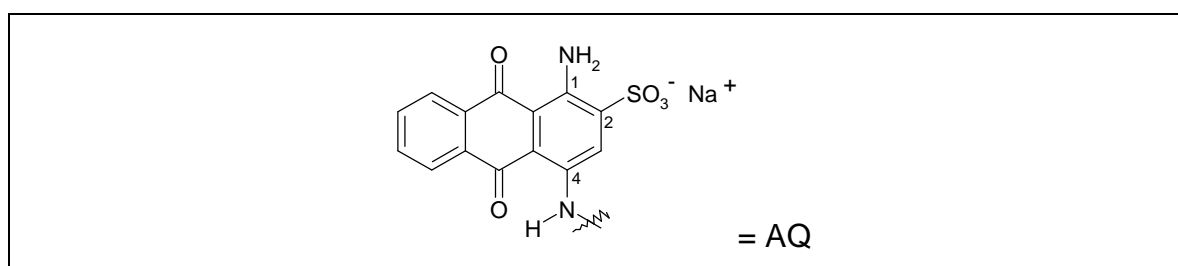


**Figure 41.** Anthraquinone scaffold of test compounds. All the test compounds share an anthraquinone scaffold, which is substituted with one sulphonate and two amino groups whereas one amino group functions as the linker to the varied residue. This scaffold structure is abbreviated in the following tables as “AQ.”

### 2.8.1 Substitution of the anthraquinone scaffold with a phenyl group

A group of anthraquinones with a single phenyl substituent at position 4 were tested, whereas the phenyl ring contained different substitution patterns (Figure 42). This group consists of 55 members, whereas 27 compounds were already characterised for at least one of the following receptors: P2Y<sub>1</sub>-like receptor, P2Y<sub>2</sub> and/or P2Y<sub>12</sub>. The results of certain compounds for the P2Y<sub>12</sub> and P2Y<sub>2</sub> receptor are especially interesting.

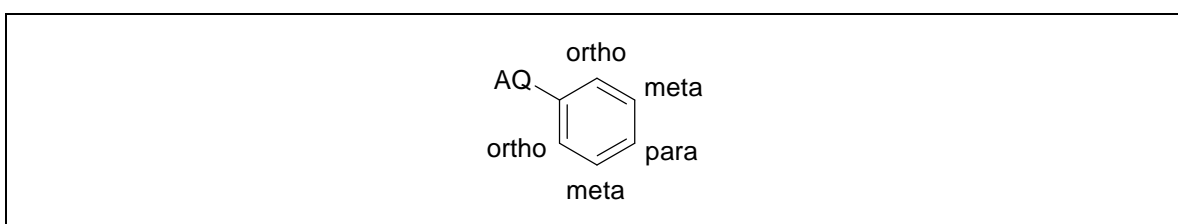


**Figure 42.** Phenyl scaffold of anthraquinone (AQ) side chains.

The IC<sub>50</sub> values for selected anthraquinones were determined for 1321N1 astrocytoma cells stably expressing P2Y<sub>2</sub> receptors in a cell population based calcium assay comparable to that already described (2.2.1) but using another microplate reader.<sup>[123-125]</sup> Anthraquinones already tested for the P2Y<sub>2</sub> receptor were potent in the following order [IC<sub>50</sub> in μM]: YB033 [3.04] > YB022 [5.31] > YB076 [5.43] > YB025 [5.61] > YB075 [7.95] > YB072 [9.26] > YB016 [9.82] > YB071 = YB015 [11.5] > YB077 [15] > YB036 [24.9] > YB062 [> 30].<sup>[119]</sup>

Baqi *et. al.* determined the K<sub>i</sub> value of selected anthraquinones for P2Y<sub>12</sub> in radioligand binding assays at human platelet membranes.<sup>[114]</sup> The affinities of the tested anthraquinones for the P2Y<sub>12</sub> receptor decrease as follows [K<sub>i</sub> in μM]: YB001 [2.1] > YB002 [2.39] > YB045 [3.13] > YB062 [6.76] > YB003 [7.07] > YB022 [7.35] > YB025 [9.83] > YB004 [12.2] > YB007 [12.3] > YB005 [25.1]. The K<sub>i</sub> values of several other compounds were ~10 or >10 (YB010, YB11 and YB020, YB019, YB028, YB023).<sup>[114]</sup>

All compounds of this series were tested for their agonistic and antagonistic behaviour at GPR17 in a cell population based calcium assay. A DRC of the compound was determined in case of activity. For this purpose compound concentrations up to a concentration of 30 μM or 100 μM were tested. Even

unspecific calcium mobilisation as a matter of compound addition was determined up to a concentration of 10  $\mu\text{M}$ . Named unspecific effects at concentrations higher than 10  $\mu\text{M}$ , which may led to the observed antagonistic effects of a test compound, could be ruled out by performing a so-called validation. Since the compounds are preincubated with the cells unspecific mobilisation events could be detected in form of a concentration-dependent enhanced background fluorescence, which was determined by the validation. Unless otherwise mentioned, no increased background fluorescence was detected at concentrations higher than 10  $\mu\text{M}$ .

Apart from YB001, YB002 shows the highest affinity towards P2Y<sub>12</sub>. YB001 and YB002 are constitutional isomers, whereas the sulphonate and amino groups are substituted with each other. However, the potency of YB001 in the 1321N1-GPR17 test system is considerably reduced ( $\text{pIC}_{50}$  4.27) compared to that of YB002, a very potent compound at GPR17 ( $\text{pIC}_{50}$  5.45).

When the sulphonate group of YB002 is substituted with a carboxylate group (YB037;  $\text{pIC}_{50}$  4.28), the potency decreases to a similar level compared to YB001 (Table 18).

All compounds which carry a single carboxylic group or an additional substitution besides this substitution are considerably less active or completely inactive. These compounds are: YB003 ( $\text{pIC}_{50}$  4.33), YB004 ( $\text{pIC}_{50}$  4.69), YB005 (inactive), YB006 ( $\text{pIC}_{50}$  4.66), YB007 ( $\text{pIC}_{50}$  4.45), YB008, YB038 (inactive), YB046 ( $\text{pIC}_{50}$  4.89), YB049, YB051 ( $\text{pIC}_{50}$  4.27), YB052 (inactive) and YB053 ( $\text{pIC}_{50}$  4.70). YB004, YB007 and YB005 are also less active on the P2Y<sub>12</sub> receptor. By contrast, YB003 shows a high affinity to P2Y<sub>12</sub> but a reduced activity towards GPR17 (Table 18).

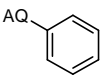
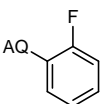
A single methylation at the meta position is well accepted (YB033;  $\text{pIC}_{50}$  5.41) but at the para position (YB036;  $\text{pIC}_{50}$  4.62) the potencies decrease considerably. The  $\text{pEC}_{50}$  value for YB033 on the P2Y<sub>2</sub> receptor is 5.52 and therefore comparable to that on GPR17 ( $\text{pIC}_{50}$  5.41) (Table 18). Furthermore, YB033 is one of the most potent compounds in this series.

A single methoxylation at the ortho (YB016;  $\text{pIC}_{50}$  4.93) or para (YB015;  $\text{pIC}_{50}$  4.99) position leads to less active compounds than methoxylation at the meta position (YB012;  $\text{pIC}_{50}$  5.26). However, a combination of both ortho and para substitution leads to a compound (YB078;  $\text{pIC}_{50}$  5.21) that is similarly potent to the single meta substituted compound (YB012).

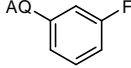
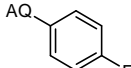
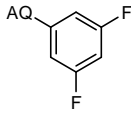
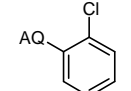
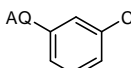
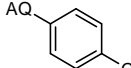
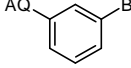
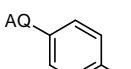
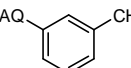
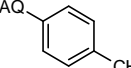
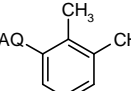
Next, compounds with a monoamino-substituted phenyl ring were tested. YB019 is para amino substituted and with a  $pI_{C_{50}}$  of 5.11 more potent than the meta amino substituted YB021 ( $pI_{C_{50}}$  4.95) and YB020 ( $pI_{C_{50}}$  4.69), which is ortho amino substituted (Table 18). The potency of YB021 is considerably enhanced when additional methylation occurs at the ortho position (YB048;  $pI_{C_{50}}$  5.29). An additional sulphonation at the meta position (YB002; 5.45) likewise increases the potency of YB019. By contrast, sulphonation of YB021 at the para position decreases the potency, resulting in a  $pI_{C_{50}}$  of 4.27 (YB001) (Table 18).

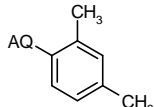
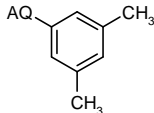
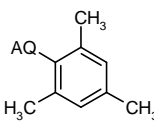
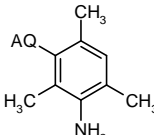
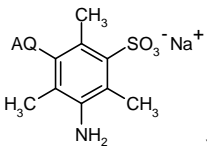
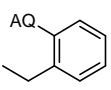
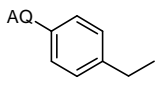
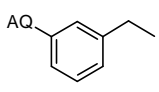
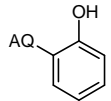
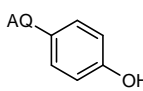
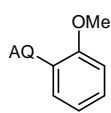
Compounds with a halogenated phenyl ring were analysed subsequently. Here, the anthraquinone with the mono chlorinated phenyl ring at the ortho position (YB084) is more potent with a  $pI_{C_{50}}$  of 5.42 than that with a mono fluorination at the meta position (YB096;  $pI_{C_{50}}$  5.34) or a bromination at the para position (YB034;  $pI_{C_{50}}$  4.97) (Table 18). YB084 is the most potent antagonist in this series at GPR17 apart from YB011 and YB002. YB011 ( $pI_{C_{50}}$  of 5.46), which was not tested on either P2Y<sub>2</sub> or P2Y<sub>12</sub>, carries a hydroxyl substitution at the para position. When the phenyl ring is hydroxylated at the ortho position (YB010), the potency decreases to a  $pI_{C_{50}}$  of 5.05 and disappears if a carboxylic group is also added at the meta position (YB046;  $pI_{C_{50}}$  4.89) (Table 18).

**Table 18.**  $pI_{C_{50}}$  and inhibition values of anthraquinone derivatives with a phenyl substitution. The increase in intracellular calcium as a result of compound addition is also summarised ( $n = 3-4$ ). Test compounds were applied in a concentration of 10  $\mu$ M (columns 3 and 4). The data are normalised to the response of 3  $\mu$ M (column 3) or 30  $\mu$ M RA-II-150 (column 4). For some compounds no  $pI_{C_{50}}$  value could be determined, because they were inactive or their potencies were too small (n.d.).

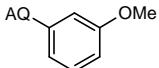
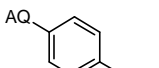
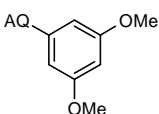
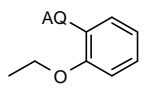
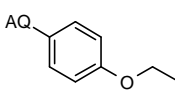
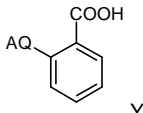
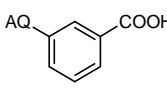
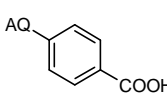
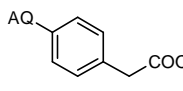
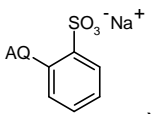
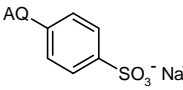
Side residue and internal designation of the test compounds	1321N1-GPR17 cells		
	$pI_{C_{50}}$ ( $\pm$ SEM)	% of inhibition by test compound ( $\pm$ SEM)	% of calcium efflux of test compound ( $\pm$ SEM)
 YB025	5.12 (0.01)	70.9 (1.68)	2.40 (1.50)
 YB095	5.34 (0.02) (not completely soluble)	62.0 (3.10)	3.14 (3.04)

## CHAPTER II: RESULTS

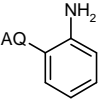
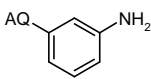
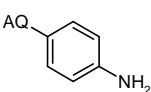
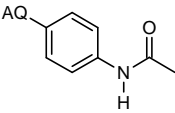
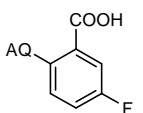
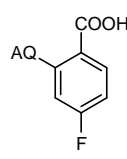
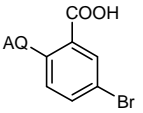
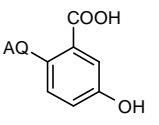
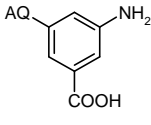
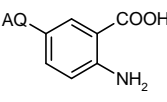
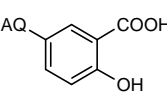
Side residue and internal designation of the test compounds	1321N1-GPR17 cells		
	pIC <sub>50</sub> (± SEM)	% of inhibition by test compound (± SEM)	% of calcium efflux of test compound (± SEM)
 YB096	5.34 (0.15)	61.4 (3.84)	1.75 (1.07)
 YB013	4.93 (0.13) (not completely soluble)	30.3 (3.27)	1.14 (0.54)
 YB079	5.13 (0.09) (not completely soluble)	61.7 (3.86)	6.44 (2.32)
 YB084	5.42 (0.06)	79.9 (3.08)	-0.31 (1.45)
 YB062	n. d. (not completely soluble)	24.7 (3.38)	2.19 (1.67)
 YB022	5.21 (0.08) (not completely soluble)	57.4 (4.79)	0.36 (0.29)
 YB014	4.93 (0.03) (stock solution not completely dissolved)	34.5 (2.27)	3.01 (1.39)
 YB034	4.97 (0.03)	41.2 (4.15)	0.02 (0.52)
 YB033	5.41 (0.07)	91.8 (2.12)	1.55 (0.62)
 YB036	4.62 (0.33)	9.56 (1.83)	-0.19 (0.37)
 YB075	5.11 (0.08) (not completely soluble)	64.3 (3.40)	0.59 (1.42)

Side residue and internal designation of the test compounds	1321N1-GPR17 cells		
	pIC <sub>50</sub> (± SEM)	% of inhibition by test compound (± SEM)	% of calcium efflux of test compound (± SEM)
 YB076	5.19 (0.18) (not completely soluble)	58.9 (3.64)	4.47 (1.20)
 YB059	4.96 (0.12)	35.8 (5.80)	0.03 (0.54)
 YB028	5.06 (0.10) (not completely soluble)	45.7 (8.13)	2.24 (1.64)
 YB023	5.14 (0.12)	66.0 (4.88)	0.14 (0.85)
 YB024	4.38 (0.34)	31.7 (4.07)	2.01 (1.48)
 YB072	5.06 (0.04)	65.7 (5.16)	2.47 (1.32)
 YB073	5.01 (0.04) (not completely soluble)	50.8 (3.52)	-0.09 (0.97)
 YB074	5.15 (0.09) (not completely soluble)	68.2 (6.66)	-2.23 (0.40)
 YB010	5.05 (0.21)	40.6 (4.88)	2.61 (0.79)
 YB011	5.46 (0.02)	92.6 (1.38)	1.51 (1.01)
 YB016	4.93 (0.03)	23.9 (3.56)	0.53 (0.97)

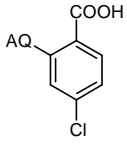
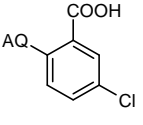
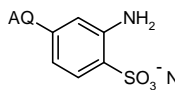
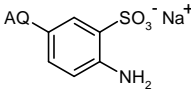
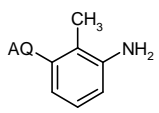
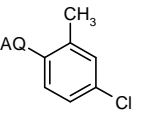
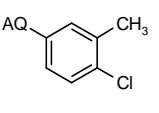
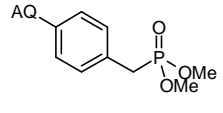
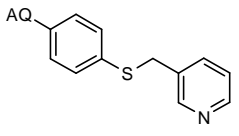
## CHAPTER II: RESULTS

Side residue and internal designation of the test compounds	1321N1-GPR17 cells		
	pIC <sub>50</sub> (± SEM)	% of inhibition by test compound (± SEM)	% of calcium efflux of test compound (± SEM)
 YB012	5.26 (0.05)	73.1 (1.08)	2.41 (0.83)
 YB015	4.99 (0.01)	51.0 (5.29)	0.03 (0.50)
 YB078	5.21 (0.02)	72.6 (3.97)	1.46 (0.57)
 YB077	4.99 (0.22)	50.1 (5.87)	0.47 (1.24)
 YB071	5.09 (0.09)	60.1 (4.08)	1.37 (0.82)
 YB005	n. d.	0.58 (1.23)	0.86 (3.19)
 YB006	4.66 (0.17)	14.2 (5.58)	0.49 (1.84)
 YB008	4.98 (0.02) (no complete inhibition up to 30 μM)	18.4 (1.97)	0.19 (0.59)
 YB038	n. d.	0.64 (2.72)	2.74 (3.32)
 YB009	5.15 (0.14)	47.1 (5.57)	-0.38 (0.73)
 YB045	4.42 (0.29)	29.2 (4.71)	1.06 (0.69)



Side residue and internal designation of the test compounds	1321N1-GPR17 cells		
	pIC <sub>50</sub> (± SEM)	% of inhibition by test compound (± SEM)	% of calcium efflux of test compound (± SEM)
 YB020	4.69 (0.24)	10.7 (5.40)	-2.67 (0.94)
 YB021	4.95 (0.03)	48.0 (2.60)	0.26 (0.71)
 YB019	5.11 (0.03)	63.2 (2.31)	1.83 (1.22)
 YB047	4.98 (0.01) (not completely soluble)	32.9 (1.97)	1.17 (0.80)
 YB052	n. d.	6.66 (4.65)	-1.18 (0.71)
 YB053	4.70 (0.61)	6.20 (4.98)	0.97 (1.86)
 YB051	4.27 (0.24)	35.2 (4.82)	1.22 (1.24)
 YB049	4.75 (0.15) (not completely soluble)	17.6 (2.02)	1.48 (0.84)
 YB003	4.33 (0.11)	9.76 (5.21)	0.15 (0.92)
 YB037	4.28 (0.33)	5.89 (2.40)	0.36 (0.42)
 YB046	4.89 (0.03)	26.3 (2.85)	2.02 (1.17)

## CHAPTER II: RESULTS

Side residue and internal designation of the test compounds	1321N1-GPR17 cells		
	pIC <sub>50</sub> (± SEM)	% of inhibition by test compound (± SEM)	% of calcium efflux of test compound (± SEM)
 YB004	4.69 (0.23)	44.1 (9.90)	-1.12 (0.51)
 YB007	4.45 (0.23)	17.3 (4.68)	-2.15 (0.67)
 YB001	4.27 (0.35)	11.0 (3.62)	0.21 (1.04)
 YB002	5.46 (0.00)	93.5 (2.29)	0.95 (1.27)
 YB048	5.29 (0.17)	70.3 (6.54)	0.14 (2.54)
 YB089	4.97 (0.20)	39.1 (4.74)	0.11 (0.56)
 YB085	5.06 (0.04) (not completely soluble)	51.2 (1.59)	2.09 (1.54)
 YB031	n. d. (not completely soluble)	10.3 (3.66)	0.38 (1.59)
 YB099	5.34 (0.14) (not completely soluble)	61.4 (6.87)	0.69 (0.87)

### 2.8.2 Substitution of the anthraquinone with a side chain containing a benzyl or phenethyl scaffold or an ethylthiophenyl side chain

This compound series consists of 10 compounds with an unsubstituted or substituted benzyl or phenethyl scaffold or an ethylthiophenyl (Table 19).

Some compounds in this series are similar to those in Table 18, except that the corresponding phenyl ring is not directly linked to the anthraquinone over the amino group but by a methyl or ethyl bridge (Table 19).

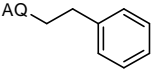
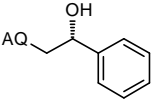
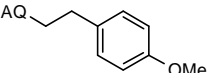
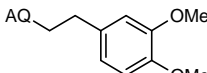
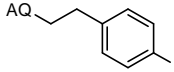
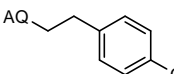
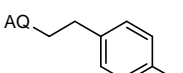
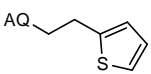
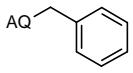
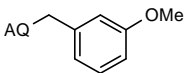
Whereas YB025 carries the phenyl ring directly at the amino group of the anthraquinone (Table 18), YB035 is the benzyl substituted derivative of YB025. YB035 has a  $K_i$  of  $\gg 10$  at P2Y<sub>12</sub> but is inactive on GPR17.<sup>[114]</sup> The ethyl bridge of YB094 does not affect the potency compared to YB025. Both compounds have a pIC<sub>50</sub> of 5.12 (Table 18 and Table 19). Whereas fluorination of the phenethyl ring at the para position (YB093) increases the potency compared to YB094 (pIC<sub>50</sub> of 5.22), the activity of YB094 decreases drastically when the ethyl linker is hydroxylated (YB088; pIC<sub>50</sub> 4.46) (Table 19).

YB029 is meta and para methoxylated and does not show any antagonistic activity (Table 19). If the phenyl ring of YB094 is replaced by a thiophene, the potency decreases considerably (pIC<sub>50</sub> 4.92).

YB082 carries a benzyl ring which is methoxylated at the meta position. In contrast to the inactive YB035, which carries the unsubstituted benzyl ring, YB082 is the most potent compound in this series with a pIC<sub>50</sub> of 5.41. This compound is similarly potent to YB011 (pIC<sub>50</sub> 5.46). YB081, with a para hydroxylated phenethyl ring, is only slightly less active than YB011 (pIC<sub>50</sub> 5.25).

## CHAPTER II: RESULTS

**Table 19.** pIC<sub>50</sub> and inhibition values of anthraquinone derivatives containing a phenyl substitution. The increase in intracellular calcium as a result of compound addition is also summarised (n = 3). Test compounds were applied in a concentration of 10 μM (columns 3 and 4). The data are normalised to the response of 3 μM (column 3) or 30 μM RA-II-150 (column 4).

Side residues and internal designation of the test compounds	1321N1-GPR17 cells		
	pIC <sub>50</sub> (± SEM)	% of inhibition by test compound (± SEM)	% of calcium efflux of test compound (± SEM)
 YB094	5.12 (0.12)	60.5 (7.44)	4.86 (4.10)
 YB088	4.46 (0.39)	14.2 (2.07)	-1.00 (1.32)
 YB080	5.03 (0.13) (not completely soluble)	43.6 (6.25)	0.45 (1.03)
 YB029	n. d.	12.7 (7.22)	0.45 (1.83)
 YB093	5.22 (0.11)	72.8 (3.71)	1.72 (0.46)
 YB087	5.47 (0.03) (not completely soluble)	60.5 (3.81)	0.84 (1.16)
 YB081	5.25 (0.06)	59.9 (4.71)	1.06 (0.50)
 YB083	4.92 (0.05)	42.6 (2.33)	-3.52 (1.60)
 YB035	n. d.	10.1 (1.97)	1.22 (0.71)
 YB082	5.41 (0.23)	77.4 (5.22)	-0.05 (3.42)

### 2.8.3 Substitution of the anthraquinone containing an aliphatic scaffold

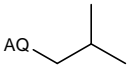
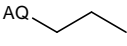
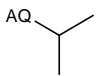
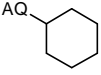
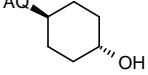
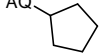
This series of anthraquinones is substituted with a relatively simple aliphatic side chain (Table 20). The compounds were not tested on other receptors.

In YB090 the cyclohexane is replaced by a cyclopentane. This replacement leads to a slightly less active compound than YB032.

Three compounds carry an isobutane (YB086), propane (YB091) or isopropane (YB092) scaffold. These compounds are less potent than YB090 or YB032 (Table 20).

YB042 carries a hydroxyl-substituted cyclohexane side chain (Table 20). This is the only inactive compound in this series. By contrast, YB032 carries a nonsubstituted cyclohexane side chain. With a  $pIC_{50}$  of 5.03 it is the most potent antagonist in this series.

**Table 20.**  $pIC_{50}$  and inhibition values of anthraquinone derivatives containing an aliphatic side chain. The increase in intracellular calcium concentration as a result of compound addition is also summarised ( $n = 3$ ). Test compounds were applied in a concentration of 10  $\mu$ M (columns 3 and 4). The data are normalised to the response of 3  $\mu$ M (column 3) or 30  $\mu$ M RA-II-150 (column 4).

Side residues and internal designation of the test compounds	1321N1-GPR17 cells		
	$pIC_{50}$ ( $\pm$ SEM)	% of inhibition by test compound ( $\pm$ SEM)	% of calcium efflux of test compound ( $\pm$ SEM)
 YB086	4.75 (0.15)	18.8 (2.22)	-2.47 (1.09)
 YB091	4.83 (0.12)	13.6 (6.16)	0.39 (0.66)
 YB092	4.65 (0.13)	10.7 (8.12)	6.21 (3.27)
 YB032	5.03 (0.05)	47.6 (3.88)	0.36 (0.75)
 YB042	n. d.	1.97 (4.81)	0.46 (0.70)
 YB090	4.96 (0.12)	32.7 (6.58)	1.35 (0.56)

### 2.8.4 Substitution of the anthraquinone with a side chain containing a naphthalene or anthracene scaffold

This series consists of nine compounds with an unsubstituted or a substituted naphthalene scaffold or an unsubstituted anthracene scaffold (Figure 43 and Table 21).

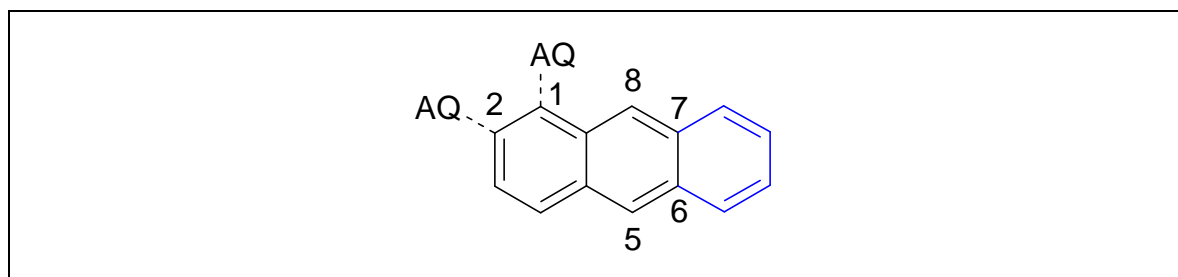


**Figure 43.** The naphthalene (black) or the anthracene (black + blue) is substituted with the anthraquinone (AQ) at positions 1 or 2. The naphthalene is also substituted at the labelled positions.

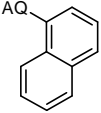
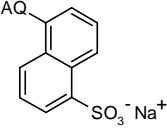
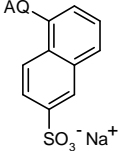
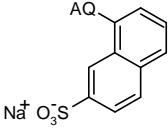
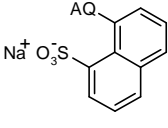
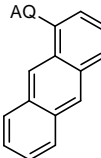
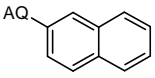
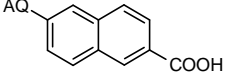
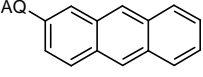
YB040 and YB041 are isomers and not substituted. The naphthalene scaffold of YB040 is coupled to the amino group of the anthraquinone at position 1 while that of YB041 is coupled at position 2 (Table 21). With a  $pIC_{50}$  of 5.47, YB041 is slightly more potent than YB040 with a  $pIC_{50}$  of 5.38. YB040 is the only compound in this series which had been tested on  $P2Y_{12}$ . A  $K_i$  value of more than 10 had been determined for  $P2Y_{12}$ .<sup>[114]</sup>

YB064 is the corresponding anthracene derivative of YB040. The potency of YB064 is increased ( $pIC_{50}$  of 5.58) while the potency of YB063, the corresponding anthracene derivative of YB041, is decreased ( $pIC_{50}$  of 4.94) (Table 21).

A single sulphonation of the 1-naphthyl ring system at positions 5 (YB055;  $pIC_{50}$  5.01), 6 (YB056;  $pIC_{50}$  4.79) and 8 (YB057;  $pIC_{50}$  5.19) lead to a further decrease in compound potency. The activity disappears in the presence of a residue being sulphonated at position 9 (YB058) (Table 21).

Carboxylation of the 2-naphthyl ring system at position 6 is tolerated (YB065) ( $pIC_{50}$  of 5.47), while the potency of the unsubstituted derivative YB041 is decreased ( $pIC_{50}$  of 5.14) (Table 21).

**Table 21.**  $pIC_{50}$  and inhibition values of anthraquinone derivatives containing side chains comprised of a naphthalene or anthracene scaffold. The increase in intracellular calcium as a result of compound addition is also summarised ( $n = 3-4$ ). Test compounds were applied in a concentration of  $10 \mu\text{M}$  (columns 3 and 4). The data are normalised to the response of  $3 \mu\text{M}$  (column 3) or  $30 \mu\text{M}$  RA-II-150 (column 4).

Side residues and internal designation of the test compounds	1321N1-GPR17 cells		
	$pIC_{50}$ ( $\pm$ SEM)	% of inhibition of $10 \mu\text{M}$ compound ( $\pm$ SEM)	% of calcium efflux of $10 \mu\text{M}$ compound ( $\pm$ SEM)
 YB040	5.38 (0.05)	81.6 (1.73)	3.79 (0.38)
 YB055	5.01 (0.07)	38.1 (5.16)	6.16 (2.36)
 YB056	4.79 (0.14)	18.9 (5.94)	2.38 (4.13)
 YB057	5.19 (0.10)	54.8 (4.16)	-0.70 (0.42)
 YB058	n. d.	8.69 (1.78)	-0.10 (0.38)
 YB064	5.58 (0.12)	95.3 (1.00)	1.14 (0.65)
 YB041	5.47 (0.05)	76.3 (4.74)	-0.93 (1.76)
 YB065	5.14 (0.11)	62.7 (2.89)	-0.59 (0.64)
 YB063	4.94 (0.01)	34.6 (4.62)	0.77 (0.89)

### 2.8.5 Substitution of the anthraquinone with a side chain consisting of two substituted or unsubstituted phenyl rings bridged by different atoms

This series of anthraquinone derivatives is comprised of 14 compounds (Table 22). Four compounds were tested on the P2Y<sub>12</sub> receptor and one of these four additionally on P2Y<sub>2</sub>. Each compound has one mono-substituted and one or two unsubstituted phenyl rings which are bridged by different atoms. The phenyl ring which is linked directly to the anthraquinone by the amino group at position 4 of this anthraquinone is referred to as ring I and the second ring as ring II (Figure 44). YB069 exhibits a methoxylated phenyl ring II at the ortho position and an amino bridging group, but the modification of ring II does not significantly influence the potency (pIC<sub>50</sub> 5.39) compared to that of the unsubstituted YB026 (pIC<sub>50</sub> 5.41). There are several other derivatives which contain oxygen as a bridging atom. These are YB030, which is sulphonated at ring I at the meta position, YB050, the ring II of which is chlorinated at the para position, and YB066, which is brominated at ring II at the para position. With a pIC<sub>50</sub> of 5.39, YB066 is more potent than YB050 (pIC<sub>50</sub> 5.08) and YB030 (pIC<sub>50</sub> 4.95) (Table 22). Interestingly, YB030 is one of the most affine compounds on the P2Y<sub>12</sub> receptor. A K<sub>i</sub> value of 0.063 μM was determined for YB030.

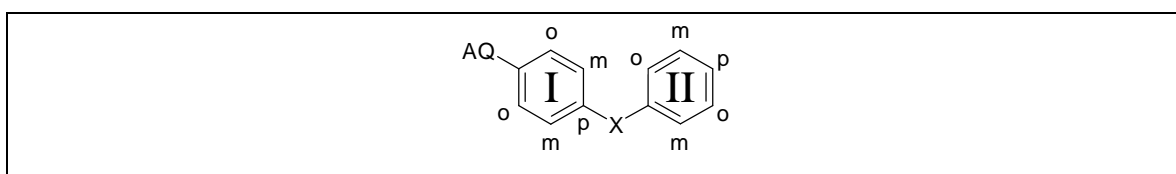


**Figure 44.** The anthraquinone (AQ) is substituted at the amino group at position 4 with two phenyl rings. Ring I is directly coupled to the anthraquinone and the second ring (ring II). The two rings are coupled to each other by different bridging atoms (X). The positions of potential substitutions are labelled (o = ortho, m = meta, p = para).

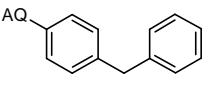
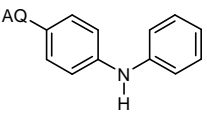
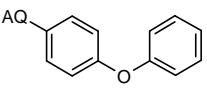
Ring II of YB129 is not coupled to ring I at its para position but at its meta position. Oxygen can be found as a bridging atom and is also active (pIC<sub>50</sub> 5.17) (Table 22). Compounds YB017, YB026, YB018 and YB027 have two unsubstituted phenyl rings but their rings are bridged by different atoms. They are linked in YB017 by a methylene, in YB026 by an amino group, in YB018 by an oxygen atom and in



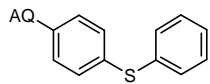
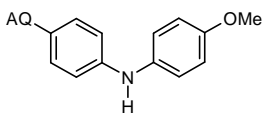
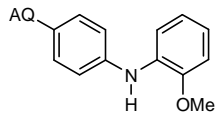
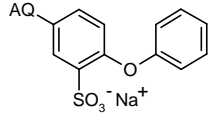
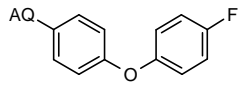
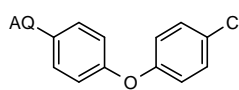
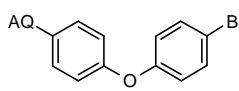
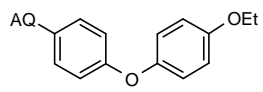
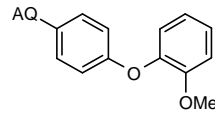
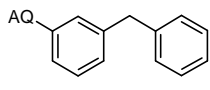
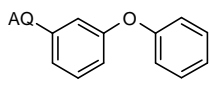
YB027 by a thioether (Table 22). YB017, YB026 and YB027 were also tested on P2Y<sub>12</sub>. A high affinity at P2Y<sub>12</sub> had been determined for all of them (YB017,  $K_i$  0.614  $\mu$ M; YB026,  $K_i$  1.85  $\mu$ M; YB027,  $K_i$  0.884  $\mu$ M).<sup>[114]</sup> YB026 is also very potent at the P2Y<sub>2</sub> receptor. The pIC<sub>50</sub> for YB026 on the P2Y<sub>2</sub> receptor is exactly the same as for GPR17 (pIC<sub>50</sub> 5.41).<sup>[119]</sup> The most potent compounds are YB017 and YB026 with similar pIC<sub>50</sub> values (5.43 and 5.41, respectively). The potency is decreased with a thioether bridging group (YB027) (pIC<sub>50</sub> 5.05) (Table 22).

Some compounds appear to have unspecific effects. These unspecific effects can be explained by the physical properties of the compounds, which lead to the absorption of the excitation wavelength for stimulating the calcium-dye complex or to the absorption of the wavelength that is emitted from the stimulated calcium-dye complex in the calcium assay. Furthermore, these observations can be explained by an unspecific elevation of the calcium concentration as a result of compound addition. This unspecific effect could be the result of activation of endogenously expressed cells on the cell surface or of cytotoxic compound properties. But there are still many very potent alternatives to these “dirty” compounds, however.

**Table 22.** pIC<sub>50</sub> and inhibition values of anthraquinone derivatives containing two substituted or unsubstituted phenyl rings as side residues. The increase in intracellular calcium as a result of compound addition is also summarised (n = 3-4). Test compounds were applied in a concentration of 10  $\mu$ M (columns 3 and 4). The data are normalised to the response of 3  $\mu$ M (column 3) or 30  $\mu$ M RA-II-150 (column 4).

Side residues and internal designation of the test compounds	1321N1-GPR17 cells		
	pIC <sub>50</sub> ( $\pm$ SEM)	% of inhibition by test compound ( $\pm$ SEM)	% of calcium efflux of test compound ( $\pm$ SEM)
 YB017	5.43 (0.07)	83.2 (2.57)	2.13 (1.98)
 YB026	5.41 (0.08)	88.1 (2.25)	-0.98 (0.47)
 YB018	4.94 (0.05) (not completely soluble)	33.2 (6.58)	0.40 (0.98)

## CHAPTER II: RESULTS

Side residues and internal designation of the test compounds	1321N1-GPR17 cells		
	pIC <sub>50</sub> (± SEM)	% of inhibition by test compound (± SEM)	% of calcium efflux of test compound (± SEM)
 YB027	5.05 (0.08)	33.6 (5.84)	2.14 (1.75)
 YB043	5.11 (0.14) (not completely soluble)	53.9 (9.86)	-0.02 (1.05)
 YB069	5.39 (0.09)	84.5 (2.72)	0.90 (0.42)
 YB030	4.95 (0.01)	40.2 (1.87)	2.82 (1.74)
 YB060	5.33 (0.07) (not completely soluble)	99.3 (0.90)	0.09 (0.50)
 YB050	5.08 (0.09)	62.4 (4.79)	-0.93 (0.28)
 YB066	5.39 (0.02)	85.8 (1.82)	0.06 (0.46)
 YB067	5.53 (0.01) (not completely soluble)	93.7 (1.96)	-0.74 (0.46)
 YB097	4.57 (0.25) (not completely soluble)	15.9 (2.44)	0.55 (0.76)
 YB128	5.26 (0.08) (not completely soluble; absorption with Fura)	67.6 (3.25)	1.03 (0.79)
 YB129	5.17 (0.14)	51.4 (4.04)	1.70 (2.14)

### 2.8.6 Substitution of the anthraquinone containing a side chain consisting of a phenyl ring and a triacetyl or pyrimidinyl ring

This series of anthraquinone derivatives consists of 9 compounds (Table 23). Five compounds were already also tested on the P2Y<sub>12</sub> receptor. Here, all anthraquinones carry a mono-substituted or unsubstituted phenyl ring which is directly coupled to the amino group at position 4 of the anthraquinone. This phenyl ring is linked by an amino group to a substituted triacetyl at the meta or para position or to an unsubstituted pyrimidinyl ring system at the para position (Figure 45).

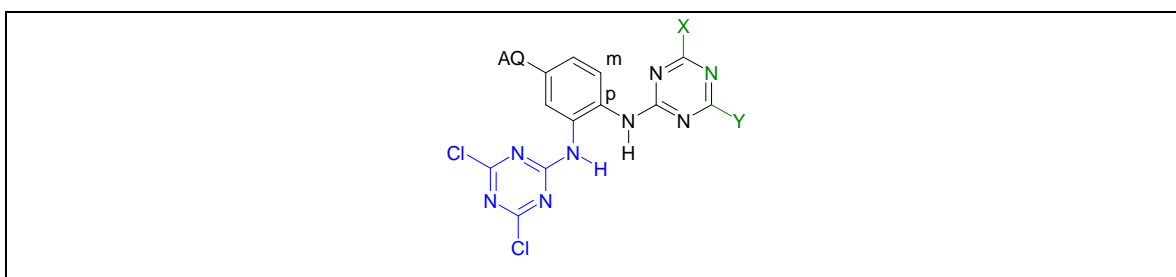


**Figure 45.** The anthraquinone (AQ) is coupled to the phenyl ring by its 4-amino group (Figure 41). This phenyl ring is linked over an amino group to an unsubstituted pyrimidinyl ring at the para (p) position (black; N (green) is replaced with a C; X and Y = H) or by a triacetyl ring with variable substituents (green) (Table 23). Furthermore, the phenyl ring can be substituted over an amino group with a dichloro triacetyl ring at the meta (m) position (blue). Equivalent substitutions at the phenyl ring are realised at the meta and para positions.

Since the phenyl ring is sulphonated at the para position in YB1-1 and the dichloro triacetyl ring is linked by the amino group at the meta position, and these two substituents are also substituted with each other in YB2-1 (Table 23), YB1-1 and YB2-1 are constitutional isomers. Whereas no data for other receptors is available for YB1-1, YB2-1 shows high affinity to P2Y<sub>12</sub>.<sup>[114]</sup> YB1-1 is the most potent antagonist at GPR17 (pIC<sub>50</sub> of 6.22). However, its isomer YB2-1 is still very potent (pIC<sub>50</sub> 5.21) and comparable with other anthraquinone antagonists.

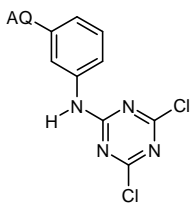
Structurally, YB21-1 is identical to YB1-1 but it lacks the sulphonate substituent at the meta position of the phenyl ring. In this case the potency is decreased to a similar level compared to YB2-1 (pIC<sub>50</sub> 5.16).

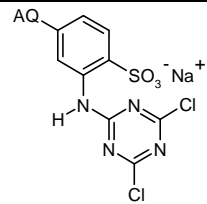
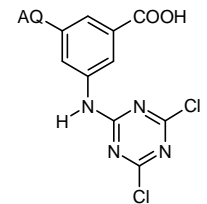
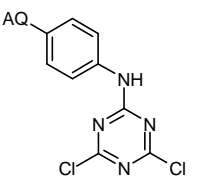
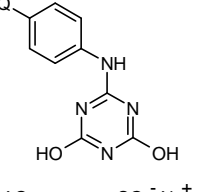
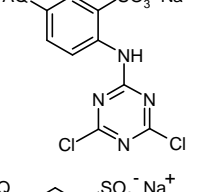
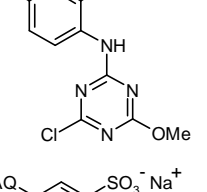
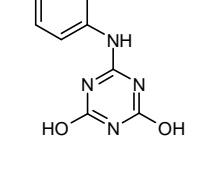
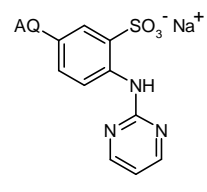
If the sulphonate group at the para position of YB1-1 is removed and a carboxylate group is inserted at the meta position, another very potent antagonist is generated (YB3 1) ( $pIC_{50}$  5.59).

The other isomers tested are YB2-1 and YB19-1, the latter being was also tested on  $P2Y_{12}$  ( $K_i$  of 1.90  $\mu$ M), as well as YB2-1-2 and YB19-1-2. YB2-1 and YB19-1 share the dichloro triacetyl ring at the para position, whereas YB19-1 lacks the sulphonate substituent at the meta position of the phenyl ring.<sup>[114]</sup> YB2-1-2 and YB19-1-2 carry a triacetyl ring which is dihydroxylated instead of being dichlorinated (Table 23). YB2-1-2 additionally carries a sulphonate group at the meta position of the phenyl ring. In the case of YB2-1-2 and YB2-1 the potency decreases when the sulphonate group is eliminated ( $pIC_{50}$ [YB2-1] 5.21;  $pIC_{50}$ [19-1] 4.94 and  $pIC_{50}$ [YB2-1-2] 5.15;  $pIC_{50}$ [19-1-2] 4.81).

YB2-1-1 is sulphonated at the meta position of the phenyl ring, while the triacetyl ring is meta chlorinated and meta methoxylated. By contrast, the substituted triacetyl ring is substituted with an unsubstituted pyrimidinyl ring (YB2-3). These compounds have a  $pIC_{50}$  of 4.50 and 4.77 respectively. Interestingly, YB2-3 shows one of the highest affinities at  $P2Y_{12}$  (Table 23). The  $K_i$  value for YB2-3 is 0.0507  $\mu$ M.<sup>[114]</sup> YB2-1-1 also has a very high affinity at  $P2Y_{12}$ . Here, the  $K_i$  value is 0.66  $\mu$ M.<sup>[114]</sup> These results indicate that it is possible to generate compounds which are selective for certain related receptors.

**Table 23.**  $pIC_{50}$  and inhibition values of anthraquinone derivatives containing a phenyl ring and a triacetyl or pyrimidinyl substitution. The increase in intracellular calcium as a result of compound addition is also summarised ( $n = 3-4$ ). Test compounds were applied in a concentration of 10  $\mu$ M (columns 3 and 4). The data are normalised to the response of 3  $\mu$ M (column 3) or 30  $\mu$ M RA-II-150 (column 4).

Side residues and internal designation of the test compounds	1321N1-GPR17 cells		
	$pIC_{50}$ ( $\pm$ SEM)	% of inhibition by test compound ( $\pm$ SEM)	% of calcium efflux of test compound ( $\pm$ SEM)
 YB21-1	5.16 (0.08)	51.0 (6.91)	0.44 (0.65)

Side residues and internal designation of the test compounds	1321N1-GPR17 cells		
	pIC <sub>50</sub> (± SEM)	% of inhibition by test compound (± SEM)	% of calcium efflux of test compound (± SEM)
 YB1-1	6.22 (0.07)	98.1 (0.84)	0.68 (0.98)
 YB3-1	5.59 (0.11)	83.3 (4.65)	2.07 (1.54)
 YB19-1	4.94 (0.18)	45.8 (5.40)	0.18 (0.92)
 YB19-1-2	4.81 (0.05)	11.5 (2.98)	1.41 (0.99)
 YB2-1	5.21 (0.18)	33.8 (4.52)	1.52 (1.68)
 YB2-1-1	4.50 (0.20)	23.3 (6.26)	0.26 (0.94)
 YB2-1-2	5.15 (0.14)	35.6 (2.05)	1.42 (1.13)
 YB2-3	4.77 (0.02)	29.9 (3.98)	4.25 (2.07)

### 2.8.7 Substitution of the anthraquinone containing a side chain consisting of a phenyl ring substituted with at least a sulphonate or carboxylate group

Finally, a series of anthraquinone derivatives consisting of 21 compounds (Table 24) was tested. None of these compounds were tested on the P2Y<sub>2</sub> or P2Y<sub>12</sub> receptor. In this group the anthraquinone scaffold is substituted at the 4-amino group (Figure 41) with a phenyl group that, as a minimum, is modified with a sulphonate or a carboxylate at the meta position (Figure 46). Other substituents are coupled to this phenyl ring by an amino group at the para position (Figure 46). The second phenyl ring of YB103 and YB105 is substituted with an ethyl or methoxyl group. YB103 is (pIC<sub>50</sub> 5.45) more potent than YB105 (pIC<sub>50</sub> 5.13) (Table 24).

YB119 and YB120 are similar compounds. A benzyl residue is coupled to the para amino group of the meta carboxylated phenyl ring of YB120 and, in the case of YB119, the benzyl residue is replaced by a phenethyl residue. The phenethyl residue is better accepted (pIC<sub>50</sub> 5.61) than the benzyl residue (pIC<sub>50</sub> 4.74) (Table 24).

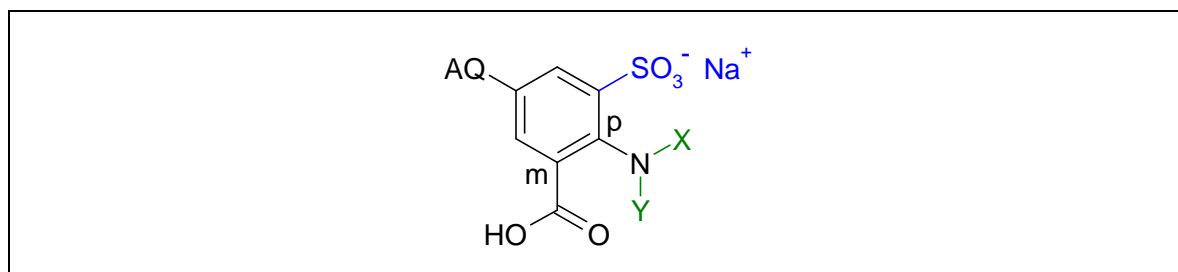


**Figure 46.** The 4-amino group of the anthraquinone (AQ) (Figure 41) is substituted, as a minimum, with a carboxylate (black) or a sulphonate (blue) at the meta position. Other substituents are added over an amino group at the para position. The residues, abbreviated as X and Y, are identical or different, respectively.

The para amino group is then substituted with a cyclohexane (YB117) and a cyclopentane (YB118). Here, the cyclopentane residue (pIC<sub>50</sub> 5.47) is better tolerated than the cyclohexane residue (pIC<sub>50</sub> 4.93) (Table 24).

Next, simple aliphatic residues are fused to the para amino group of the meta carboxylated phenyl ring. YB123 is substituted with an iso-propanyl while YB122 is

modified with an n-propanyl, YB121 with an iso-butanyl and YB127 with two n-propanyl residues (Table 24). They are very potent with the exception of YB127, which has a  $pIC_{50}$  value of 4.79 ( $pIC_{50}[YB121]$  5.35,  $pIC_{50}[YB122]$  5.11,  $pIC_{50}[YB123]$  5.03).

YB126 is the only compound in this series with no free linking amino group. The linking amino group is integrated in a cyclopentane ring (Table 24). The potency of this compound is 5.02 (Table 24).

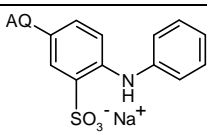
YB039 is the only compound in this series that carries a sulphonate group at the meta position of the phenyl ring. All other compounds are modified at this position with a carboxylate. Furthermore, a second phenyl ring is linked to the first one by an amino group at the para position.

Radioligand binding assays with membranes carrying  $P2Y_{12}$  receptors had identified YB039 as the antagonist with the highest affinity. The  $K_i$  value determined for this compound is  $0.0249 \mu M^{[114]}$ , though for GPR17 it is only a weak antagonist ( $pIC_{50}$  4.91).

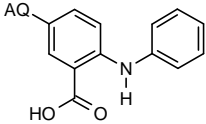
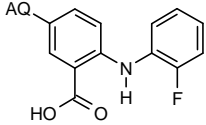
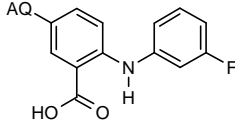
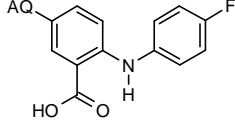
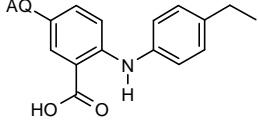
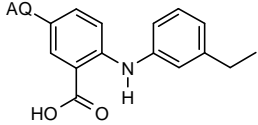
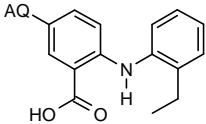
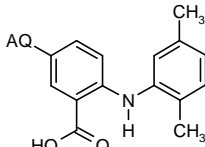
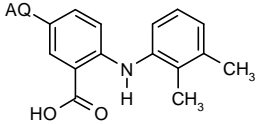
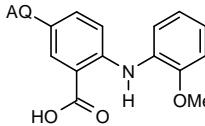
YB100 is a related structure of YB039. However, the sulphonate group is substituted with a carboxylate group. Compared to YB039 the potency of YB100 ( $pIC_{50}$  5.57) is considerably increased (Table 24).

The  $pIC_{50}$  values of YB124 (ortho fluorophenyl), YB125 (meta fluorophenyl) and YB108 (para fluorophenyl) are not significantly influenced compared to YB100 by the insertion of single fluoro substituents into the second phenyl ring (Table 24).

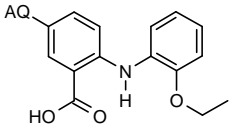
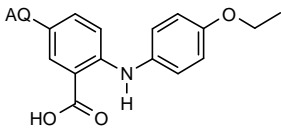
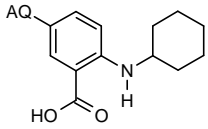
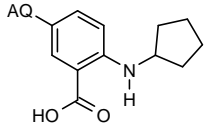
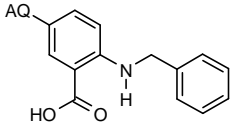
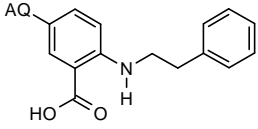
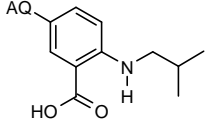
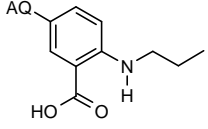
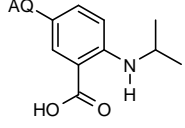
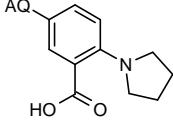
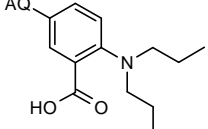
**Table 24.**  $pIC_{50}$  and inhibition values of anthraquinone derivatives containing a phenyl ring substituted, as a minimum, with a sulphonate or carboxylate group. The increase in intracellular calcium as a result of compound addition ( $n = 3-4$ ) is also summarised. Test compounds were applied in a concentration of  $10 \mu M$  (columns 3 and 4). The data are normalised to the response of  $3 \mu M$  (column 3) or  $30 \mu M$  RA-II-150 (column 4).

Side residues and internal designation of the test compounds	1321N1-GPR17 cells		
	$pIC_{50}$ ( $\pm$ SEM)	% of inhibition by test compound ( $\pm$ SEM)	% of calcium efflux of test compound ( $\pm$ SEM)
 YB039	4.91 (0.09)	91.7 (2.15)	2.69 (2.07)

## CHAPTER II: RESULTS

Side residues and internal designation of the test compounds	1321N1-GPR17 cells		
	pIC <sub>50</sub> (± SEM)	% of inhibition by test compound (± SEM)	% of calcium efflux of test compound (± SEM)
 YB100	5.57 (0.10)	91.9 (1.25)	1.67 (1.04)
 YB124	5.20 (0.09)	80.1 (3.78)	0.34 (1.80)
 YB125	5.70 (0.08)	92.7 (1.23)	6.81 (1.22)
 YB108	5.13 (0.11)	76.2 (4.32)	0.92 (0.73)
 YB101	5.71 (0.12) (not completely soluble)	75.8 (5.46)	13.6 (2.46) (unspecific background)
 YB102	5.83 (0.14) (absorption or raised background depending on the fluorescent dye)	90.2 (2.83)	23.2 (1.96) (unspecific background)
 YB103	5.45 (0.02)	95.0 (2.03)	2.04 (0.71)
 YB111	5.48 (0.04) (absorption or raised background depending on the fluorescent dye)	96.8 (1.95)	3.39 (0.78)
 YB114	5.68 (0.13) (absorption or raised background depending on the fluorescent dye)	86.2 (3.42)	12.7 (2.92) (unspecific background)
 YB105	5.13 (0.08)	66.3 (4.91)	-2.73 (2.72)



Side residues and internal designation of the test compounds	1321N1-GPR17 cells		
	pIC <sub>50</sub> (± SEM)	% of inhibition by test compound (± SEM)	% of calcium efflux of test compound (± SEM)
 YB115	5.41 (0.03) raised background with Fura and OG at high concentrations	90.1 (1.92)	1.92 (1.60)
 YB116	5.63 (0.09) raised background with Fura and OG at high concentrations	97.0 (1.08)	2.52 (0.47)
 YB117	4.93 (0.04)	50.4 (7.95)	0.21 (0.54)
 YB118	5.47 (0.07)	83.3 (2.84)	-0.30 (0.63)
 YB120	4.74 (0.20) (only partial DRC)	19.5 (6.00)	0.23 (0.63)
 YB119	5.61 (0.08)	94.1 (1.96)	3.34 (0.91)
 YB121	5.35 (0.07)	74.8 (2.65)	0.14 (0.81)
 YB122	5.11 (0.04)	57.2 (1.67)	-0.19 (0.50)
 YB123	5.03 (0.05)	47.3 (0.88)	0.96 (0.47)
 YB126	5.02 (0.14)	45.0 (3.17)	-0.60 (1.05)
 YB127	4.79 (0.09)	19.4 (3.34)	0.99 (1.22)

It has been shown that GPR17 is inhibited by a wide variety of anthraquinone derivatives. Even though they are also active on other closely related receptors, there are anthraquinones that prefer GPR17 and evidence exists of structural elements that are important to enhance their selectivity. At this point the characterised inhibitors are very useful tools for the *in vitro* characterisation of GPR17 and they are novel lead structures for the development of highly selective GPR17 inhibitors.

---

## CHAPTER III: DISCUSSION

---

### 3.1 Identified GPR17 ligands – useful *in vitro* tools

A major aim in the development of new therapies for the treatment of diseases is to identify the cellular components involved in these diseases. For several decades now, the family of G protein-coupled receptors has been one of the most important drug target families, because GPCRs play a role in many human diseases such as stroke, asthma, schizophrenia, cancer, neurological pain, migraine, allergies, gastric ulcers, diabetes, obesity and hypertension.<sup>[2-4]</sup> It is thus of outstanding importance to deorphanise the approximately 100 human orphan GPCRs. GPR17 was only deorphanised quite recently and has been less extensively pharmacologically investigated in comparison to other GPCRs. However, since there are contrary reports concerning the agonistic properties of the proposed GPR17 agonists, the major goal of this thesis was to identify and characterise novel lead structures for the activation and inhibition of GPR17.

Like the members of the P2Y receptor family and the related cysteinyl-receptor family, GPR17 has certain highly conserved ligand binding motifs such as the H-X-X-R/K motif in transmembrane domain 6.<sup>[126]</sup> In GPR17 this motif consists of the amino acids histidine 252 and arginine 255.<sup>[127]</sup> The corresponding basic arginine residues in the P2Y receptor family mediate ligand binding by interacting with the negatively charged phosphate groups of the nucleotide.<sup>[127]</sup> The presence of this important residue in transmembrane domain 6 of GPR17 implicates at least one negatively charged substructure in a putative GPR17 ligand. In the case of the P2Y<sub>1</sub>, P2Y<sub>2</sub>, P2Y<sub>4</sub>, P2Y<sub>6</sub> and P2Y<sub>11</sub> receptors the arginines at positions 128 and 310 have been identified as essential basic residues for ligand binding and receptor activation.<sup>[128]</sup> Since both residues are lacking in GPR17, it is self-evident

---

that GPR17 is not activated, or only weakly activated, by nucleotides.<sup>[127]</sup> Nevertheless, Ciana *et. al.* proposed that GPR17 is activated by uracil nucleotides. However, our results from different functional assays and a label-free assay are in line with the assumption, derived from the sequence comparison and other reports, that GPR17 cannot be activated by the proposed nucleotidic agonists.<sup>[30, 51]</sup> Unfortunately, molecular modelling and dynamics studies of GPR17 published previously give no explanation for the decreased compound potency or failed activity of pranlukast and montelukast, which were proposed GPR17 antagonists in our studies.<sup>[51, 127]</sup> Screening of negatively charged compounds that mimic nucleotidic phosphates identifies RA-II-150, a GPR17 ligand with two carboxylic groups and an indole scaffold. The relevance of at least one of these two carboxylic groups was shown, since the deletion of the 3-(2-carboxyethyl) group leads to a loss of activity, indicating that basic residues such as arginine 255 mediate RA-II-150 binding. The involvement of arginine 255 and other residues in ligand binding and activation must be verified in future by site directed mutagenesis.

However, on the one hand the charged structures are necessary for receptor binding and activation, while on the other hand this feature limits the utilisation of the compound and its derivatives as a potential therapeutical drug. Since it has been shown that GPR17 is mainly expressed in brain under certain conditions, it has to pass the brain-blood-barrier to reach the affected cells. The brain-blood-barrier is a physiological border that separates brain from blood. The brain-blood-barrier hence consists of endothelial cells that are linked by tight junctions, which limit the compound permeability. Furthermore, there are several mechanisms that limit access to the brain by the brain-blood-barrier, such as very effective transporters, enzymatical degradation and alternate transport pathways, so that 100% of large-molecule drugs and more than 98% of small-molecule drugs do not cross this barrier.<sup>[129, 130]</sup> The brain-blood-barrier can be traversed by multiple, highly specific, endogenous transporters within this barrier, however, as well as by passive diffusion. Small molecules with appropriate lipophilicity, molecular weight and charge will diffuse from blood into the brain. Since it has been reported that more than one carboxylic group aborts brain-blood-barrier transport, it is obvious that the identified novel GPR17 agonist RA-II-150 and its active derivatives are not appropriate drugs for the treatment of brain injuries after

ischemic events.

Several pharmacological approaches have been established to enhance the brain penetration of a drug. Functional groups of a drug that limits penetration can be modified by acetylation, methylation, conjugation with amantadine and adamantidine derivatives or the attachment of fatty acid or cholesterol esters.<sup>[131-133]</sup> Unfortunately, these modifications which are necessary for drugs to cross the brain-blood-barrier often result in loss of the desired activity or turn it into a substrate for the efflux pumps.<sup>[129]</sup> Since the carboxylic groups must be modified to permit GPR17 agonists to pass the brain-blood-barrier and these groups appear to be essential for agonist activity, these modifications may lead to a loss of function. Nevertheless, RA-II-150 and its derivatives are suitable *in vitro* tools for the characterisation of GPR17 and the signal transduction pathways coupled to the receptor. Furthermore, it has been shown that RA-II-150 is very potent and selective for GPR17, since related P2Y receptor cannot be activated by RA-II-150.

## **3.2 First indications of functionally selective GPR17 ligands**

Functionally selective ligands activate a fraction of the signal transduction pathways coupled to a receptor. It has been shown that even small changes in the chemical structure of a compound can lead to functional selectivity. Fenoterol is a selective  $\beta_2$ -adrenoceptor agonist. Whereas the (*S,R*) stereoisomer of fenoterol activates  $G_s$  and  $G_i$  pathways, the (*R,R*) stereoisomer only activates the  $G_s$  signal transduction pathway in native rat cardiomyocytes.<sup>[134, 135]</sup> The selective activation of the  $G_s$  pathway eliminates side effects of unselective  $\beta_2$ -adrenoceptor agonist. These side effects, which are due to the  $G_i$  activation, disappear upon application of the functionally selective stereoisomer.<sup>[135]</sup> Functionally selective ligands have also been reported for the  $CB_1$  cannabinoid receptor and there are several publications dealing with functionally selective ligands.<sup>[134, 136-139]</sup>

Since GPR17 couples to at least the  $G_i$ ,  $G_s$  and cell type specifically to the  $G_q$  pathway and exhibits positive and negative features that may be due to the

activated signal transduction pathways, it would be interesting to develop functionally selective GPR17 ligands for the development of therapies that prevent brain injury and promote remodelling processes after ischemic events. Preliminary unpublished data supplied by Marieke Böckmann genannt Dallmeyer, suggest that certain substitution patterns may lead to functionally selective GPR17 compounds.<sup>[72]</sup> These preliminary results are supported by the comparison of the results of the calcium assay and the inositol phosphate accumulation assay within this thesis. Since the potency of KL16-1 in the calcium assay is also at the upper border confidence interval, the considerable big part of the  $G_i$  pathway to the overall calcium signalling of GPR17 upon receptor activation with KL16-1 is indicated. A structural analysis reveals that KL16-1, which is monochlorinated, has  $G_i$  pathway preference. It is necessary to investigate whether the functional selectivity of KL16-1 for the  $G_i$  pathway can be enhanced, so that the  $G_i$  is exclusively activated. The substitution of the chlorination at position 6 with other functional groups probably increases functional selectivity. Furthermore, the development of functionally selective agonists, which activate certain other pathways exclusively, would be interesting because there has so far been no investigation to determine which pathway or pathways mediate the different GPR17 functions.

### **3.3 Novel calcium mobilisation mechanism proposed for GPR17**

Investigations within the scope of this thesis of a proposed novel calcium mobilisation mechanism led to the identification of several involved components, such as a PTX sensitive  $G_i$  protein, a phosphatidylinositol-specific phospholipase C (PI-PLC) and  $IP_3$  receptors on intracellular stores, which are the major calcium source. However, calcium release is independent of an inositol phosphate accumulation, due to the classical activation of a phospholipase C like the involved PI-PLC. Similar observations have been already reported by Mirabet *et. al.* They describe a calcium release mechanism which is independent of an inositol

phosphate production for the  $A_{2b}$  adenosine receptor expressed in Jurkat cells.<sup>[140]</sup> Since all components of the novel calcium release mechanism are localised in the plasma membrane or the membrane of the endoplasmic reticulum (ER), they are in close proximity as required for signal transduction. The close proximity of the two membrane systems and the interactions between proteins localised in these membrane systems have been reviewed.<sup>[141, 142]</sup> The following model was claimed for the novel calcium release mechanism: A  $G_i$  protein is activated upon receptor stimulation. A PI-PLC is then recruited by the  $G_i$  protein. The two proteins form a complex which binds to  $IP_3$  sensitive calcium channels localised in the ER. These  $IP_3$  receptors are activated by the complex, and calcium is subsequently released from the ER (Figure 47). Since it is not possible with functional assays under the usage of PTX to discriminate whether the  $G_{\alpha i}$  or the  $G_{\beta\gamma}$  subunit mediates the PI-PLC activation, it remains unclear which subunit transduces the signal to the ER. However, there is one indication that the  $G_{\beta\gamma}$  subunit recruits the PI-PLC, since in 2003 Zeng *et. al.* described a novel calcium release mechanism, where a direct interaction between a  $G_{\beta\gamma}$  subunit and  $IP_3$  receptors is proposed.<sup>[143]</sup> Interestingly, the calcium release mechanism chosen by GPR17 is independent of a PI-PLC-dependent inositol phosphate accumulation as deduced from inositol phosphate accumulation with 1321N1-GPR17 cells (2.5.4).

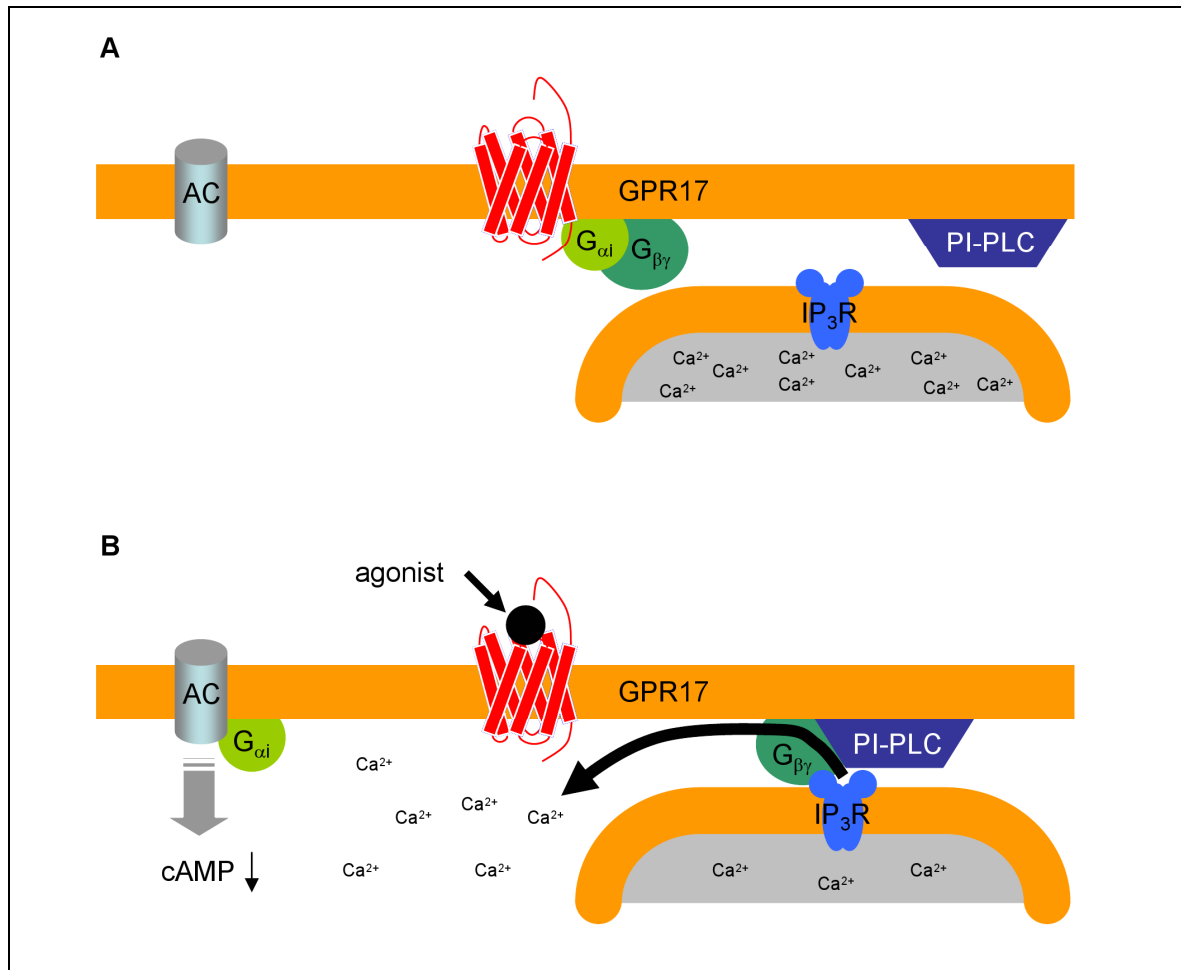


**Figure 47.** Model of a novel calcium release mechanism being involved in GPR17 signalling. In panel (A) all cellular constituents involved are shown in their initial state. (B) After agonist-dependent receptor stimulation the associated inhibitory heterotrimeric  $G_i$  protein dissociates into its active  $G_{\alpha i}$  and  $G_{\beta\gamma}$  subunits. Whereas the  $G_{\alpha i}$  subunit inhibits the adenylyl cyclase (AC), the  $G_{\beta\gamma}$  subunit recruits a phosphatidylinositol-specific phospholipase C (PI-PLC). The  $G_{\beta\gamma}$ -PI-PLC complex moves to the inositol 1,3,4-triphosphate sensitive receptors ( $IP_3R$ ) located in the membrane of intracellular calcium stores (ER) and activates them. Upon activation, calcium ( $Ca^{2+}$ ) is gated by  $IP_3R$  into the cytoplasm.

### 3.4 Screening of natural products does not deorphanise GPR17, but identifies novel antagonist lead structures

In literature several examples of originally orphan G protein-coupled receptors have been described. Endogenous ligands of these receptors are intermediates of metabolism pathways or other unusual ligands previously not known to modulate



GPCRs. For example GPR91 and GPR99 are activated by intermediates of the citric acid cycle, GPR40 by long-chain fatty acids, the endothelial differentiation gene-1 receptor by sphingosine 1-phosphate and GPR109A, GPR109B and GPR81 by hydroxy-carboxylic acids.<sup>[144-147]</sup> For this reason several native compounds and intermediates of metabolism pathways were tested on GPR17 within the scope of this thesis. The tested compounds were due to structural similarities either with the lead compound RA-II-150 and its derivatives or with the proposed nucleotidic GPR17 agonists (2.2.1 and 2.3.1). Unfortunately, all the compounds tested here failed to activate or inhibit GPR17, so that GPR17 could not be deorphanized.

A wide variety of natural products have been described as modulators of GPCR functions. Morphine and codeine are ligands of the  $\mu$ -,  $\kappa$ -, and  $\delta$ -opioid receptors while caffeine acts as a nonselective adenosine  $A_1$  and  $A_{2A}$  receptor antagonist.<sup>[148, 149]</sup> These few selected examples show the potential of natural products as GPCR ligands. Therefore in order to identify novel agonist and antagonist lead structures compound libraries comprised of natural products, kindly provided by the group of Professor G. M. König and Professor E. Leistner, Institute of Pharmaceutical Biology, University of Bonn, as well as commercially available natural compounds were screened. Screening these compounds allowed several new GPR17 antagonists to be identified. Since natural products are often cytotoxic and they occur in small amounts in the producing organism, the access to these compounds is limited. Moreover, their complex structure is difficult or impossible to synthesize, which is why natural products are often not suitable as drugs. Even though the compounds identified as GPR17 antagonists are not very potent and their antagonistic activity is particularly nonselective for GPR17, these compounds reveal novel lead structures for the development of GPR17 antagonists. The modification of these GPR17 antagonists probably enhances compound potency and selectivity.

### 3.5 Anthraquinone derivatives as potent *in vitro* GPR17 antagonists

Anthraquinone and its derivatives such as emodin, aloe-emodin, and rhein have anti-cancer and laxative properties.<sup>[150]</sup> Furthermore, anthraquinone derivatives have been described as potent P2Y<sub>1</sub>-like receptors, P2X receptors, P2Y<sub>2</sub> receptors, P2Y<sub>12</sub> receptors and ectonucleoside triphosphate diphosphohydrolases antagonists.<sup>[115-120]</sup> Owing to the close relationship to this receptor family, the potential of anthraquinone derivatives as potent P2Y receptor antagonists indicates that these compounds may also inhibit GPR17. The majority of the tested anthraquinone derivatives, kindly provided by the group of Professor C. E. Müller, Pharmaceutical Institute, Pharmaceutical Chemistry I, University of Bonn, inhibit GPR17, as shown in 2.8.

The structural analysis of these compounds reveals several similarities between YB1-1, the most potent antagonist, and the lead GPR17 agonist RA-II-150. The two chloro substitutions of the triacetyl ring and the secondary amine of YB1-1 are thus in the same steric configuration compared to RA-II-150. Additionally, it is possible that the sulphonate group mimics the 2-carboxyethyl group of RA-II-150, even they do not exhibit in the same steric configuration (Figure 48). A similar arrangement of certain structural elements in YB1-1 on the one hand and RA-II-150 on the other hand is probably responsible for the high potency of YB1-1, whereas the anthraquinone substructure mediates the inhibitory effect in general. It would be interesting to see whether sulphonation or carboxylation at the ortho position of the first ring, which is more equivalent to the steric arrangement of the 2-carboxyethyl group of RA-II-150, or the substitution of the sulphonate with a carboxylate leads to a further increase in compound potency.

Nevertheless, these structures are not suitable for the *in vivo* application owing to side effects such as the increased colorectal cancer risk and cytotoxicity, both of which are due to the anthraquinone scaffold.<sup>[151]</sup> Furthermore, access of these compounds to the brain is restricted by the brain-blood-barrier and their activity is not very selective. Even though their utilisation in light and fluorescence based functional assays is limited due to their intensive colour, they are very useful tools for *in vitro* analysis.

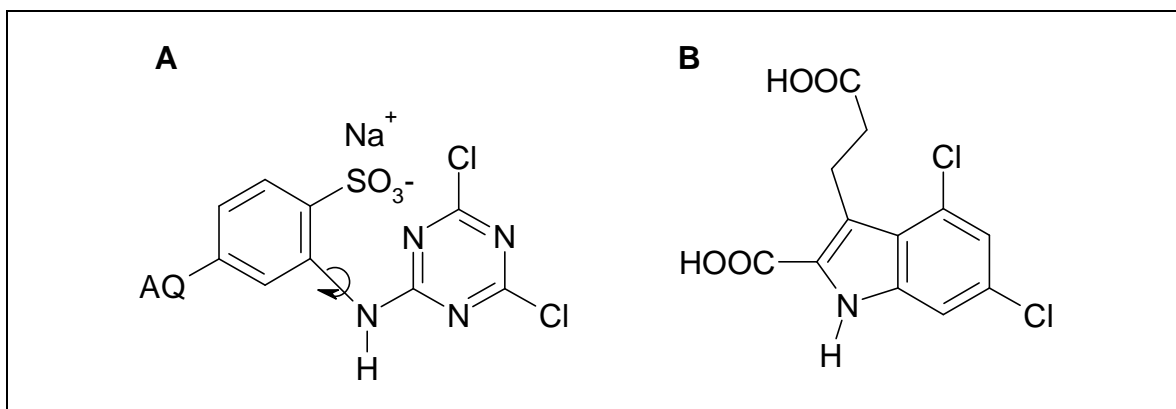


**Figure 48.** Structural similarities between the side chain of the antagonist YB1-1 (A) and the agonist RA-II-150 (B). The 4,6-dichloro triacyl ring of YB1-1 mimics the 4,6-dichlorobenzoyl ring of RA-II-150. Furthermore, both compounds share a secondary amine in the same steric configuration. The benzol ring of YB1-1 is twisted around the bridging group while the indole is planar. The sulphonate of YB1-1 may mimic the 2-carboxylethyl group.

### 3.6 Putative *in vivo* role of GPR17

Lecca *et. al.* reported that GPR17 expression is up-regulated at the boundaries of the lesioned area in phases following ischemia. This has been attributed to the initiation of local remodelling and repair responses, suggesting that GPR17 acts as a coordinator of brain remodelling processes.<sup>[56]</sup> It has been shown that the endogenous cAMP level, controlled for example by G protein-coupled receptors, modulates neurite outgrowth in the central nervous system, whereby high amounts promote neurite outgrowth and small amounts attenuate it.<sup>[13, 14, 152, 153]</sup> However, other findings assert that  $G_{o/i}$  coupled receptors, like the cannabinoid receptor  $CB_1$ , the D2 dopamine receptor and the serotonin receptor, induce neurite outgrowth by reducing cAMP levels.<sup>[154-157]</sup> It has been demonstrated in this thesis that GPR17 couples to both  $G_i$  and  $G_s$  pathways and that the signalling of GPR17 is dependent on the cellular background (2.5). Furthermore, there are indications that certain agonists display functional selectivity. Even though the endogenous ligand of GPR17 has still not been identified, the function of GPR17 is dependent on the ligand and the cells expressing the receptor. Summarizing the results from this thesis and from literature the following model can be proposed for the *in vivo*

function of GPR17. The destructive function of GPR17 is probably due to its signalling as well as to its negative regulatory function with regard to CysLT<sub>1</sub>, while its remodelling function in later phases following ischemia is attributable to the activation of GPR17 by a specific endogenous ligand that appears subsequently. This ligand is presumed to be a compound that is released when cells are decomposed, so that the ligand concentration increases after ischemia. The G<sub>i</sub> pathway is activated at low agonist concentrations immediately following ischemia, so that the cAMP level within the cells is decreased, inhibiting remodelling processes. In later phases the agonist concentration increases, so that there is a switch from the G<sub>i</sub> pathway to the G<sub>s</sub> pathway; the intracellular cAMP level also increases, subsequently promoting neurite outgrowth and remodelling processes. Assuming that GPR17 is not affected in the presence of CysLT<sub>1</sub>, the initially low ligand concentrations and the delayed presence of GPR17 on the cell surface in the lesioned area together explain why GPR17 does not attenuate neuronal cell death. It is difficult to develop a therapy that exploits the dualistic function of GPR17. On the one hand its presence is unwanted because of its destructive inhibitory CysLT<sub>1</sub> function, while on the other this presence is desired because of its remodelling function. If it is possible to interrupt the GPR17-CysLT<sub>1</sub> dimer formation by modulation of GPR17 activity immediately after the ischemic event, the progression of ischemia could be delayed or even halted. Furthermore, the activation of GPR17 in later phases may decrease the consequences of injury.

---

## CHAPTER IV: SUMMARY

---

In order to discover a set of tools suitable to be employed in its *in vitro* characterization, the recently orphanized G protein coupled receptor GPR17 was investigated by using different classical second messenger assays and the new dynamic mass redistribution technology.

Contrary to reports from the literature which claim a function of GPR17 as a nucleotide receptor or as ligand and signalling independent, the receptor was found to be activated by a new class of GPCR ligands sharing an indole scaffold. Besides agonists, different classes of natural and synthetic compounds have been identified and characterised to display antagonistic activity at the receptor.

Detailed compound analysis shows first evidence of functional selectivity. Both, the identified agonists and antagonists are potent lead structures for the development of novel therapies for ischemia and inflammation, two diseases which are promoted or modulated by GPR17.

Furthermore, it could be shown that the receptor, upon activation, dependent on the cellular background is linked to the  $G_q$ ,  $G_i$  and  $G_s$  signal transduction pathways.

A detailed analysis of the signal transduction network reveals a novel calcium release mechanism in 1321N1 astrocytoma cells recombinantly expressing GPR17. This mechanism is characterized by a  $G_i$  dependent activation of a phosphatidylinositol (PI) specific phospholipase C. According to a hypothesis this in turn leads to a stimulation of intracellular calcium stores by  $IP_3$  receptors which is independent from inositol phosphate formation. Our model proposes the activation of  $IP_3$  receptors by the formation of a  $G_i$ -PI-PLC- $IP_3$  receptor complex.

---

## CHAPTER V: EXPERIMENTAL SECTION

---

### 5.1 Devices and materials

#### 5.1.1 Devices

Autoclave	3850 ELV, Systec
Incubator for bacteria	Innova 4200 Incubator Shaker, New Brunswick Scientific, NJ 08818-4005, USA
Balances	TE64, Sartorius, D-37075 Göttingen (precision balances) TE6101, Sartorius, D-37075 Göttingen
Camera	Imago charge-coupled device camera, Till Photonics, D-82166 Gräfelfing
Flasks for cell culture	25 cm <sup>2</sup> , 75 cm <sup>2</sup> , 175 cm <sup>2</sup> , Sarstedt, D-51582 Nümbrecht and Corning <sup>®</sup> Incorporated, NY 14831 USA
Centrifuges	Allgegra™ 21 R, Beckman Coulter™, CA 92822-8000, USA Avanti™ J-20I, Beckman Coulter™, CA 92822-8000, USA Biofuge pico, Heraeus, D-63450 Hanau

Centrifuges	MiniSpin, Eppendorf, D-22339 Hamburg Centrifuge 5810, Eppendorf, D-22339 Hamburg
CO <sub>2</sub> incubator	HERAcell <sup>®</sup> 240, Heraeus, D-63450 Hanau
Dry block heater	Thermomixer <sup>®</sup> comfort, Eppendorf, D-22339 Hamburg
Electrophoresis chambers	Schütt Labortechnik, D-37079 Göttingen Mini-Sub <sup>®</sup> cell GT, Bio Rad, CA 94547, USA Wide Mini-Sub <sup>®</sup> cell GT, Bio Rad, CA 94547, USA
Microbiological safety cabinets	S@fe flow 1.2, Nunc <sup>™</sup> , NY 14625-2385, USA Miroflow <sup>®</sup> Biological Safety Cabinet, Nunc <sup>™</sup> , NY 14625-2385, USA HeraSafe HS12, Thermo Electron Corporation, MA 02454, USA
Microplate readers	NOVOstar <sup>®</sup> , BMG LABTECH, D-77656 Offenburg Mithras LB940 Multimode reader, Berthold Technologies, D-75323 Bad Wildbad TopCount NXT <sup>™</sup> microplate scintillation counter, PerkinElmer Life Sciences, MA 02451, USA
Microscopes	Axiovert 25, Zeiss Wilovert 30, hund WETZLAR, D-35580 Wetzlar CKX31, Olympus, D-20097 Hamburg Axiovert 100 microscope, Zeiss
Microwave	Microwave 800, Severin, D-59846 Sundern
Monochromator	Polychrome II monochromator, Till Phototomics, D-82166 Gräfelfing
UV/VIS spectrophotometer	DU <sup>®</sup> 530, Beckman Coulter <sup>™</sup> , CA 92822- 8000, USA

PCR cyclers	Px2 Thermal Cycler, Thermo Electron Corporation, MA 02454, USA GeneAmp <sup>®</sup> PCR System 9700, Applied Biosystems 2720 Thermal Cycler, Applied Biosystems, CA 92008, USA
pH meter	SevenEasy <sup>™</sup> , Mettler Toledo, D-35353 Giessen
Objective	Oil immersion F-Fluar 40x, Zeiss
Photo documentation system	Universal Hood II, Bio Rad, CA 94547, USA De Vision DBOX, Decon Science Tec
Pipettes	0.5-10 µl; 10-100 µl; 20-200 µl; 100-1000 µl physiocare concept pipettes, Eppendorf research (Eppendorf, D-22339 Hamburg) 25-250 µl MultiMate Liquidsystems, Mettler Toledo
Pipette tips	Sarstedt, D-51582 Nümbrecht CyBio, D-07745 Jena 384/25 µl (for the Epic <sup>®</sup> system)
Power supplies (electrophoresis)	PowerPac 300, Bio Rad, CA 94547, USA PowerPac HC <sup>™</sup> , Bio Rad, CA 94547, USA Elite 300 plus, Bio Rad, CA 94547, USA
Vortex	Vortex genius 3, IKA <sup>®</sup> , D-79219 Staufen
Freezer (-80°C)	Ultra Low, Sanyo, D-81829 Munich

### 5.1.2 Consumables

Agarose UltraPure	Invitrogen <sup>™</sup> , D-64293 Darmstadt; #15510-27
Aloin	Sigma, D-21147 Hamburg; #B6906
Ampicillin sodium salt	Roth, D-76231 Karlsruhe; #K029.1
γ-Aminobutyric acid	Sigma, D-21147 Hamburg; #A44401



---

2-Aminoethoxydiphenylborane (2-APB)	Biozol, D-85386 Eching; #64970
Arbutin	Sigma, D-21147 Hamburg; #A4256
Betulinic acid	Sigma, D-21147 Hamburg; #855057
Bisindolylmaleimidel (GF 109203X)	Tocris, Bristol BS11 0QL, UK; #0741
Bromphenol blue	Fluka, D-21147 Hamburg; #32712
Calcium chloride, dehydrate	Sigma, D-21147 Hamburg; #C3306
Capsaicin	Sigma, D-21147 Hamburg; #M2028
p-Coumaric acid	Sigma, D-21147 Hamburg; #C9008
Dantrolene, sodium salt	Tocris, Bristol BS11 0QL, UK; #0507
DMSO	Riedel-de Haen, D-30926 Seelze; #60153
dNTP Mix	Promega, WI 53711, USA; #U1511
Edelfosine	Tocris, Bristol BS11 0QL, UK; #3022
EDTA, disodium salt, dihydrate	Roth, D-76231 Karlsruhe; #8040.3
EGTA	Roth, D-76231 Karlsruhe; #3054
Emodin	Sigma, D-21147 Hamburg; #E7881
Ferulic acid	Sigma, D-21147 Hamburg; #46278
Forskolin	Tocris, Bristol BS11 0QL, UK; #1099
Fura-2/AM	Molecular Probes, D-64293 Darmstadt; #F-1221
D-(+)-glucose	Sigma, D-21147 Hamburg; #G7021
Fluphenazine dihydrochloride	Sigma, D-21147 Hamburg; #F4765
Glycerol	Sigma, D-21147 Hamburg; #G2025
HBSS-buffer	Invitrogen™, D-64293 Darmstadt; #14025
HEPES (free acid)	Applichem; #A3268
Herniarin	Sigma, D-21147 Hamburg; #64951
Hydrochloric acid	Applichem, D-64291 Darmstadt; #0659
H 89 (N-[2-(p-Bromocinnamylamino) ethyl]- 5-isoquinolinesulphonamide dihydrochloride	Sigma, D-21147 Hamburg; #B1427
3-Isobutyl-1-methylxanthine (IBMX)	Tocris, Bristol BS11 0QL, UK; #2845
Imperatorin	Sigma, D-21147 Hamburg; #I6659

---

## CHAPTER V: EXPERIMENTAL SECTION

---

Lipofectamine™ 2000	Invitrogen™, D-64293 Darmstadt; #11668019
Lithium chloride solution	Sigma, D-21147 Hamburg; #L7026
LB agar	Invitrogen™, D-64293 Darmstadt; #22700041
LB powder medium (Luria/Miller)	Applichem, D-64291 Darmstadt; #A0854
Magnesium chloride, hexahydrate	Fluka, D-21147 Hamburg; #63068
Magnesium sulphate, heptahydrate	Applichem, D-64291 Darmstadt; #A1037
Montelukast	Biozol, D-85386 Eching; #10008318
Oregon Green® BAPTA-1/AM	Molecular Probes, D-64293 Darmstadt; #O6807
Pertussis toxin (PTX)	Sigma, D-21147 Hamburg; #2980
Phenol red	Sigma, D-21147 Hamburg; #P0290
Pluronic®-F127	Molecular Probes, D-64293 Darmstadt; #O6807
Polybrene	Aldrich, D-21147 Hamburg; #10,768-9
Polylysine coated yttrium silicate scintillation proximity assay (SPA) beads	Amersham Biosciences, Buckinghamshire HP7 9NA, UK; #TRK911
Potassium chloride	Fluka, D-21147 Hamburg; #60128
Potassium dihydrogen phosphate	ZVE, D-53121 Bonn; #234984
Pranlukast	Biozol, D-85386 Eching; #10008319
Purpurin	Sigma, D-21147 Hamburg; #82631
Sodium acetate	Applichem, D-64291 Darmstadt; #4555
Sodium butyrate	Fluka, D-21147 Hamburg; #19364
Sodium chloride	Fluka, D-21147 Hamburg; #71376
Sodium dodecyl sulphate (SDS)	Applichem, D-64291 Darmstadt; #1502
Disodium hydrogen phosphate, dihydrate	Roth, D-76231 Karlsruhe; #4984
Sodium hydrogen carbonate	Merck, D-64293 Darmstadt; #1.06323.2500
Sodium hydroxide	Fluka, D-21147 Hamburg; #71689
Thapsigargin	Tocris, Bristol BS11 0QL, UK; #1138
TRIS UltraPure	Roth, D-76231 Karlsruhe; #5426
Tryptone	Roth, D-76231 Karlsruhe; #8952.1

---

U-73343	Enzo Life Sciences, PA 19462-1202, USA; #BML-ST392-0005
U-73122	Biozol, D-85386 Eching; #70740
Umbelliferone	Sigma, D-21147 Hamburg; #93979
W-7 (N-(6-Aminohexyl)-5-chloro- 1-naphthalenesulphonamide hydrochloride	Aldrich, D-21147 Hamburg; #283916
Xanthine	Sigma, D-21147 Hamburg; #X7375
Yeast extract	Applichem, D-64291 Darmstadt; #3732
Zafirlukast	Biozol, D-85386 Eching; #10008282

### 5.1.3 Kits

IP-One HTRF <sup>®</sup> assay kit	Cisbio Bioassays, BP 84175, France; #62P1APEB
cAMP Dynamic 2 HTRF <sup>®</sup> assay kit (cell based assay)	Cisbio Bioassays, BP 84175, France; #62AM4PEC
QIAquick <sup>®</sup> Gel Extraction Kit	QIAGEN GmbH, D-40724 Hilden; #28706
QIAquick <sup>®</sup> PCR purification Kit	QIAGEN GmbH, D-40724 Hilden; #28106
QIAprep <sup>®</sup> Spin Miniprep Kit	QIAGEN GmbH, D-40724 Hilden; #27106
Plasmid Midi Kit	QIAGEN GmbH, D-40724 Hilden; # 12145

### 5.1.4 Radioligands

[2- <sup>3</sup> H]Myo-inositol	Amersham Biosciences, Buckinghamshire HP7 9NA, UK; #TRK911
---------------------------------	---

### 5.1.5 Software

Office Excel 2002	Microsoft® Corporation, D-85716 Unterschleißheim
Office PowerPoint®	Microsoft® Corporation, D-85716 Unterschleißheim
Office Word 2002	Microsoft® Corporation, D-85716 Unterschleißheim
Prism® 4.02	GraphPad Software, Inc, CA 92037, USA
MicroWin 2000 AdvII v4.41	Mikrotek Laborsysteme GmbH, D-51491 Overath
Quantity One® Version 4.4.0	Bio Rad, CA 94547, USA
DeVision G v1.0	Decon Science Tec GmbH, D-37318 Hohengandern
Assay Development Mode Epic™ V1.22.2	Corning® Incorporated, NY 14831, USA
Microplate Analyzer v1.5 modified for Excel 2002	Corning® Incorporated, NY 14831, USA
NOVOstar® 1.20-0	BMG LABTECH, D-77656 Offenburg
TopCount NXT™ 1.06	PerkinElmer Life Sciences, MA 02451, USA
TILLvisION imaging system	Till Photonics, D-82166 Gräfelfing
EndNote 9.0.0 (Bld 1425)	Thomson, PA 19130, USA
ClustalW 2.0.12	Des Higgins, Julie Thompson and Toby Gibson
ClustalX 2.0.12	Des Higgins, Julie Thompson and Toby Gibson
TreeView (Win32) 1.6.6	Roderic D. M. Page
MDL ISIS™/Draw 2.5	MDL Information System, Inc., CA 95051, USA

## 5.2 Cell culture

### 5.2.1 Cell lines

Cell line	Species	Organ	Source
GPR17-1321N1	Human	Brain	Recombinant cell line which was created within this PhD thesis
1321N1	Human	Brain	Working group of Professor C. E. Müller, Pharmaceutical Institute, Pharmaceutical Chemistry I, University of Bonn
GPR17-CHO	Chinese hamster	Ovaries	Recombinant cell line; working group Professor E. Kostenis, Institute of Pharmaceutical Biology, University of Bonn
CHO-K1	Chinese hamster	Ovaries	ATCC® number CCL-61
GP+envAM12	Mouse	Embryonic fibroblasts	Recombinant cell line; AK Professor W. Kolanus, Institute of Molecular Physiology and Developmental Biologie, University of Bonn

### 5.2.2 Materials and supplements for cell culture

Blasticidin	InvivoGen; #ant-bl-1
Doxycycline hyclate	Sigma, D-21147 Hamburg; # D9891
Foetal calf serum (FCS)	Sigma, D-21147 Hamburg; #-0804
Geneticin 418 (G418)	Gibco, Paisley PA4 9RF, UK; #11811
Hygromycin B	Merck, D-64293 Darmstadt; #400052
Hypoxanthine	Applichem, D-64291 Darmstadt; #A0700
Mycophenolic acid	Tocris, Bristol BS11 0QL, UK; #1505
Penicillin-Streptomycin solution	Invitrogen™, D-64293 Darmstadt; #15140-122
Trypsin	Lonza, 4002 Basel, Switzerland; #17-160

### 5.2.3 Solutions for cell culture

#### Phosphate buffered saline (PBS)

150 mM NaCl, 2.5 mM KCl, 7.5 mM Na<sub>2</sub>HPO<sub>4</sub>, 1.5 mM KH<sub>2</sub>PO<sub>4</sub> are dissolved in a. dem.. The pH value of 7.2 is adjusted with hydrochloric acid and the solution afterwards autoclaved.

#### Trypsin/EDTA solution (0.05%/0.6 mM)

For the preparation of 1 l of a trypsin/EDTA solution 6 ml of a 0.1 M EDTA stock solution are filled up to 1 l with PBS and autoclaved. Afterwards 20 ml of a sterile 2.5% trypsin solution and 750 µl of a sterile 0.5% phenol red solution (final concentration 0.01%) are added under sterile conditions. The solution is splitted and stored at 4°C.

#### Hypoxanthine solution (10 mg/ml)

Hypoxanthine is suspended in 80% of the final amount of a. dem.. 1 N hydrochloric acid is added in portions until the substance is completely dissolved.

Afterwards the residual amount of a. dem. is added and sterilised. The solution is stored at -20°C.

**Xanthine solution (10 mg/ml)**

Xanthine is suspended in 80% of the final amount of a. dem.. 1 N hydrochloric acid is added in portions until the substance is completely dissolved. Afterwards the residual amount of a. dem. is adjoined and sterilised. The solution is stored at -20°C.

**Solution of mycophenolic acid (10 mg/ml)**

Mycophenolic acid is suspended in 80% of the final amount of a. dem.. 1 N hydrochloric acid is added in portions until the substance is completely dissolved. Afterwards the residual amount of a. dem. is adjoined and sterilised. The solution is stored at -20°C in the absence of light.

**Solution of sodium butyrate (500 mM)**

55.05 mg sodium butyrate are dissolved in 1 ml of a. dem. The solution is sterilised and stored at -20°C.

**Polybrene solution (4 mg/ml)**

For the preparation of 5 ml polybrene solution, 20 mg of the substance are dissolved in the above-mentioned amount of a. dem. Afterwards the solutions is sterilised and stored at 4°C.

**Genitacin 418 (G418) (50 mg/ml)**

50 mg of active substance of genitacin is dissolved in 1 ml of a. dem. The final concentration of G418 in the selection medium is 800 µg/ml. The solution is sterilised and stored at -20°C.

### **Doxycycline (1 mg/ml)**

1 mg of doxycycline is dissolved in 1 ml of a. dem. The final concentration of doxycycline in the medium for the induction of receptor expression in CHO-GPR17 cells is 1 µg/ml. Doxycycline stock solution is stored at -20°C.

## **5.2.4 Media for mammalian cells**

### **HXM medium for GP+envAM12 packaging cells**

50 ml of foetal calf serum (FCS), 5 ml of penicillin G / streptomycin solution (final concentration 100 U/ml penicillin, 100 µg/ml streptomycin), 1% ultra glutamine, 0.75 ml of hypoxanthine (10 mg/ml), 12.5 ml of xanthine (10 mg/ml), 1.25 ml of mycophenolic acid (10 mg/ml) and 2 ml of hygromycin B (50 mg/ml) are added to 500 ml DMEM. If necessary, the pH value must be adjusted again by adding a few drops of concentrated hydrochloric acid. In this case the medium has to be sterilised by filtering.

### **Medium for native 1321N1 astrocytoma cells**

DMEM medium, including 10% foetal calf serum (FCS), is used for culturing native 1321N1 astrocytoma cells.

### **Medium for retrovirally transfected 1321N1 astrocytoma cells**

G418 (800 µg/ml G418) is added to DMEM medium with 10% FCS for preparation of medium to cultivate 1321N1 astrocytoma cells stably expressing GPR17.

### **Medium for native Chinese hamster ovary (CHO) cells**

DMEM/F-12 medium with 10% FCS is used to cultivate native CHO cells.



**Medium for Flp-In T-rex-CHO (FLIPR) cells (= CHO-GPR17 cells)**

DMEM/F-12 medium with 10% FCS, 30 µg/ml of blasticidin and 500 µg/ml of hygromycin B is used for culturing stable CHO cells generated by using the Flp-In T-rex system. Doxycycline is added up to a concentration of 1 µg/ml for the induction of receptor expression in this cell line.

**5.2.4 Cell culture techniques****Breeding of cells**

Eukaryotic cells are cultured in an incubator at 37°C, 5% carbon dioxide and a humidity of 95%. Normally, cells grow adherent at the bottom of a cell culture flask of different sizes (T25 cm<sup>2</sup>, T75 cm<sup>2</sup> or T175 cm<sup>2</sup>). When cells are grown confluent, up to 80-90%, cells have to be subcultured by removing the medium and rinsing the cell monolayer with PBS buffer (5.2.3). Afterwards PBS buffer is removed and a trypsin/EDTA solution is added (0.5 ml, 1 ml and 1.5 ml respectively; 5.2.3). The cells are incubated until they are detached. The reaction of trypsin is stopped by adding fresh medium. After resuspension with a pipette, cells are transferred to a new cell culture flask. The amount of cells which are transferred depends on the required splitting ratio. Afterwards fresh medium (5.2.4) is added to obtain a total volume of 5 ml, 12 ml and 20 ml respectively.

**Thawing of cells**

A cryotube is taken out of the liquid nitrogen and incubated in a water bath (37°C) until the ice has just about melted. The cells are transferred to a centrifuge tube with fresh, warmed-up medium (5.2.4). They are then pelleted by centrifugation for 5 min at 200 g. The supernatant is aspirated and the cells are resuspended with fresh medium without antibiotics (corresponding to the medium used for native cells; 5.2.4). The cells are transferred to a fresh T75 cm<sup>2</sup> cell culture flask prefilled with culture medium without antibiotics (5.2.4). The next day the medium is replaced with cultivation medium (if necessary with antibiotics; 5.2.4).

### **Freezing of cells**

The cells are harvested as described previously (5.2.4) and transferred to a centrifuge tube. After being pelleted by centrifugation (200 g at 4°C), the cells are resuspended in precooled freezing medium consisting of 90% FCS and 10% DMSO. The cell suspension is transferred to cryotubes. The cryotubes are placed into a special freezing container, which in turn is placed into a -80°C freezer overnight. The next day, the cryotubes are transferred to a liquid nitrogen tank for long-time storage.

### **Counting of cells**

An improved Neubauer counting chamber is used for counting of cells. 10 µl of a cell suspension are injected between the counting surface and a cover slip. The numbers of cells of four big squares, each subdivided into 16 smaller squares, are counted. Finally, the cell number can be calculated by the following term: cells per ml = (counted cells x 10000)/4.

### **Retroviral transfection of 1321N1 astrocytoma cells**

#### **Background**

Retroviruses are viruses whose RNA genome is transcribed into DNA by a reverse transcriptase after infection of a host cell. Then DNA is inserted into the host genome. The advantages of a transfection method using retroviruses are the generation of stably transfected cells and the high efficiency.

The virus genome consists of the essential genes gag, env, pol and the packaging signal Ψ (psi), which are flanked by long terminal repeats (LTR). The gag gene codes for capsid polypeptides, the env gene for virus envelope polypeptides and the pol gene for the virus reverse transcriptase and integrase. LTR regions function as a promoter, enhancer, regulatory sequences for the reverse transcription and the insertion of virus genes into the host genome. The sequences between the flanking LTR regions are also reversely transcribed and inserted.<sup>[158]</sup>

A helper cell line, a so-called packaging cell line which produces replication deficient viruses, is used for the retroviral transfection. It is important that deficient viruses are used for the infection of the host cell, because wild type retroviruses weaken and destroy the host cell by virus production. In this case the amphotropic packaging cell line GP+envAM12, which is derived from mouse embryonic fibroblasts, is used.<sup>[159, 160]</sup> The packaging cell line is stably transfected with two plasmids. The first plasmid carries the envelope gene and the gene for the resistance against the aminoglycoside hygromycin B. The second gene carries the information for capsid proteins (gag), reverse transcriptase (pol) of the murine leukaemia virus (MuLV) and a gpt gene which codes a xanthine-guanine-phosphoribosyl transferase. The packaging cell line is cultivated by adding hygromycin B, xanthine, hypoxanthine and mycophenolic acid to the medium as supplements under selective conditions. Mycophenolic acid inhibits the endogenous purine synthesis, so that the cell line is dependent on the xanthine-guanine-phosphoribosyl transferase which produces purines. The packaging cell line lacks the packaging signal  $\Psi$ , so that no virus production takes place.<sup>[159, 161, 162]</sup> All components necessary for the production of infectious viruses are not present until the packaging cell line is transfected with the vector pLXSN containing the receptor DNA of interest, because the vector also carries the packaging signal  $\Psi$ . In this case the information for the inserted receptor, viral promoters and packaging signal is packed into the virus in contrast to the information about the other viral proteins, so that no new viruses can be produced in the host cell.<sup>[158]</sup> To enhance the efficiency of infection by the virus, the packaging cell line is co-transfected with a second retroviral pLXSN plasmid, which carries the information for the G glycoprotein of the envelope of the vesicular stomatitis virus (VSV-G). The so-called pseudo-typing facilitates the virus by the presentation of the glycoprotein, to bind not only to specific receptors on the surface but to all phospholipids of the host cell.<sup>[163]</sup> After the transfection of the host cell with the deficient viruses which carry the receptor information, the successfully transfected cells can be selected by the addition of the neomycin derivative G418, because the resistance against this antibiotic is transfected together with the receptor information (Figure 49).

### Procedure

The retroviral transfection of 1321N1 astrocytoma cells is performed as described.<sup>[66]</sup> The packaging cell line GP+envAM12 is cultivated in HXM medium (5.2.4). One day before transfection  $1.5 \times 10^6$  cells are seeded and incubated overnight at 37°C, 5% CO<sub>2</sub> and 95% humidity in a 25 cm<sup>2</sup> cell culture flask containing medium without antibiotics (5.2.4). For at least two hours before transfection the medium is exchanged for 6.25 ml DMEM medium without any additive. Two solutions are prepared for the transfection. The first solution consists of 25 µl of Lipofectamine™ 2000 (final concentration 2%) and 600 µl of DMEM medium without any additives while the second solution is composed of 6.25 µg of pLXSN-GPR17 and 3.75 µg of pLXSN-VSV-G vector DNA. The second solution is filled up with DMEM medium without any additives. Solution one is incubated for 5 min at room temperature before both solutions are combined and incubated for 20 min, also at room temperature. Afterwards the sample is added to the packaging cell line and incubated for 12-15 h. The medium is then replaced with 3 ml of fresh medium containing 30 µl of a 500 mM sodium butyrate solution. The virus production is stimulated by sodium butyrate and takes place by incubation for 48 h at 32°C and 95% humidity. One day before infection 500,000 of 1321N1 astrocytoma cells are seeded in a 25 cm<sup>2</sup> cell culture flask. After 48 h of virus production, the retroviruses are harvested and sterilised by filtration through a filter with a pore size of 45 µm. The host cell medium is replaced with the sterilised virus supernatant containing 6 µl of polybrene solution (5.2.3) and the infection of the host cells takes place for further 48 h of incubation at 37°C, 95% humidity and 5% CO<sub>2</sub>. After incubation, the transfected cells are transferred to a 175 cm<sup>2</sup> cell culture flask and selected by adding medium containing G418 (5.2.4). The efficiency of infection and stable transfection using this method is up to 95%.

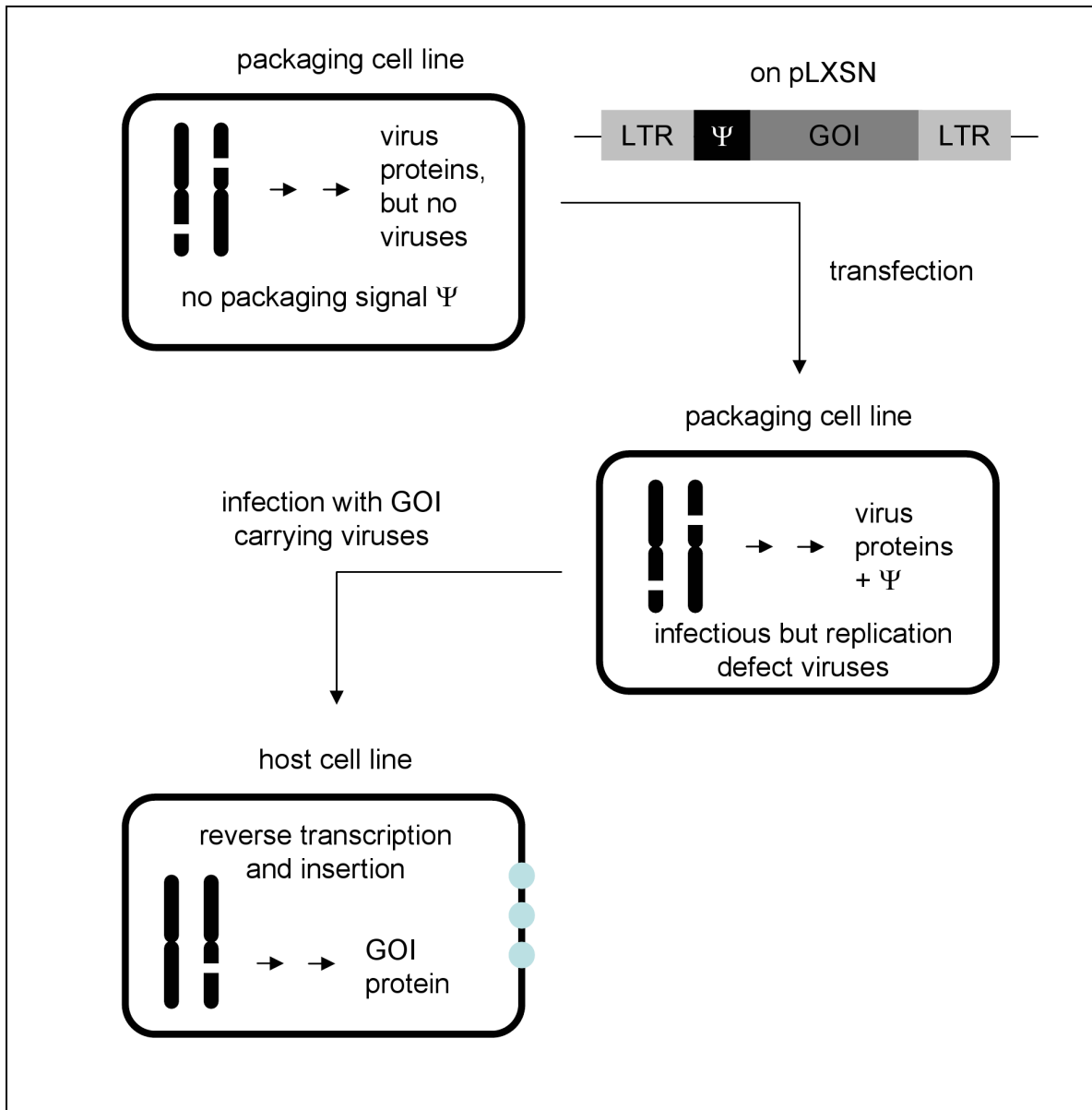


**Figure 49.** Scheme of a retroviral transfection. The packaging cell line produces virus proteins but it lacks the packaging signal  $\Psi$ . Upon transfection with a plasmid carrying a packaging signal and a gene of interest (GOI), the packaging cell line starts to produce infectious but replication defect viruses, whereas the viruses are loaded with GOI transcripts but lack the information for other virus proteins. After infection, the GOI is inserted via the GOI flanking long terminal repeat (LTR) regions into the genome of the host cell line, and the GOI protein biosynthesis takes place. The figure is modified according to Hu and Pathak.<sup>[158]</sup>

## **5.3 Molecular biology**

### **5.3.1 Solutions for molecular biology**

#### **TAE buffer for agarose gel electrophoresis (50x)**

TAE buffer consists of 2 M TRIS and 50 mM EDTA in a. dem.. The pH value is adjusted by adding 57.1 ml of glacial acetic acid. The solution is autoclaved and stored at room temperature. Before usage the buffer is diluted to 1-fold.

#### **DNA loading dye (6x)**

DNA loading dye is prepared by dissolving 25 mg of bromphenol blue (0.25%) in equivalent amounts of glycerol and a. dem.. The dye is stored at 4°C.

#### **Ribonuclease A (RNase A) solution for DNA preparation**

20 mg of RNase A are dissolved in 1 ml of 50 mM TRIS/1 mM EDTA buffer. For the inactivation of DNases the solution is incubated for 10 min at 99°C. The sample is splitted (40 µl) and stored frozen at -20°C. Before usage the sample is filled up to 1 ml with sterile a. dem..

#### **10 mM EDTA, pH value 8.0**

EDTA is dissolved in a. dem. and the pH value of 8.0 is calibrated by adding 1 N sodium hydroxide solution. Afterwards the solution is autoclaved.

#### **TRIS-EDTA/sodium hydroxide/SDS solution for DNA preparation**

The following buffers are needed for the preparation of 500 ml of TENS solution. 50 ml 100 mM TRIS-buffer are prepared by dissolving 605 mg of TRIS in 45 ml of

a. dem. (final concentration 10 mM) and adjusting the pH value to 7.4. Afterwards the solution is filled up to 50 ml with a. dem.. In addition, 50 ml of 10 mM EDTA (final concentration 1 mM) are separately prepared by staggering 146 mg of EDTA with 45 ml of a. dem.. EDTA is dissolved by adding sodium hydroxide (pH 8.0). Then the solution is filled up to 50 ml with a. dem.. Afterwards the two solutions are pooled and 12.5 ml of a 20% SDS solution (final concentration 0.5%), and 50 ml of a 1 N sodium hydroxide (final concentration 0.1 N) solution are added. The buffer is filled up to 500 ml with a. dem., autoclaved and stored at room temperature.

### **Sodium acetate solution (3 M) for DNA preparation**

For the preparation of 100 ml of 3 M sodium acetate solution, 24.6 g of sodium acetate are dissolved in 90 ml of a. dem. and the pH value is adjusted up to 5.2. Finally, the solution is filled up to 100 ml by adding the required amount of a. dem.. The solution can be stored at room temperature.

### **Ampicillin stock solution (100 mg/ml)**

100 mg of ampicillin are dissolved in 1 ml of a. dem.. For the selection of recombinant bacteria, the stock solution has to be diluted to a concentration of 100 µg/ml of ampicillin in LB medium (5.3.3).

### **5.3.2 Bacteria**

One Shot<sup>®</sup> TOP 10 chemically competent *E. coli*      Invitrogen<sup>™</sup>, D-64293  
Darmstadt; #C4040-10

### 5.3.3 Media for bacterial cultures

#### LB-medium for bacteria

25 g of LB powder medium are dissolved in 900 ml of a. dem., and the pH value of the medium is adjusted up to 7.5 with 1 N sodium hydroxide solution. The volume is filled up to 1 l and afterwards the medium is autoclaved. If necessary, antibiotics are added after cooling down.

#### LB agar plates for cultivation of bacteria

For the preparation of 1 l of medium for LB agar plates, 32 g of an LB agar ready-to-use mixture (according to manufacturer's instructions; Invitrogen™, D-64293 Darmstadt) are dissolved in a. dem.. The solution is autoclaved and cooled down to a temperature of approximately 50°C. At this point antibiotics (if necessary for selection) are added to the liquid solution and the solution is spilled into 10 cm dishes. The agar sets while cooling down at room temperature. The plates are stored upside down at 4°C.

#### SOC medium for bacteria

20 g of tryptone, 5 g of yeast extract, 0.5 g of sodium chloride, 10 ml of a 0.25 M KCl stock solution, 5 ml of a 2 M MgCl<sub>2</sub> stock solution and 20 ml of a 1 M glucose solution are dissolved in 1 l of a. dem. for the preparation of 1 l SOC medium. The pH value of the medium is adjusted up to 7.0 and afterwards the medium is autoclaved.

### 5.3.4 Enzymes

Vent <sub>R</sub> ® DNA polymerase	New England BioLabs®, MA 01938-2723, USA; #M0254S
<i>Xho</i> l (restriction endonucleases)	New England BioLabs®, MA 01938-2723,



	USA; #R0146S
<i>Eco</i> RI (restriction endonucleases)	New England BioLabs <sup>®</sup> , MA 01938-2723, USA; #R0101S
T4-DNA ligase	New England BioLabs <sup>®</sup> , MA 01938-2723, USA; #M0202S

### 5.3.5 Vectors and molecular weight markers

pLXSN	Working group of Professor R. Nicolas, Department of Pharmacology, University of North Carolina, Chapel Hill, USA
Lambda DNA/ <i>Eco</i> RI+ <i>Hind</i> III	Fermentas, D-68789 St. Leon-Rot, #SM0191
PhiX174 DNA/ <i>Bsu</i> RI ( <i>Hae</i> III)	Fermentas, D-68789 St. Leon-Rot, #SM0251

### 5.3.6 Protocols for molecular biological techniques

#### Breeding of bacteria

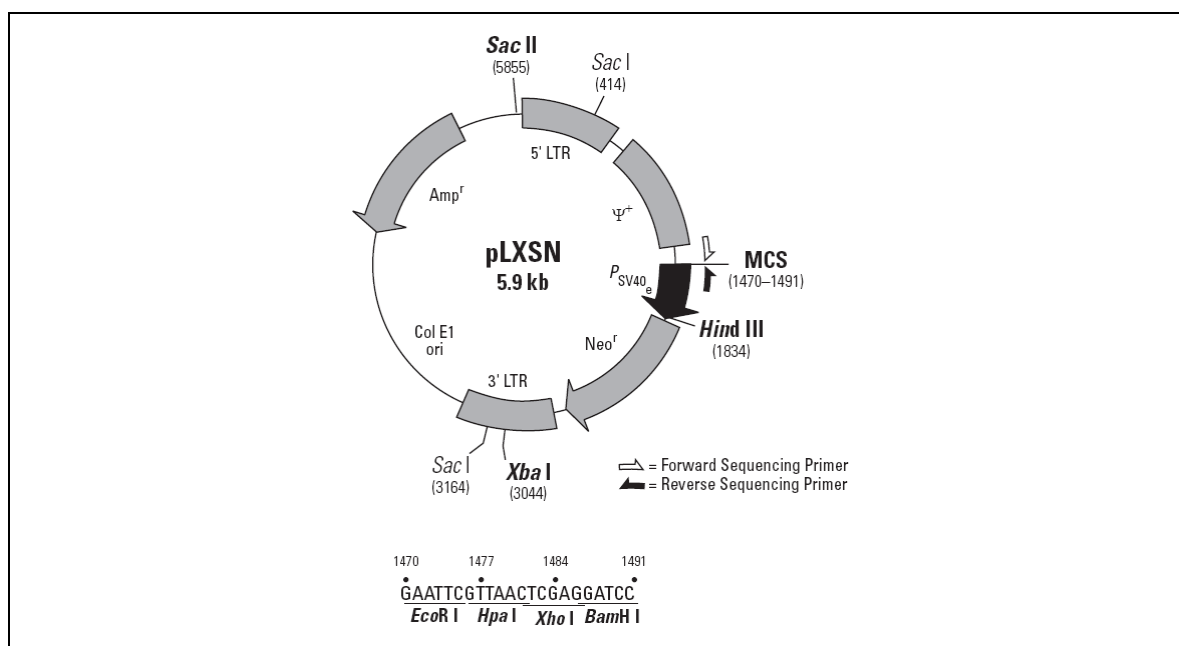
Prokaryotic cells are bred in 4 ml of LB-medium (with antibiotics, if required) overnight at 200 rpm and 37°C. The LB-medium is inoculated by a single bacterial colony or from a frozen glycerol stock by picking with a sterile pipette tip into the stock and discarding the used pipette tip into a prepared liquid LB-medium culture.

#### Freezing of bacteria

Prokaryotic cells are grown as described above and settled by centrifugation. The supernatant is removed and the cells are resuspended in LB-medium with 15% glycerol. The bacterial suspension is stored at -80°C.

### Insertion of receptor DNA into the retroviral expression vector pLXSN

The sequence for the human GPR17 was present as a cDNA clone and had to be subcloned into the vector pLXSN, which can be used for retroviral transfection of the human astrocytoma cell line 1321N1. The vector pLXSN is commercially available from Clontech Laboratories, CA 94043, USA (catalogue number #631509; GenBank accession no. M28248) and was kindly provided by the working group of Professor C. E. Müller, Pharmaceutical Institute, Pharmaceutical Chemistry I, University of Bonn.



### Primer design

Two flanking oligonucleotides were designed for the subcloning of receptor DNA. Both oligonucleotides consist of a restriction site, a short sequence which is homologous to parts of the GPR17 sequence and a short overhang. An *EcoRI* restriction site and a *XhoI* restriction site, respectively, have been introduced into the forward primer and the reverse primer. Both sites are unique restriction sites in the multiple cloning site of the target plasmid pLXSN.

	Sequence	Melting point
Forward oligonucleotide	5'-ata tat ata <u>tG'A ATT ,CAT</u> GAA TGG CCT TG-3'	58.2°C
Reverse oligonucleotide	5'-ata tat ata <u>tC'T CGA ,GTC</u> ACA GCT CTG ACT T-3'	62.9°C

The overhang is marked with lower case letters. Sequences representing restriction sites are underlined, the cutting site is marked with a single quotation mark and a comma, and the start and stop codons are on a grey background. Information concerning the melting points was provided by the supplier MWG-Biotech AG, D-85560 Ebersberg.

### Polymerase chain reaction (PCR)

The proof reading Vent<sub>R</sub><sup>®</sup> DNA polymerase (5.3.4) is used to reduce the mutation frequency for the amplification of receptor DNA and two specific oligonucleotides (5.3.6) are added in a final concentration of 10 pmol/μl each. Each deoxyribonucleotide triphosphate at 0.5 mM dNTPs and 2.5 mM MgSO<sub>4</sub> are used. A standard sample for the polymerase chain reaction is composed of the following ingredients:

	1 μl	forward primer
+	1 μl	reverse primer
+	5 μl	Vent <sub>R</sub> <sup>®</sup> DNA polymerase buffer (10x)
+	0.5 μl	Vent <sub>R</sub> <sup>®</sup> DNA polymerase (1 U)
+	0.5 μl	dNTP-Mix
+	2.5 μl	MgSO <sub>4</sub>
+	1 μl	template (~ 20 ng)
+	38.5 μl	a. dem.
	<hr/>	
	50 μl	

The protocol for the amplification is as follows:

94°C	2 min		
94°C	1 min	}	25 cycles
45°C	45 sec		
72°C	1.5 min		
72°C	7 min		
4°C	∞		

### Agarose gel electrophoresis

Agarose is suspended in 1-fold TAE buffer (5.3.1). 1-2% agarose gels are used, depending on the DNA fragment length. Fragments with a length of 500-6000 bp are differentiated on a 1% gel while smaller fragments are analysed on a 2% agarose gel. The suspension is boiled in a microwave until the agarose is completely dissolved. Afterwards ethidium bromide is added at a ratio of 1 to 1000 (v/v) to the liquid agarose solution. The solution is transferred to a prepared gel chamber with a comb. The comb forms the slots for the DNA samples in the solid gel. The gel is transferred to an electrophoresis chamber which is filled with 1-fold TAE buffer, so that the gel is completely covered with buffer. DNA samples are prepared by mixing with 6-fold DNA loading dye (final concentration 1-fold) and if necessary with a. dem. before they are added to the gel. A DNA molecular weight marker (5.3.5) is also pipetted into one slot for analysing the fragment length and/or concentration. A current of 100 V is used to separate DNA fragments. The fragments are analysed using a photo documentation system (5.1.1) (Figure 50).

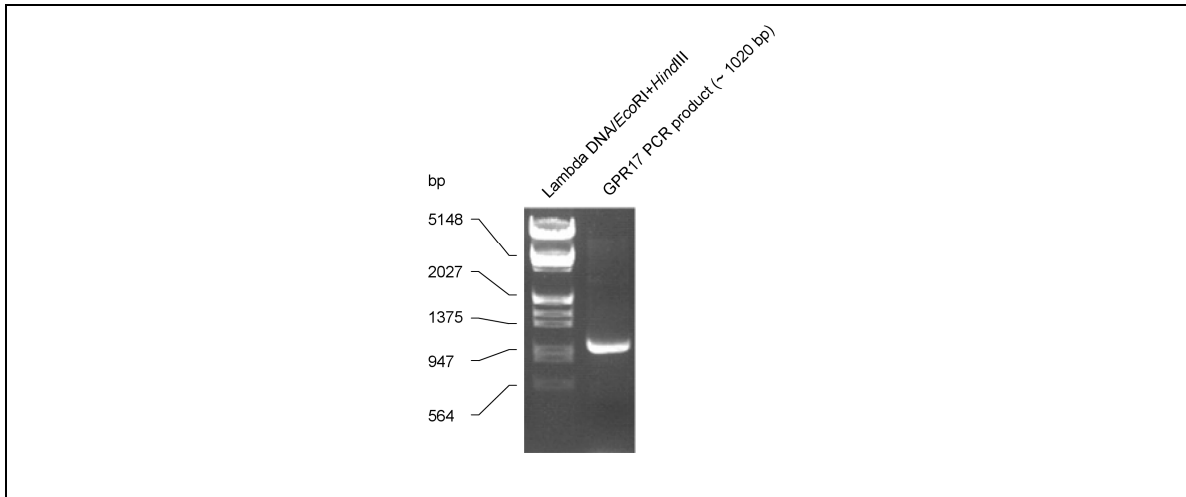


**Figure 50.** Agarose gel electrophoresis of a PCR (5.3.6) for the amplification of GPR17 receptor DNA. A DNA fragment with a molecular mass of approximately 1020 bp was expected.

### Extraction of DNA from agarose gels

The agarose gel is exposed to UV radiation for a short time period and the fragments of choice are cut out of the gel with a sharp scalpel. The piece of gel is transferred to an Eppendorf tube and the DNA is extracted with the QIAquick<sup>®</sup> Gel Extraction Kit from QIAGEN GmbH, D-40724 Hilden. The DNA extraction is performed accordingly to the manufacturer's instructions.

### Restriction digest

Vector DNA and PCR products are digested with restriction endonucleases under buffer conditions which are recommended by the manufacturer. Buffer conditions under which both enzymes have maximum activity are chosen for digestion with two different enzymes. If recommended by the manufacturer, albumin from bovine serum (BSA) is added to the digestion. The digestion takes place in a dry block heater for 1 h at 37°C and is terminated by incubating the sample for 20 min at 80°C (if possible; see manufacturers' instructions).

A standard composition for restriction digest is as follows:

	X $\mu$ l	Vector DNA or PCR products
+	0.5 $\mu$ l	<i>Eco</i> RI (10 U)
+	0.5 $\mu$ l	<i>Xho</i> I (10 U)
+	2.5 $\mu$ l	<i>Eco</i> RI-buffer
+	2.5 $\mu$ l	BSA (10-fold)
+	Y $\mu$ l	a. dem.
25 $\mu$ l		

### Purification of the digestion products

The digestion of vector DNA and PCR products is normally performed to prepare these DNA molecules for ligation (Figure 51). To eliminate side products, the fragments of choice are purified with the QIAquick<sup>®</sup> PCR Purification Kit from QIAGEN GmbH, D-40724 Hilden following the manufacturer's instructions.

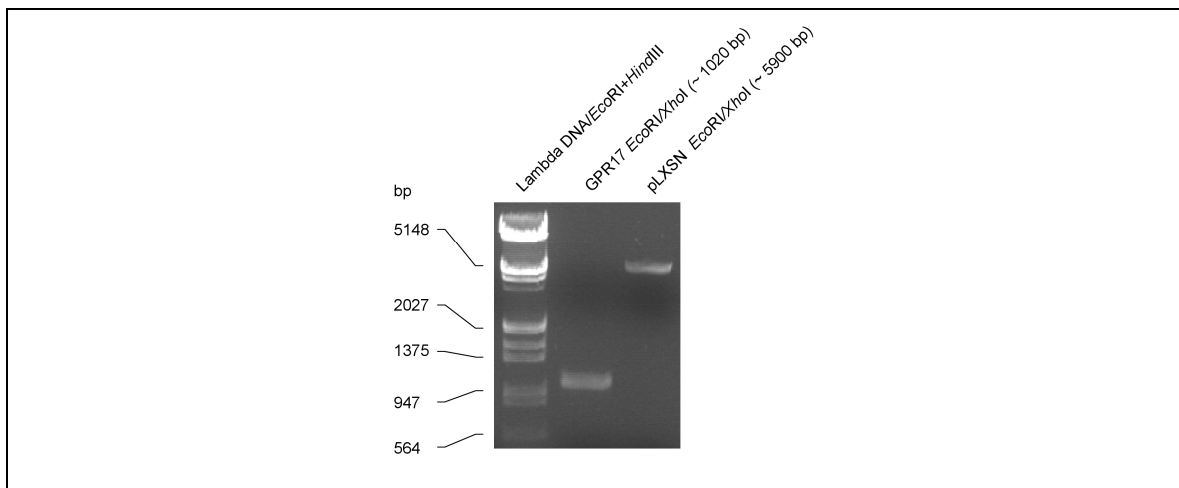


**Figure 51.** Agarose gel electrophoresis of the GPR17 PCR and pLXSN vector fragments after restriction with *Eco*RI and *Xho*I (5.3.6.7) and purification (5.3.6.8).

### Ligation of DNA fragments

The ligation of two DNA fragments which are prepared by digestion and purification is performed using T4-DNA ligase (5.3.4). The insert (GPR17-DNA) and the vector (pLXSN) are used in a molar ratio of 4:1, which corresponds to a

molecular weight ratio of approximately 1:1. Combined DNA of 0.1 to 0.4 µg is used. The ligation takes place at 16°C overnight in a dry block heater. A standard composition is as follows:

	X µl	Digested GPR17 insert-DNA (0.05-0.2 µg)
+	Y µl	Digested pLXSN vector-DNA (0.05-0.2 µg)
+	0.5 µl	T4-DNA ligase (200 U)
+	2 µl	T4-DNA ligase buffer (10-fold)
+	2 µl	ATP (100 mM)
+	Z µl	a. dem.
	<hr/>	
	20 µl	

### **Transformation of competent bacteria**

10 to 50 ng of plasmid DNA or 2 µl of a ligation sample (5.3.6) are added to 100 µl of competent *E. coli* TOP10 bacteria from Invitrogen™, D-64293 Darmstadt (5.3.2), then thawed on ice and mixed carefully with a pipette tip. After 30 min of incubation on ice, a heat shock is applied by placing the tube with the bacteria for 2 min into a water bath preheated to 37°C. Afterwards the bacteria are cooled down on ice for 2 min and 200 µl of SOC medium (5.3.3) are added to the sample. Within 1 h of incubation at 37°C and 200 rpm the bacteria develop the antibiotic resistance which is provided by the transformed plasmid. They are then pelleted by centrifugation (17900 g for 1 min) and the supernatant is removed by decanting. Bacteria are resuspended in residual medium by pipetting and distributed with a Drigalski applicator on an LB agar plate (5.3.3) containing the suitable antibiotic. Successfully transformed bacteria form colonies after incubation overnight at 37°C.

### **Preparation of plasmid DNA from bacteria**

For the amplification of a plasmid of choice, bacteria were transformed (5.3.6) and grown under selection conditions (5.3.6). There are two protocols for the preparation of plasmid DNA. The TENS protocol (see below) is used to prepare the plasmid DNA from many cultures to check whether the subcloning was

successful. The second protocol for preparation using a kit is preferred when purified plasmid DNA for sequencing or further steps are needed (Figure 52).

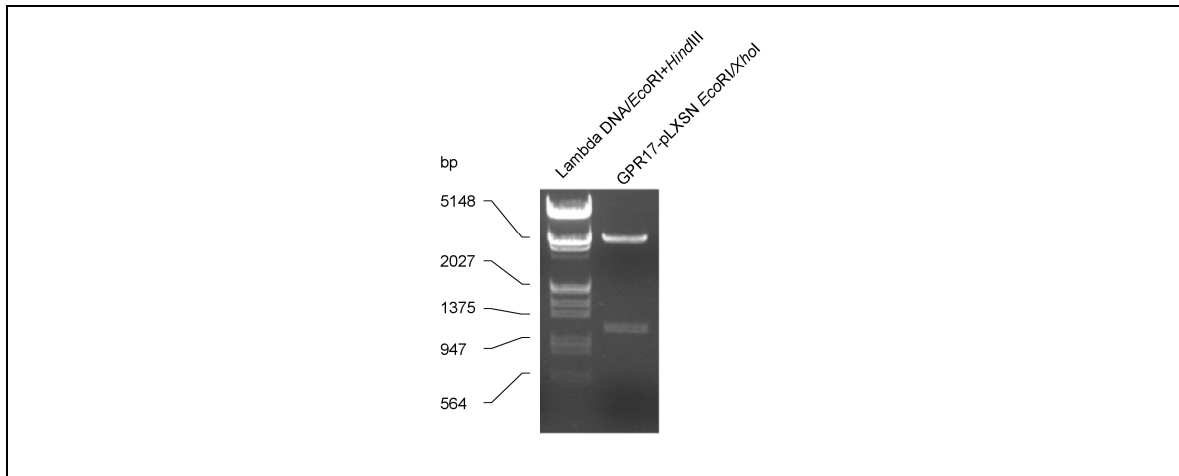


**Figure 52.** After subcloning, the vector DNA is isolated from the bacteria. To verify the isolated vector DNA, it was digested with the restriction enzymes *EcoRI* and *XhoI* (5.3.6.7). A vector fragment (~ 5900 bp) and a GPR17 insert fragment (1020 bp) were detected.

### Preparation of plasmid DNA using the TENS method

Bacteria are settled by centrifugation for 2 min at 17900 g. The supernatant is discarded and the bacteria are resuspended in 40  $\mu$ l of RNase A solution. Bacteria are lysed by the addition of 300  $\mu$ l of TENS solution (5.3.1). After adding 150  $\mu$ l of 3 M sodium acetate, the sample is mixed carefully and the developing precipitate is pelleted by centrifugation for 10 min at 17900 g. The supernatant is transferred to a new Eppendorf tube. Plasmid DNA precipitates after the addition of 900  $\mu$ l of ice-cold absolute ethanol. After precipitation, the plasmid DNA is separated from other soluble cell components by centrifugation (2 min, 17900 g). The supernatant is discarded and the plasmid DNA pellet is washed carefully with 1 ml of ice-cold ethanol (70%). After another centrifugation step, the ethanol is removed and the pellet is dried in a dry block heater. Plasmid DNA is dissolved in 40  $\mu$ l of sterile a. dem. after the pellet has dried completely. Plasmid DNA which has been isolated in this way cannot be used, for example for sequencing because applied EDTA when not removed completely interferes with this.



**Preparation of plasmid DNA using a kit**

If clean plasmid DNA is needed, it can be prepared from bacteria using the QIAprep® Spin Miniprep Kit from QIAGEN GmbH, D-40724 Hilden. The preparation is performed according to manufacturer's recommendations.

**Midi-preparation of plasmid DNA**

Large amounts of plasmid DNA are needed for the transfection of astrocytoma cells. In this case a midi-preparation of plasmid DNA is necessary. The preparation is performed using the Plasmid Midi Kit from QIAGEN GmbH, D-40724 Hilden and handled as described according to the manufacturer's instructions.

**Photometrical determination of DNA concentration**

For the photometrical determination of the concentration of a DNA sample 2 µl of the DNA are diluted in 1 ml of a. dem., and the absorption of that dilution is detected at a wavelength of 260 nm in a photometer. For reference a. dem. is used.

**Determination of the receptor DNA sequence inserted in the vector pLXSN**

The receptor DNA subcloned into the retroviral vector pLXSN is sequenced by GATC-Biotech, D-78467 Konstanz. 1 µg of plasmid DNA dissolved in sterile a. dem. is needed for sequencing. The oligonucleotides used for sequencing were designed by Dr. Petra Hillmann, Institute for Pharmaceutical Chemistry I, University of Bonn. The sequences of the primers are as follows:

	Sequence
Forward oligonucleotide	5'-CCC TTG AAC CTC CTC GTT CGA CC-3'
Reverse oligonucleotide	5'-CCA CAC CTG CTT GCT GAC TA-3'

Both oligonucleotides bind to pLXSN sequences which are close to the multiple cloning site of the vector where the receptor DNA is inserted.

## 5.4 Functional assays

### 5.4.1 Solutions for functional assays

#### Solutions for measuring intracellular calcium release

##### Krebs HEPES buffer (KHB)

The KHB buffer consists of an aqueous solution of 118.6 mM NaCl, 4.7 mM KCl, 1.2 mM  $\text{KH}_2\text{PO}_4$ , 4.2 mM  $\text{NaHCO}_3$ , 11.7 mM D-glucose, 10 mM HEPES (free acid). A 5-fold concentrated buffer without  $\text{CaCl}_2$  and  $\text{MgSO}_4$  is prepared and stored at  $-20^\circ\text{C}$ . After diluting this buffer to 1-fold,  $\text{MgSO}_4$  and  $\text{CaCl}_2$  are added at 1.3 mM and 1.2 mM, respectively. The pH value of 7.4 is adjusted by adding 1 N sodium hydroxide.

##### Calcium-free Krebs HEPES buffer

The composition of the calcium-free KHB buffer is the same as for the standard KHB except that 1.2 mM  $\text{CaCl}_2$  of the standard KHB buffer is exchanged for 1.2 mM  $\text{MgCl}_2$ . EGTA is added to a final concentration of 100  $\mu\text{M}$ . The pH value of this solution is adjusted up to 7.4.

##### Oregon Green<sup>®</sup> stock solution

A 1 mM stock solution is prepared by adding 39.7  $\mu\text{l}$  of DMSO to 50  $\mu\text{g}$  of the fluorescence dye Oregon Green<sup>®</sup> 488 BAPTA-1/AM ( $M_r = 1258.07$  g/mol). Since the dye is sensitive towards light, the dissolution should take place in the absence of light. The sample is splitted to amounts of 3  $\mu\text{l}$ . The aliquots are stored at  $-20^\circ\text{C}$  in the absence of light.

**Fura-2 stock solution**

A 1 mM stock solution of the calcium indicator fura-2/AM ( $M_r = 1001.86$  g/mol) is prepared by dissolving 50  $\mu$ g of the dye in 49.9  $\mu$ l of DMSO. The sample is splitted to amounts of 3  $\mu$ l. Since the dye is sensitive to light, the aliquots are stored in the absence of light at  $-20^\circ\text{C}$ .

**Pluronic<sup>®</sup>-F127 stock solution**

The stock solution is prepared by dissolving 200 mg of pluronic<sup>®</sup>-F127 in 800  $\mu$ l of DMSO. The solution is stored at room temperature.

**2-Aminoethoxydiphenylborane (2-APB) (10 mM)**

2-APB is dissolved in DMSO up to a concentration of 10 mM. Inositol 1,4,5-triphosphate ( $\text{IP}_3$ ) receptors, which gate the calcium release from intracellular calcium stores, can be blocked by the cell-permeable antagonist 2-APB.<sup>[80, 164]</sup> For inhibition, 10  $\mu$ M of this compound are incubated for 30 min together with the cells before being measured. The solution is stored at  $-20^\circ\text{C}$ .

**Dantrolene (10 mM)**

Dantrolene is dissolved in DMSO up to a concentration of 10 mM. Dantrolene inhibits the release of  $\text{Ca}^{2+}$  from sarcoplasmic reticulum by inhibiting ryanodine receptor (RYR) channels.<sup>[77, 165, 166]</sup> It displays selectivity for RYR1 and RYR3 over RYR2. For the inhibition of ryanodine receptor channels, 20  $\mu$ M of the substance are incubated for 30 min together with the cells before being measured. The stock solution is stored at  $-20^\circ\text{C}$ .

**H 89 (10 mM)**

A H 89 stock solution is dissolved in DMSO up to a concentration of 10 mM. As a very potent and selective inhibitor of the protein kinase A, it is preincubated in a final concentration of 1  $\mu$ M with both 1321N1 and CHO cells for 30 min before starting measurement in.<sup>[91]</sup> The solution is stored at  $-20^\circ\text{C}$ .

**GF 109203X (10 mM)**

A GF 109203X stock solution is dissolved in DMSO up to a concentration of 10 mM. As a very potent and selective inhibitor of the protein kinase C (selective for the  $\alpha$  and  $\beta_1$  isoforms), it is preincubated in a final concentration of 1  $\mu$ M with both 1321N1 and CHO cells for 30 min before starting measurement.<sup>[92, 167-169]</sup> The solution is stored at -20°C.

**Thapsigargin (10 mM)**

Thapsigargin solid is dissolved in DMSO up to a concentration of 10 mM. The SERCA inhibitor is preincubated in a final concentration of 1  $\mu$ M with both 1321N1 and CHO cells for 30 min before starting measurement.<sup>[76, 170, 171]</sup> The stock solution is stored at -20°C.

**Edelfosine (10 mM)**

Edelfosine is dissolved in DMSO up to a concentration of 10 mM. Edelfosine inhibits phosphatidylinositol-specific phospholipase C.<sup>[73, 74]</sup> The effective final concentration is 5  $\mu$ M. The compound is preincubated with the cells for 30 min before being measured. The stock solution is stored at -20°C.

**U-73122 (1 mM)**

U-73122 is dissolved in DMSO up to a concentration of 1 mM. As an inhibitor of PLC-dependent processes, it is preincubated in a final concentration of 2.5  $\mu$ M with 1321N1 cells and 5  $\mu$ M in CHO cells 5 min before starting measurement.<sup>[172-174]</sup> The stock solution is stored at -20°C.

**U-73343 (1 mM)**

U-73343 is dissolved in DMSO up to a concentration of 1 mM. The inactive derivative of U-73122 is preincubated in a final concentration of 2.5  $\mu$ M with 1321N1 cells and 5  $\mu$ M in CHO cells 5 min before starting measurement. The stock solution is stored at -20°C.

**N-(6-Aminohexyl)-5-chloro-1-naphthalenesulphonamide hydrochloride (W-7)  
(10 mM)**

W-7 is a calmodulin inhibitor that is dissolved in DMSO up to a concentration of 10 mM. It is preincubated in a final concentration of 30  $\mu$ M with both 1321N1 and CHO cells 30 min before starting measurement.<sup>[84]</sup> The stock solution is stored at -20°C.

**Fluphenazine (10 mM)**

Fluphenazine is a calmodulin inhibitor that is dissolved in DMSO up to a concentration of 10 mM. It is preincubated in a final concentration of 30  $\mu$ M with both 1321N1 and CHO cells 30 min before starting measurement.<sup>[85]</sup> The stock solution is stored at -20°C.

**Solutions for single cell calcium imaging**

**Superfusion-buffer**

An aqueous buffer containing 135 mM sodium chloride, 4.8 mM potassium chloride, 1.3 mM calcium chloride, 1.2 mM potassium dihydrogen phosphate, 10 mM glucose and 10 mM HEPES is prepared for the superfusion of cells in a superfusion chamber. The solution is stored at 4°C.

**Solutions for measurement of inositol phosphate accumulation**

**Formic acid (1 M)**

Solid formic acid is dissolved in DMSO up to a concentration of 1 mM. The solution is stored at 4°C and has to be diluted 100-fold in HBSS-buffer without lithium chloride before use.

**Solutions to determine the accumulation of cAMP****Forskolin (10 mM)**

Forskolin is dissolved in DMSO up to a concentration of 10 mM. The solution is stored at -20°C.

**3-isobutyl-1-methylxanthine (IBMX) (50 mM)**

IBMX is dissolved in ethanol up to a concentration of 50 mM. The stock solution is stored at -20°C.

**Assay buffer**

An HBSS buffer (5.1.2) supplemented with 20 mM HEPES is used to perform the assay.

**5.4.2 Microplates for functional assays**

<b>Number of wells</b>	<b>Plate ID</b>	<b>Assay</b>
96	Rotilabo <sup>®</sup> microplate V-profile; Roth, D-76231 Karlsruhe #9292.1	Calcium assay
96	Clear F-bottom UV-Transparent microplate; Corning <sup>®</sup> Incorporated, NY 14831, USA; #3635	Calcium assay (fura-2/AM)
96	PS, F-bottom µclear, black; Greiner bio one, 4550 Kremsmünster, Austria #655096	Calcium assay (Oregon Green <sup>®</sup> BAPTA-1/AM)
96	Solid white F-bottom, PS, TC-treated, with lid, sterile; Corning <sup>®</sup> Incorporated, NY 14831, USA; #3917	Radioactive IP <sub>3</sub> accumulation assay

---

96	TC, F-bottom with lid, sterile; Sarstedt, D-51582 Nümbrecht; #83.1835	Radioactive IP <sub>3</sub> accumulation assay
384	LIA plate, white, TC, F-form Greiner bio one, 4550 Kremsmünster, Austria; #784080	HTRF <sup>®</sup> IP-One assay and HTRF <sup>®</sup> cAMP assay
384	Epic <sup>®</sup> fibronectin-coated cell assay microplate; Corning <sup>®</sup> Incorporated, NY 14831, USA; #5042	DMR assay
384	Clear round bottom, PP, untreated, without lid, nonsterile; Corning <sup>®</sup> Incorporated, NY 14831, USA; #3657	DMR assay

### 5.4.3 Protocols for functional GPCR analysis

#### Measurement of intracellular calcium efflux using the NOVOstar<sup>®</sup> microplate reader

##### Background

PLC activation and IP<sub>3</sub> accumulation result in a release of calcium from intracellular calcium stores, for example the endoplasmic reticulum. In order to detect the released calcium, cells are loaded with a cell membrane permeable dye, which is converted within the cell into its active form by the cleavage of ester bonds. The active form of the dye binds the released calcium. The fluorescence properties of the dye change after calcium binds to the dye. These changes can be detected automatically (in this case the NOVOstar<sup>®</sup> microplate reader, BMG LABTECH, D-77656 Offenburg) and represent the ligand-dependent receptor activation (Figure 53).

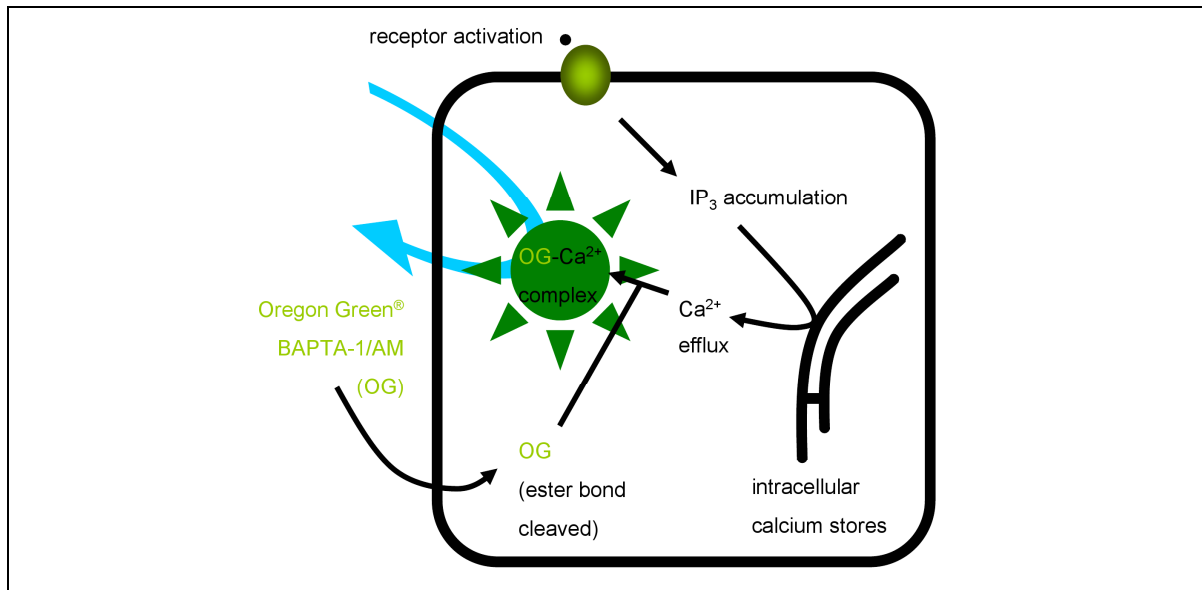


**Figure 53.** Principle of calcium efflux from intracellular calcium stores and its detection using Oregon Green® BAPTA-1/AM (OG) dye. Cells are loaded with the cell permeable calcium chelator OG (alternatively fura-2/AM), the ester bonds of which are cleaved intracellularly. After receptor activation, the built inositol phosphates stimulate the calcium channels of intracellular calcium stores. The activated channels pump calcium into the cytoplasm where they form a complex with the fluorescence dye. This complex can be stimulated, and the emitted fluorescence of the complex is detected.

### Procedure

The assay is performed as described previously.<sup>[66, 124, 125]</sup> Cells from two confluent grown (80 to 90%) 175 cm<sup>2</sup> cell culture flasks are needed for a calcium assay using the NOVOstar® microplate reader (approximately 150,000 cells per well).

Cells are harvested after removing the medium, washed once with PBS buffer and detached using a trypsin/EDTA solution. After incubation for 45 min at 37°C and 5% CO<sub>2</sub>, the cells are pelleted by centrifugation (5 min, 200 g). Cells are resuspended in 994 µl of Krebs HEPES buffer (KHB; 5.4.1) and loaded in the absence of light with one of two available fluorescents, namely Oregon Green® 488 BAPTA-1/AM dye or fura-2/AM (5.4.1), by incubating them for one hour at 28°C and 700 rpm in an Eppendorf Thermomixer (Eppendorf, D-22339 Hamburg) (5.1.1) in the presence of Pluronic® F-127 (5.4.1). Pluronic® F-127 is supplemented so that the cells can better absorb the dye. The cells are washed twice with 1 ml of KHB buffer (three centrifugation steps, each for 15 sec at



2700 rpm) before being seeded in a 96-well microplate in a total volume of 160  $\mu\text{l}$  or 180  $\mu\text{l}$  for antagonist or agonist testing respectively. In the case of antagonist testing the antagonists are submitted to the plate in 10-fold concentration (20  $\mu\text{l}$ ) before addition of the cell suspension. A 10-fold concentrated agonist solution (35  $\mu\text{l}$ ) is added to another 96-well microplate with a V-profile. Both plates are placed into the NOVOstar<sup>®</sup> microplate reader and incubated there for 20 min. If pathway inhibitors are used, the incubation time must be matched to the time at which the inhibitor effect occurs.

After incubation, the required gain is determined by the microplate so that the fluorescence background of the cells is between 38,000 and 42,000 fluorescence units. This background is an optimal range for starting the measurement, because it is in the middle of the reader's detection range. Normally, the background in each well of a microplate should be the same. The background is determined by performing a so-called validation. A validation is performed to detect irregularities in cell densities between different wells, fluorescence or absorption properties as well as unspecific antagonist effects. These irregularities are noticeable when the background is significantly increased or decreased compared to the normal range. Afterwards, 20  $\mu\text{l}$  of agonist are injected from the source plate to the measurement plate by the injector unit of the NOVOstar<sup>®</sup>, and the increase in fluorescence is determined as a function of the calcium efflux resulting from receptor stimulation (Figure 54).

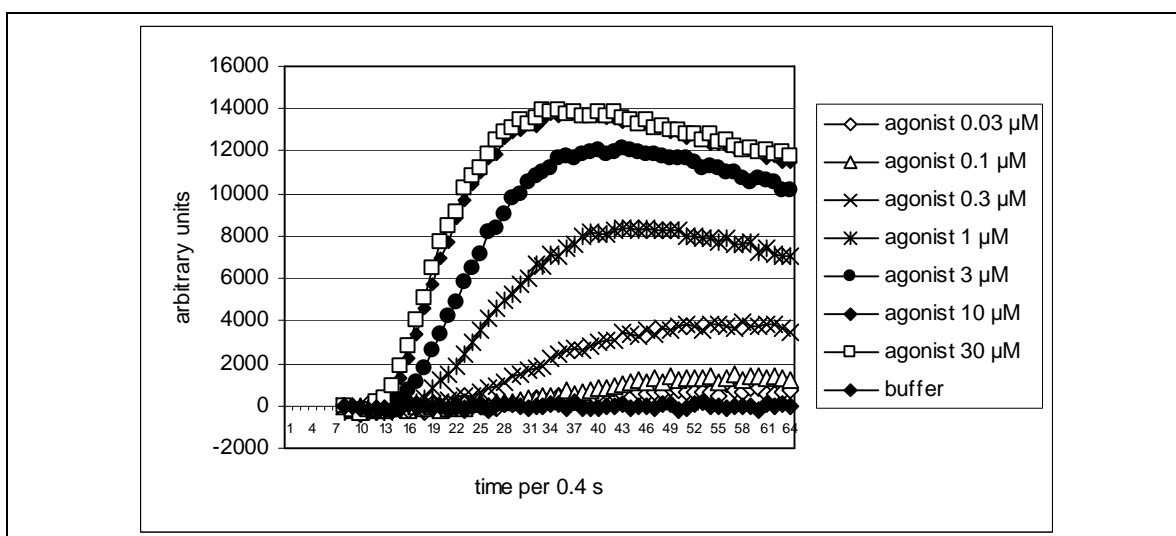


**Figure 54.** Plot of the intracellular calcium increase in a cell population assay as a function of time. The calcium response after agonist addition is dependent on the agonist concentration.

Parameters of measurement	Oregon Green <sup>®</sup> BAPTA-1/AM	Fura-2/AM
Excitation wavelength	485 nm (band width: 25 nm)	320 nm (band width: 25 nm)
Emission wavelength	520 nm (band width: 20 nm)	520 nm (band width: 20 nm)
Number of flashes per well and interval (validation)	10 (10)	10 (10)
Gain	Variable	Variable
Number of intervals (validation)	60 (1)	60 (1)
Interval time	0.4 s	0.4 s
Injection start time	11.5 s	11.5 s
Pump speed [ $\mu$ l/s]	65	65
Positioning delay	0.2 s	0.2 s
Temperature	Room temperature	Room temperature
Cell number per well	Approximately 150,000	Approximately 150,000

### Data evaluation of calcium assays

The evaluation of the data starts with Microsoft<sup>®</sup> Excel (5.1.5). Fluorescence units measured immediately after injection are used for reference purposes. These values are subtracted from each additional data point. A mean value is determined for all data points of one well. This mean value is plotted against the agonist and antagonist concentrations in order to generate a dose response curve (DRC). Each data point of a single experiment represents the mean of a triplicate. Further data evaluation is performed using GraphPad Prism<sup>®</sup> 4.02 (5.1.5). Dose response curves are generated by a non-linear sigmoidal fit (variable slope). DRC parameters are calculated by the software. Each DRC shown in this thesis is the mean of at least three independent experiments.

To permit a comparison of the potencies of different compounds, the EC<sub>50</sub> or IC<sub>50</sub> value (molar concentration of an agonist or antagonist which produces 50% of that agonist or antagonist's maximum possible effect) is converted into a pEC<sub>50</sub> or

pIC<sub>50</sub> value, which is the negative logarithm to the base of 10.<sup>[65]</sup>

## **Single cell calcium imaging**

### **Realisation**

Single cell calcium imaging is performed as described previously.<sup>[175]</sup> 1321N1-GPR17 cells cultured overnight on cover slips in cell culture dishes with medium are incubated with fura-2/AM (final concentration 2  $\mu$ M) for 30 min at 37°C, 5% CO<sub>2</sub> and 95% humidity. A cover slip is fixed between two platinum electrodes in a superfusion chamber and mounted on the stage of a Zeiss Axiovert 100 microscope equipped with an oil immersion F-Fluar 40x objective (Zeiss, Jena, Germany). The cells are superfused with superfusion buffer at 1 ml/min. After a presuperfusion period of 20 min, cells are superfused with test compound solution in the final concentration. A second compound can be tested after a wash-out phase of 12 min with superfusion buffer. The dead time between starting superfusion and signal appearance depends on the length of the flexible tube and the position of the analysed cells on the cover slip. Fluorescence emission is measured after alternating excitation at 340 nm and 380 nm, each applied for 5 to 9 ms and repeated every 1 s using a Polychrome II monochromator, an Imago charge-coupled device camera and the TILLvisION imaging system (Till Photonics, D-82166 Gräfelfing) (Figure 55).

### **Evaluation of single cell imaging data**

The term (fluorescence emission due to excitation at 340 nm)/(fluorescence emission due to excitation at 380 nm) (F<sub>340 nm</sub>/F<sub>380 nm</sub>) is evaluated in order to estimate the changes in intracellular calcium concentration (Figure 55).

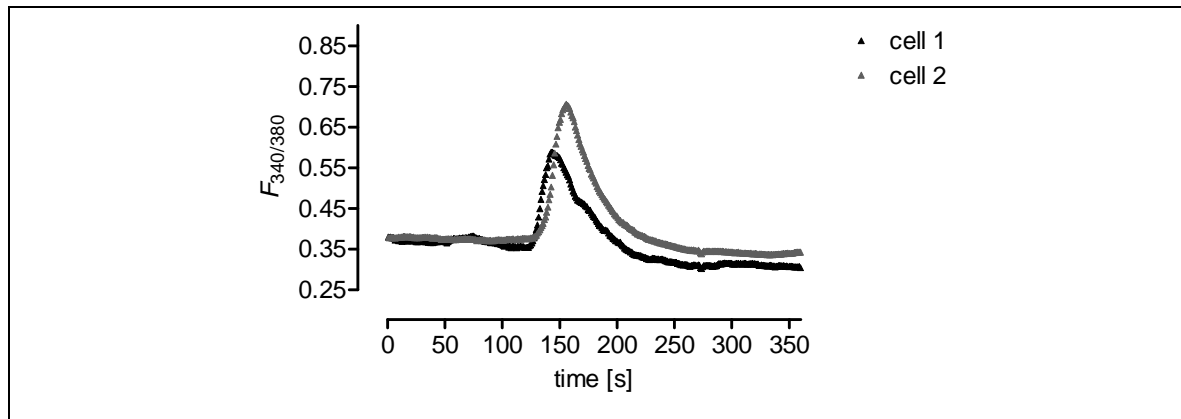


**Figure 55.** Plot of the intracellular calcium increase resulting from a single cell assay as a function of time using fluorescence microscopy. Each signature represents the response of a single cell. The signal is described as the ratio of the fluorescence at 340 nm and 380 nm.

## Radioactive inositol phosphate (IP) accumulation assays

### Background

The yttrium silicate scintillation proximity bead assay (YSi-SPA) is based on the radioactive decay of tritiated inositol phosphates and contains beads with a polylysine coated surface and an yttrium core.

Cells expressing the receptor of interest are fed with tritiated *myo*-inositol which is incorporated into cellular phosphatidylinositol 4,5-bisphosphate (PIP<sub>2</sub>). The latter is degraded to radioactive IP<sub>3</sub> and DAG according to the activation of phospholipase C. Tritiated IP<sub>3</sub> and unlabeled IP<sub>3</sub> bind with their negatively charged phosphate groups to the positively charged polylysine coated bead surface after cell lysis. The tritiated IP<sub>3</sub> and the yttrium core, which functions as a scintillator, are in close proximity after binding. The scintillator converts the radioactive radiation, which is a  $\beta^-$ -decay, into detectable, non-radioactive radiation. For this reason, the amount of detected light reflects the amount of radioactive IP<sub>3</sub> bound to the beads and thus the activity of PLC representing receptor activation.

**Procedure**

The inositol phosphate accumulation assay is performed as described previously.<sup>[176]</sup> 40,000 CHO cells and 30,000 1321N1 cells are seeded in 100  $\mu$ l of culture medium in 96-well tissue culture plates and loaded with 0.5  $\mu$ Ci (18,500 Bq) of [2-<sup>3</sup>H]myo-inositol per well. The next day, the cells are washed twice in 200  $\mu$ l of HBSS-buffer (5.1.2). The supernatant is completely removed, and 80  $\mu$ l of HBSS-buffer with 10 mM LiCl are added to the cells. Receptor activation is stimulated by adding 20  $\mu$ l of a 5-fold concentrated agonist solution in HBSS buffer supplemented with 10 mM LiCl and incubated for 45 min at 37 °C. In the case of antagonist testing, 60  $\mu$ l of HBSS-buffer with LiCl are added as well as 20  $\mu$ l of antagonist solution 10 min before agonist supplementation. Reactions are terminated by aspiration and by the addition of 50  $\mu$ l of 10 mM ice-cold formic acid per well. After a 90 min incubation on ice, 20  $\mu$ l of the resulting cell extract is transferred to 80  $\mu$ l of yttrium silicate scintillation proximity assay beads (12.5 mg/ml; Amersham Biosciences, Buckinghamshire HP7 9NA, UK), and shaken for 60 min at 4°C. Yttrium silicate beads are centrifuged to settle before counting on a TopCount NXT™ microplate scintillation counter (PerkinElmer Life Sciences, MA 02451, USA).

**Data evaluation of the IP accumulation assay**

GraphPad Prism® 4.02 (5.1.5) is used for data evaluation. Inositol phosphate accumulation is plotted against agonist concentration. Each data point of a single experiment represents the mean of a triplicate. Dose response curves are generated by a non-linear sigmoidal fit (variable slope). DRC parameters are calculated by the software. Each DRC shown in this thesis is the mean of at least three independent experiments.

**Homogeneous time resolved fluorescence (HTRF®) assays****Background**

Homogeneous time-resolved fluorescence (HTRF®) technology is a combination of

fluorescence resonance energy transfer (FRET) and time-resolved fluorometry (TRF).

FRET uses two fluorophores, a donor and an acceptor. Both fluorophores have defined excitation and emission spectra. When the emission spectrum of the donor overlaps with the excitation spectrum of the acceptor, energy transfer takes place if the donor is stimulated by light with a certain wavelength and both fluorophores are within a certain distance of, and have a certain orientation to each other. The light emitted by the acceptor is less energetic than the excited light for stimulating the donor.

TRF combines long-lived fluorophores and fluorescence detection is delayed between excitation and emission. Lanthanides are complexed for this purpose with organic moieties that harvest light and transfer it to the lanthanide by means of intramolecular, non-radiative processes.

### **HTRF<sup>®</sup> cAMP accumulation assays**

Two signal transduction pathways that influence the activity of the adenylyl cyclase in oppositional ways can be activated upon receptor activation. Whereas the  $G_s$  pathway stimulates the adenylyl cyclase-dependent catalysation of cAMP formation, the  $G_i$  pathway inhibits it. The detection of cAMP accumulation is based on the HTRF<sup>®</sup> technology described above. In this case a monoclonal antibody specific to cAMP is the donor fluorophore while the acceptor fluorophore d2 is fused to cAMP. Total  $G_i$  signalling of the cell has to be blocked by treatment with pertussis toxin in order to analyse the  $G_s$  pathway. The analysis of the  $G_i$  pathway is based on the direct activation of the adenylyl cyclase, for example, by forskolin. Upon activation, the  $G_i$  pathway inhibits the forskolin-dependent activation of the adenylyl cyclase, leading to decreased cAMP accumulation.

The inhibition of forskolin-stimulated cAMP accumulation in 1321N1 or CHO cells is performed as described above using the HTRF<sup>®</sup> cAMP dynamic kit (Cisbio Bioassays, BP 84175, France).<sup>[176]</sup> Cells are resuspended in assay buffer with 1 mM 3-isobutyl-1-methylxanthine (IBMX) supplemented and dispensed in 384-well microplates at a density of 50,000 cells/well in a volume of 5  $\mu$ l. After preincubation in assay buffer for 30 min, the cells are stimulated by adding 5  $\mu$ l of agonist in the respective concentration of forskolin. The final concentration of

forskolin is dependent on the cell line which is employed in the assay. Adenylyl cyclase is stimulated with 1  $\mu\text{M}$  forskolin in 1321N1-GPR17 cells and with 10  $\mu\text{M}$  forskolin in CHO-GPR17 cells, followed by incubation for 30 min at room temperature. The reaction is terminated by lysis of the cells, which results from the addition of 5  $\mu\text{l}$  of  $d_2$ -conjugate followed by the addition of 5  $\mu\text{l}$  of anti-IP<sub>1</sub>-cryptate (both supplements are diluted in conjugate and lysis buffer). The assay is incubated for 60 min at room temperature and time-resolved FRET signals are measured at an excitation wavelength of 320 nm using the Mithras LB 940 multimode reader (Berthold technologies, D-75323 Bad Wildbad).

### **Data evaluation of HTRF<sup>®</sup> accumulation assays**

The evaluation of HTRF<sup>®</sup> data is performed following the instructions of the kit manufacturer. Data analysis is based on the fluorescence ratio emitted by labelled cAMP (665 nm) over the light emitted by the europium cryptate-labelled anti-cAMP (620 nm). Levels of cAMP are normalised to the amount of cAMP elevated by 10  $\mu\text{M}$  or 1  $\mu\text{M}$  forskolin alone.

### **Dynamic mass redistribution (DMR) assay using the EPIC<sup>®</sup> system**

#### **Background**

A beta version of the Corning<sup>®</sup> Epic<sup>®</sup> system (Corning<sup>®</sup> Incorporated, NY 14831 USA), consisting of a temperature control unit, an optical detection unit and an on-board robotic liquid handling device, was used in the experiments of the present thesis. Each well of the 384-well Epic<sup>®</sup> microplate contains a resonant waveguide grating biosensor. The system measures changes in the local index of refraction upon mass redistribution within the cell monolayer grown on the biosensor. Amongst other things, mass redistribution is a result of receptor activation after ligand addition. Following receptor activation, specific macromolecules are activated within the cell and start to move. If macromolecules move into or out of the range of the biosensor (up to 150 nm above the sensor surface) the DMR in living cells is manifested as a shift in the wavelength of light that is reflected from the sensor. The magnitude of this wavelength shift is proportional to the amount of

DMR. An increase in mass contributes negatively to the overall response.<sup>[177, 178]</sup> The shape of the signature obtained depends on the respective signal transduction pathway(s). In contrast to the other measurement techniques, this technology does not measure a single pathway or a defined second messenger but all processes in parallel that are initiated upon receptor activation in real time (Figure 56).

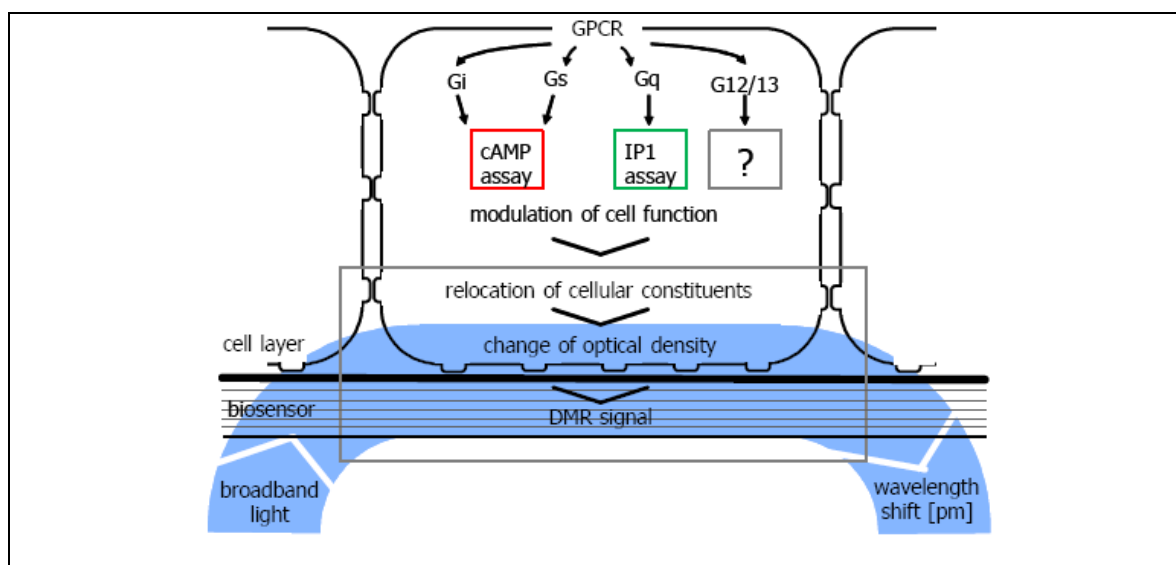


**Figure 56.** Measurement principle of live cell imaging using dynamic mass redistribution.<sup>[67]</sup> After the application of a ligand, the downstream signalling cascade of a GPCR is activated, leading to a movement of masses in the form of signalling molecules within the cell. One consequence of this movement is a change in the optical density within the range of the biosensor which is integrated in the bottom of the measurement plate. This change in the optical density results in a wavelength shift, which is reflected in comparison to the shift that was reflected before agonist addition. The signalling molecules which are activated are characteristic of a certain receptor and its signal transduction pathways.

## Procedure

Dynamic mass redistribution in 1321N1 or CHO cells is performed as described above.<sup>[176]</sup> On the day prior to the measurement, cells are seeded onto fibronectin-coated 384-well Epic<sup>®</sup> sensor microplates at a density of 12,500 cells/well for 1321N1 cells or 15,000 cells/well (in 40  $\mu$ l of medium per well) for CHO cells, then cultured for 16-20 h at 37°C, 5% CO<sub>2</sub> and 95% humidity to obtain a confluent monolayer. The cells are washed twice with assay buffer. The supernatant is completely removed to 10  $\mu$ l by an eight-channel manifold for this purpose, and



30  $\mu\text{l}$  of assay buffer (5.4.1) are added. This step is repeated once and then finally 20  $\mu\text{l}$  of assay buffer are added to the wells. A second plate, the source plate, is loaded with 20  $\mu\text{l}$  of the 4-fold concentrated test compounds. Both plates are kept simultaneously for 1 h in the Epic<sup>®</sup> reader at a constant temperature of 28°C. Afterwards the sensor plate is scanned and a baseline optical signature is recorded for five minutes. Then 10  $\mu\text{l}$  of the test compounds are injected onto the sensor plate by the on-board liquid handling device and DMR is monitored for at least 3600 s.

### **Data evaluation**

Data from DMR assays are evaluated by calculating the area under curve (AUC) of a signature which has been baseline-corrected. The AUCs from three or more single wells with cells treated with a defined agonist concentration are averaged. Other parameters were specified for the calculation of the area under curve: the time limit for summarising data points was set to 1000 sec and the baseline to an ordinate value of -10 or -20. The measured DMR signal does not fall below a value of -10 or -20 within 1000 sec. Since the baseline is set to -10 or -20, it is possible to calculate an AUC for the baseline-corrected buffer signature.

---

## CHAPTER VI: TABLE OF ABBREVIATIONS

---

### A

a. dem.	demineralised water
ADP	adenosine 5'-diphosphate
AC	adenylyl cyclase
AMP	adenosine monophosphate
ATP	adenosine 5'-triphosphate
AQ	anthraquinone
AUC	area under curve

### B

bp	base pairs
BSA	bovine serum albumin

### C

cAMP	cyclic adenosine monophosphate
cDNA	complementary DNA
CHO	Chinese hamster ovary
Ci	Curie
CREB	cAMP-response element binding protein
CysLT	cysteinyl-leukotriene
CysLT <sub>1</sub>	type 1 cysteinyl-leukotriene receptor
CysLT <sub>2</sub>	type 2 cysteinyl-leukotriene receptor

**D**

DAG	diacylglycerol
DMEM	Dulbecco's modified eagle medium
DMR	dynamic mass redistribution
DMSO	dimethyl sulfoxide
DNA	deoxyribonucleic acid
dNTP	deoxynucleotide phosphate
DRC	dose response curve

**E**

EBI2	Epstein–Barr virus-induced receptor 2
EBV	Epstein-Barr virus
<i>E. coli</i>	<i>Escherichia coli</i>
EC <sub>50</sub>	concentration of half maximum effect
EDTA	ethylenediaminetetraacetic acid
EGTA	ethylene glycol-bis(2-aminoethylether) <i>N,N,N',N'</i> -tetraacetic acid
EPAC	exchange protein activated by cAMP
ER	endoplasmic reticulum
ET-18-OCH <sub>3</sub>	Edelfosine

**F**

FCS	fetal bovine serum
FLIPR	Flp-In T-rax
FRET	fluorescence resonance energy transfer
FRT	Flp Recombination Target site
Fsk	forskolin

**G**

g	acceleration by gravity
G418	geneticin 418
GDP	guanosine 5'-diphosphate
GEF	guanine nucleotide exchange factor
GMP	guanosine 5'-monophosphate

## CHAPTER VI: TABLE OF ABBREVIATIONS

---

GOI	gene of interest
GPCR	G protein-coupled receptor
GRK	G protein-coupled receptor kinases
GTP	guanosine 5'-triphosphate
<b>H</b>	
h	human
h	hours
H 89	N-[2-(p-Bromocinnamylamino)ethyl]- 5-isoquinolinesulphonamide dihydrochloride
HBSS	Hanks' balanced salt solutions
H <sub>4</sub> -folat	tetrahydrofolate
5-HIAA	5-hydroxyindoleacetic acid
HTRF <sup>®</sup>	homogeneous time resolved fluorescence
HEPES	4-(2-Hydroxyethyl)piperazine-1- ethanesulphonic acid
HXM	hypoxanthine, xanthine and mycophenolic acid
<b>I</b>	
IBMX	3-Isobutyl-1-methylxanthine
IC <sub>50</sub>	concentration of half maximum inhibition
IP <sub>1</sub>	inositol 4-phosphate
IP <sub>3</sub>	inositol 1,3,4-triphosphate
IP <sub>3</sub> R	IP <sub>3</sub> receptor
<b>K</b>	
KHB	Krebs-HEPES-buffer
<b>L</b>	
LB-medium	Lennox-Broth-medium
LTR	long terminal repeats

**M**

MAPK	mitogen-activated protein kinase
min	minutes
Mrg	Mas-related gene
MT <sub>1</sub>	subtype 1 melatonin receptor
MuLV	murine leukaemia virus

**N**

n	number
n. d.	not detectable
NGF	nerve growth factor
no.	number

**O**

OG	Oregon Green <sup>®</sup> BAPTA-1/AM
----	--------------------------------------

**P**

PC12	pheochromocytoma cells
pEC <sub>50</sub>	negative logarithm of EC <sub>50</sub>
PI	phosphatidylinositol
PI-PLC	phosphatidylinositol specific phospholipase C
pIC <sub>50</sub>	negative logarithm of IC <sub>50</sub>
PIP <sub>2</sub>	phosphatidylinositol 4,5-bisphosphate
PBS	phosphate buffered saline
PCR	polymerase chain reaction
PKA	protein kinase A
PKC	protein kinase C
PLC	phospholipase C
PP	polypropylene
PP2A	protein phosphatase 2A
PS	polystyrene
PTX	Pertussis toxin

## CHAPTER VI: TABLE OF ABBREVIATIONS

---

### R

rpm	rounds per minute
RNA	ribonucleic acid
RNase A	ribonuclease A
RT	room temperature
RYR	ryanodine receptor channel

### S

s	seconds
SDS	sodium dodecyl sulfate
SEM	standard error of mean
SERCA	Sarco/endoplasmic Ca <sup>2+</sup> -ATPase
SOC	super optimal broth with glucose
SPA	scintillation proximity assay

### T

TAE	TRIS-acetate EDTA solution
TC	tissue culture
TENS	TRIS-EDTA sodium hydroxide-SDS-solution
TM	transmembrane
TRF	time resolved fluorometry
TRIS	tris(hydroxymethyl)aminomethane

### U

U	units
UniProtKB	Universal Protein Resource
UTR	untranslated region
UV	ultraviolet

### V

VIS	visible light
VSV-G	glycoprotein G of the vesicular Stomatitis-virus

**W**

W-7 N-(6-Aminohexyl)-5-chloro-1-naphthalenesulphonamide hydrochloride

**Y**

$\Psi$  retroviral packaging signal

YSi Yttrium silicate

---

## CHAPTER VII: REFERENCES

---

1. Millar, R. P. & Newton, C. L. *The year in G protein-coupled receptor research* (2010) *Mol Endocrinol* **24**, 261-74.
2. Jacoby, E., Bouhelal, R., Gerspacher, M. & Seuwen, K. *The 7 TM G-protein-coupled receptor target family* (2006) *ChemMedChem* **1**, 761-82.
3. Chung, S., Funakoshi, T. & Civelli, O. *Orphan GPCR research* (2008) *Br J Pharmacol* **153 Suppl 1**, S339-46.
4. Overington, J. P., Al-Lazikani, B. & Hopkins, A. L. *How many drug targets are there?* (2006) *Nat Rev Drug Discov* **5**, 993-6.
5. Simon, M. I., Strathmann, M. P. & Gautam, N. *Diversity of G proteins in signal transduction* (1991) *Science* **252**, 802-8.
6. Ferris, C. D., Haganir, R. L., Bredt, D. S., Cameron, A. M. & Snyder, S. H. *Inositol trisphosphate receptor: phosphorylation by protein kinase C and calcium calmodulin-dependent protein kinases in reconstituted lipid vesicles* (1991) *Proc Natl Acad Sci U S A* **88**, 2232-5.
7. Schmid, R. S., Graff, R. D., Schaller, M. D., Chen, S., Schachner, M., Hemperly, J. J. & Maness, P. F. *NCAM stimulates the Ras-MAPK pathway and CREB phosphorylation in neuronal cells* (1999) *J Neurobiol* **38**, 542-58.
8. Métrich, M., Lucas, A., Gastineau, M., Samuel, J. L., Heymes, C., Morel, E. & Lezoualc'h, F. *Epac mediates  $\beta$ -adrenergic receptor-induced cardiomyocyte hypertrophy* (2008) *Circ Res* **102**, 959-65.
9. Chepurny, O. G., Kelley, G. G., Dzhura, I., Leech, C. A., Roe, M. W., Dzhura, E., Li, X., Schwede, F., Genieser, H. G. & Holz, G. G. *PKA-dependent potentiation of glucose-stimulated insulin secretion by Epac activator 8-pCPT-2'-O-Me-cAMP-AM in human islets of Langerhans* (2010) *Am J Physiol Endocrinol Metab* **298**, E622-33.
10. Kinukawa, M., Oda, S., Shirakura, Y., Okabe, M., Ohmuro, J., Baba, S. A., Nagata, M. & Aoki, F. *Roles of cAMP in regulating microtubule sliding and flagellar bending in demembrated hamster spermatozoa* (2006) *FEBS Lett* **580**, 1515-20.
11. Datta, N. S., Chen, C., Berry, J. E. & McCauley, L. K. *PTHrP signaling targets cyclin D1 and induces osteoblastic cell growth arrest* (2005) *J Bone Miner Res* **20**, 1051-64.
12. Sands, W. A., Woolson, H. D., Milne, G. R., Rutherford, C. & Palmer, T. M. *Exchange protein activated by cyclic AMP (Epac)-mediated induction of suppressor of cytokine signaling 3 (SOCS-3) in vascular endothelial cells* (2006) *Mol Cell Biol* **26**, 6333-46.
13. Cai, D., Qiu, J., Cao, Z., McAtee, M., Bregman, B. S. & Filbin, M. T. *Neuronal cyclic AMP controls the developmental loss in ability of axons to*



- regenerate (2001) *J Neurosci* **21**, 4731-9.
14. Tanaka, S., Ishii, K., Kasai, K., Yoon, S. O. & Saeki, Y. *Neural expression of G protein-coupled receptors GPR3, GPR6, and GPR12 up-regulates cyclic AMP levels and promotes neurite outgrowth* (2007) *J Biol Chem* **282**, 10506-15.
  15. Sands, W. A. & Palmer, T. M. *Regulating gene transcription in response to cyclic AMP elevation* (2008) *Cell Signal* **20**, 460-6.
  16. Vanderheyden, V., Devogelaere, B., Missiaen, L., De Smedt, H., Bultynck, G. & Parys, J. B. *Regulation of inositol 1,4,5-trisphosphate-induced  $Ca^{2+}$  release by reversible phosphorylation and dephosphorylation* (2009) *Biochim Biophys Acta* **1793**, 959-70.
  17. Nakade, S., Rhee, S. K., Hamanaka, H. & Mikoshiba, K. *Cyclic AMP-dependent phosphorylation of an immunoaffinity-purified homotetrameric inositol 1,4,5-trisphosphate receptor (type I) increases  $Ca^{2+}$  flux in reconstituted lipid vesicles* (1994) *J Biol Chem* **269**, 6735-42.
  18. Ferris, C. D., Cameron, A. M., Bredt, D. S., Huganir, R. L. & Snyder, S. H. *Inositol 1,4,5-trisphosphate receptor is phosphorylated by cyclic AMP-dependent protein kinase at serines 1755 and 1589* (1991) *Biochem Biophys Res Commun* **175**, 192-8.
  19. Bird, G. S., Burgess, G. M. & Putney, J. W., Jr. *Sulfhydryl reagents and cAMP-dependent kinase increase the sensitivity of the inositol 1,4,5-trisphosphate receptor in hepatocytes* (1993) *J Biol Chem* **268**, 17917-23.
  20. Daaka, Y., Luttrell, L. M. & Lefkowitz, R. J. *Switching of the coupling of the  $\beta_2$ -adrenergic receptor to different G proteins by protein kinase A* (1997) *Nature* **390**, 88-91.
  21. Bugrim, A. E. *Regulation of  $Ca^{2+}$  release by cAMP-dependent protein kinase. A mechanism for agonist-specific calcium signaling?* (1999) *Cell Calcium* **25**, 219-26.
  22. Mochizuki, N., Ohba, Y., Kiyokawa, E., Kurata, T., Murakami, T., Ozaki, T., Kitabatake, A., Nagashima, K. & Matsuda, M. *Activation of the ERK/MAPK pathway by an isoform of rap1GAP associated with  $G\alpha_i$*  (1999) *Nature* **400**, 891-4.
  23. Lopez-Illasaca, M., Crespo, P., Pellici, P. G., Gutkind, J. S. & Wetzker, R. *Linkage of G protein-coupled receptors to the MAPK signaling pathway through PI 3-kinase  $\gamma$*  (1997) *Science* **275**, 394-7.
  24. Camps, M., Carozzi, A., Schnabel, P., Scheer, A., Parker, P. J. & Gierschik, P. *Isozyme-selective stimulation of phospholipase C- $\beta_2$  by G protein  $\beta\gamma$ -subunits* (1992) *Nature* **360**, 684-6.
  25. Park, D., Jhon, D. Y., Lee, C. W., Lee, K. H. & Rhee, S. G. *Activation of phospholipase C isozymes by G protein  $\beta\gamma$  subunits* (1993) *J Biol Chem* **268**, 4573-6.
  26. Buhl, A. M., Johnson, N. L., Dhanasekaran, N. & Johnson, G. L.  *$G\alpha_{12}$  and  $G\alpha_{13}$  stimulate Rho-dependent stress fiber formation and focal adhesion assembly* (1995) *J Biol Chem* **270**, 24631-4.
  27. Fromm, C., Coso, O. A., Montaner, S., Xu, N. & Gutkind, J. S. *The small GTP-binding protein Rho links G protein-coupled receptors and  $G\alpha_{12}$  to the serum response element and to cellular transformation* (1997) *Proc Natl Acad Sci U S A* **94**, 10098-103.
  28. Seasholtz, T. M., Majumdar, M. & Brown, J. H. *Rho as a mediator of G protein-coupled receptor signaling* (1999) *Mol Pharmacol* **55**, 949-56.
  29. Sah, V. P., Seasholtz, T. M., Sagi, S. A. & Brown, J. H. *The role of Rho in G*

- protein-coupled receptor signal transduction* (2000) *Annu Rev Pharmacol Toxicol* **40**, 459-89.
30. Maekawa, A., Balestrieri, B., Austen, K. F. & Kanaoka, Y. *GPR17 is a negative regulator of the cysteinyl leukotriene 1 receptor response to leukotriene D<sub>4</sub>* (2009) *Proc Natl Acad Sci U S A* **106**, 11685-90.
  31. Milasta, S., Pediani, J., Appelbe, S., Trim, S., Wyatt, M., Cox, P., Fidock, M. & Milligan, G. *Interactions between the Mas-related receptors MrgD and MrgE alter signalling and trafficking of MrgD* (2006) *Mol Pharmacol* **69**, 479-91.
  32. Levoye, A., Dam, J., Ayoub, M. A., Guillaume, J. L., Couturier, C., Delagrangé, P. & Jockers, R. *The orphan GPR50 receptor specifically inhibits MT<sub>1</sub> melatonin receptor function through heterodimerization* (2006) *Embo J* **25**, 3012-23.
  33. White, J. H., Wise, A., Main, M. J., Green, A., Fraser, N. J., Disney, G. H., Barnes, A. A., Emson, P., Foord, S. M. & Marshall, F. H. *Heterodimerization is required for the formation of a functional GABA<sub>B</sub> receptor* (1998) *Nature* **396**, 679-82.
  34. Xu, H., Staszewski, L., Tang, H., Adler, E., Zoller, M. & Li, X. *Different functional roles of T1R subunits in the heteromeric taste receptors* (2004) *Proc Natl Acad Sci U S A* **101**, 14258-63.
  35. Wei, H., Ahn, S., Shenoy, S. K., Karnik, S. S., Hunyady, L., Luttrell, L. M. & Lefkowitz, R. J. *Independent  $\beta$ -arrestin 2 and G protein-mediated pathways for angiotensin II activation of extracellular signal-regulated kinases 1 and 2* (2003) *Proc Natl Acad Sci U S A* **100**, 10782-7.
  36. Sun, Y., Cheng, Z., Ma, L. & Pei, G.  *$\beta$ -arrestin2 is critically involved in CXCR4-mediated chemotaxis, and this is mediated by its enhancement of p38 MAPK activation* (2002) *J Biol Chem* **277**, 49212-9.
  37. Barnes, W. G., Reiter, E., Violin, J. D., Ren, X. R., Milligan, G. & Lefkowitz, R. J.  *$\beta$ -Arrestin 1 and G $_{\alpha q/11}$  coordinately activate RhoA and stress fiber formation following receptor stimulation* (2005) *J Biol Chem* **280**, 8041-50.
  38. Beaulieu, J. M., Sotnikova, T. D., Marion, S., Lefkowitz, R. J., Gainetdinov, R. R. & Caron, M. G. *An Akt/ $\beta$ -arrestin 2/PP2A signaling complex mediates dopaminergic neurotransmission and behavior* (2005) *Cell* **122**, 261-73.
  39. Luttrell, L. M., Ferguson, S. S., Daaka, Y., Miller, W. E., Maudsley, S., Della Rocca, G. J., Lin, F., Kawakatsu, H., Owada, K., Luttrell, D. K., Caron, M. G. & Lefkowitz, R. J.  *$\beta$ -arrestin-dependent formation of  $\beta_2$  adrenergic receptor-Src protein kinase complexes* (1999) *Science* **283**, 655-61.
  40. Kim, J., Ahn, S., Ren, X. R., Whalen, E. J., Reiter, E., Wei, H. & Lefkowitz, R. J. *Functional antagonism of different G protein-coupled receptor kinases for  $\beta$ -arrestin-mediated angiotensin II receptor signaling* (2005) *Proc Natl Acad Sci U S A* **102**, 1442-7.
  41. Ren, X. R., Reiter, E., Ahn, S., Kim, J., Chen, W. & Lefkowitz, R. J. *Different G protein-coupled receptor kinases govern G protein and  $\beta$ -arrestin-mediated signaling of V2 vasopressin receptor* (2005) *Proc Natl Acad Sci U S A* **102**, 1448-53.
  42. Liu, S., Premont, R. T., Kontos, C. D., Zhu, S. & Rockey, D. C. *A crucial role for GRK2 in regulation of endothelial cell nitric oxide synthase function in portal hypertension* (2005) *Nat Med* **11**, 952-8.
  43. Jiménez-Sainz, M. C., Murga, C., Kavelaars, A., Jurado-Pueyo, M., Krakstad, B. F., Heijnen, C. J., Mayor, F., Jr. & Aragay, A. M. *G protein-coupled receptor kinase 2 negatively regulates chemokine signaling at a*

- level downstream from G protein subunits (2006) *Mol Biol Cell* **17**, 25-31.
44. Rosenkilde, M. M., Kledal, T. N. & Schwartz, T. W. *High constitutive activity of a virus-encoded seven transmembrane receptor in the absence of the conserved DRY motif (Asp-Arg-Tyr) in transmembrane helix 3* (2005) *Mol Pharmacol* **68**, 11-9.
45. Rosenkilde, M. M., Benned-Jensen, T., Andersen, H., Holst, P. J., Kledal, T. N., Lüttichau, H. R., Larsen, J. K., Christensen, J. P. & Schwartz, T. W. *Molecular pharmacological phenotyping of EBI2. An orphan seven-transmembrane receptor with constitutive activity* (2006) *J Biol Chem* **281**, 13199-208.
46. Ledent, C., Demeestere, I., Blum, D., Petermans, J., Hämäläinen, T., Smits, G. & Vassart, G. *Premature ovarian aging in mice deficient for Gpr3* (2005) *Proc Natl Acad Sci U S A* **102**, 8922-6.
47. Mehlmann, L. M., Saeki, Y., Tanaka, S., Brennan, T. J., Evsikov, A. V., Pendola, F. L., Knowles, B. B., Eppig, J. J. & Jaffe, L. A. *The Gs-linked receptor GPR3 maintains meiotic arrest in mammalian oocytes* (2004) *Science* **306**, 1947-50.
48. Libert, F., Vassart, G. & Parmentier, M. *Current developments in G-protein-coupled receptors* (1991) *Curr Opin Cell Biol* **3**, 218-23.
49. Bläsius, R., Weber, R. G., Lichter, P. & Ogilvie, A. *A novel orphan G protein-coupled receptor primarily expressed in the brain is localized on human chromosomal band 2q21* (1998) *J Neurochem* **70**, 1357-65.
50. Raport, C. J., Schweickart, V. L., Chantry, D., Eddy, R. L., Jr., Shows, T. B., Godiska, R. & Gray, P. W. *New members of the chemokine receptor gene family* (1996) *J Leukoc Biol* **59**, 18-23.
51. Ciana, P., Fumagalli, M., Trincavelli, M. L., Verderio, C., Rosa, P., Lecca, D., Ferrario, S., Parravicini, C., Capra, V., Gelosa, P., Guerrini, U., Belcredito, S., Cimino, M., Sironi, L., Tremoli, E., Rovati, G. E., Martini, C. & Abbracchio, M. P. *The orphan receptor GPR17 identified as a new dual uracil nucleotides/cysteinyl-leukotrienes receptor* (2006) *Embo J* **25**, 4615-27.
52. Banfi, C., Ferrario, S., De Vincenti, O., Ceruti, S., Fumagalli, M., Mazzola, A., N, D. A., Volonte, C., Fratto, P., Vitali, E., Burnstock, G., Beltrami, E., Parolari, A., Polvani, G., Biglioli, P., Tremoli, E. & Abbracchio, M. P. *P2 receptors in human heart: upregulation of P2X<sub>6</sub> in patients undergoing heart transplantation, interaction with TNF $\alpha$  and potential role in myocardial cell death* (2005) *J Mol Cell Cardiol* **39**, 929-39.
53. Itagaki, K., Barton, B. E., Murphy, T. F., Taheri, S., Shu, P., Huang, H. & Jordan, M. L. *Eicosanoid-Induced Store-Operated Calcium Entry in Dendritic Cells* (2009) *J Surg Res*.
54. Benned-Jensen, T. & Rosenkilde, M. M. *Distinct expression and ligand-binding profiles of two constitutively active GPR17 splice variants* (2010) *Br J Pharmacol* **159**, 1092-105.
55. Maisel, M., Herr, A., Milosevic, J., Hermann, A., Habisch, H. J., Schwarz, S., Kirsch, M., Antoniadis, G., Brenner, R., Hallmeyer-Elgner, S., Lerche, H., Schwarz, J. & Storch, A. *Transcription profiling of adult and fetal human neuroprogenitors identifies divergent paths to maintain the neuroprogenitor cell state* (2007) *Stem Cells* **25**, 1231-40.
56. Lecca, D., Trincavelli, M. L., Gelosa, P., Sironi, L., Ciana, P., Fumagalli, M., Villa, G., Verderio, C., Grumelli, C., Guerrini, U., Tremoli, E., Rosa, P., Cuboni, S., Martini, C., Buffo, A., Cimino, M. & Abbracchio, M. P. *The*

- recently identified P2Y-like receptor GPR17 is a sensor of brain damage and a new target for brain repair (2008) *PLoS One* **3**, e3579.
57. Ceruti, S., Villa, G., Genovese, T., Mazzon, E., Longhi, R., Rosa, P., Bramanti, P., Cuzzocrea, S. & Abbracchio, M. P. *The P2Y-like receptor GPR17 as a sensor of damage and a new potential target in spinal cord injury* (2009) *Brain* **132**, 2206-18.
  58. Chen, Y., Wu, H., Wang, S., Koito, H., Li, J., Ye, F., Hoang, J., Escobar, S. S., Gow, A., Arnett, H. A., Trapp, B. D., Karandikar, N. J., Hsieh, J. & Lu, Q. R. *The oligodendrocyte-specific G protein-coupled receptor GPR17 is a cell-intrinsic timer of myelination* (2009) *Nat Neurosci* **12**, 1398-406.
  59. Cahoy, J. D., Emery, B., Kaushal, A., Foo, L. C., Zamanian, J. L., Christopherson, K. S., Xing, Y., Lubischer, J. L., Krieg, P. A., Krupenko, S. A., Thompson, W. J. & Barres, B. A. *A transcriptome database for astrocytes, neurons, and oligodendrocytes: a new resource for understanding brain development and function* (2008) *J Neurosci* **28**, 264-78.
  60. Pugliese, A. M., Trincavelli, M. L., Lecca, D., Coppi, E., Fumagalli, M., Ferrario, S., Failli, P., Daniele, S., Martini, C., Pedata, F. & Abbracchio, M. P. *Functional characterization of two isoforms of the P2Y-like receptor GPR17: [<sup>35</sup>S]GTP $\gamma$ S binding and electrophysiological studies in 1321N1 cells* (2009) *Am J Physiol Cell Physiol* **297**, C1028-40.
  61. Maekawa, A., Xing, W., Austen, K. F. & Kanaoka, Y. *GPR17 regulates immune pulmonary inflammation induced by house dust mites* (2010) *J Immunol* **185**, 1846-54.
  62. Daniele, S., Lecca, D., Trincavelli, M. L., Ciampi, O., Abbracchio, M. P. & Martini, C. *Regulation of PC12 cell survival and differentiation by the new P2Y-like receptor GPR17* (2010) *Cell Signal* **22**, 697-706.
  63. Communi, D., Piroton, S., Parmentier, M. & Boeynaems, J. M. *Cloning and functional expression of a human uridine nucleotide receptor* (1995) *J Biol Chem* **270**, 30849-52.
  64. Communi, D., Gonzalez, N. S., Detheux, M., Brezillon, S., Lannoy, V., Parmentier, M. & Boeynaems, J. M. *Identification of a novel human ADP receptor coupled to G(i)* (2001) *J Biol Chem* **276**, 41479-85.
  65. Neubig, R. R., Spedding, M., Kenakin, T. & Christopoulos, A. *International Union of Pharmacology Committee on Receptor Nomenclature and Drug Classification. XXXVIII. Update on terms and symbols in quantitative pharmacology* (2003) *Pharmacol Rev* **55**, 597-606.
  66. Hillmann, P., Ko, G. Y., Spinrath, A., Raulf, A., von Kügelgen, I., Wolff, S. C., Nicholas, R. A., Kostenis, E., Höltje, H. D. & Müller, C. E. *Key determinants of nucleotide-activated G protein-coupled P2Y<sub>2</sub> receptor function revealed by chemical and pharmacological experiments, mutagenesis and homology modeling* (2009) *J Med Chem* **52**, 2762-75.
  67. Schröder, R., Janssen, N., Schmidt, J., Kebig, A., Merten, N., Hennen, S., Müller, A., Blättermann, S., Mohr-Andrä, M., Zahn, S., Wenzel, J., Smith, N. J., Gomeza, J., Drewke, C., Milligan, G., Mohr, K. & Kostenis, E. *Deconvolution of complex G protein-coupled receptor signaling in live cells using dynamic mass redistribution measurements* (2010) *Nat Biotechnol* **28**, 943-49.
  68. Lynch, K. R., O'Neill, G. P., Liu, Q., Im, D. S., Sawyer, N., Metters, K. M., Coulombe, N., Abramovitz, M., Figueroa, D. J., Zeng, Z., Connolly, B. M., Bai, C., Austin, C. P., Chateauneuf, A., Stocco, R., Greig, G. M., Kargman,

- S., Hooks, S. B., Hosfield, E., Williams, D. L., Jr., Ford-Hutchinson, A. W., Caskey, C. T. & Evans, J. F. *Characterization of the human cysteinyl leukotriene CysLT<sub>1</sub> receptor* (1999) *Nature* **399**, 789-93.
69. Rebecchi, M. J. & Pentylala, S. N. *Structure, function, and control of phosphoinositide-specific phospholipase C* (2000) *Physiol Rev* **80**, 1291-335.
70. Lee, C. W., Lee, K. H., Lee, S. B., Park, D. & Rhee, S. G. *Regulation of phospholipase C- $\beta$ 4 by ribonucleotides and the  $\alpha$  subunit of G<sub>q</sub>* (1994) *J Biol Chem* **269**, 25335-8.
71. Katada, T. & Ui, M. *Direct modification of the membrane adenylate cyclase system by islet-activating protein due to ADP-ribosylation of a membrane protein* (1982) *Proc Natl Acad Sci U S A* **79**, 3129-33.
72. Böckmann genannt Dallmeyer, M. *Etablierung verschiedener funktioneller Testverfahren zur Aufdeckung molekularer Signaltransduktionswege des orphanen G-Protein gekoppelten Rezeptors GPR17* (2009) *Diploma thesis*.
73. Powis, G., Seewald, M. J., Gratas, C., Melder, D., Riebow, J. & Modest, E. J. *Selective inhibition of phosphatidylinositol phospholipase C by cytotoxic ether lipid analogues* (1992) *Cancer Res* **52**, 2835-40.
74. Wong, R., Fabian, L., Forer, A. & Brill, J. A. *Phospholipase C and myosin light chain kinase inhibition define a common step in actin regulation during cytokinesis* (2007) *BMC Cell Biol* **8**, 15.
75. Sagara, Y. & Inesi, G. *Inhibition of the sarcoplasmic reticulum Ca<sup>2+</sup> transport ATPase by thapsigargin at subnanomolar concentrations* (1991) *J Biol Chem* **266**, 13503-6.
76. Treiman, M., Caspersen, C. & Christensen, S. B. *A tool coming of age: thapsigargin as an inhibitor of sarco-endoplasmic reticulum Ca<sup>2+</sup>-ATPases* (1998) *Trends Pharmacol Sci* **19**, 131-5.
77. Zhao, F., Li, P., Chen, S. R., Louis, C. F. & Fruen, B. R. *Dantrolene inhibition of ryanodine receptor Ca<sup>2+</sup> release channels. Molecular mechanism and isoform selectivity* (2001) *J Biol Chem* **276**, 13810-6.
78. Mackrill, J. J. *Ryanodine receptor calcium channels and their partners as drug targets* (2010) *Biochem Pharmacol* **79**, 1535-43.
79. Foskett, J. K., White, C., Cheung, K. H. & Mak, D. O. *Inositol trisphosphate receptor Ca<sup>2+</sup> release channels* (2007) *Physiol Rev* **87**, 593-658.
80. Maruyama, T., Kanaji, T., Nakade, S., Kanno, T. & Mikoshiba, K. *2APB, 2-aminoethoxydiphenyl borate, a membrane-penetrable modulator of Ins(1,4,5)P<sub>3</sub>-induced Ca<sup>2+</sup> release* (1997) *J Biochem* **122**, 498-505.
81. Rodney, G. G., Williams, B. Y., Strasburg, G. M., Beckingham, K. & Hamilton, S. L. *Regulation of RYR1 activity by Ca<sup>2+</sup> and calmodulin* (2000) *Biochemistry* **39**, 7807-12.
82. Yamada, M., Miyawaki, A., Saito, K., Nakajima, T., Yamamoto-Hino, M., Ryo, Y., Furuichi, T. & Mikoshiba, K. *The calmodulin-binding domain in the mouse type 1 inositol 1,4,5-trisphosphate receptor* (1995) *Biochem J* **308** (Pt 1), 83-8.
83. Saimi, Y. & Kung, C. *Calmodulin as an ion channel subunit* (2002) *Annu Rev Physiol* **64**, 289-311.
84. Hidaka, H., Sasaki, Y., Tanaka, T., Endo, T., Ohno, S., Fujii, Y. & Nagata, T. *N-(6-aminoethyl)-5-chloro-1-naphthalenesulfonamide, a calmodulin antagonist, inhibits cell proliferation* (1981) *Proc Natl Acad Sci U S A* **78**, 4354-7.
85. Mahon, M. J. & Shimada, M. *Calmodulin interacts with the cytoplasmic tails*

- of the parathyroid hormone 1 receptor and a sub-set of class b G-protein coupled receptors* (2005) *FEBS Lett* **579**, 803-7.
86. Patel, S., Morris, S. A., Adkins, C. E., O'Beirne, G. & Taylor, C. W. *Ca<sup>2+</sup>-independent inhibition of inositol trisphosphate receptors by calmodulin: redistribution of calmodulin as a possible means of regulating Ca<sup>2+</sup> mobilization* (1997) *Proc Natl Acad Sci U S A* **94**, 11627-32.
87. Cardy, T. J. & Taylor, C. W. *A novel role for calmodulin: Ca<sup>2+</sup>-independent inhibition of type-1 inositol trisphosphate receptors* (1998) *Biochem J* **334 (Pt 2)**, 447-55.
88. Hill, T. D., Campos-Gonzalez, R., Kindmark, H. & Boynton, A. L. *Inhibition of inositol trisphosphate-stimulated calcium mobilization by calmodulin antagonists in rat liver epithelial cells* (1988) *J Biol Chem* **263**, 16479-84.
89. Khan, S. Z., Longland, C. L. & Michelangeli, F. *The effects of phenothiazines and other calmodulin antagonists on the sarcoplasmic and endoplasmic reticulum Ca<sup>2+</sup> pumps* (2000) *Biochem Pharmacol* **60**, 1797-806.
90. Khan, S. Z., Dyer, J. L. & Michelangeli, F. *Inhibition of the type 1 inositol 1,4,5-trisphosphate-sensitive Ca<sup>2+</sup> channel by calmodulin antagonists* (2001) *Cell Signal* **13**, 57-63.
91. Lochner, A. & Moolman, J. A. *The many faces of H89: a review* (2006) *Cardiovasc Drug Rev* **24**, 261-74.
92. Toullec, D., Pianetti, P., Coste, H., Bellevergue, P., Grand-Perret, T., Ajakane, M., Baudet, V., Boissin, P., Boursier, E., Loriolle, F. & et al. *The bisindolylmaleimide GF 109203X is a potent and selective inhibitor of protein kinase C* (1991) *J Biol Chem* **266**, 15771-81.
93. Gulaj, E., Pawlak, K., Bien, B. & Pawlak, D. *Kynurenine and its metabolites in Alzheimer's disease patients* (2010) *Adv Med Sci* **55**, 1-8.
94. Cozzi, A., Carpenedo, R. & Moroni, F. *Kynurenine hydroxylase inhibitors reduce ischemic brain damage: studies with (m-nitrobenzoyl)-alanine (mNBA) and 3,4-dimethoxy-[N-4-(nitrophenyl)thiazol-2yl]-benzenesulfonamide (Ro 61-8048) in models of focal or global brain ischemia* (1999) *J Cereb Blood Flow Metab* **19**, 771-7.
95. Moroni, F., Alesiani, M., Facci, L., Fadda, E., Skaper, S. D., Galli, A., Lombardi, G., Mori, F., Ciuffi, M., Natalini, B. & et al. *Thiokynurenates prevent excitotoxic neuronal death in vitro and in vivo by acting as glycine antagonists and as inhibitors of lipid peroxidation* (1992) *Eur J Pharmacol* **218**, 145-51.
96. Chen, J., Graham, S., Moroni, F. & Simon, R. *A study of the dose dependency of a glycine receptor antagonist in focal ischemia* (1993) *J Pharmacol Exp Ther* **267**, 937-41.
97. Pellegrini-Giampietro, D. E., Cozzi, A. & Moroni, F. *The glycine antagonist and free radical scavenger 7-Cl-thio-kynurenate reduces CA1 ischemic damage in the gerbil* (1994) *Neuroscience* **63**, 701-9.
98. Fukuwatari, T., Morikawa, Y., Sugimoto, E. & Shibata, K. *Effects of fatty liver induced by niacin-free diet with orotic acid on the metabolism of tryptophan to niacin in rats* (2002) *Biosci Biotechnol Biochem* **66**, 1196-204.
99. Gerber, A. P. & Keller, W. *An adenosine deaminase that generates inosine at the wobble position of tRNAs* (1999) *Science* **286**, 1146-9.
100. Höller, U., Wright, A. D., Matthee, G. F., König, G. M., Draeger, S., Aust, H.-J. & Schulz, B. *Fungi from marine sponges: diversity, biological activity and secondary metabolites* (2000) *Mycol. Res.* **104**, 1354-65.

101. Blunt, J. W., Copp, B. R., Munro, M. H. G., Northcote, P. T. & Prinsep, M. R. *Marine natural products* (2005) *Nat. Prod. Rep.* **22**, 15-61.
102. Hill, R. A. *Marine natural products* (2006) *Annu. Rep. Prog. Chem., Sec. B* **102**, 123-37.
103. Mayer, A. M., Rodriguez, A. D., Berlinck, R. G. & Hamann, M. T. *Marine pharmacology in 2005-6: Marine compounds with anthelmintic, antibacterial, anticoagulant, antifungal, anti-inflammatory, antimalarial, antiprotozoal, antituberculosis, and antiviral activities; affecting the cardiovascular, immune and nervous systems, and other miscellaneous mechanisms of action* (2009) *Biochim Biophys Acta* **1790**, 283-308.
104. Pontius, A., Krick, A., Kehraus, S., Foegen, S. E., Müller, M., Klimo, K., Gerhäuser, C. & König, G. M. *Noduliprevenone: a novel heterodimeric chromanone with cancer chemopreventive potential* (2008) *Chemistry* **14**, 9860-3.
105. Pontius, A., Krick, A., Mesry, R., Kehraus, S., Foegen, S. E., Müller, M., Klimo, K., Gerhäuser, C. & König, G. M. *Monodictyochromes A and B, Dimeric Xanthone Derivatives from the Marine Algicolous Fungus Monodictys putredinis* (2008) *J Nat Prod.*
106. Pontius, A., Mohamed, I., Krick, A., Kehraus, S. & König, G. M. *Aromatic polyketides from marine algicolous fungi* (2008) *J Nat Prod* **71**, 272-4.
107. Abdel-Lateff, A., Klemke, C., König, G. M. & Wright, A. D. *Two new xanthone derivatives from the algicolous marine fungus Wardomyces anomalus* (2003) *J Nat Prod* **66**, 706-8.
108. Utkina, N. K., Denisenko, V. A., Scholokova, O. V., Virovaya, M. V., Gerasimenko, A. V., Popov, D. Y., Krasokhin, V. B. & Popov, A. M. *Spongiadioxins A and B, two new polybrominated dibenzo-p-dioxins from an Australian marine sponge Dysidea dendyi* (2001) *J Nat Prod* **64**, 151-3.
109. Fu, X., Schmitz, F. J., Govindan, M., Abbas, S. A., Hanson, K. M., Horton, P. A., Crews, P., Laney, M. & Schatzman, R. C. *Enzyme Inhibitors: New and Known Polybrominated Phenols and Diphenyl Ethers from Four Indo-Pacific Dysidea Sponges* (1995) *J. Nat. Prod.* **58**, 1384-91.
110. Cox, C. D., Rinehart, K. L., Jr., Moore, M. L. & Cook, J. C., Jr. *Pyochelin: novel structure of an iron-chelating growth promoter for Pseudomonas aeruginosa* (1981) *Proc Natl Acad Sci U S A* **78**, 4256-60.
111. Chin, Y. W., Balunas, M. J., Chai, H. B. & Kinghorn, A. D. *Drug discovery from natural sources* (2006) *Aaps J* **8**, E239-53.
112. Leistner, E. *Isolation, Identification and Biosynthesis of Anthraquinones in Cell Suspension Cultures of Morinda citrifolia* (1975) *Planta Med* **28**, 214-24.
113. Bauch, H. R. & Leistner, E. *Aromatic metabolites in cell suspension cultures of Galium mollugo L.* (1978) *Plant physiology and biochemistry* **33**, 105-23.
114. Baqi, Y., Atzler, K., Köse, M., Glänzel, M. & Müller, C. E. *High-affinity, non-nucleotide-derived competitive antagonists of platelet P2Y<sub>12</sub> receptors* (2009) *J Med Chem* **52**, 3784-93.
115. Tuluc, F., Bultmann, R., Glänzel, M., Frahm, A. W. & Starke, K. *P2-receptor antagonists: IV. Blockade of P2-receptor subtypes and ecto-nucleotidases by compounds related to reactive blue 2* (1998) *Naunyn Schmiedebergs Arch Pharmacol* **357**, 111-20.
116. Brown, J. & Brown, C. A. *Evaluation of reactive blue 2 derivatives as selective antagonists for P2Y receptors* (2002) *Vascul Pharmacol* **39**, 309-15.

117. Glänzel, M., Bültmann, R., Starke, K. & Frahm, A. W. *Constitutional isomers of Reactive Blue 2 - selective P2Y-receptor antagonists?* (2003) *Eur J Med Chem* **38**, 303-12.
118. Glänzel, M., Bültmann, R., Starke, K. & Frahm, A. W. *Structure-activity relationships of novel P2-receptor antagonists structurally related to Reactive Blue 2* (2005) *Eur J Med Chem* **40**, 1262-76.
119. Weyler, S., Baqi, Y., Hillmann, P., Kaulich, M., Hunder, A. M., Müller, I. A. & Müller, C. E. *Combinatorial synthesis of anilinoanthraquinone derivatives and evaluation as non-nucleotide-derived P2Y<sub>2</sub> receptor antagonists* (2008) *Bioorg Med Chem Lett* **18**, 223-7.
120. Baqi, Y., Weyler, S., Iqbal, J., Zimmermann, H. & Müller, C. E. *Structure-activity relationships of anthraquinone derivatives derived from bromaminic acid as inhibitors of ectonucleoside triphosphate diphosphohydrolases (E-NTPDases)* (2009) *Purinergic Signal* **5**, 91-106.
121. Baqi, Y. & Müller, C. E. *Rapid and efficient microwave-assisted copper(0)-catalyzed ullmann coupling reaction: general access to anilinoanthraquinone derivatives* (2007) *Org Lett* **9**, 1271-4.
122. Baqi, Y. & Müller, C. E. *Synthesis of alkyl- and aryl-amino-substituted anthraquinone derivatives by microwave-assisted copper(0)-catalyzed Ullmann coupling reactions* (2010) *Nat Protoc* **5**, 945-53.
123. El-Tayeb, A., Qi, A. & Müller, C. E. *Synthesis and structure-activity relationships of uracil nucleotide derivatives and analogues as agonists at human P2Y<sub>2</sub>, P2Y<sub>4</sub>, and P2Y<sub>6</sub> receptors* (2006) *J Med Chem* **49**, 7076-87.
124. Kaulich, M., Streicher, F., Mayer, R., Müller, I. & Müller, C. E. *Flavonoids - novel lead compounds for the development of P2Y<sub>2</sub> receptor antagonists* (2003) *Drug Dev. Res.* **59**, 72-81.
125. Kassack, M. U., Hofgen, B., Lehmann, J., Eckstein, N., Quillan, J. M. & Sadee, W. *Functional screening of G protein-coupled receptors by measuring intracellular calcium with a fluorescence microplate reader* (2002) *J Biomol Screen* **7**, 233-46.
126. Abbracchio, M. P., Boeynaems, J. M., Barnard, E. A., Boyer, J. L., Kennedy, C., Miras-Portugal, M. T., King, B. F., Gachet, C., Jacobson, K. A., Weisman, G. A. & Burnstock, G. *Characterization of the UDP-glucose receptor (re-named here the P2Y<sub>14</sub> receptor) adds diversity to the P2Y receptor family* (2003) *Trends Pharmacol Sci* **24**, 52-5.
127. Parravicini, C., Ranghino, G., Abbracchio, M. P. & Fantucci, P. *GPR17: molecular modeling and dynamics studies of the 3-D structure and purinergic ligand binding features in comparison with P2Y receptors* (2008) *BMC Bioinformatics* **9**, 263.
128. Costanzi, S., Mamedova, L., Gao, Z. G. & Jacobson, K. A. *Architecture of P2Y nucleotide receptors: structural comparison based on sequence analysis, mutagenesis, and homology modeling* (2004) *J Med Chem* **47**, 5393-404.
129. Gabathuler, R. *Approaches to transport therapeutic drugs across the blood-brain barrier to treat brain diseases* (2010) *Neurobiol Dis* **37**, 48-57.
130. Pardridge, W. M. *Blood-brain barrier delivery* (2007) *Drug Discov Today* **12**, 54-61.
131. Oldendorf, W. H., Hyman, S., Braun, L. & Oldendorf, S. Z. *Blood-brain barrier: penetration of morphine, codeine, heroin, and methadone after carotid injection* (1972) *Science* **178**, 984-6.
132. Tsuzuki, N., Hama, T., Kawada, M., Hasui, A., Konishi, R., Shiwa, S., Ochi,



- Y., Futaki, S. & Kitagawa, K. *Adamantane as a brain-directed drug carrier for poorly absorbed drug. 2. AZT derivatives conjugated with the 1-adamantane moiety* (1994) *J Pharm Sci* **83**, 481-4.
133. Bradley, M. O., Webb, N. L., Anthony, F. H., Devanesan, P., Witman, P. A., Hemamalini, S., Chander, M. C., Baker, S. D., He, L., Horwitz, S. B. & Swindell, C. S. *Tumor targeting by covalent conjugation of a natural fatty acid to paclitaxel* (2001) *Clin Cancer Res* **7**, 3229-38.
134. Seifert, R. & Dove, S. *Functional selectivity of GPCR ligand stereoisomers: new pharmacological opportunities* (2009) *Mol Pharmacol* **75**, 13-8.
135. Woo, A. Y., Wang, T. B., Zeng, X., Zhu, W., Abernethy, D. R., Wainer, I. W. & Xiao, R. P. *Stereochemistry of an agonist determines coupling preference of  $\beta_2$ -adrenoceptor to different G proteins in cardiomyocytes* (2009) *Mol Pharmacol* **75**, 158-65.
136. Bosier, B., Muccioli, G. G., Hermans, E. & Lambert, D. M. *Functionally selective cannabinoid receptor signalling: therapeutic implications and opportunities* (2010) *Biochem Pharmacol* **80**, 1-12.
137. Mailman, R. B. *GPCR functional selectivity has therapeutic impact* (2007) *Trends Pharmacol Sci* **28**, 390-6.
138. Urban, J. D., Clarke, W. P., von Zastrow, M., Nichols, D. E., Kobilka, B., Weinstein, H., Javitch, J. A., Roth, B. L., Christopoulos, A., Sexton, P. M., Miller, K. J., Spedding, M. & Mailman, R. B. *Functional selectivity and classical concepts of quantitative pharmacology* (2007) *J Pharmacol Exp Ther* **320**, 1-13.
139. Leduc, M., Breton, B., Galés, C., Le Guill, C., Bouvier, M., Chemtob, S. & Heveker, N. *Functional selectivity of natural and synthetic prostaglandin  $EP_4$  receptor ligands* (2009) *J Pharmacol Exp Ther* **331**, 297-307.
140. Mirabet, M., Mallol, J., Lluís, C. & Franco, R. *Calcium mobilization in Jurkat cells via  $A_{2b}$  adenosine receptors* (1997) *Br J Pharmacol* **122**, 1075-82.
141. English, A. R., Zurek, N. & Voeltz, G. K. *Peripheral ER structure and function* (2009) *Curr Opin Cell Biol* **21**, 596-602.
142. Lebiezinska, M., Szabadkai, G., Jones, A. W., Duszynski, J. & Wieckowski, M. R. *Interactions between the endoplasmic reticulum, mitochondria, plasma membrane and other subcellular organelles* (2009) *Int J Biochem Cell Biol* **41**, 1805-16.
143. Zeng, W., Mak, D. O., Li, Q., Shin, D. M., Foskett, J. K. & Muallem, S. *A new mode of  $Ca^{2+}$  signaling by G protein-coupled receptors: gating of  $IP_3$  receptor  $Ca^{2+}$  release channels by  $G\beta\gamma$*  (2003) *Curr Biol* **13**, 872-6.
144. He, W., Miao, F. J., Lin, D. C., Schwandner, R. T., Wang, Z., Gao, J., Chen, J. L., Tian, H. & Ling, L. *Citric acid cycle intermediates as ligands for orphan G-protein-coupled receptors* (2004) *Nature* **429**, 188-93.
145. Briscoe, C. P., Tadayyon, M., Andrews, J. L., Benson, W. G., Chambers, J. K., Eilert, M. M., Ellis, C., Elshourbagy, N. A., Goetz, A. S., Minnick, D. T., Murdock, P. R., Sauls, H. R., Jr., Shabon, U., Spinage, L. D., Strum, J. C., Szekeres, P. G., Tan, K. B., Way, J. M., Ignar, D. M., Wilson, S. & Muir, A. I. *The orphan G protein-coupled receptor GPR40 is activated by medium and long chain fatty acids* (2003) *J Biol Chem* **278**, 11303-11.
146. Lee, M. J., Van Brocklyn, J. R., Thangada, S., Liu, C. H., Hand, A. R., Menzeleev, R., Spiegel, S. & Hla, T. *Sphingosine-1-phosphate as a ligand for the G protein-coupled receptor EDG-1* (1998) *Science* **279**, 1552-5.
147. Ahmed, K., Tunaru, S. & Offermanns, S. *GPR109A, GPR109B and GPR81, a family of hydroxy-carboxylic acid receptors* (2009) *Trends Pharmacol Sci*

- 30**, 557-62.
148. Mignat, C., Wille, U. & Ziegler, A. *Affinity profiles of morphine, codeine, dihydrocodeine and their glucuronides at opioid receptor subtypes* (1995) *Life Sci* **56**, 793-9.
  149. Hsu, C. W., Wang, C. S. & Chiu, T. H. *Caffeine and a selective adenosine A<sub>2A</sub> receptor antagonist induce sensitization and cross-sensitization behavior associated with increased striatal dopamine in mice* (2010) *J Biomed Sci* **17**, 4.
  150. Huang, Q., Lu, G., Shen, H. M., Chung, M. C. & Ong, C. N. *Anti-cancer properties of anthraquinones from rhubarb* (2007) *Med Res Rev* **27**, 609-30.
  151. van Gorkom, B. A., Timmer-Bosscha, H., de Jong, S., van der Kolk, D. M., Kleibeuker, J. H. & de Vries, E. G. *Cytotoxicity of rhein, the active metabolite of sennoside laxatives, is reduced by multidrug resistance-associated protein 1* (2002) *Br J Cancer* **86**, 1494-500.
  152. Gordon, T. & Gordon, K. *Nerve regeneration in the peripheral nervous system versus the central nervous system and the relevance to speech and hearing after nerve injuries* (2010) *J Commun Disord* **43**, 274-85.
  153. Monk, K. R., Naylor, S. G., Glenn, T. D., Mercurio, S., Perlin, J. R., Dominguez, C., Moens, C. B. & Talbot, W. S. *A G protein-coupled receptor is essential for Schwann cells to initiate myelination* (2009) *Science* **325**, 1402-5.
  154. Lotto, B., Upton, L., Price, D. J. & Gaspar, P. *Serotonin receptor activation enhances neurite outgrowth of thalamic neurones in rodents* (1999) *Neurosci Lett* **269**, 87-90.
  155. He, J. C., Gomes, I., Nguyen, T., Jayaram, G., Ram, P. T., Devi, L. A. & Iyengar, R. *The G $\alpha_{o/i}$ -coupled cannabinoid receptor-mediated neurite outgrowth involves Rap regulation of Src and Stat3* (2005) *J Biol Chem* **280**, 33426-34.
  156. Jordan, J. D., He, J. C., Eungdamrong, N. J., Gomes, I., Ali, W., Nguyen, T., Bivona, T. G., Philips, M. R., Devi, L. A. & Iyengar, R. *Cannabinoid receptor-induced neurite outgrowth is mediated by Rap1 activation through G $\alpha_{o/i}$ -triggered proteasomal degradation of Rap1GAPII* (2005) *J Biol Chem* **280**, 11413-21.
  157. Reinoso, B. S., Undie, A. S. & Levitt, P. *Dopamine receptors mediate differential morphological effects on cerebral cortical neurons in vitro* (1996) *J Neurosci Res* **43**, 439-53.
  158. Hu, W. S. & Pathak, V. K. *Design of retroviral vectors and helper cells for gene therapy* (2000) *Pharmacol Rev* **52**, 493-511.
  159. Markowitz, D., Goff, S. & Bank, A. *Construction and use of a safe and efficient amphotropic packaging cell line* (1988) *Virology* **167**, 400-6.
  160. Markowitz, D., Goff, S. & Bank, A. *A safe packaging line for gene transfer: separating viral genes on two different plasmids* (1988) *J Virol* **62**, 1120-4.
  161. Cornstock, K. E., Watson, N. F. & Olsen, J. C. *Design of retroviral expression vectors*. (1997) *Methods Mol. Biol.* **62**, 207-222.
  162. Mulligan, R. C. & Berg, P. *Selection for animal cells that express the Escherichia coli gene coding for xanthine-guanine phosphoribosyltransferase*. (1981) *Proc. Natl. Acad. Sci. U. S. A.* **78**, 2072-2076.
  163. Burns, J. C., Friedmann, T., Driever, W., Burrascano, M. & Yee, J. K. *Vesicular stomatitis virus G glycoprotein pseudotyped retroviral vectors: concentration to very high titer and efficient gene transfer into mammalian*

- and nonmammalian cells* (1993) *Proc Natl Acad Sci U S A* **90**, 8033-7.
164. Ma, H. T., Patterson, R. L., van Rossum, D. B., Birnbaumer, L., Mikoshiba, K. & Gill, D. L. *Requirement of the inositol trisphosphate receptor for activation of store-operated Ca<sup>2+</sup> channels* (2000) *Science* **287**, 1647-51.
165. O'Mara, S. M., Rowan, M. J. & Anwyl, R. *Dantrolene inhibits long-term depression and depotentiation of synaptic transmission in the rat dentate gyrus* (1995) *Neuroscience* **68**, 621-4.
166. Hotchkiss, R. S. & Karl, I. E. *Dantrolene ameliorates the metabolic hallmarks of sepsis in rats and improves survival in a mouse model of endotoxemia* (1994) *Proc Natl Acad Sci U S A* **91**, 3039-43.
167. Martiny-Baron, G., Kazanietz, M. G., Mischak, H., Blumberg, P. M., Kochs, G., Hug, H., Marme, D. & Schachtele, C. *Selective inhibition of protein kinase C isozymes by the indolocarbazole Go 6976* (1993) *J Biol Chem* **268**, 9194-7.
168. Jacobson, P. B., Kuchera, S. L., Metz, A., Schachtele, C., Imre, K. & Schrier, D. J. *Anti-inflammatory properties of Gö 6850: a selective inhibitor of protein kinase C* (1995) *J Pharmacol Exp Ther* **275**, 995-1002.
169. Coultrap, S. J., Sun, H., Tenner, T. E., Jr. & Machu, T. K. *Competitive antagonism of the mouse 5-hydroxytryptamine<sub>3</sub> receptor by bisindolylmaleimide I, a "selective" protein kinase C inhibitor* (1999) *J Pharmacol Exp Ther* **290**, 76-82.
170. Yu, M., Zhong, L., Rishi, A. K., Khadeer, M., Inesi, G. & Hussain, A. *Specific substitutions at amino acid 256 of the sarcoplasmic/endoplasmic reticulum Ca<sup>2+</sup> transport ATPase mediate resistance to thapsigargin in thapsigargin-resistant hamster cells* (1998) *J Biol Chem* **273**, 3542-6.
171. Davidson, G. A. & Varhol, R. J. *Kinetics of thapsigargin-Ca<sup>2+</sup>-ATPase (sarcoplasmic reticulum) interaction reveals a two-step binding mechanism and picomolar inhibition* (1995) *J Biol Chem* **270**, 11731-4.
172. Bleasdale, J. E., Thakur, N. R., Gremban, R. S., Bundy, G. L., Fitzpatrick, F. A., Smith, R. J. & Bunting, S. *Selective inhibition of receptor-coupled phospholipase C-dependent processes in human platelets and polymorphonuclear neutrophils* (1990) *J Pharmacol Exp Ther* **255**, 756-68.
173. Hildebrandt, J.-P., Plant, T. D. & Meves, H. *The effects of bradykinin on K<sup>+</sup> currents in NG108-15 cells treated with U73122, a phospholipase C inhibitor, or neomycin* (1997) *Br J Pharmacol* **120**, 841-50.
174. Smith, R. J., Sam, L. M., Justen, J. M., Bundy, G. L., Bala, G. A. & Bleasdale, J. E. *Receptor-coupled signal transduction in human polymorphonuclear neutrophils: effects of a novel inhibitor of phospholipase C-dependent processes on cell responsiveness* (1990) *J Pharmacol Exp Ther* **253**, 688-97.
175. Kulick, M. B. & von Kügelgen, I. *P2Y-receptors mediating an inhibition of the evoked entry of calcium through N-type calcium channels at neuronal processes* (2002) *J Pharmacol Exp Ther* **303**, 520-6.
176. Schröder, R., Merten, N., Mathiesen, J. M., Martini, L., Kruljac-Letunic, A., Krop, F., Blaukat, A., Fang, Y., Tran, E., Ulven, T., Drewke, C., Whistler, J., Pardo, L., Gomeza, J. & Kostenis, E. *The C-terminal tail of CRTH2 is a key molecular determinant that constrains G<sub>α</sub> and downstream signaling cascade activation* (2009) *J Biol Chem* **284**, 1324-36.
177. Fang, Y., Ferrie, A. M., Fontaine, N. H. & Yuen, P. K. *Characteristics of dynamic mass redistribution of epidermal growth factor receptor signaling in living cells measured with label-free optical biosensors* (2005) *Anal Chem*

- 77**, 5720-5.
178. Fang, Y., Ferrie, A. M., Fontaine, N. H., Mauro, J. & Balakrishnan, J. *Resonant waveguide grating biosensor for living cell sensing* (2006) *Biophys J* **91**, 1925-40.

---

## ACKNOWLEDGEMENTS

---

An dieser Stelle möchte ich allen danken, die mich auf meinem bisherigen Lebensweg begleitet und unterstützt haben. Ohne sie wäre diese Arbeit nicht möglich gewesen.

Recht herzlich möchte ich mich bei meinen Poppelsdorfer Kolleginnen und Kollegen Stefanie Blättermann, Ralf Schröder, Dr. Christel Drewke, Ulrike Rick, Marianne Vasmer Ehses, Stephanie Hennen, Dr. Nicole Merten, Anke Müller, Lucas Peters, Johannes Schmidt und Daniel Schulz dafür bedanken, dass sie immer so erfreut waren, als ich mal im Institut war. Außerdem möchte ich mich bei euch für einzigartige Weihnachtsfeiern, Weihnachtsmarktbesuche und Betriebsausflüge bedanken. Die unzähligen Umräumaktionen und Putzaktionen werden unvergesslich bleiben.

Ganz herzlichen Dank gilt auch den Endericher Kolleginnen und Kollegen, die mich in ihre Arbeitsgruppe aufgenommen und mir das Gefühl gegeben haben, einer der Ihren zu sein. Insbesondere Dominik Tobias Thimm, Bernt Bruno Albert Alsdorf und Anja Scheiff möchte ich für die unzähligen Spieleabende und Kinoabende bedanken. Das perfekte Dinner und die Reise nach Stockholm mit euch waren phantastisch. Ihr seid echte Freunde geworden. Dominik möchte ich außerdem dafür danken, dass er meiner Frau und mir die Ehre erwiesen hat mein Trauzeuge zu sein und Taufpate unserer Tochter zu werden.

Dr. Daniela Bertarelli, Dr. Andrea Behrenswerth und Dr. Petra Hillmann möchte ich für die schöne Zeit im Büro und Labor danken und dafür, dass wir uns trotz der teilweise großen Entfernung immer noch bei jeder Gelegenheit treffen. Ich hoffe das bleibt so.

Dr. Rhallid Akkari, Kirsten Ritter und Dr. Younis Baqi möchte ich für die Synthese meiner Testsubstanzen danken. Karen Schmeling möchte ich für die Unterstützung bei meiner Arbeit bedanken.

## ACKNOWLEDGEMENTS

---

Allen Kolleginnen und Kollegen der Arbeitsgruppe von Frau Professorin Dr. Christa E. Müller, die hier nicht namentlich erwähnt sind, möchte ich natürlich auch für die schöne Arbeitsatmosphäre danken.

Den Arbeitsgruppen von Frau Professorin Dr. G. M. König und Herr Professor E. Leistner möchte ich für die Bereitstellung ihrer Substanzbibliotheken bedanken. Der Arbeitsgruppe von Herr Professor I. von Kügelgen möchte ich dafür danken, dass ich kurzfristig meine Versuche bei ihnen durchführen konnte.

Für die freundliche Übernahme der Korrektur meiner Arbeit möchte ich mich bei Dr. Christel Drewke, Dominik Tobias Thimm und Martin Lund bedanken.

Allen Mitgliedern des Graduiertenkollegs 677 danke ich für die zahlreichen interessanten gemeinsamen Workshops und Symposien.

Außerdem möchte ich mich bei Christian Degering, meinem alten Freund und Studienkollege aus Düsseldorfer Zeit, und seiner Frau Sara danken. Die regelmäßigen Telefonate, bei denen wir uns gegenseitig immer wieder Mut zugesprochen haben, und gemeinsamen Spieleabende waren klasse.

Abschließend möchte ich mich bei meiner Familie, insbesondere meinen Eltern dafür bedanken, dass sie es mir und meinen Geschwistern ermöglicht haben, alles zu erreichen was wir möchten.

Mein größter Dank gilt jedoch meiner Frau Marieke, die mich und meine Launen all die Jahre ertragen hat. Sie hat mich stets unterstützt und wenn es notwendig war in den Hintern getreten. Danke, dass du mich geheiratet und uns unsere Tochter Annemarie geschenkt hast.

---

## REGISTER OF PUBLICATIONS

---

### Publications

Christiansen, E., Urban, C., Merten, N., Liebscher, K., Karlsen, K. K., Hamacher, A., Spinrath, A., Bond, A. D., Drewke, C., Ullrich, S., Kassack, M. U., Kostenis, E. & Ulven, T. *Discovery of potent and selective agonists for the free fatty acid receptor 1 (FFA<sub>1</sub>/GPR40), a potential target for the treatment of type II diabetes* (2008) *J Med Chem* **51**, 7061-4.

Hillmann, P., Ko, G. Y., Spinrath, A., Raulf, A., von Kügelgen, I., Wolff, S. C., Nicholas, R. A., Kostenis, E., Höltje, H. D. & Müller, C. E. *Key determinants of nucleotide-activated G protein-coupled P2Y<sub>2</sub> receptor function revealed by chemical and pharmacological experiments, mutagenesis and homology modeling* (2009) *J Med Chem* **52**, 2762-75.

### Posters

Spinrath, A., Hillmann, P., Kostenis, E. & Müller, C. E. *Structural requirements for ligand binding and activation of the P2Y<sub>2</sub> receptor* Second Joint Italian-German Club Meeting, Leipzig, Germany 12.-15. September 2007.

Spinrath, A., Hennen, S., Akkari, R., von Kügelgen, I., Müller, C. E., Gomeza, J. & Kostenis, E. *GPR17: a new dual uracil nucleotide/cysteinyl-leukotriene receptor or still an orphan?* Minisymposium of the Graduate College GRK 677 - Structure and Molecular Interaction as Basis of Drug Action, Bonn, Germany, 1. April 2009.

Spinrath, A., Hennen, S., Dallmeyer, M., von Kügelgen, I., Müller, C. E., Gomeza, J. & Kostenis, E. *Uracil nucleotides do not activate the orphan G protein coupled*

*receptor GPR17* Small Purine Meeting, Stockholm, Sweden, 18.-19. September 2009.

Spinrath, A., Hennen, S., Dallmeyer, M., von Kügelgen, I., Müller, C. E., Gomeza, J. & Kostenis, E. *GPR17: an orphan G protein-coupled receptor on a journey to find its identity...*, International Symposium of the Graduate College GRK 677 - Structure and Molecular Interaction as Basis of Drug Action, Bonn, Germany, 21.-23. September 2009.